U.PORTO

FEUP FACULDADE DE ENGENHARIA UNIVERSIDADE DO PORTO

STRUCTURAL CONDITION ASSESSMENT OF DAMS BASED ON CONTINUOUS DYNAMIC MONITORING

SÉRGIO BOUÇA PEREIRA

A dissertation presented to the Faculty of Engineering of the University of Porto for the degree of Doctor in Civil Engineering.

Supervisors: Filipe Magalhães (Assistant Professor); Álvaro Cunha (Full Professor).

FCT Fundação para a Ciência e a Tecnologia
MINISTÉRIO DA CIÊNCIA, TECNOLOGIA E ENSINO SUPERIOR

REPÚBLICA PORTUGUESA

CONSTRUCT


REPÚBLICA PORTUGUESA
CIÊNCIA, TECNOLOGIA E ENSINO SUPERIOR
FCT Fundação para a Ciência e a Tecnologia
NORTE2020
POCH
PORTUGAL 2020
UNIÃO EUROPEIA
Fundo Social Europeu

To my parents

ABSTRACT

Dams play a fundamental role in human societies, providing water for population and irrigation and serving as well as an important instrument for energy production. However, the enormous amount of potential energy held by dams in their reservoirs becomes a tremendous threat to human lives and properties in case of a structural failure. Thus, the risks of a malfunction in the structure, caused by external actions or simply by ageing, must be minimized by continuous monitoring and maintenance procedures. Structural health monitoring based on operational modal analysis is an adequate methodology to continuously assess the condition of civil engineering structures and has already been successfully implemented in bridges, buildings, wind turbines, towers and stadia.

This work focuses on the development of numerical and experimental tools to assess the dynamic behaviour of dams during reservoir filling and operational phases, and to evaluate their structural condition using vibration-based monitoring systems. With this purpose, the present work involves, on the one hand, the performance of ambient vibration tests in a group of dams with different characteristics, and on the other hand the exploration of continuous dynamic monitoring systems installed in two recently built concrete arch dams.

To achieve the presented goals and verify the structural integrity of dams, algorithms for automatic and continuous identification of modal parameters are implemented and applied, as well as tools to minimize the effects of environmental and operational conditions on the referred modal estimates, allowing the detection of structural anomalies. Numerically simulated damages are used to test the ability of damage detection tools to find these anomalies. Additionally, results obtained from ambient vibration tests are used to analyse the suitability of operational modal analysis to concrete dams, and the level of accuracy achieved during these tests using different types of sensors is studied.

RESUMO

As barragens desempenham um papel fundamental nas sociedades humanas, fornecendo água às populações e para irrigação e servindo ainda como um instrumento para a produção de energia. No entanto, a enorme quantidade de energia potencial detida pelas barragens nos seus reservatórios torna-se uma tremenda ameaça à vida e propriedades humanas, em caso de falha estrutural. Assim, os riscos de um mau funcionamento da estrutura causados por ações externas, ou simplesmente pelo envelhecimento, devem ser minimizados por procedimentos de monitorização e manutenção contínuos. A monitorização da integridade estrutural baseada em análise modal operacional é uma metodologia adequada para avaliar a condição de estruturas de engenharia civil de forma contínua e já foi implementada com sucesso em pontes, edifícios, turbinas eólicas, torres e estádios.

Este trabalho foca-se no desenvolvimento de ferramentas numéricas e experimentais para avaliar o comportamento dinâmico de barragens durante as fases de enchimento e de operação, e avaliar a sua condição estrutural utilizando sistemas de monitorização dinâmica. Desta forma, o presente trabalho envolve, por um lado, a realização de ensaios de vibração ambiental num conjunto de barragens com diferentes características e, por outro, a exploração de sistemas de monitorização dinâmica contínua instalados em duas barragens de betão construídas recentemente.

Para atingir os objetivos apresentados e verificar a integridade estrutural de barragens, são implementados e aplicados algoritmos de identificação automática de parâmetros modais, além de ferramentas para minimizar os efeitos das condições ambientais e operacionais nas referidas estimativas modais, permitindo a deteção de anomalias estruturais. Danos numericamente simulados são usados para testar a capacidade das ferramentas de deteção de danos em encontrar essas anomalias. Além disso, os resultados obtidos a partir de ensaios de vibração ambiental são usados para analisar a aptidão da análise modal operacional em barragens de betão, e é estudado o nível de precisão alcançado durante esses testes usando diferentes tipos de sensores.

RÉSUMÉ

Les barrages jouent un rôle fondamental dans les sociétés humaines en fournissant de l'eau pour la population et l'irrigation et en servant également d'instrument important pour la production d'énergie. Toutefois, l'énorme quantité d'énergie potentielle des barrages dans leurs réservoirs représente une menace considérable pour les biens et vies humaines en cas de défaillance structurelle. Ainsi, les risques de dysfonctionnement de la structure, dus à des actions externes, ou simplement au vieillissement, doivent être minimisés par des procédures de surveillance et de maintenance continues. La surveillance de l'état des structures basée sur l'analyse modale opérationnelle est une méthodologie adéquate pour évaluer en permanence l'état des ouvrages de génie civil, qu'a déjà été mise en œuvre avec succès dans les ponts, les bâtiments, les éoliennes, les tours et les stades.

Ce travail porte sur le développement d'outils numériques et expérimentaux pour évaluer le comportement dynamique des barrages pendant les phases de remplissage et d'exploitation, ainsi que pour évaluer leur état structurel à l'aide de systèmes de surveillance basés sur les vibrations. À cette fin, les travaux en cours portent, d'une part, sur la réalisation d'essais de vibrations ambiantes dans un groupe de barrages présentant des caractéristiques différentes, et, d'autre part, sur l'exploration de systèmes de surveillance dynamique en continu installés dans deux barrages en béton.

Pour atteindre les objectifs présentés et vérifier l'intégrité structurelle des barrages, des algorithmes d'identification automatique des paramètres modaux sont mis en œuvre et appliqués, ainsi que des outils permettant de minimiser les effets des conditions environnementales et opérationnelles sur les estimations modales référées, permettant ainsi de détecter des anomalies structurelles. Des dommages simulés numériquement permettent de tester la capacité des outils de détection des dommages à détecter ces anomalies. En outre, les résultats des tests de vibrations ambiantes permettent d'analyser l'adéquation de l'analyse modale opérationnelle aux barrages en béton et d'étudier le niveau de précision obtenu lors de ces tests avec différents types de capteurs.

ACKNOWLEDGMENTS

To all my family, friends and colleagues, who through their friendship and support helped me prepare this thesis, here I present my sincere gratitude. Nevertheless, I want to express a special thanks:

- to Professor Filipe Magalhães, my advisor, for all the support, the commitment, the time, the sympathy, the precious pieces of advice and the enormous patience when my countless "what-ifs" and "something's wrong" were followed by his demonstrations of knowledge and kind motivational words;

- to Professor Álvaro Cunha, my co-advisor, for challenging me with this adventure and always making sure I had the necessary resources to develop my work, for encouraging me to participate in so many international conferences, but mostly for the close, gentle and constant support, motivation and guidance;

- to Doctors Jorge Pereira Gomes and José Vieira de Lemos, from the National Laboratory for Civil Engineering (Portugal), for receiving me at the Concrete Dams Department during almost two months, for their hospitality and for the time so kindly spent giving me insights about the numerical modelling of dams. Additionally, for all the support related with the monitoring of Baixo Sabor and Foz Tua dams;

- to Professor Edwin Reynders, from Katholieke Universiteit Leuven (Belgium) for all the support validating the routines for uncertainty quantification and the generous and useful suggestions on the topic;

- to Professor Carlo Rainieri, from the University of Molise (Italy), for the insights on automatic operational modal analysis and the conversations about the specific case of Baixo Sabor dam, which helped improve this thesis;

- to Doctor Gustavo Oliveira for the cared reading of my Research Thesis Project, and the interesting suggestions that followed;

- to Energias de Portugal (EDP), in particular to Engineers Domingos Silva Matos and Ilídio Ferreira, for the opportunity of testing Aguieira, Alto Lindoso, Bouçã, Caldeirão, Castelo do Bode and Santa Luzia dams, and for the access to data related with the monitoring of Baixo Sabor and Foz Tua dams;

- to Professor Elsa Caetano for introducing me to the topic of operational modal analysis during my master thesis, which helped me take the decision to pursue this PhD, and for the interesting suggestions and constant incentive throughout this period of my life;

- to Professor Carlos Moutinho, for the good time spent with him inside and outside the lab, working with sensors around bridges and tuned mass dampers and, mostly, learning from him;

- to Engineer João Pacheco, for his help during the preparation and performance of ambient vibration tests on dams;

- to Mrs. Ana Matos for keeping me on track with the paperwork, always with a smile and a kind word;

- to Fundação para a Ciência e a Tecnologia (FCT), for the financial support through the PhD fellowship SFRH/BD/100587/2014 and to projects POCI-01-0145-FEDER-007457 - CONSTRUCT - Institute of R&D in Structures and Construction and PTDC/ECM-EST/0805/2014|16761 – DAM_AGE - Advanced Online Dynamic Structural Health Monitoring of Concrete Dams, funded by FEDER through COMPETE2020 - Programa Operacional Competitividade e Internacionalização (POCI) – and by national funds through FCT - Fundação para a Ciência e a Tecnologia;

- to my colleagues at the "Civil-FEUP" futsal team, for letting me be part of such a group of stars and for the amazing fellowship;

- to my work colleagues and friends Aires, Ana Gomes, André, Gustavo, Ricardo, Ruben, Silvia, Alex, Ana Luísa, Cássio, Cláudio, João, Rodrigo, Lázaro and Paulo, for the great time that was working in our H304, and for all those hours discussing meaningless topics and getting older together;

- à Rute, pelo amor e pela paciência sempre que estive presente em corpo, mas não em mente. Pelo conforto que me dá quando se senta ao meu lado e olha o futuro de frente comigo;

- aos meus avós, para quem sempre fui e serei "filho";

- aos meus pais, pelo amor, pelo tempo, por me porem sempre à frente, por me darem tudo o que tenho e sou.

Contents

1. INTRODUCTION

1.1. RESEARCH CONTEXT

Water has always been a crucial factor of progress. Since early in the evolution of human civilization, the need to control water's natural cycle led to the construction of reservoirs, in order to assure the supply for agriculture and population, in a first stage, and then to attempt the control of floods, thus liberating fertile areas in the river banks for agriculture. However, ancient dams had limited dimensions and accidents were common.

Science and technology brought new materials, construction techniques and structural design methods allowing the construction of higher, safer and long-lasting dams. New purposes such as electricity production, recreational events or even fish breeding emerged. So, nowadays, these structures are scattered all over the world. According to the International Commission on Large Dams (ICOLD), and the present edition of the World Register of Dams, there are more than 55000 dams in the world, 40% of whom are located in China and about 10% in Europe. About half the dams in the world are single purposed and the most common purpose for a dam is irrigation, followed by hydropower and water supply.

However, higher dams and larger reservoirs also mean major concentration of potential energy that may become an enormous threat to human life and property in case of structural failure. A dam failure can be caused by miscalculations or inadequate evaluation of any critical design condition, such as hydrological or geotechnical conditions, or by an error in operational procedures (Betâmio de Almeida et al., 2003). In the first three quarters of the 20th century there were about 200 serious dam failures in the world, resulting in the death of more than 8000 people (Jansen, 1980), and

deadly accidents are still occurring nowadays (BBC, 2019), though quite not as frequently, and mainly with earth and tailing dams. In the case of concrete dams, there are many examples of structures that needed to be repaired after being submitted to extreme loading conditions, but the last major catastrophe occurred in France, in 1959. The failure of Malpasset dam (Londe, 1987), a 66 meters high arch dam, was due to a combination of severe rains and design and operation errors. Figure 1.1 presents a comparison of Malpasset dam before and after failure.

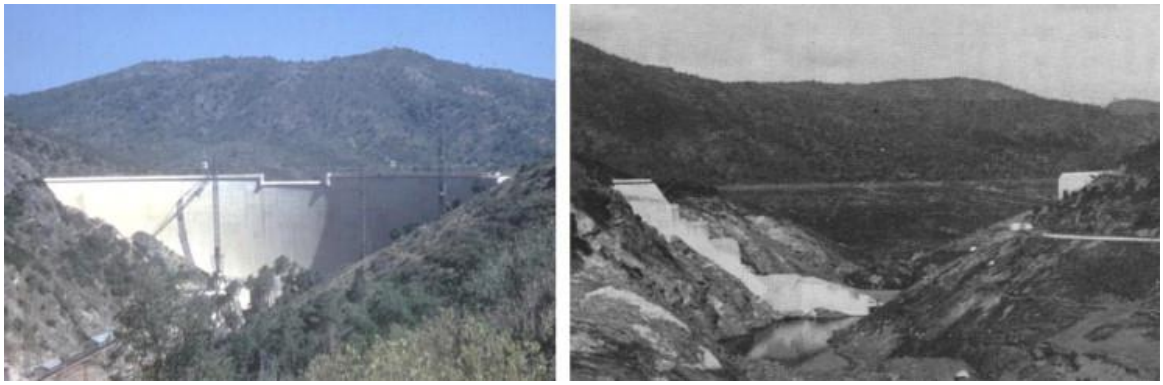

Figure 1.1 – Malpasset dam at the end of construction on the left, and soon after failure on the right (Duffaut, 2013).

Most times, after the occurrence of accidents or structural damages, studies initiate to understand its causes and prevent it from happening again. Learning from past mistakes led to safer structures and more efficient emergency plans, resulting in less human and material losses. Nonetheless, it is also important to be capable of predicting when a structural malfunction may arise. For this it is essential that the scientific community keeps investigating and improving knowledge on how to properly model, analyse, design, maintain, monitor, manage, predict and optimise the life-cycle performance of structures and infrastructures under uncertainty (Frangopol, 2011). Moreover, to confidently maintaining civil infrastructures such as dams with high levels of performance and safety, decisions should be supported by integrated monitoring systems considering real continuous data, directly obtained from the structures.

Mosul dam, in Iraq, is a relevant case of a structure where continuous monitoring and maintenance are extremely important. The dam finished in 1984 sits on a foundation of soluble rock, so to keep it stable, workers have to pump a cement mixture into the earth below (Filkins, 2017). However, the latest political conflicts in the region left the structure nearly abandoned and the maintenance processes were stopped. American authorities used satellite pictures to study the dam's movement and warned that a break was likely to occur, which would be a catastrophic scenario for the

country's second largest city. Fortunately, the political situation in the region has been stabilizing and maintenance processes are being conducted once again.

Regular condition assessment, through dynamic tests and vibration-based health monitoring, play a significant role in determining structural integrity and protecting the longevity of structures, especially for long-life ones (A. C. Altunişik et al., 2016). Health monitoring systems are historically associated with static data. This is the case with dams, which are classically equipped with systems capable of measuring displacements, strains, relative movements between joints or temperatures, with the aim of studying the structures static behaviour. However, vibration-based health monitoring systems have also already been successfully implemented in many different structures such as bridges (Magalhães, Cunha, et al., 2012), wind turbines (G. Oliveira et al., 2016), stadia roofs (Martins et al., 2014) or bell-towers (Ubertini et al., 2016). In the case of dams, besides the more common forced vibration tests (J. Gomes & Carvalho, 2014) (J. Gomes & J. V. Lemos, 2016b), also dynamic tests using ambient vibration have been performed (Darbre & Proulx, 2002) and a vibration-based health monitoring system worked for a period of almost a year in Cabril dam (P. Mendes, 2010) with good results.

The nowadays-available dynamic monitoring equipment integrating very sensitive low noise sensors creates an opportunity to implement continuously operating dynamic monitoring systems in dams and validate the suitability of these systems to monitor these more massive structures and detect damage.

For the purpose of damage detection, robust operational modal analysis techniques are needed to accurately and automatically estimate modal parameters from measured structural responses, and statistical methods to remove the effects of environmental and operational conditions (such as thermal and reservoir water level variations) from the obtained modal properties must be implemented.

The detection of structural novel behaviour, that may indicate the occurrence of damage, can be based on control charts and is associated with shifts in the modal parameters values that are not explained by other physical phenomena but a change in the structure's stiffness.

1.2. OBJECTIVES AND MAIN CONTRIBUTIONS

Considering the previously presented background, the main goals of the present thesis consist on better understanding the dynamic behaviour of dams, on assessing the suitability of applying operational modal analysis to dams and on the development of a vibration-based monitoring system capable of detecting the presence of small damages in this type of structures.

In order to achieve these goals, the following objectives are addressed in this thesis:

- implementation of operational modal analysis tools for the identification of modal properties, including the quantification of the uncertainties associated with these estimates, and validation of the implemented tools with real data recorded in concrete dams;

- implementation and development of tools and strategies for continuous and automatic tracking of modal properties and mitigation of the effects of operational and environmental conditions in the context of concrete dams;

- conception and implementation of long-term dynamic programs in concrete dams to test and validate the implemented routines and demonstrate the usefulness of vibration-based health monitoring systems in this type of structures.

It is expected for the tools here implemented, developed and validated, as well as for the obtained results, to represent an important step in the vibration-based testing and monitoring of concrete dams, contributing to better understand the dynamic behaviour of these structures, on the one hand, and to the increase of safety and lifetime, on the other. In this context, the main contributions of the present work are the following:

- description of the general structural characteristics of dams, of the major concerns to have in consideration when testing and numerically modelling these type of structures and how each part of the system dam-foundation-reservoir affects their dynamic behaviour (chapter 2);

- synthesis of the main procedures used in the dynamic testing of dams and of the tools in which these procedures are based, taking into consideration the major sources of uncertainties in operational modal analysis and the quantification of these uncertainties (chapter 3);

- application and validation of the tools implemented for operational modal analysis in the dynamic testing of six concrete dams with different typologies, assuring the suitability of such tools for the testing of such massive structures and creating accurate records that can be used in the future for the comparison of modal properties and updating of numerical models (chapter 4);

- analysis of the accuracy achieved in the identification of the modal properties of two concrete arch dams considering sensors with different functioning principles, using real data and numerically simulated noise (section 4.9);

- synthesis of the theory behind the available methods to minimize the influence of operational and environmental factors on modal parameters, with the goal of obtaining features suited for the application of routines that allow the automatic identification of abnormal structural behaviour (chapter 5);

- conception, assembly and operation for more than three years of a dynamic monitoring system on a concrete arch dam (Baixo Sabor dam, in Portugal), where all the stages of a vibration-based monitoring system were implemented, tested and validated, including modal properties identification and comparison with results from numerical models and forced vibration tests, continuous modal tracking, mitigation of the effects of operational and environmental conditions and damage detection, using numerically simulated damages (chapter 6);

- quantification of the uncertainties associated with the estimated natural frequencies and damping ratios through the entire period of monitoring of Baixo Sabor arch dam and incorporation of these uncertainties both in the modal tracking routines and in the procedures used for minimization of operational and environmental effects on natural frequencies (sections 6.5 and 6.6);

- operation for more than one year of a dynamic monitoring system in Foz Tua arch dam, in Portugal, which was important to demonstrate the good results achieved with Baixo Sabor arch dam did not consist of an isolated case and that the routines for automatic identification and tracking of modal properties are adequate for these type of structures, even with challenging scenarios such as the ones observed in this dam, which required the use of moving references for modal tracking (chapter 7).

1.3. ORGANIZATION OF THE TEXT

The present thesis is divided in 8 chapters and, at the end, it is presented the list of references introduced throughout the text. Chapters 2, 3 and 5 are introductory and present general concepts and state-of-art tools and applications. On the other hand, chapters 4, 6 and 7 present case studies where the tools previously introduced are applied. Finally, in the eighth chapter, the conclusions achieved are presented and the foreseen future research is described. A summarized description of the contents addressed in each chapter is presented in the following paragraphs.

Chapter 1 introduces the present work with a concise contextualization, which is followed by the present description of the text's organization.

Chapter 2 presents a brief overview on dams, classifying these structures taking into account their shape and the materials composing them. Additionally, important aspects regarding the system dam-foundation-reservoir and the interaction between their parts are addressed. The last section of the chapter is dedicated to the numerical modelling of dams, giving special relevance to case studies where operational modal analysis is used to validate and update the models.

Chapter 3 addresses the topic of operational modal analysis, which is the core of a dynamic monitoring system. Some output-only identification algorithms such as the Peak Picking, the Enhanced Frequency Domain Decomposition, the Covariance driven Stochastic Subspace Identification and the poly-reference Least Squares Complex Frequency Domain methods are introduced along with short application examples. Finally, the importance of estimating the uncertainty in modal parameters is addressed and tools to accomplish it are described.

Chapter 4 presents ambient vibration tests performed in a group of six Portuguese dams with different typologies, including arch dams (Alto Lindoso dam, Bouçã dam, Santa Luzia dam and Caldeirão dam), an arch-gravity dam (Castelo do Bode dam) and a multiple arch dam (Aguieira dam), as well as the processing applied to the acceleration time-series obtained during the tests to identify the dams modal properties. The chapter concludes with a sensitivity analysis on the ability of sensors with different functioning principles to be successfully used in the dynamic testing of concrete dams.

In **chapter 5** the topic of structural health monitoring is introduced along with methodologies to automatically process data obtained from the continuous dynamic monitoring of structures and

methods to mitigate the effects of operational and environmental conditions on modal properties are described. Tools and indicators used for damage detection are presented.

Chapter 6 describes the continuous dynamic monitoring of Baixo Sabor arch dam as a case study. The structure and the installed monitoring system are presented, and the methods explained in previous chapters are used to continuously and automatically estimate modal parameters and respective uncertainties and to mitigate the influence of operational and environmental conditions. At the end, control charts are used to identify damages simulated with a numerical model of the dam and then artificially introduced in the data resulting from operational modal analysis.

Chapter 7 describes a second case study, which consists in the continuous dynamic monitoring of Foz Tua arch dam. Once again, the structure and the installed monitoring system are presented. The structure vibration levels are characterized and automatic operational modal analysis is used to continuously identify and track the structure's modal properties during the first year of monitoring.

Chapter 8 ends the thesis with the presentation of the conclusions achieved throughout the work and the foreseen future research on the topic.

2. GENERAL CONSIDERATIONS ON DAMS

2.1. INTRODUCTION

Commonly known as a synonym of life and prosperity, water is one of our most import resources, apart from air and land. As Leonardo Da Vinci put it "water is the driving force of all nature" (Hay, 2016). Therefore, it is no surprise that most of the civilizations in early humankind history began in river valleys. Mesopotamia, a region widely considered to be one of the cradles of the civilization was situated between the rivers Euphrates and Tigris. The name itself, "Meso-potamia", comes from the Greek and means "between rivers", which denotes the importance of water for the rising of this ancient culture.

However, freshwater resources are generally unevenly distributed, both geographically and during the year. Thus, all early civilizations, as those who rose in Egypt, Middle East, India or China, have been identified with the construction of storage reservoirs appropriate to their needs, in the earliest instances to satisfy irrigation demands arising through the development and expansion of organized agriculture (Novak et al., 2007). This concept of water resources management was later widespread through Europe by the Roman Empire, which developed new dam structural solutions, such as arch dams, as well as a kind of water-proof hydraulic mortar, allowing the construction of higher, safer and longer lasting dams (Henkel, 2015). Roman hydraulic engineering, which also included plumbing and the construction of aqueducts and mills, was the most advanced at the time and one of the pillars that made possible the maintenance of such an empire. Cornalvo dam in Spain, which has been in use for almost two millennia, is a good example of such long-term roman engineering. This gravity dam is presented in Figure 2.1.

Figure 2.1 – Cornalvo dam: Roman structure in Spain (Henkel, 2015).

Nowadays, a great variety of dams, with different structural solutions and purposes are scattered around the world. Such as during the last 5000 years, since the first dams arose, dams also serve today to ensure an adequate supply of water, for irrigation or population's consumption, by storing it in times of surplus and releasing it in times of scarcity, thus also preventing floods or, at least, mitigating their effects. Still, these are not their only finalities, as dams are now also used for allowing navigation in rivers, sedimentation control, recreation, fish farming and hydroelectric power production. In addition, modern dams are often multipurpose structures, serving populations directly and at the same time aiding in the production of energy, thus clearly making a significant contribution to the efficient management and harnessing of water resources.

According to the *World Register of Dams* (ICOLD) almost half of the world's dams are used for irrigation, making this the most common purpose for a dam. Taking into account the large population growth expected for the next decades (the United Nations predicted a growth of 50% of the world's population until the end of the century (UN, 2015)), and that irrigated land is much more productive than non-irrigated land, it is reasonable to think that irrigation will be expanded to increase the world's food capacity production. Consequently, even with the widespread measures to conserve water by improvements in irrigation technology and the introduction of low water consumption crops, the construction of more dams with this purpose will probably be required. In the same way, water supply needs for domestic and industrial use should also follow population growth, hence increasing the pressure on water reserves. Simultaneously, climate change is likely to promote the occurrence of extreme droughts which in turn boosts deforestation, decreasing soils capacity to retain water, thus resulting in a self-driving process of regional desertification. Consequently, properly planned and located dams may assume an extremely important role to

ensure daily population demand of water and, mostly, to guarantee basic supply needs in time of severe shortage caused by climate conditions.

Dams and reservoirs can also be effectively used to regulate river levels and flooding downstream of the dam by temporarily storing the flood volume and releasing it later. For this, integrated plans for water management of the entire basin must be created. Flood control is particularly important in The Netherlands, for instance, where a net of dykes maintains a major part of the country's surface from being flooded by the sea and the primary rivers.

Even though fossil fuels are still the major energy source in the world, corresponding to more than 80% of the total consumed energy during 2015 (WECouncil, 2016), renewable ways of producing energy have been spreading. The international consensus to protect the environment and reduce carbon emissions points to the expansion of all the renewable forms of energy production, including the hydroelectric, which is worldwide leaded by China. Figure 2.2, which presents the installed capacity of power plants in Portugal by source, shows that nearly half of the country's capacity related to renewable energy corresponds to hydroelectric developments and that the capacity of reversible hydro has been increasing. The latest point is relevant in the sense that wind and hydroelectric production have been used together, harnessing the surplus of energy produced by wind to pump river water upstream, which is then used to produce electricity when demanded by the distribution network. This strategy makes the hydroelectric production of energy, together with other renewable based sources such as wind or solar, the core of a concept that regards hydroelectric developments as giant batteries that can help manage power production without fossil fuels (Times, 2018).

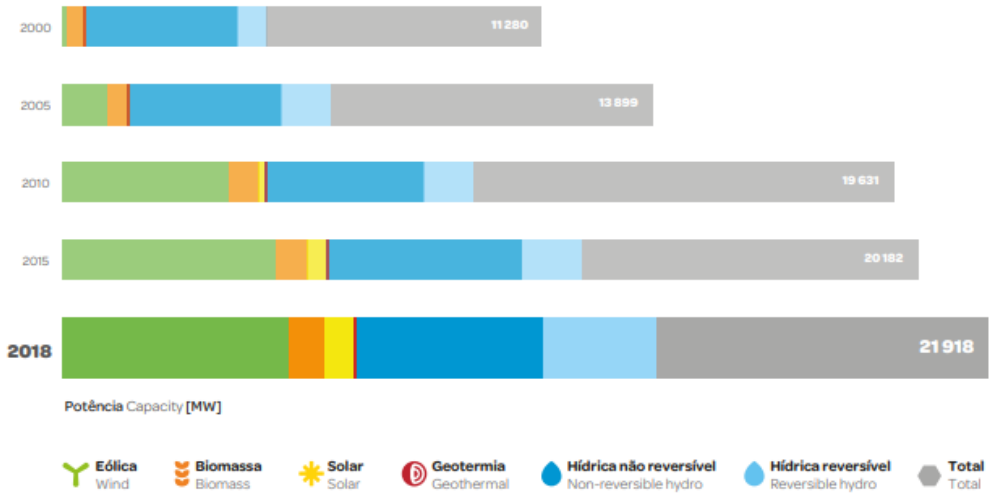

Figure 2.2 – Installed capacity of powerplants in Portugal by source (APREN, 2019).

2.2. STRUCTURAL CLASSIFICATION

Dams can be classified according to their function, to the materials that compose them and to their forms and structural schemes. Considering their purposes, dams can be built and used for water retention and water supply, both for population or industrial consumption, for irrigation, for power production, for recreational activities, for flood control, for fish farming or for tailing, and many dams are used for more than one function at the same time, thus being called multipurpose dams.

Regarding the materials used to build dams, these structures are usually made of concrete, soil or rock, but masonry dams are common as well, and even timber and steel dams can be found. Concrete dams, the main study object of this thesis, are generally large and massive structures whose construction requires enormous volumes of concrete, poured at high placing rates and subjected to lower compressive stresses, when compared to other structures. Mass concrete for use in dams should present satisfactory density, strength, durability and resistance to cracking and low thermal volume change and permeability. It is worth taking into account that, concrete is a superficially inert but chemically and physically complex construction material. Its merits lie in its adaptability, its use of readily available mineral resources and, above all, its low bulk cost (Novak et al., 2007). The primary constituents of concrete are cement, mineral aggregates and water, but ashes and pozzolans may also be added to partially substitute cement and reduce hydration heat and gain resistance against aggressive chemical agents, without diminishing mechanical properties.

Finally, taking into account their structural schemes and building processes, dams can be classified as gravity dams, buttress dams, arch dams, multiple arch dams, roller-compacted concrete dams or embankment dams, which are divided in earthfill and rockfill dams. All these types of dams are presented in the next few subsections.

2.2.1. GRAVITY DAMS

Gravity dams are concrete, or masonry, structures designed and calculated to withstand the momentum of the water they retain only by the use of their own weight. The cross section of a typical gravity dam is approximately triangular, mostly to ensure stability and to avoid overstressing of the dam or its foundation, and the top view, which is generally rectangular, may have a slight curvature. If this curvature is important enough to mobilize an arch effect it allows a rather slimmer profile. In this last case, the term arch-gravity dam may be employed. Gravity dams are classified as solid or hollow, depending on the existence, or not, of voids in their cross sections. Figure 2.3

presents the cross section of Guilhofrei dam, a solid triangular shaped cross section dam, in Ave river, in the north of Portugal.

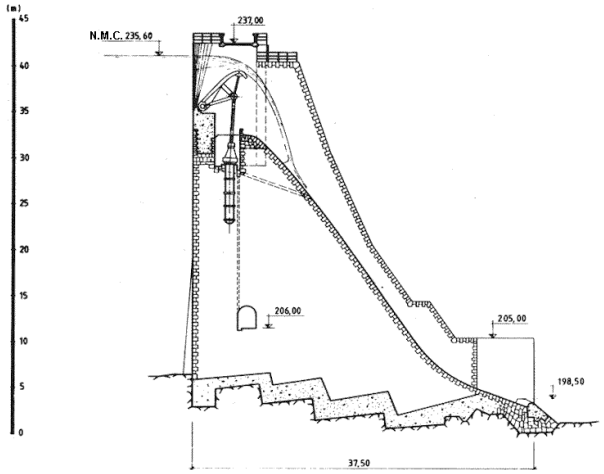

Figure 2.3 – Cross section of Guilhofrei dam (CNPGB).

The design of gravity dams must always take into account the following safety requirements (Novak et al., 2007):

- The structure must not be overthrown over any horizontal line, defined in the dam's body or along the contact with the foundation;
- The structure must not slide over any horizontal plane, defined in the dam's body or along the contact with the foundation or any of its geological discontinuities;
- The structure must present a shape such that the stresses in the dam's body and in the foundation do not exceed admissible values.

The main forces to be taken into account in the design process are those resulting from hydrostatic pressure, self-weight and subpressions at the base of the dam, from a static point of view, and the inertia forces of the dam's body and the hydrodynamic pressures at the upstream wall, from a dynamic point of view. It is also of utmost importance to consider the deformations imposed by thermal variations, due to the release of the heat of hydration of the cement during construction, and due to environmental conditions.

Figure 2.4 shows a picture of Bemposta dam, an example of an arch-gravity dam with hollowed cross section, located in the Portuguese part of the Douro river, right in the boundary between Portugal and Spain.

Figure 2.4 – Bemposta dam: aeriel view (EDP) and cross section (CNPGB).

2.2.2. BUTTRESS DAMS

In the design of a dam, whatever its type, two essential objectives are aimed: to resist the impulse of the water that it retains and to guarantee the watertightness of the structure and of its foundation. In the case of both gravity and arch dams, the structure's body is designed to guarantee these two requirements simultaneously. In buttress dams, however, strength and watertightness are guaranteed by different structural parts. The resistant structure consists of a series of parallel and generally equidistant buttresses of triangular profile, on which it is supported the watertight part of the structure. This becomes most evident by the observation of Pracana dam's plan and cross section, presented in Figure 2.5, where the dam's twelve buttresses are easily perceived. To utilize some of the reservoir water pressure to resist overturning moment, the upstream face is usually sloped (Penman, 1989), as it is the case in the represented cross section.

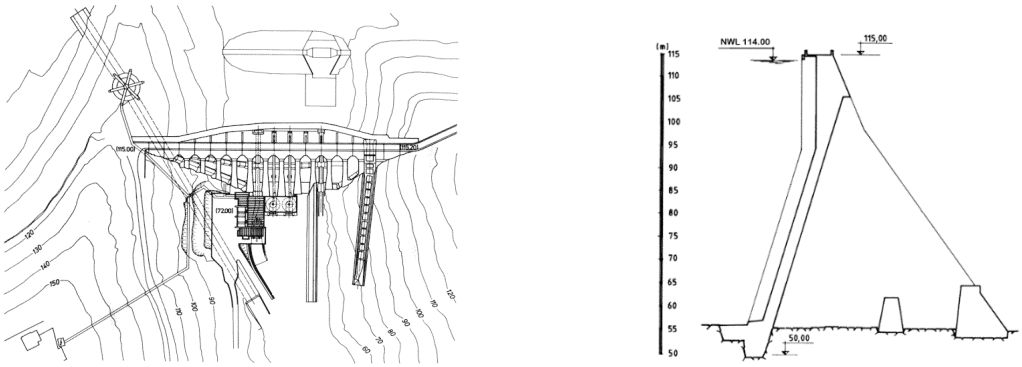

Figure 2.5 – Pracana dam: plan on the left; cross section on the right (CNPGB).

There are several types of buttress dams, whose differences mostly depend on the nature of the watertight part of the structure: dams where this structure is a slab; dams where this structure is a continuation of the buttress, forming a massive round or diamond-shaped head; dams in which this structure is an arch, commonly known as multiple arch dams (Instituto da Água, 2001). This last type will be presented later in this work.

The previously referred Pracana dam, located in Ocreza river, central Portugal, is presented in Figure 2.6, along with Miranda dam, an example of a diamond-shaped head dam, located at the beginning of the international stretch of the Douro river.

Figure 2.6 – Buttress dams: Pracana dam on the left; Miranda dam on the right (EDP).

2.2.3. ARCH DAMS

Arch dams are curved structures in plan, with the convexity facing upstream, designed to transmit the water impulse mainly to the abutments and not to the bottom of the valley, using for that the compressive strength of the material of which they are made. The first constraints in determining the shape to be given to an arch dam are the topographical and geological conditions of the foundation. Generally, the best shape is the double curvature arch which reduces bending and twisting side-effects, leading to uniform compressive stresses and limited tensile stresses under all loading conditions (Serafim, 1987).

These structures are much lighter than gravity dams and represent the most slender type of dams. In general, the relative thickness of arch dams is described by the ratio between T/H, where T is the base thickness of the central cantilever and H the height of the dam. A thin arch dam is defined as having a ratio of 0,2 or smaller, a medium-thick arch dam is defined as having a ratio between 0,2 and 0,35 and ratios above 0,35 represent thick arch dams or arch-gravity dams (Chen, 2015).

However, the lower thickness of arch dams implies some extra costs through the necessity of more monitoring instruments, when compared to dams where stresses are lower, and the manifest need for a higher quality concrete (Serafim, 1987). Nowadays, most arch dams are double curved, both in horizontal and vertical views, which is the case of Salamonde arch dam, in Cávado river, Portugal, presented in Figure 2.7.

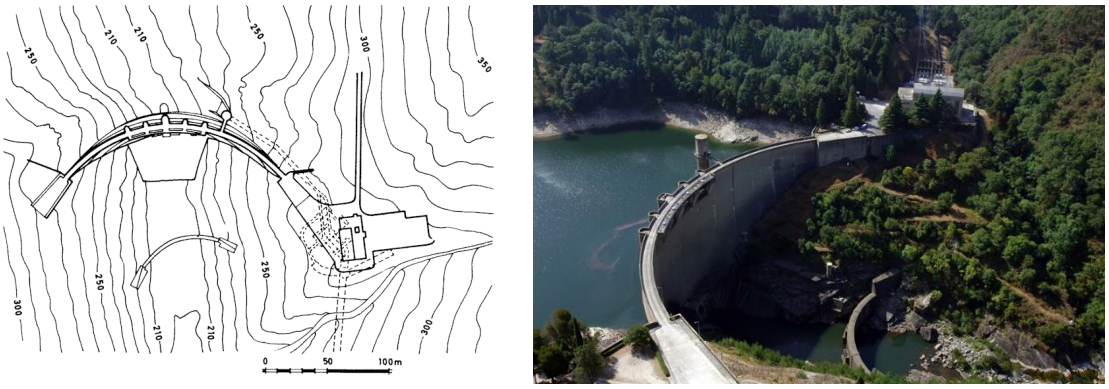

Figure 2.7 – Salamonde dam: plan view (CNPGB); dam's picture (EDP).

The loads to be considered in the design of an arch dam are essentially the same as for gravity dams (deadweight, hydrostatic thrust, uplift pressure, temperature effects, earthquakes, etc). However, the effect of these actions and the way they are accommodated by the structure are much different. The oldest concept of dimensioning an arch dam is simply that the arches must carry the water impulse to its supports, a concept which has led to the admission of a safety criterion mostly focused on the admissible compression stress of the dam's material. In order to guarantee the permanent good behaviour of the dam, compression pressures and tensile stresses must assume values that are relatively low when compared to the respective resistances.

One of the most important criteria to consider in the design of an arch dam is the angle that the resultant of the tensions in the arch extremities makes with the surface of the rock insertion, which should be higher than 30º (Serafim, 1987). Additionally, the angle with the directions of the foundations' main families of fractures must be considered, and studies of the global stability of the dam and its foundation for static and dynamic demands must be performed.

Cabril dam, in Zêzere river, and Alto Lindoso dam, in Lima river, respectively with 136 m and 110 m of maximum height, are two outstanding civil engineering structures and two of the highest Portuguese dams as well. These double arched dams are presented in Figure 2.8.

Figure 2.8 – Arch dams: Cabril dam on the left; Alto Lindoso dam on the right (EDP).

2.2.4. MULTIPLE ARCH DAMS

Finally, a brief mention to multiple arch dams should be made. These are complex structures that result from the combination of buttress dams with arch dams, through the implantation of two or more concrete arches next to each other, which are supported by buttresses located between consecutive arches. An extraordinary example of a multiple arch dam is Aguieira dam, in Mondego river, which is formed by three double-curvature arches and two central buttresses. The buttresses support the central arch, and the lateral arches are supported both by the buttresses and the abutments.

According to (Structurae), Aguieira dam is the second tallest multiple arch dam in the world with 89 meters of height, being second only to Daniel-Johnson dam in Canada, which is 214 meters high. Both these dams are presented in Figure 2.9.

Figure 2.9 – Multiple arch dams: Aguieira dam on the left (EDP) and Daniel-Johnson dam on the right (Gauron et al., 2018).

2.2.5. ROLLER-COMPACTED CONCRETE DAMS

Roller-compacted concrete (RCC) dams present similarities with both conventional concrete gravity dams and embankment dams, also resisting the water thrust with their own weight. In these structures, compacting is achieved through the passing of vibrating cylinders that circulate over concrete layers that are successively placed. RCC dams stem from the intention of combining the material properties of concrete with the speed of execution and the simplicity of concept and adaptability of embankment dams.

This type of dam corresponds to a technology with only a few decades of existence. When compared to embankment dams it presents the advantage of needing less volume of material (Instituto da Água, 2001). On the other hand, there is a larger area available to work, during construction, and a lower risk of concrete shrinkage, when compared to other concrete dams. However, the dependence on vibrating equipment and weather conditions entails a bigger uncertainty linked to the structure execution.

The first Portuguese RCC dam, Pedrogão dam, was inaugurated in 2006. The Pedrogão dam is located in the Guadiana River and was built with the purposes of irrigation and energy production. This dam is presented in the left side of Figure 2.10, while the right side of the figure presents the highest RCC dam in the world, the Gibe III dam, in Ethiopia. With a power capacity of 1870 MW, the Gibe III dam, which was finished in 2018, is the third of five dams planned for this part of the Omo river (Pietrangeli, 2015) and it is 620 meters long and 250 meters high.

Figure 2.10 – Pedrogão dam on the left (EDP); Gibe III dam, in Ethiopia, on the right (Pietrangeli, 2015).

2.2.6. EMBANKMENT DAMS

Embankment dams are generally made of natural resources that are preferably excavated or quarried from nearby sites. The two main types of embankment dams are earthfill dams, made up mostly from compacted earth, and rock fill dams, made up primarily by dumped and compacted rockfill. The previous types may be combined to form a third one composed by one slope of each kind. Both earthfill and rockfill dams will be addressed in the next sections.

Earthfill Dams

As long as adequately designed, earthfill dams may be constituted by a wide range of natural soils. This kind of dams are particularly recommended for sites presenting compressible or very permeable foundations, since the tensions applied to it by the dam's weight are generally low, when compared to other solutions, and on the other hand the path of the water percolated through the foundation is necessarily long. Nonetheless, the referred tensions and the deformations that may develop must be consistent with the foundation resistant capacity, and the percolation intensity must be controlled in order to prevent the occurrence of internal erosion (Instituto da Água, 2001).

Earthfill dams are divided in homogeneous and zoned fill dams, depending on the distribution of the composing materials along the dam's cross section, and they may also present a central nucleus.

In the case of homogeneous fill dams, the entire structure works as a barrier to control the percolation and in the distribution of weight to the foundation. Small sized particle materials such as clays and sandy clays generally compose these dams, however, materials composed by bigger particles like sand and gravel may be used, as long as it results in a tolerable percolation. Figure 2.11 shows the representation of Capinha dam cross-section, an 18 meter high homogeneous fill dam in Fundão, Portugal, which is used for irrigation and water supply.

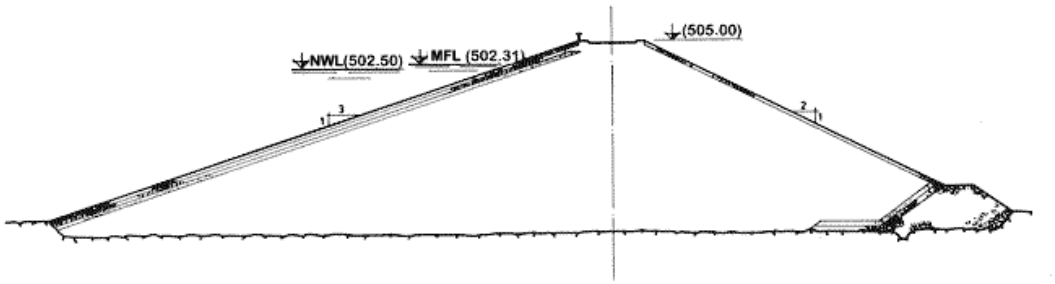

Figure 2.11 – Capinha dam: homogeneous fill dam (CNPGB).

Many different variants of homogeneous fill dams, combining filters and drains, were developed and implemented through the years in order to control percolation and the arising of erosion problems. Even so, many ruptures have occurred, as explained by (Zhang et al., 2009), who analysed the failure of more than 1600 dams worldwide.

Earthfill dams may instead be divided in zones composed by different materials, submitted to different compaction energies and presenting different water content, constituting zoned fill dams. These structures may be composed by several zones and normally present a central core made of a low-permeability material such as clay or concrete. Alijó earthfill dam, in Portugal, whose cross-section is presented in Figure 2.12 is an example of an earthfill dam with a central clay core.

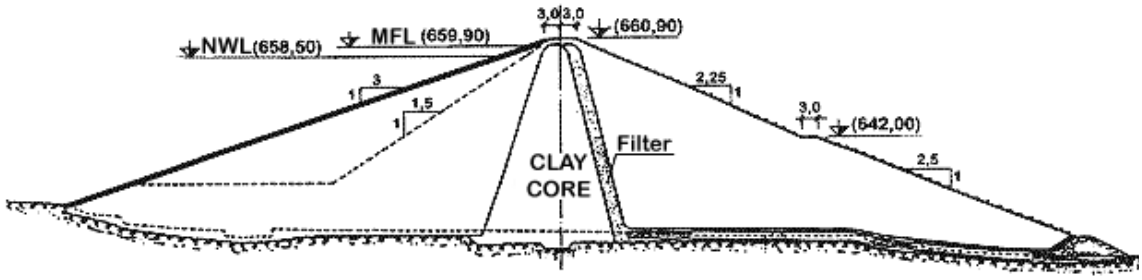

Figure 2.12 – Alijó dam: zoned fill dam (CNPGB).

Sabugal dam, presented in Figure 2.13, is another example of a zoned earthfill dam in Portugal. Completed in 2000, the dam is 58 meters high above the foundation and is used for irrigation, water supply and hydroelectric power generation.

Figure 2.13 – Sabugal dam: zoned fill dam (CNPGB).

Rockfill Dams

Rockfill dams may either have an internal watertight element or an upstream deck. In the case of the former, the element is generally positioned in the central part of the structure and may be of earthfill or, in the absence of suitable soils, of asphaltic concrete. The alternative upstream face membrane or deck can be constructed of reinforced or of asphaltic concrete (Novak et al., 2007). Either way the deck represents a relatively thin layer of the structure. If properly protected and reinforced, rockfill dams have the ability to accept limited overflow of flood water without serious damage.

Rockfill dams are particularly suitable for areas with high precipitation, where landfilling with soils is unwise and in places with good rocky foundations. The major advantages of rockfill as an embankment construction material are high frictional shear strength, allowing the construction of much steeper face slopes than earthfill, and relatively high permeability, eliminating problems associated with pore water pressures. On the other hand, rockfill dams present difficulties of controlling the grading of crushed rock, for instance, from excavations and tunnels, and in the construction and post-construction settlements, which are relatively high. This can result in interface problems where rockfill shoulders are adjacent to a compressible clay core.

Concrete Face Rockfill Dams (CFRDs), which as the name suggests possess a concrete slab working as an impervious layer, can be low-cost and effective alternatives to other rockfill dams and to concrete dams, both in narrow and in wide valleys (Cruz et al., 2009). The design and construction of CFRDs have improved substantially in the last few decades, so the limits of maximum height have been consecutively increasing, and have already exceeded 200 meters in some cases. An example of a CFRD in Portugal, is Paradela dam in Cávado river, presented in Figure 2.14, which was built in 1958 and is 112 meters high (Dams, 1992).

Figure 2.14 – Concrete Face Rockfill dam: Paradela dam (EDP).

2.3. LOADS ON DAMS

Dams are three-dimensional, frequently asymmetrical, structures, founded over non-uniform and anisotropic natural formations, made of materials that may be chemically reactive and present complex physical behaviour. During their lifetime, dams are submitted to a wide range of loads and processes that may be constantly present or arise sporadically. All these peculiarities must be adequately considered so that in all foreseeable circumstances the stability of the dam and foundation is ensured, with stresses contained at acceptable levels, and watertight integrity fully assured (Novak et al., 2007).

The set of loads that may affect the dam-foundation-reservoir system can be classified according to several criteria. Taking into account the proper appreciation of load combination for design purposes, these loads may be divided in primary, secondary and exceptional. The first group is of prime importance to all dams, such as self-weight, water pressure and seepage loads, that may arise under the dam or along discontinuities. The second group includes loads regularly present but of lower intensity or loads that are most important only to some types of dams, as sediments loads or thermal actions, respectively. Hydrodynamic wave loads, or ice loads in extreme conditions, may be included, but are normally not significant. Lastly, a group of exceptional loads, which have a lower probability of occurrence, such as earthquakes and foundation slides (Novak et al., 2007).

A general set of the referred loads is schematically represented in Figure 2.15, applied to a gravity dam.

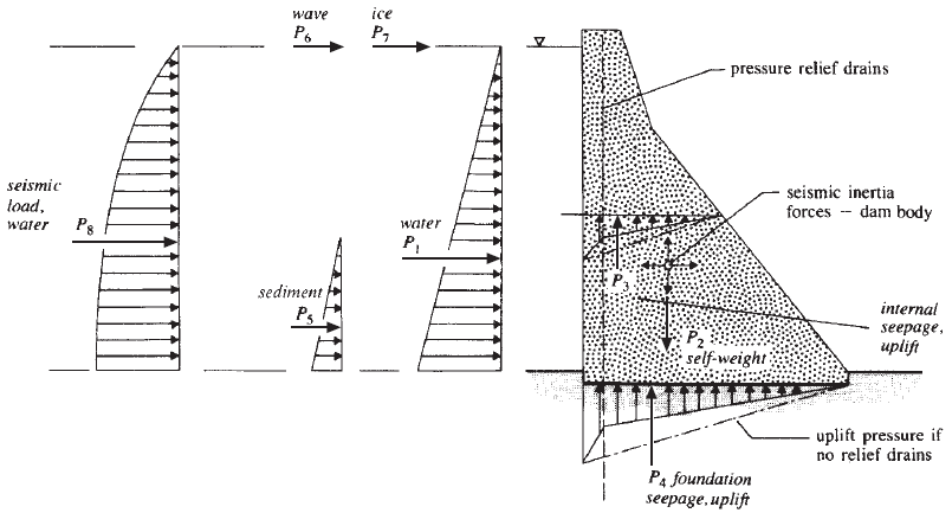

Figure 2.15 – Scheme of loads on a gravity dam profile (Novak et al., 2007).

However, different classifications may also be of good use. On the one hand, water, thermal and seismic actions may be considered external actions, while chemical reactions and thermo-hygrometric variations correspond to internal actions. On the other hand., actions may also be divided as static, such as self-weight and hydrostatic pressure, or dynamic, which is the case of earthquakes and vibrations due to the operation of turbines (Oliveira, 2000).

There are still some actions that occur only, or are most important, during certain periods. During the construction period, it is important to take into account the self-weight of individual blocks, in concrete arch dams, the heat released by the cement hydration in different layers of concrete, in concrete dams, or the pressure of the injections in contraction joints or in the foundation. In turn, during the first filling period, hydrostatic pressure arises on the upstream face of the dam, foundation movements and small-induced earthquakes may occur due to the weight of the water, and a faster cooling of the upstream face of the dam takes place as well.

As stated before, loads related to water are extremely important and may manifest themselves in different ways. Besides the hydrostatic pressures in the upstream face, and sometimes in the lower part of the downstream face, hydrostatic pressures may occur in cracks, in the foundation or in the insertion surface, seismicity may be induced by the reservoir in the case of the existence of faults, chemical reactions may take place, and erosion may develop in the discharge organs, as well as in the dissipation basin. The percolation of water in the foundation may lead to a combined event of internal erosion and chemical reactions in the discontinuities, which may drive to a long term wear. The foundation and dam materials are pervious to a certain extent, and seepage will occur, depending on porosity, cracks and discontinuities of materials. Nonetheless, for lower pervious materials such as concrete, it may take decades to form a stable field of seepage (Chen, 2015).

It is also worth noting that the reservoir exploration, paired with contrasting rainfall levels along the year, imply high variations of water levels in the reservoir that affect the dam-reservoir system dynamic response. When the water level rises, an enormous mass is added to the system, but in the case of arch dams at the same time, the extra water weight on the dam compresses the contraction joints and stiffens the structure.

In turn, in the analysis of the dam's self-weight there are two different scenarios. When analysing the behaviour of the structure in service, the process can be simplified to consider that the distribution of stresses due to self-weight corresponds to the distribution that would occur if all the weight is applied instantaneously in the structure already completely constructed. Nonetheless, the

construction period must also be taken into account. In the case of arch dams, for example, the growth and weight of each individual block should be carefully evaluated.

Temperature is another action that should be considered for the study of different stages in a dam's lifetime. The generation and dissipation of heat through the cement hydration occurs essentially during the construction phase and during the dam's initial life. In the course of the pooring phase, the cooling of a recent layer, connected to a stiffer lower layer in a more advanced cooling state, can cause horizontal stresses that lead to the emergence of vertical cracking. To prevent this outcome, concrete layer thickness must be minimized (Batista, 1998) and cooled aggregates and cement, with low rates of hydration heat generation and good capacity of stress relaxation, are used. On the other hand, during its service time, the dam is submitted to high temperature variations, both daily and annually, which may lead to important elastic deformations (Escuder-Bueno et al., 2013). Yet, the latter only influence a small depth of concrete, and generally does not produce significant structural effects (Oliveira, 2000).

In addition to the physical actions stated before, chemical reactions of an expansive nature, particularly the alkali-aggregate reaction and internal sulfate reaction, may develop between concrete constituents and impair the structure on the long term. For the alkali-aggreagate reactions to occur the aggregates must be potentially reactive, the alkali concentration in the concrete pore solution must be high and the concrete must be exposed to high humidity conditions (Bérubé et al., 2002), which is the case with dams. In turn, the sulfate attack is caused by the reaction of sulfate ions with the cement hydration products, resulting in expansions that can cause cracking and, in extreme cases, may lead to the disintegration of the concrete (Campos et al., 2016). The products that result from these reactions lead to an increase in volume that provoke the rise of the dam's crest and horizontal radial displacements. Although these reactions may start during the dam construction, their consequences may only be detected long after.

Additionally, possible foundation movements due to underground works, geological phenomena or internal landslides induced by the adjustment of the hydraulic balance to the new reservoir should be mentioned.

Finally, some basic issues related to the safety of concrete dams, namely the stability of the structure and the foundation, are presented and discussed in (Amberg, 2015).

2.4. DAM-RESERVOIR-FOUNDATION SYSTEM

Dam, foundation and reservoir constitute a system whose parts strongly influence each other, both statically and dynamically. Even after the structure construction is completed the system static behaviour will fluctuate over time accordingly to the intensity of the static loads acting on it, especially the pressures imposed by the water in the reservoir. In turn, the system dynamic characteristics will also be affected, and alter to match each new global structural scenario. Moreover, the system dam-reservoir-foundation may be submitted to dynamic excitation with many diverse sources: seismic actions with high intensity, or small induced seismicity; wind acting on the dam's upstream face; vibrations due to the operation of energy production turbines; vibrations due to the operation of the dam's overflow units; vibrations due to nearby occurrences such as explosions, traffic or other human activities.

The system dynamic behaviour may also be influenced by auxiliary structures. Besides the frequency associated with the power production turbines, which is commonly identified in the analysis of ambient vibration tests performed on dams, the paper (Mendes & Oliveira, 2009) presents the interference of the intake tower of a hydroelectric development (Figure 2.16) in Portugal, which is connected to the dam by a walkway, on the dam's modal properties.

Figure 2.16 – Cabril arch dam and intake tower (EDP).

The behaviour of the foundation, for instance, is conditioned by the existence of geological joints and faults, which are normally filled with deformable and low resistance materials. During earthquakes, rocky blocks defined by the foundation geological joints may slide and cause both new geological joints and cracks in the dam, which may later generate seepage and internal water pressures, decreasing watertightness and structural performance.

The reservoir foundation behaviour, in turn, is much influenced by the water it contains. During the first filling enormous pressures provoked by the water weight will compress the foundation, which will accommodate the new load and adapt into a new stress condition. This process may induce small seismic actions, originated by internal collapses.

After the reservoir first filling, water levels will continue to vary, in some cases many meters, due to the reservoir exploration and the different rainfall levels over the year. The extra water, and sediments accrued near the dam's upstream face, increase the system mass and the natural frequencies values may largely decrease. Additionally, the extra water may also facilitate the dissipation of energy through the propagation of pressure waves, and alter the system damping values. On the other hand, in the case of arch dams, for instance, contraction joints between concrete blocks tend to close as water level rise, since water compresses the dam from upstream to downstream, increasing the structure stiffness, and thus affecting the system dynamic behaviour. Figure 2.17 presents a picture of Foz Tua arch dam during construction phase, when each concrete block was still working independently, and the block's lateral faces that will work as contraction joints are visible. Joints within each block, between concrete layers, are also important, since it is common the appearance of cracks along the joints, where the tensile resistance is lower.

Figure 2.17 – Foz Tua arch dam contraction joints (EDP).

The direct foundation of the structure is a vital part of the entire system and deformations in any part of the structure foundation may play an important role in its structural integrity. In the case of Beauregard dam in Italy, for instance, movements in the left bank led to important cracks in the dam's downstream face, ending with the rehabilitation of the structure and part of it being demolished (Frigerio & Mazza, 2013).

Finally, it is imperative to mention that as the behaviour of all the parts of the system dam-foundation-reservoir depend on each other, the whole system should be considered when performing numerical studies, that is, to accurately model and study a dam, both reservoir and foundation should be modelled as well. More considerations about this topic are presented in section 2.5.4., where the importance of carefully modelling each part of the system dam-foundation-reservoir is addressed.

2.5. DAM MODELLING

2.5.1. INTRODUCTION

During the first half of the 20th century, the behaviour of dams used to be analysed mostly using physical models scaled to a laboratory compatible size, since available numerical methods were still dependent on considerable simplifications (Oliveira, 2000). Nevertheless, scaled physical models are still being used nowadays to evaluate the global behaviour of dams in terms of dynamic properties, displacements, principal stresses and strains (Altunisik, 2018), to study failure scenarios in concrete dams (Oliveira & Faria, 2006), to study the behaviour of very high arch dams and the interaction between dam, reservoir and foundation when submitted to earthquakes (Wang & Li, 2006) (Wang & Li, 2007), to test the effects of cracking in the dynamic behaviour of a dam (Sevim et al., 2012b) and the ability of methods based in neural networks to detect natural frequencies variations due to cracking (Wang & He, 2007), or to analyse shifts in the dynamic behaviour after repair and strengthening with composite materials (Altunisik et al., 2017), and also to study the interaction between fluid and structure, as an alternative to computational fluid dynamics (CFD) modelling (Savage & Johnson, 2001).

However, from the second half of the last century until our days, two major developments took place: on the one hand, serious progress occurred in the field of structural analysis, with the emergence of new and powerful numerical methods, such as the finite element method, and on the other hand, computational capacity has been extraordinarily increased, allowing researchers and structural designers to take full advantage of the mentioned methods and allowing the implementation of new ones.

Nowadays, there are several computational applications that allow numerical studies based on a great diversity of hypotheses. Thus, in each particular structural analysis, appropriate methods must be used to achieve specific purposes. Different methods may be adequate to model the geometrical and physical characteristics of the structure, as well as its behaviour and the acting loads, while discontinuities, joints or failure mechanisms may be better defined by other approaches. Anyhow, the same problem may be assessed with simpler or more complex models, depending on the problem itself and on the precision required for the analysis. It is up to the user to choose, at any moment, which kind of model suits better the required evaluation.

Simple models are extremely important since they may provide good results with fast and straightforward analyses that may then be taken as a basis for more complex approaches. In these models some simplifying assumptions can be made, such as taking concrete behaviour as linear elastic; do not consider the existence of contraction joints, or take them as closed and behaving linear elastically as well; adopt an elastic foundation, with no mass, which translates as despising its dynamic characteristics; use the Westergaard hypothesis (Westergaard, 1933) to simulate the water dynamic pressure on the dam's upstream wall by means of concentrated masses; or consider damping proportional to mass and stiffness (Mendes, 2010).

On the other hand, after an initial stage when simpler models are used to study the structure, if necessary, more sophisticated models may be developed using different types of methods and elements. These may take into account the possibility of cracks arising in the concrete due to nonlinear behaviour, the use of finite elements to model cracks and joints opening and closing, the consideration of pressure waves both in the reservoir and in the foundation as well as the foundation nonlinear behaviour and slide along joints (Mendes, 2010). It should be considered, though, that more complex models are likely to be more computationally demanding, and more prone to human induced errors, both during the building of the model and during the analysis of the results.

The dynamic interaction between dam, foundation and reservoir is essential for the study of the dynamic behaviour of dams, particularly the importance of the reservoir water level, which may largely influence the values of the structure modal parameters. The rise of water level increases the mass of the system, may increase its stiffness due to the closure of vertical contraction joints, and it implicates a variation in damping as well. In dam-foundation-reservoir systems, energy dissipation occurs through internal mechanisms of deformation of materials, through the formation of cracks and by wave radiation to the foundation and the reservoir. Thus, when modelling a dam, especially when aiming to obtain the structure modal parameters, to prepare an ambient or forced vibration test, or on the contrary, when using results from tests to calibrate numerical models, the reservoir must be properly considered, as it will be detailed in section 2.5.4.

Finally, it is worth mentioning that numerical models of dam's most common purpose is the analysis of the structural integrity of the dam, either at design stage or during condition assessment at operation stage, for which national codes and international guidelines should be followed. A comparison between the applications of different guidelines to the seismic verification of an arch dam using numerical models is presented in (Gunn & Tzenkov, 2015).

2.5.2. Applications of the Finite Element Method (FEM) to the Study of Dams

The finite element method, referenced by (Clough & Wilson, 1999) to have been developed during the early 1950s in the aerospace industry, is nowadays widespread in both industry and academic works, being the most common method used to solve structural mechanics problems, mostly because of its extreme versatility. Though a formulation based on stresses may be used, the classical formulation of this method is based on displacements. Generally, the finite element method consists of dividing a domain in simpler parts, called finite elements. The method fundaments may be found in several classical references such as (Oñate, 2009) and (Zienkiewicz et al., 2014). In addition, a straightforward presentation focused on its application to dams, including a general formulation for dynamic actions, may be found in (Mendes, 2010).

It is worth noticing that this method was first introduced in Portugal by (Pedro, 1977), to analyse the behaviour of dams. It was later applied by (Delgado, 1984) to study the dynamic behaviour of both gravity and arch dams, studying also the interaction between fluid and structure, and by (Cunha, 1990) to obtain the natural frequencies values of two arch dams symmetrical modes (Alto Lindoso and Caldeirão) and to evaluate their response to seismic actions using stochastic methods. The Alto Lindoso seismic performance was also studied by (Faria, 1994), together with the Foz Coa arch dam and the Koyna gravity dam, using damage models.

Nowadays, the use of the finite element method in the numerical modelling of dams is generalized, and numerical models may be used for many different purposes, from the design stage to health condition evaluation or the study of specific mechanisms. To produce good models, able to accurately reproduce the structures behaviour, real in situ information obtained from testing is extremely important. In the context of this thesis, which is focused on dynamic testing and monitoring, special relevance is given to examples of numerical models of dams that were calibrated or updated based on information provided by vibration-based monitoring. This is the case of the works described by (Alves & Hall, 2006), (Bayraktar et al., 2011), (Makha & Moyo, 2012) (Calcina et al., 2014) and (García-Palacios et al., 2016), where modal properties obtained from ambient vibrations tests or from recorded earthquakes are used to compare experimental results with numerical ones and calibrate the numerical models when necessary. A scheme of the model used in the last mentioned work is presented in Figure 2.18.

Experimental data can be used not just to calibrate models, but to validate new approaches as well. This is the case in (Chopra & Wang, 2012), where the response of two arch dams, Mauvoisin arch

dam in Switzerland and Pacoima arch dam in the USA, to ground motions recorded during earthquakes is computed by a linear analysis procedure that includes dam-water-foundation interaction effects, and the computed responses are compared with recorded responses to demonstrate the effectiveness of the analysis procedure.

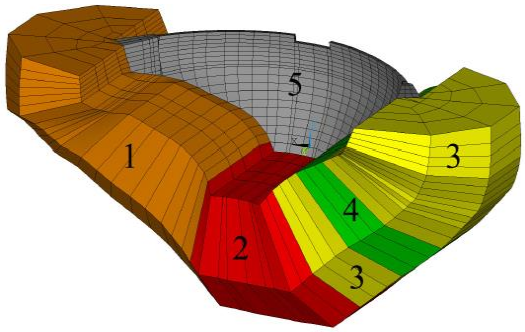

Figure 2.18 – La Tejera dam and foundation finite element model (García-Palacios et al., 2016).

Because of their versatility, besides being used to study dam's global behaviour and response to static and dynamic loads, numerical models based in finite elements methods can also be used to study specific problems and mechanisms. This is the case with the works presented by (Song et al., 2016) and (Zelin et al., 2016), where nonsymmetrical problems, which are common in high arch dams due to both topological and geological conditions at the dams sites, and the impact of interlayer shear zones on the stability of an arch dam, are respectively studied with finite element numerical models.

2.5.3. Applications of the Discrete Element Method (DEM) to the Study of Dams

Though the finite element method is the most common method used in the modelling of dams, the Discrete Element Method (DEM) is worth of a mention as well. This method was first developed in the field of rock mechanics (Cundall, 1971), and is therefore quite suitable for the study of the discontinuous nature of rock, which may include fluid flow through the discontinuities. The method was used by (Lemos, 1987) in the dynamic analysis of jointed rock and some of its first applications to engineering problems were described by (Pande et al., 1990). In turn, (Williams & Pentland, 1992), (Bićanić, 2004) and (Bobet et al., 2009) presented works revising the methods and their application.

Comparing the discrete element method to the finite element method, previously addressed, it is noteworthy that in the case of DEM, materials are represented by a discontinuous particle structure without any need of a mesh, being the infinite number of material points of the continuum replaced by a finite number of particles of finite extent that interact through collisions with each other (Santasusana, 2012), that is, elements representing physical objects.

The term *discrete element method* is generally associated with the definition presented by (Cundall, 1989) which refers to any computational modelling framework that allows finite displacements and rotations of discrete bodies and that allows new contacts automatically (Bićanić, 2004). Different numerical approaches are used to calculate the motion of a large number of elements, ranging from molecules to particles like grains of sand, or bigger elements like concrete blocks. Particles and blocks are the discrete elements most commonly used in civil engineering.

Being especially suited for the field of rock mechanics, the discrete element method may be used to study the foundation of large structures such as dams, and it has been widely used with masonry structures as well. For instance, a numerical model for analysis of masonry gravity dams based on the discrete element method is presented in (Bretas et al., 2014), where the dam and rock foundation are represented as block assemblies. Additionally, in (Lemos & Antunes, 2011), the method is used to study foundation failure scenarios using as examples Alto Ceira and Baixo Sabor arch dams.

Block type discrete elements may be rigid or deformable. The latter may be combined with finite elements to generate hybrid models that take advantage of parts of both methods. A method combining discrete and finite elements, aiming the resolution of problems involving static and dynamic behaviour of systems containing a large number of solid deformable bodies, is addressed in (Munjiza, 2004). Additionally, a DEM/FEM coupling algorithm has been presented by (Azevedo & Lemos, 2006) for fracture analysis, which enables the use of rigid circular particles only on the fracture processes, being the remaining part of the structure modelled with finite elements. A combination of the two methods is used as well in (Lemos et al., 2008), where vertical blocks are modelled using the DEM, allowing the consideration of contraction joints between the blocks, which are discretized using the FEM.

2.5.4. DAM-RESERVOIR-FOUNDATION INTERACTION

Dam-reservoir-foundation interaction resumes a series of physical processes and mechanisms that alter dam's behaviour due to the dependency of the structure to the physical environment in which

it is inserted. Thus, to correctly model the behaviour of a dam, it is important to study how the parts of this system interact between each other and how relevant they are to the whole in different analysis scenarios. For this purpose, finite elements, discrete elements, boundary elements or hybrid methods may be used, and the numerical results may be complemented and validated by physical models.

Modal identification is also an important tool to better understand the integrated behaviour of the system's parts since it provides the opportunity of evaluating how their interaction influences the modal parameters. This is the case of the work developed in (Mendes & Oliveira, 2007), where the dynamic interaction between water and structure is studied with a physical model of a tank wall, which is filled with water at different levels and submitted to ambient and hammer excitation. A 2D finite element model of the tank was built and the water pressure was considered by two different processes: i) using Westergaard added water masses; ii) using water finite elements. Natural frequencies were obtained for both numerical models considering the same water levels used for the physical model. In Figure 2.19 experimental and numerical results of the structure first mode natural frequency for the studied set of water levels are compared. The authors concluded that both added water masses and water finite elements formulations presented a good agreement with the experimental results. Furthermore, since the numerical models were built using a concrete Young's modulus obtained from ultrasonic tests, it was concluded as well that this is a reliable way of estimating this parameter.

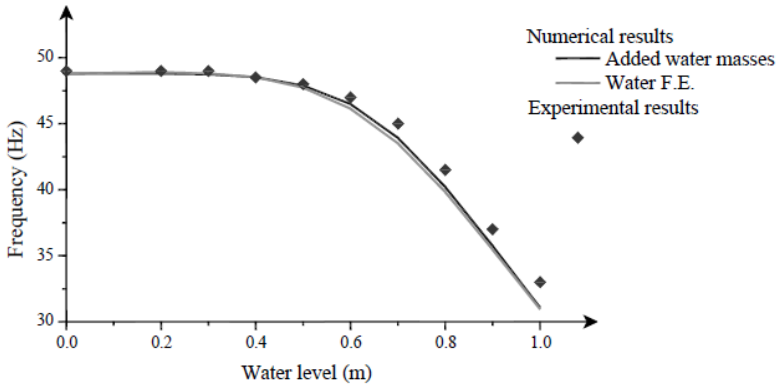

Figure 2.19 – Comparison between numerical and test results (Mendes & Oliveira, 2007).

Reservoir effects on the dam are more commonly studied for arch dams, since the structures greater flexibility, when compared to gravity dams for instance, makes it more dependent on the reservoir level. In (García et al., 2014) an analysis of the influence that reservoir levels and bottom sediment

properties have on the dynamic response of arch dams is carried out. Also in (Akkose et al., 2008) the effects of reservoir water level on nonlinear dynamic response of arch dams are investigated.

In arch dams, concrete blocks are separated by vertical contraction joints that may move relatively to each other during major external events, such as earthquakes, resulting in opening and closing movements and eventually on the development of shear movements at the joint surfaces. In (Lau et al., 1998) a concrete arch dam finite element model was developed considering contraction joints and submitted to an earthquake in order to demonstrate the capability of a proposed joint model. The results show that joint movement can have significant effects on the response of an arch dam.

In (Lemos, 2008) the influence of contraction joints in the dynamic behaviour of Cabril arch dam was studied. Two different models were built, the first one considering a linear elastic behaviour of the dam and the second one taking into account the effect of contraction joints. These models were then compared with each other in many water level scenarios, simulated with Westergaard masses. Additionally, both rigid supports and an elastic foundation were considered. Finally, the natural frequencies obtained with the models considering all these hypotheses were compared to results from ambient and forced vibration tests, which helped to validate the models. Similar work is presented in (Hamidian et al., 2013) which uses a finite element model to study the seismic response of Morrow Point dam for different reservoir and support conditions, and compares its results to those obtained in (Tan & Chopra, 1996) for the same dam.

Since earthquakes are capable of releasing huge amounts of energy and provoking massive damage to structures, their evaluation is extremely important. In (Alembagheri & Ghaemian, 2013) the seismic damage of concrete dams was investigated by applying the Incremental Dynamic Analysis method to the Morrow Point arch dam, which was modeled using finite-elements. The dam's interaction with the reservoir and foundation was considered and for the effects resulting from the foundation flexibility two scenarios were equated, the first considering the ratio between the dam's concrete Young's modulus and the foundation rock Young's modulus equal to one, and in the second case considering this ratio equal to 0.5.

Several key issues regarding the seismic safety evaluation of high concrete dams, such as cracking and the opening of contraction joints, are addressed in (Zhang, 2013) through a case study, with finite elements models based on different foundation characteristics. Collapse scenarios in numerical arch dams models, backed up by reduced scale models of Alto Lindoso and Alqueva dam, are simulated in (Oliveira & Faria, 2006). In the first case concrete strength was gradually

reduced until failure, and in the second one a relative displacement was prescribed on a foundation fault.

The references mentioned in this subchapter are meant, on the one hand, to expose the complexity of modelling dam-reservoir-interaction and, on the other, to alert for the many specific points that may influence such interaction and should thus be taken into account when numerically modelling dams and their surroundings. In this sense, it is worth mentioning the set of works presented in (Goldgruber, 2014), "Theme A – Fluid Structure Interaction: Arch Dam – Reservoir at Seismic Loading", where an artificially generated symmetric arch dam is modelled by 11 different teams, from different countries, using the same geometry and boundary conditions but different modelling techniques and tools. The comparison of the results obtained by all the participants show that despite all the constraints imposed by the problem formulation to assure base similarity and that the results across participants could be compared, still significant differences are found between solutions. Therefore, it is important to keep in mind that numerical simulations, though extremely useful, should be performed carefully, in order to prevent human induced errors, and their results should be treated critically. Additionally, whenever possible, the analyst should seek validation for the results obtained from numerical simulations, either through comparing them to a reference solution from a former comparable project, or through experimental data obtained from tests performed in situ.

Finally, the numerical model of Baixo Sabor arch dam developed at the Portuguese National Laboratory for Civil Engineering (LNEC), which is used in Chapter 6 to simulate damages in the structure and study their effect on modal properties, should be mentioned. The model was built with 3DEC (Itasca, 2017), a discrete element code widely used in the field of rock mechanics that allows the consideration of deformable blocks, which are discretized into an internal finite element mesh (Lemos et al, 2019). The dam model has 32 cantilever blocks separated by vertical contraction joints that were discretized into 20-node brick elements, the hydrodynamic interaction is modelled through the consideration of Westergaard added masses and a simplified representation of the foundation rock mass was used. More details on this numerical model are presented in section 6.3.2.

2.6. FINAL CONSIDERATIONS

Dams and reservoirs have always played an important role in the development of human societies, which keeps occurring to this day, ensuring an adequate supply of water, for agriculture and for population's consumption, by storing it in times of surplus and releasing it in times of scarcity, working as well in the mitigation of the effects of floods. More recently, dam's reservoirs have been used for navigation, sedimentation control, recreation, fish farming and hydroelectric power production. In addition, modern dams are often used as multipurpose structures, serving populations directly and at the same time aiding in the production of energy.

Most commonly, dams are either built with concrete, earth, rocks or masonry, but there are examples of structures where more than one these are used. This thesis will focus on concrete dams which, depending on the characteristics of the site where the structure will be inserted and in the characteristics of the development to be constructed, may assume many different typologies, from gravity to buttress, arch or even multiple arch dams, with the possibility of hybrid solutions to arise.

During their life span dams are submitted to many different types of loads. Some of these are continuous, such as the self-weight of the structure and the hydrodynamic pressure of the reservoir, some other present seasonal and daily variation patterns, which is the case of the environmental thermal wave and the exploration of water from the reservoir, and finally major actions such as earthquakes may occur only from time to time. The combination of all these actions with time deterioration may lead to a loss in safety and operation conditions that must be fought with maintenance based on continuous monitoring programs.

The monitoring of a structure may be based on inspections, the recording of data from several devices and imbedded sensors or the performance of tests, and may be supported by the construction of models, that can be used to study its behaviour. Though they are still used today, physical scaled models of dams were more common in the past, whereas nowadays the modelling of dams is mostly based on numerical methods. The finite element methods is widely used in the numerical modelling of structures in general, and dams in particular, but the discrete element method deserves to be mentioned in this context as well, for its adequacy to the field of rock mechanics, being thus particularly suited for the study of dam's foundations and fracture scenarios.

In the next chapter, the dynamic testing of dams is addressed with special emphasis to operational modal analysis and input-output modal identification methods.

3. OPERATIONAL MODAL ANALYSIS TOOLS FOR DAMS

3.1. INTRODUCTION

Ageing and deterioration of structures have encouraged the development of accurate vibration-based damage detection techniques supported by structural health monitoring systems (Cunha & Caetano, 2006) that may play a fundamental role in the management of maintenance programs for civil engineering structures, increasing their durability, safety and operation standards . This is possible because of the emergence of new transducers and analog-to-digital converters that brought the possibility of identifying the structures modal properties without using any other excitation than that provoked by ambient and operational conditions.

In this context, operational modal analysis and its application to civil engineering structures in general, and more specifically to dams, are addressed in the first part of the present chapter, after a brief introduction to experimental modal analysis and forced vibration tests, which represent the procedures still most commonly used to obtain the dynamic properties of dams. Then, the chapter focuses on the presentation of a group of well-established output-only methods working in both time and frequency domain, which are used to identify the dynamic properties of structures and on the application of such methods to time series recorded in a concrete arch dam.

Finally, the importance of quantifying and minimizing the uncertainty associated with modal parameters estimates is addressed and tools to accomplish it are described.

3.2. EXPERIMENTAL MODAL ANALYSIS BASED ON FORCED VIBRATION TESTS

Periodic structural-condition monitoring of structures is necessary to ensure their continuous service in safe conditions. It is common for condition assessment to rely on visual inspections which, though very important and useful since in situ insights are obtained, present some limitations as well: (1) concealed and inaccessible parts of the structure are difficult, if not impossible, to inspect; (2) the quality of the inspection process is often dependent on the inspection personnel's experience and knowledge; (3) results from one area of a structure does not necessarily represent conditions at another, thus broad inspections are needed to produce a good representation of the global structural condition. These constraints imply that the process is time consuming, labour-intensive and may be expensive (Salawu & Williams, 1995). In this sense, visual inspection programs should be complemented with structural assessment using global indexes, which allow distresses or integrity losses to be detected by measuring global parameters at a few easily accessible points. Global indexes such as the dynamic properties of the structure can be achieved with vibration testing and modal analysis.

In this context, Experimental Modal Analysis (EMA), the experimental identification of modal parameters, which is a subject that has been long studied, should now be introduced. It was first explored by mechanical engineering with the aim of estimating modal frequencies, damping ratios and mode shapes of small laboratory sized structures, and is nowadays widespread trough many different areas from aerospace to civil engineering, and more recently it has even been used in the field of dental implant prostheses (Suzuki et al., 2019). These tests consist on the application of a known input force to the structure and on measuring its reaction (output), thus becoming usually known as input-output methods. EMA is currently a well-established field founded on solid theoretical bases extensively documented in reference books, such as (Heylen et al., 2007), (Ewins, 2000) or (Maia & Silva, 1997).

These techniques have been applied to civil engineering structures like bridges, dams and buildings through the performance of forced vibration tests. These tests consist essentially of applying controlled excitation at one or more points of a structure and in measuring the response at various points. Since the excitation forces are known, it becomes possible to evaluate Frequency Response Functions (FRF) that relate the measured responses with the applied forces. Later, modal identification is performed based on these functions.

In small and medium-sized structures, the excitation can be induced by an impulse hammer, which as the advantage of providing a wide-band input that is able to stimulate different modes of vibration. However, the relatively low frequency resolution of the spectral estimates (due to the short time series), can preclude the accurate estimation of modal damping factors, and the lack of energy provided by the input may prevent the excitation of some relevant modes of vibration. Therefore, the equipment must suit the structure for the excitation to be adequate to activate all the vibration modes and produce good results. Forced vibration tests performed in large-sized structures, for instance, require the use of suitable equipment such as servo-hydraulic shakers, electro-dynamic shakers, or eccentric mass vibrators, such as those represented in Figure 3.1 (Cunha & Caetano, 2006). The excitation forces that are used may present impulsive, harmonic, or white noise characteristics over a given frequency range (Rodrigues, 2004).

Figure 3.1 - a) Eccentric Mass Vibrator (FEUP); b) Horizontal electro-hydraulic shaker (EMPA).

Forced vibration tests produce accurate and reliable results providing useful information about the structures dynamic behaviour, which can be used for comparison with previous tests or as benchmark for comparison with future tests. It can be used as well to validate design assumptions relative to the structure, to tune and update numerical models, to analyse solutions for vibration control and to design continuous vibration-based monitoring systems for structural health monitoring.

However, a few drawbacks related with the performance of forced vibration tests should be mentioned as well. As it was addressed before, in the case of large-sized structures the equipment used to excite the structure is usually of large dimensions and weight, so its transportation and operation may be expensive and arduous. For this reason, their execution may occur only from time to time, thus not allowing a regular prospection of the dynamic characteristics of a structure,

meaning they are not suited for continuous monitoring. Additionally, when the excitation equipment is operating on a bridge or on a dam's crest it implies the interruption of the road traffic during the test, and the levels of excitation used do not necessarily correspond to operation conditions.

These were the first type of field tests conducted on dams with the aim of understanding their dynamic behaviour, and help as well for the validation and calibration of numerical models. In Portugal, there is much work done in this field, essentially due to the activity developed by the National Laboratory of Civil Engineering (LNEC) since the beginning of the second half of the XX century, until our days. With the aim of characterizing the dynamic behaviour of some Portuguese large dams with higher potential risk, many forced vibration tests have been performed. Examples of tested structures are Aguieira, Alto Lindoso, Crestuma, Cabril, Alto Ceira and Alqueva dams. Some of these works are documented by (A. Portugal, 1990), (A. C. Portugal & Caetano, 1992), (Câmara et al., 1993), (Pina & Gomes, 1996), as cited by (P. Mendes, 2010). More recently, several forced vibration tests are being performed by LNEC in the context of new dams construction or of repowering operations, as is the case of Baixo Sabor dam, as documented in (J. P. Gomes & J. V. d. Lemos, 2016). At international level, there are also some references about forced vibration tests performed on dams as, for instance, those conducted by (Abdel-Ghaffar & Scott, 1981) on an earth dam in California, the series of tests performed by (Ellis & Jeary, 1984) both on concrete and rock-fill dams in England, and the tests performed by (Paultre et al., 2002) on a concrete gravity dam in Canada to evaluate the effects of ice cover on the dam's dynamic behaviour. A review on this topic may be found in (Bukenya et al., 2014).

3.3. OPERATIONAL MODAL ANALYSIS BASED ON AMBIENT VIBRATION TESTS

Technological developments allowed for lower vibration levels to be measured, thus opening a window for ambient vibration tests, and the development of identification methods requiring only the measurement of the structure response, to gain relevance. These tests, also known as output-only tests, rely on ambient and operational excitation, like the wind, small earthquakes or traffic circulating over or nearby the structure, hence revealing to be practical and economical to perform. Since no artificially induced input is needed, the test may be conducted maintaining the structure under operation and consequently this process is usually called Operational Modal Analysis (OMA). Therefore, as modal information is derived from structural responses while the structure is in operational conditions, in case of existence of non-linear behaviour, the obtained results are associated with realistic levels of vibration (Magalhães, 2010). Additionally, OMA's characteristics make it suitable for continuous vibration-based health monitoring as well as for damage detection.

Nevertheless, there are some disadvantages associated with ambient vibration tests when compared to forced vibration tests. For instance, the lower levels of excitation require very sensitive sensors and high resolution digitizers to be used and much lower signal to noise ratios should be expected. Also, the modal mass is not estimated, that is the mode shapes are not scaled in an absolute way, and the frequency content of the excitation (idealized as a white noise) may not cover the whole spectrum of interest, especially in the case of very stiff structures with high natural frequencies (Magalhães & Cunha, 2011).

Still, nowadays, operational modal analysis represents a robust and trustworthy alternative to experimental modal analysis and it is widely implemented in several engineering domains. OMA has been successfully applied to several different types of civil engineering structures such as cable-stayed bridges (Cunha et al., 2001), suspension bridges (Brownjohn et al., 2010), footbridges (Wei-Hua, 2012), viaducts (Magalhães, Caetano, et al., 2012), stadia roofs (Magalhães, Caetano, et al., 2008), dams (P. Mendes, 2010), buildings (Shi et al., 2012), towers (Gentile et al., 2014), wind turbines (G. Oliveira, 2016) and nuclear power plants (Nour et al., 2016). OMA has been also applied in mechanical engineering to study the dynamic behaviour of helicopters (Bart Peeters et al., 2007), commercial aircrafts (Hermans & Van Der Auweraer, 1999) and aerospace vehicles (Goursat et al., 2011).

3.4. APPLICATION OF OMA TO DAMS

When compared to other structures, such as bridges, buildings or wind turbines, concrete dams are much more massive and stiff, thus presenting lower levels of vibration. However, as it was already mentioned in this chapter, the remarkable technological progress on high sensitivity low-noise accelerometers and very high resolution digitizers that occurred during the past few decades, allied with the evolution on the accuracy level provided by different types of time or frequency-domain modal identification techniques, strengthens the perspective of applying OMA to dams with good results.

OMA relies on operational and ambient induced vibrations, which in the case of dams may be due to turbines operation, outflow, nearby or crest traffic, wind, small earthquakes or to the dynamic interaction between dam and reservoir. However, since most dams are situated in remote locations, traffic induced vibrations are sporadic, leaving the structure essential excitation to the turbines operation of the power plant, if existent, which may produce relevant vibration levels on dams if the power plant is located nearby the structure. However, when the turbines are not operating the vibration levels measured on dams are very low. An example is presented in Figure 3.2, where the effective accelerations measured on Baixo Sabor arch dam during five days are presented. During most of the first three days presented, the turbines are not operating (if not for a short period during the 24th of December) and vibration levels are about ten times lower than those measured when the turbines are operating, as occurred between the 26th and 28th of December. Even so, the highest effective vibration level registered during this period was inferior to 15 micro g. This level of vibration turns the identification process into a challenge, complicating it and sometimes even precluding the complete modal identification.

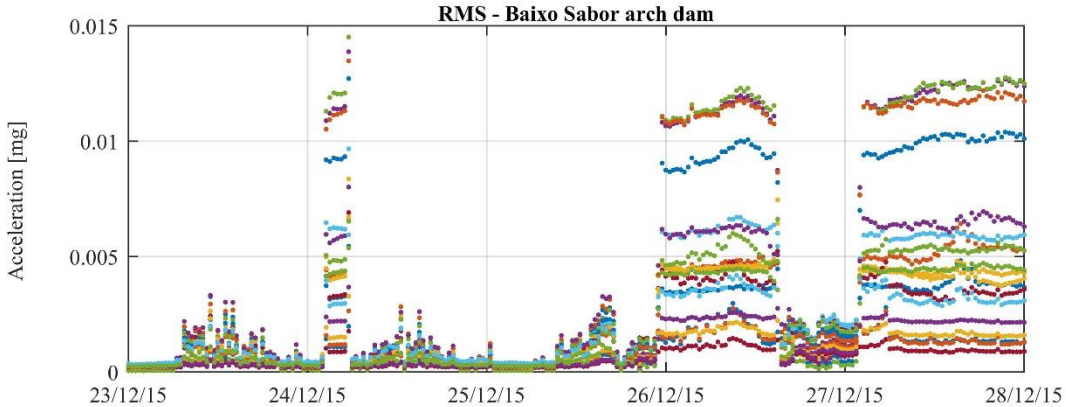

Figure 3.2 – Vibration levels at Baixo Sabor arch dam.

On the other hand, despite playing a major role on inducing vibrations, operational conditions may at the same time disturb the modal identification process and motivate the appearance of delicate challenges, since turbine operation may produce harmonics with frequencies close to those of the structure natural vibration modes making it harder to accurately identify those modes.

In turn, ambient conditions, as temperature or reservoir level variations during the year, may significantly change the natural frequencies values, making it imperative to correct the modal identification outcome by means of statistical methods. Studies about the effect of the water level on the dam dynamic properties were performed by Proulx et al. (2001) on Emosson arch dam, in France's border with Switzerland. Forced vibration and ambient vibration tests were executed in different times of the year, with very different reservoir levels, to access its effect on the dam natural frequencies and then build a model that relates the two variables. Identical work is presented by (P. Mendes et al., 2007) with tests executed in Cabril dam in Portugal and, more recently, by (Calcina et al., 2014) with tests performed in Punta Gennarta dam in Italy. A comparison between the effect of empty and full reservoir on natural frequencies and damping ratios was also executed by (A. C. Altunişik et al., 2016) on a dam model.

As it was already mentioned in this chapter, forced vibration tests are not suitable for continuous health monitoring because these tests can only be performed from time to time. Contrarily, OMA's characteristics are particularly convenient for this purpose since once a monitoring system is installed it can provide continuous results automatically. A system of this type was installed in Baixo Sabor arch dam, in Portugal, as described in (Pereira et al., 2018), and in chapter 6.

Nonetheless, OMA can be applied to dams with other purposes. For instance, the results obtained from the execution of ambient vibration tests are especially helpful for the calibration of numerical models, both to update existing models and to improve the future creation of new models. Results of ambient vibration tests have been compared to those of numerical models, and permitted the upgrading of the referred models, in works developed for instance by (B. Sevim et al., 2012a) about Berke arch dam, in Turkey, and more recently by (García-Palacios et al., 2016) about La Tejera arch dam, in Spain. Another interesting work of the application of OMA to dams was developed by (Yang et al., 2017) presenting the identification of modal characteristics of an arch dam situated in south-western China. In this case, the modal analysis was not based on ambient vibration tests but on earthquake response records, thus producing results important to earthquake design, since the structure is analysed when submitted to real earthquake scenarios. A group of ambient vibration tests performed in six Portuguese concrete dams is described in chapter 4 of this thesis.

3.5. OUTPUT-ONLY IDENTIFICATION METHODS

In this section it is presented an overview of the output-only algorithms implemented in Matlab (Mathworks, 2016) and used in this work, some of which were also integrated in the dynamic monitoring systems described in chapters 6 and 7. The Peak Picking method (PP), the Enhanced Frequency Domain Decomposition method (EFDD), the Covariance driven Stochastic Subspace Identification method (SSI-Cov) and the poly-reference Least Squares Complex Frequency Domain method (p-LSCF) constitute the group of output-only identification methods addressed in the following subsections. Most of these identification methods, and some other that are not mentioned in this work, are described in (Carlo Rainieri & Fabbrocino, 2014), as well as some background theory that helps understanding both the mathematical and the physical part of the identification problem.

After each algorithm is explained, an example of application is presented. The examples involve the identification of natural frequencies and modal damping ratios as well as the determination of mode shapes. All the examples are based on a set of acceleration time series measured by the 12 accelerometers of the Baixo Sabor arch dam dynamic monitoring system situated in the upper visit gallery (see Figure 6.8), which are presented in Figure 3.3. These time series were measured simultaneously, while the structure was only excited by ambient vibration, thus with accelerations generally inferior to 0.02 mg. The time series were previously submitted to a pre-processing that includes a decimation from 50 to 25 Hz and the application of high-pass filters with a cut-off frequency of 1.0 Hz. Although a higher number of vibration modes could be identified, only the first four vibration modes will be discussed in these examples.

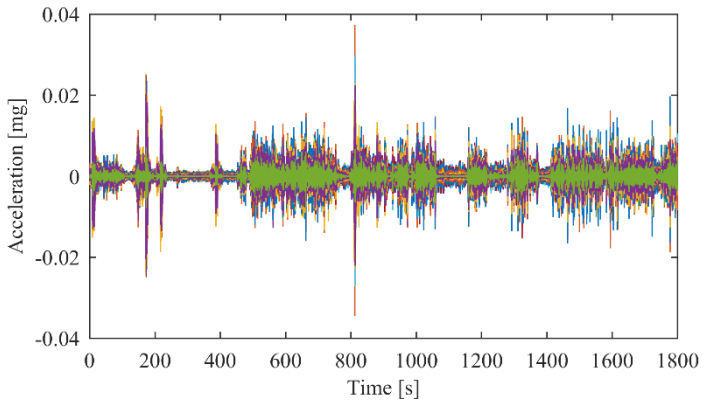

Figure 3.3 – Time series of accelerations measured by the Baixo Sabor arch dam monitoring system.

3.5.1. PEAK PICKING

The peak picking is a simple and straightforward identification method, and the first one developed to perform the dynamic identification of structures based on their responses to ambient vibration. It is still commonly used for an initial assessment of the data, since it can quickly provide good results. Though some previous works had already been developed, Bendat and Piersol (Bendat & Piersol, 1980) are considered responsible for the current methodology.

This method consists on the analysis of the structure response in the frequency domain. For a structure excited by a white noise, the output spectrum only depends on the system transfer function, since the input spectrum is constant:

$$S_{yy}(\omega) = H(\omega) \, . S_{uu} \, . H(\omega)^H \tag{3.1}$$

With:

S_{yy}	Output spectrum
H	Transfer function
S_{uu}	Input spectrum
$*^H$	Complex conjugate transpose

The output spectrum presents local maxima (*peaks*) at the damped frequencies of the structure. If the structure damping is low, as it generally is in civil engineering structures, the damped frequencies constitute a proper estimation of the structural frequencies. The relationship between the damped and structural frequencies is defined by:

$$\omega_n(\omega) = \frac{\omega_{d_n}}{\sqrt{1 - \xi_n^2}} \tag{3.2}$$

With:

ω_{n}	Natural frequency
ω_{d_n}	Damped frequency
ξ_n	Damping ratio

In this way, an output spectrum must be estimated for each degree-of-freedom. Next, the procedure defined by Felber (Felber, 1993) may be used to construct an averaged normalized power spectrum density function (ANPSD), that contains the information of all spectra:

$$ANPSD(\omega) = \frac{1}{l}\sum_{i=1}^{l} NPSD_i(\omega) \tag{3.3}$$

$$NPSD(\omega) = \frac{PSD_i(\omega)}{\sum_{k=1}^{N} PSD(\omega_k)} \tag{3.4}$$

With:

l	Number of measured degrees-of-freedom
NPSD	Normalized power spectrum density
N	Number of points of discretization of the spectrum

Then, the values of the natural frequencies of the vibration modes may be identified analyzing the ANPSD's peaks. In turn, the calculation of modal damping can be computed through the half-power method (Clough & Penzien, 1995), even though it is widely connoted with lack of accuracy. Lastly, for the determination of the mode shapes, a reference degree-of-freedom must be defined. The modal components associated with the other degrees-of-freedom (i) are defined in relation to the reference one (ref). The configuration of the mode shape with angular frequency ω is defined by the transfer function:

$$T_{i,ref} = \frac{S_y(\omega)_{i,ref}}{S_y(\omega)_{ref,ref}} \tag{3.5}$$

After the estimation of the T functions, it is possible to obtain the amplitude and phase of the mode shapes for every instrumented degree-of-freedom of each vibration mode.

The Peak Picking method is characterized by its simplicity and swiftness. However, it presents some drawbacks, such as leading to inaccurate results if the modes are not well separated, and not being suitable for the estimation of damping ratios. An application example is presented hereafter.

Application Example

The Peak Picking method was applied to a set of acceleration time series obtained with the dynamic monitoring system installed in Baixo Sabor dam, as mentioned before. During the selected setup, with 30 minutes of duration, the structure was loaded only by ambient excitation.

The output spectrum was computed with segments of 8192 points and an overlapping of 50%. The averaged normalized spectrum obtained is presented in Figure 3.4 – a), from 2 to 5 Hz, interval that contains the natural frequencies of the first four modes. The four peaks are easily distinguishable and were highlighted with black circles.

In Figure 3.4 – b) an averaged normalized spectrum from a different setup is presented with the aim of showing the effect of the operating conditions on the identification process. In this case, a well-defined, very sharp peak appears above most of the modes peaks. Its frequency corresponds exactly to the frequency of the power plant turbines rotation frequency. Even though the harmonic itself is quickly identifiable, because of its characteristic shape, its position may interfere with the identification of a mode's peak, when both frequencies coincide. Additionally, the peaks on the second setup are shifted to the left, when compared to the peaks on the first one, due to operational and environmental factors affecting the values of natural frequencies.

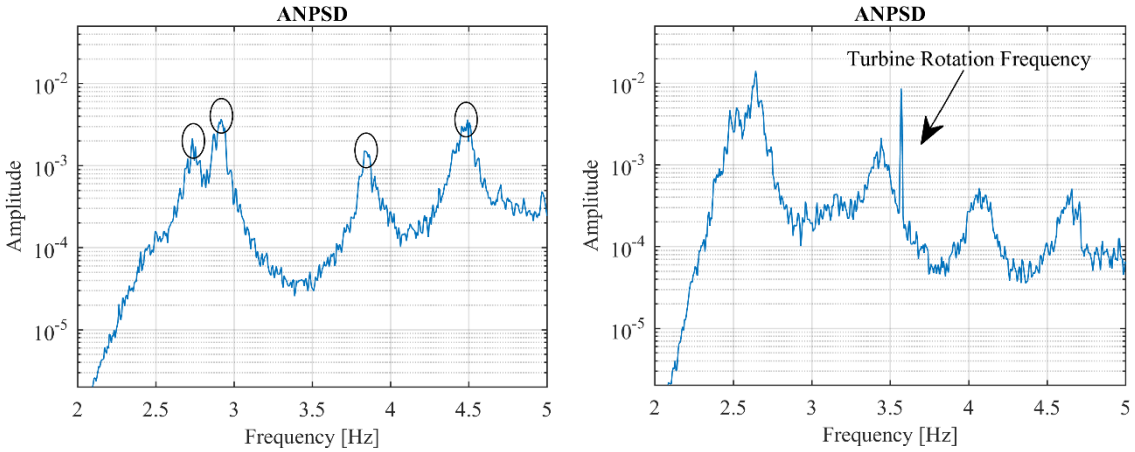

Figure 3.4 – Averaged normalized spectrum: a) ambient vibration only; b) turbines operating.

The frequencies of the vibration modes identified through the evaluation of the four peaks highlighted in Figure 3.4 – a) are presented in Table 3.1.

Table 3.1 – Natural frequencies obtained with the Peak Picking method

Mode	Peak Picking
	Identified Frequencies [Hz]
1	2.734
2	2.917
3	3.845
4	4.492

The transfer functions T were then computed with equation (3.5) and from them the mode shapes were obtained. Modal configurations of the four vibration modes are presented in Figure 3.5, with a 2D visualization. Blue dots correspond to the position of accelerometers, hence their values were obtained through the amplitude and phase of the transfer functions, while the blue lines were achieved by interpolation, with Matlab function *spline* (Mathworks, 2016).

As shown by Figure 3.5, the configurations of the first and third modes are symmetric and the configurations of the second and fourth modes are antisymmetric. The central part of the figure is blank in all the cases, since the dam's spillway prevented the installation of accelerometers in that area. In this application example, modal damping ratios were not calculated since the results produced by the half-power method are often associated with gross errors.

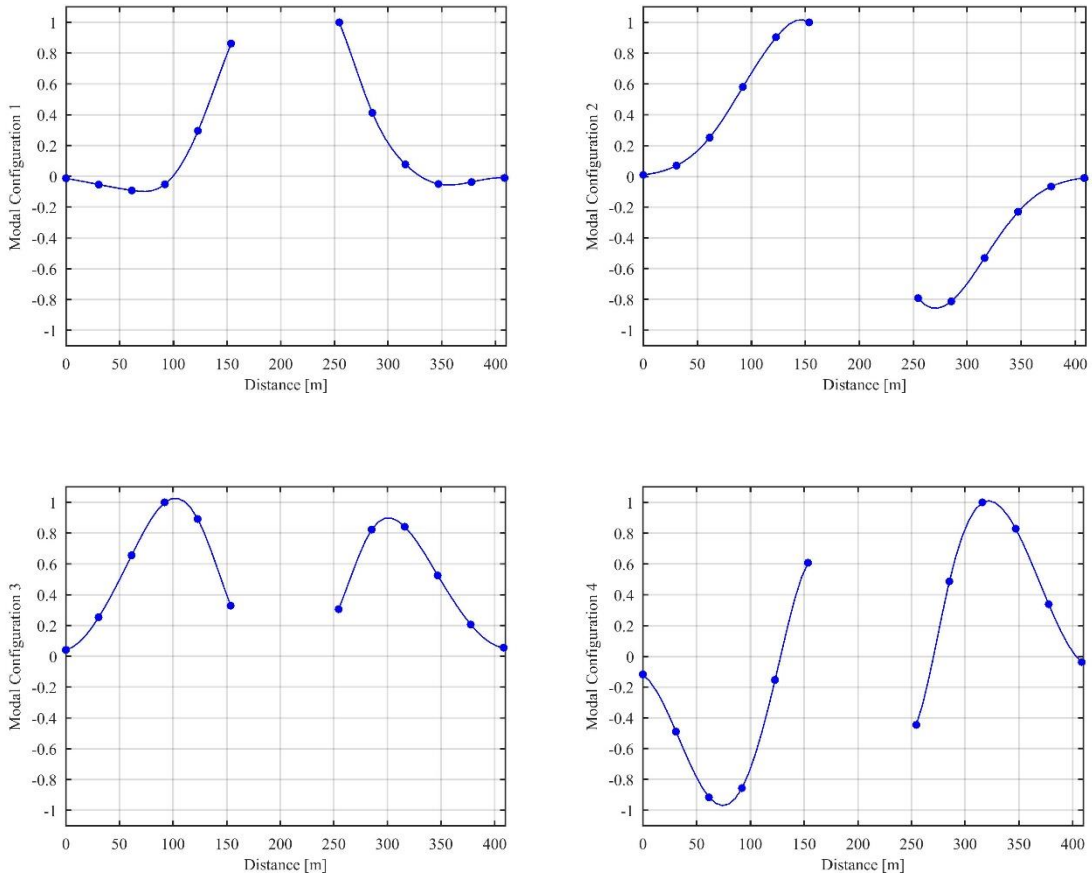

Figure 3.5 – Modal configurations obtained with Peak Picking.

3.5.2. EFDD

The Frequency Domain Decomposition method (FDD) was proposed by Brincker et al. (Brincker et al., 2000) for the dynamic identification of structures and represents an evolution of the Peak Picking method. The FDD is also a non-parametric method in the frequency domain; however, it makes possible the identification of closely spaced modes and it allows much more accurate estimation of the modal damping ratios.

In order to achieve good results with this method, it is referred by (Brincker et al., 2000) the need of a white noise excitation and a lightly damped structure, whose closely spaced modes should have geometrically orthogonal mode shapes. Nonetheless, if these assumptions are not fulfilled, this method can still be applied and, in most cases, the produced results, although approximate, will still be better than those obtained with PP.

FDD method initiates with the application of the Singular Value Decomposition (SVD) to the estimate of the output spectrum matrix (Syy):

$$\hat{S}_{yy}(\omega_i) = U_i \,.\, S_i \,.\, U_i^H \tag{3.6}$$

With:

$\hat{*}$	Estimate of the matrix *
U_i	Unitary matrix that contains the singular vectors
S_i	Diagonal matrix that contains the scalar singular values

For each value ω_i, matrix S_i contains as many singular values as the number of measuring points, that is the size of matrix $\hat{S}_{yy}$. The singular values are related with the ordinates of scalar spectra of single degree of freedom systems with the same modal parameters as the structure modes. When the modes are well separated, the exclusive evaluation of the peaks present in the first singular value will be sufficient to detect the modes. In turn, when there are closely spaced modes, the dominant vibration mode may be detected by evaluating the first singular value, while the detection of the other modes may require the evaluation of the subsequent singular values.

Matrix *U* is associated with the singular vectors and, for each detected mode, contains the estimate of the mode shape associated with the corresponding singular value.

An improved version of this method, called Enhanced Frequency Domain Decomposition (EFDD), is presented by (Brincker et al., 2001), introducing a strategy to estimate modal damping ratios This methodology relies in the selection of the points of the spectra associated with each mode, and in converting them to the time domain through an inverse Fast Fourier Transformation (iFFT), obtaining the auto-correlation functions associated with each mode. The points are selected through the Modal Assurance Criterion (MAC):

$$MAC_{\phi_i\phi_j} = \frac{(\phi_i^T \phi_j)^2}{(\phi_i^T \phi_i)(\phi_j^T \phi_j)} \tag{3.7}$$

With:

$*^T$	Transpose of the vector/matrix *
ϕ	Mode shape configuration

The segment of the spectra is padded with zeros in the points where the criterion is not met, and then the iFFT is applied, so an auto-correlation function with the contribution of the only mode under study is obtained. Taking into account that the output correlation of a dynamic system excited by a white noise is proportional to its impulsive response, to obtain an estimate of the modal damping ratio, it is possible to fit an exponential decay to the relative maxima of the auto-correlation function or to use the following expression (Clough & Penzien, 1995):

$$\xi = \frac{\ln(^{\upsilon_n}/_{\upsilon_{n+m}})}{2 \,.\, \pi \,.\, m} \tag{3.8}$$

With:

$\upsilon_n, \upsilon_{n+m}$	Peaks of the decay function spaced by m cycles

Through the inverse of the mean value of the period of cycles of the auto correlation function, it is possible to obtain an estimation of the damped frequency, which can be transformed into the natural frequency by equation (3.2).

Application Example

The application of the EFDD method started with the computation of the output spectrum matrix and then the singular value decomposition was applied. In this case, instead of 8196, only 2048 points were used to compute the output spectra. Twelve singular values were obtained per frequency, however the information gathered by most of them reveals itself irrelevant. Taking this into account, only the first three singular values are presented in Figure 3.6, which unveils four main resonance peaks, as it was expected.

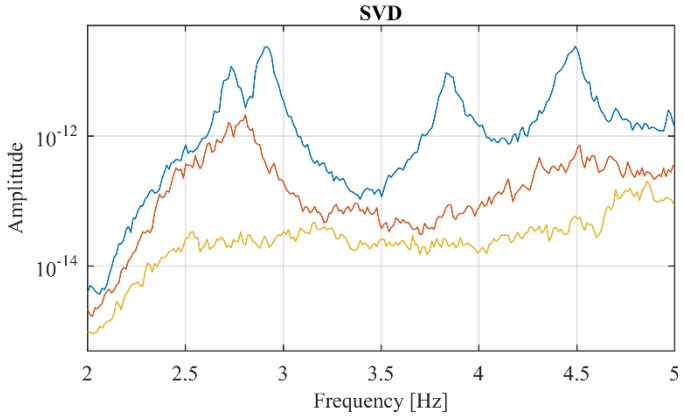

Figure 3.6 – First three singular values of the spectrum matrix.

The modal configurations associated with the first singular value of each of the four peaks were identified and the MAC values (3.7) between those references and all the other modal configurations associated with the first singular value were computed. A MAC value of 0.80 was considered for the definition of the singular values that were relevant to characterize each mode. The selected singular values are highlighted with dark blue in Figure 3.7.

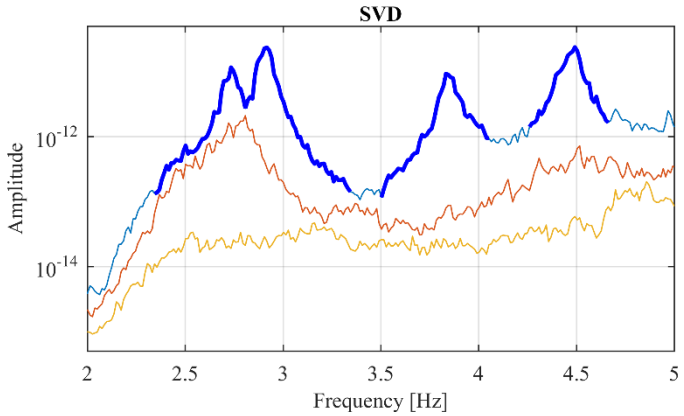

Figure 3.7 – Singular values that meet the Modal Assurance Criterion (MAC) highlighted in dark blue.

The following step comprises the creation of a spectrum for each mode, containing the selected singular values at the respective positions and zeros at the remaining frequencies. Then, the four spectra were converted back to time-domain through the application of an inverse Fast Fourier Transformation (iFFT), and the four auto-correlation functions presented in Figure 3.8 were obtained.

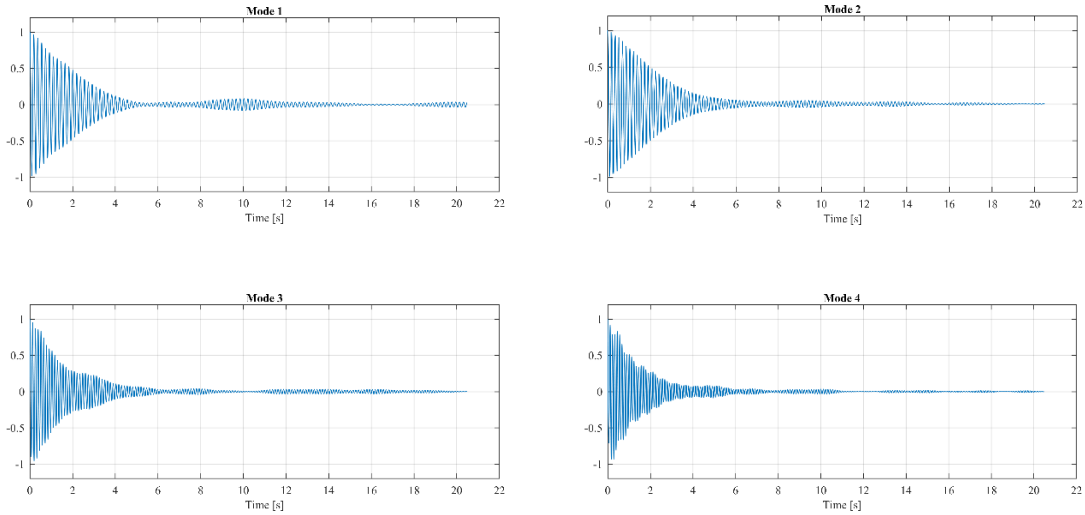

Figure 3.8 – Normalized auto-correlation functions.

With the auto-correlation functions now defined, it was possible to identify the frequency and damping ratios values. On the one hand, if the number of cycles are represented as a function of the evolution of time, the frequency value is determined through a linear regression. On the other hand, the damping ratio values are also determined through a linear regression but, in this case, using the representation of the logarithm of the local maxima as a function of the number of cycles. All these regressions are presented in Figure 3.9.

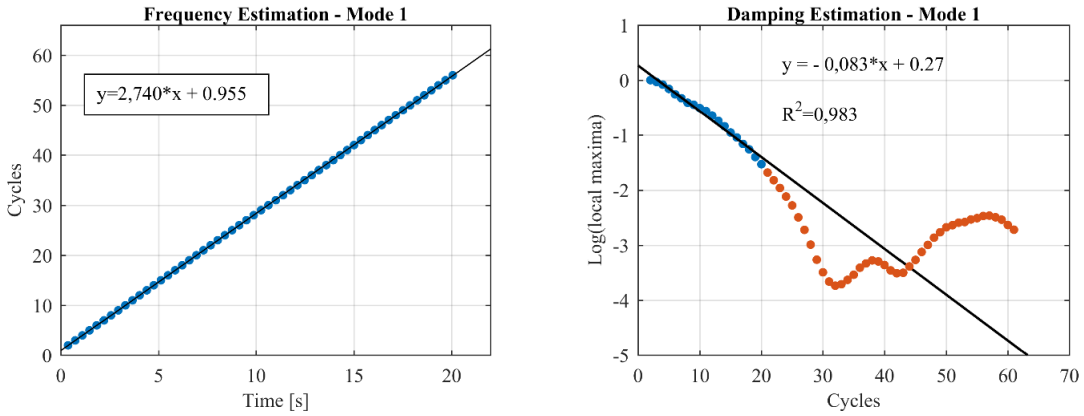

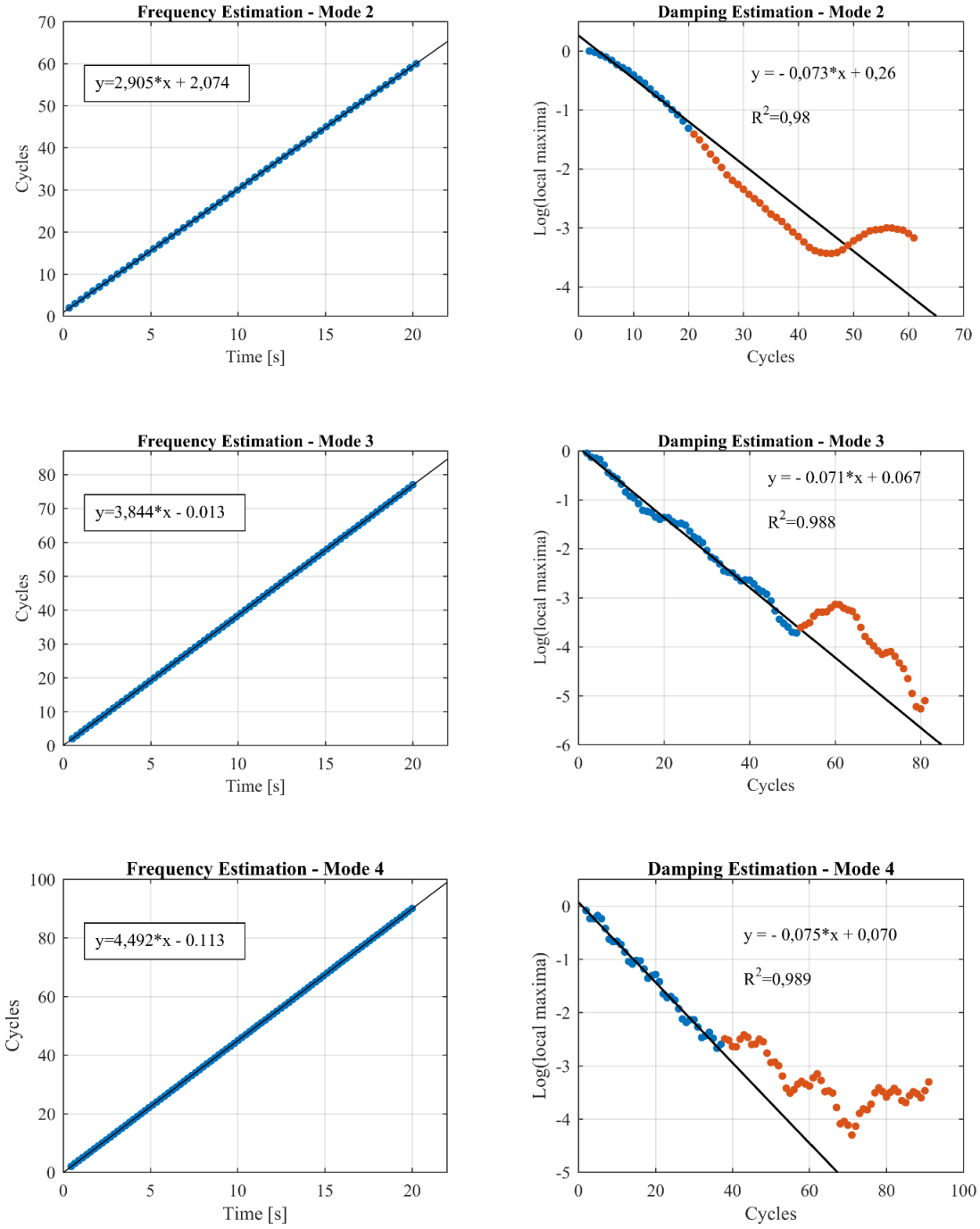

Figure 3.9 – Frequencies and damping values estimations.

For each mode, the slope of the line equation, on the left, corresponds to the identified frequency. On the right, the slope of the line equation was used with equation (3.8) to obtain the damping ratios. Both these quantities are presented in Table 3.2, along with the natural frequencies identified with Peak Picking method for comparison.

Table 3.2 – Natural frequencies obtained with Peak Picking and EFDD

Mode	Frequencies [Hz]		Damping Ratios [%]
	Peak Picking	EFDD	EFDD
1	2.731	2.734	1.32
2	2.921	2.917	1.16
3	3.833	3.845	1.13
4	4.504	4.492	1.20

The modal configurations of the modes were calculated through the average of the configurations associated with the singular values that met the modal assurance criterion (MAC). The obtained modal configurations of the four vibration modes are very similar to those that resulted from the application of the Peak Picking method, with two symmetric and two antisymmetric modes. These configurations are presented in Figure 3.10.

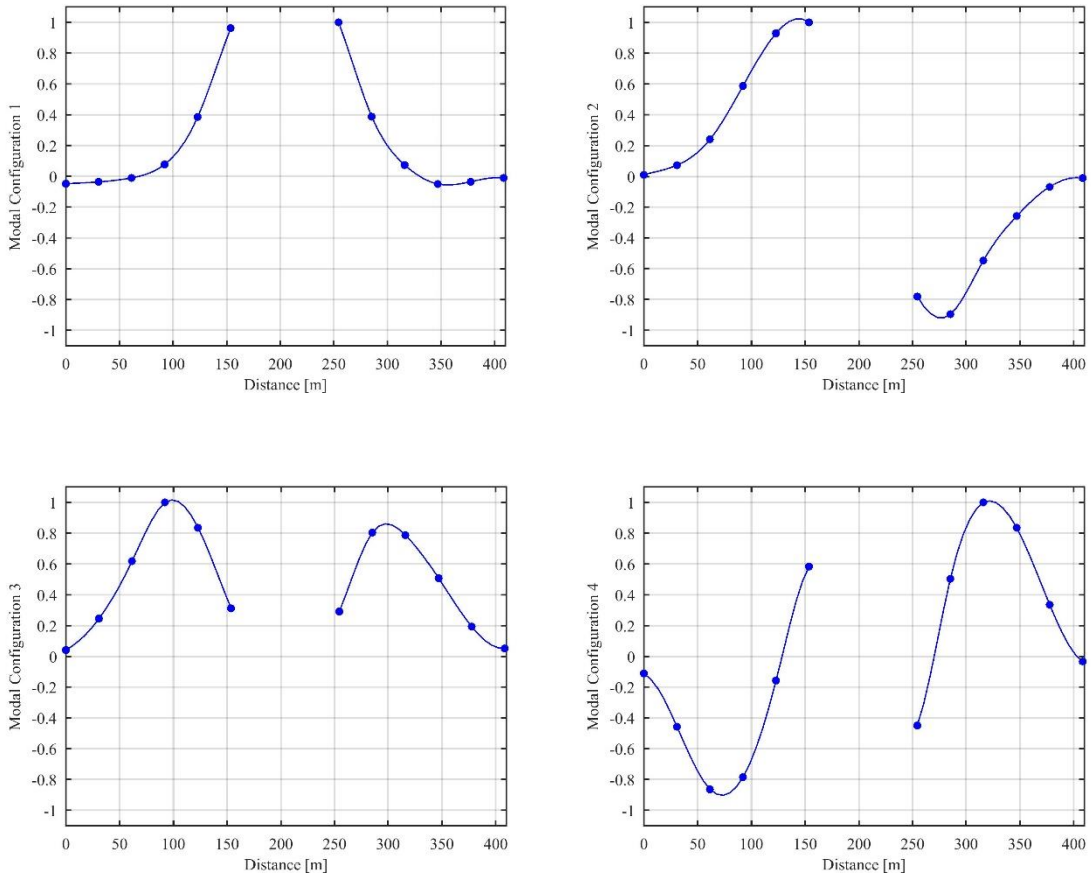

Figure 3.10 – Modal configurations obtained with EFDD.

3.5.3. SSI-Cov

The Covariance driven Stochastic Subspace Identification method (SSI - Cov) is a parametric method for the identification of a stochastic state-space model in the time domain, well-established in the field of operational modal analysis due to its reliability. For a better understanding of this method, some basic considerations about state-space models are introduced next.

State-Space model

A stochastic state-space model is an alternative time domain formulation of a dynamic system. In its discrete version, a stochastic state-space model is characterized by (Juang, 1994):

$$x_{k+1} = A.x_k + B.u_k + w_k \tag{3.9}$$

$$y_k = C.x_k + D.u_k + v_k \tag{3.10}$$

With:

x	State vector (which contains the displacement and velocity vectors of the system)
y	Output vector (which contains the measured output values)
u	Input vector
A	State matrix
B	Influence matrix
C	Output matrix
D	Direct transmission matrix
w	Vector containing noise due to disturbances and modelling inaccuracies
v	Vector containing noise due to sensor inaccuracy

The main goal of the SSI-Cov method is to estimate the matrix A, since it characterizes the structural system. Plus, in the context of Operational Modal Analysis, the system input is unknown, so the terms related to u_k should be grouped together with the noise terms as:

$$x_{k+1} = A.x_k + w_k \tag{3.11}$$

$$y_k = C.x_k + v_k \tag{3.12}$$

This model assumes that the system inputs are idealized as realizations of white noise processes, and that the state vector can be characterized by a stationary stochastic process with zero mean, which allows the factorization of the correlation matrix presented in equation (3.13). Many other properties that support the identification algorithm presented in the next subsection are described and proven in (Overschee & Moor, 1996).

$$R_j = C.A^{j-1}.G \tag{3.13}$$

SSI – Cov Algorithm

The Covariance driven Stochastic Subspace Identification method is a time-domain, parametric method that identifies a stochastic state-space model from the output covariance matrix (Magalhães, 2010). In this work, it will be presented the version described in (B. Peeters, 2000).

The algorithm is based in the main assumption that the correlation functions of the response of a structure excited by a white noise are defined by a sum of sinusoids with exponential decrement. Since these sinusoids are related with the impulsive structural response, the dynamic characteristics of the structure can be then extracted through these functions (B. Peeters, 2000).

The algorithm initiates with the organization of a Toeplitz matrix. This matrix, presented in equation (3.14) contains the estimates of the output correlation functions computed for positive time lags varying from $1 \cdot \Delta t$ to $(2i-1) \cdot \Delta t$.

$$T_{1|i}^{ref} = \begin{bmatrix} R_i^{ref} & R_{i-1}^{ref} & \dots & R_1^{ref} \\ R_{i+1}^{ref} & R_i^{ref} & \dots & R_2^{ref} \\ \dots & \dots & \dots & \dots \\ R_{2\cdot i-1}^{ref} & R_{2\cdot i-2}^{ref} & \dots & R_i^{ref} \end{bmatrix} \tag{3.14}$$

With:

$R_i{}^{ref}$	Correlation matrix evaluated at time lag *i*, containing the correlation between all the sensors and a selected set of sensors (reference sensors)

If the factorization property of the correlation matrix presented in equation (3.13) is applied to all the correlation functions stored in the Toeplitz matrix, the follow decomposition may be obtained:

$$T_{1|i}^{ref} = \begin{bmatrix} C \\ C \cdot A \\ \vdots \\ C \cdot A^{i-1} \end{bmatrix} \cdot \begin{bmatrix} A^{i-1} \cdot G^{ref} & \cdots & A \cdot G^{ref} & G^{ref} \end{bmatrix} = O_i \cdot \Gamma_i^{ref} \tag{3.15}$$

With:

O	Extended observability matrix
Γ	Reverse extended stochastic controllability matrix

In turn, the computation of the singular value decomposition of the Toeplitz matrix reveals

$$T_{1|i}^{ref} = U \cdot S \cdot V^H = \begin{bmatrix} U_1 & U_2 \end{bmatrix} \cdot \begin{bmatrix} S_1 & 0 \\ 0 & 0 \end{bmatrix} \cdot \begin{bmatrix} V_1^T \\ V_2^T \end{bmatrix} = U_1 \cdot S_1 \cdot V_1^T \tag{3.16}$$

and so, the comparison of equations (3.15) and (3.16) takes to a different definition of O and Γ matrices, that can be calculated from the outputs of the SVD:

$$O_i = U_i \cdot S_1^{1/2} \tag{3.17}$$

$$\Gamma_i = S_1^{1/2} \cdot V_1^T \tag{3.18}$$

Since matrix C can be extracted from the first l lines of the observability matrix O (being l the number of measured outputs), the identification of matrix A, and the characterization of the dynamic behaviour of the structural system are solved. In order to obtain the matrix A, the following formulation may be used:

$$\begin{bmatrix} C \\ C \cdot A \\ \vdots \\ C \cdot A^{i-2} \end{bmatrix} \cdot A = \begin{bmatrix} C \cdot A \\ C \cdot A^2 \\ \vdots \\ C \cdot A^{i-1} \end{bmatrix} \Leftrightarrow A = \begin{bmatrix} C \\ C \cdot A \\ \vdots \\ C \cdot A^{i-2} \end{bmatrix}^{\dagger} \cdot \begin{bmatrix} C \cdot A \\ C \cdot A^2 \\ \vdots \\ C \cdot A^{i-1} \end{bmatrix} \tag{3.19}$$

With:

$*^{\dagger}$	Moore-Penrose pseudo-inverse

The decomposition of the matrix A as follows

$$A = \Psi \cdot \Lambda_d \cdot \Psi^{-1} \tag{3.20}$$

With:

Ψ	Matrix with eigenvectors in each column
Λ_d	Matrix with eigenvalues in the diagonal

allows for the eigenvectors and for the eigenvalues (μ_n) in discrete time to be obtained. The natural frequencies and modal damping for each vibration mode are then obtained with the conversion of the eigenvalues from the discrete time to the continuous time model:

$$f_n = \frac{Abs\left(\ln(\mu_n)/\Delta t\right)}{2\pi} \tag{3.21}$$

$$\zeta_n = -\frac{Re\left(\ln(\mu_n)/\Delta t\right)}{Abs\left(\ln(\mu_n)/\Delta t\right)} \tag{3.22}$$

With:

f_n	Frequency value of the n^{th} vibration mode
ζ_n	Damping ratio of the n^{th} vibration mode
Δt	Sampling interval of the outputs
$Abs(*)$	Absolute value of *
$Re(*)$	Real part of *

To end the identification process, only the mode shapes are missing, which can be obtained through the calculation:

$$\phi = C.\Psi \tag{3.23}$$

With:

ϕ	Matrix with the mode shape configurations

In the context of practical applications of the SSI-Cov method, there are some considerations that must be mentioned. For instance, the output correlation matrix actually consists of a matrix composed by estimates and there are always noise contaminating the signals. This implicates that the higher singular values, obtained from the decomposition of the Toeplitz matrix, that would theoretically be equal to zero, present in practice residual values, not allowing for the model order

to be identified. Thus, it is common to calculate the results for different orders of matrices A and C, and then select the best model by the analysis of the corresponding modal parameters. However, higher orders may lead to the emergence of numerical modes, which have little to none physical meaning.

To separate these numerical modes from the physical ones, as well as to assist the user in the process of choosing the most adequate model order, stabilization diagrams are constructed. These diagrams consist on the representation of the estimated modal parameters for each model order, taking into account if the variation between parameters of successive orders is within a previously defined limit, in which case the result parameter (or pole) is considered stable. Physical modes are likely to present stable poles for most of the orders, while spurious modes appear only in some model orders.

Application Example

The SSI – Cov method was applied considering all the sensors as references, and model orders between 1 and 30. The stabilization diagram presented in Figure 3.11 was achieved considering maximum variations of frequency and damping ratios between consecutive poles of 1%, and a minimum MAC value between consecutive poles of 95%. Four clear alignments of stable poles appear between the 2 and 5 Hz, as it was expected.

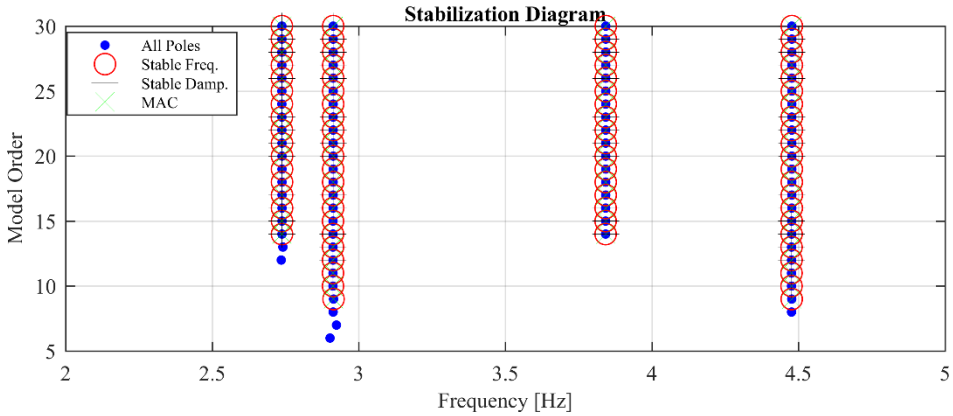

Figure 3.11 – Stabilization diagram obtained with the SSI - COV method.

In Figure 3.12 the damping ratios of the stable poles are presented as a function of natural frequencies, and each colour represents a mode. The low variability of the circles position proves the consistency of the results for models of different orders.

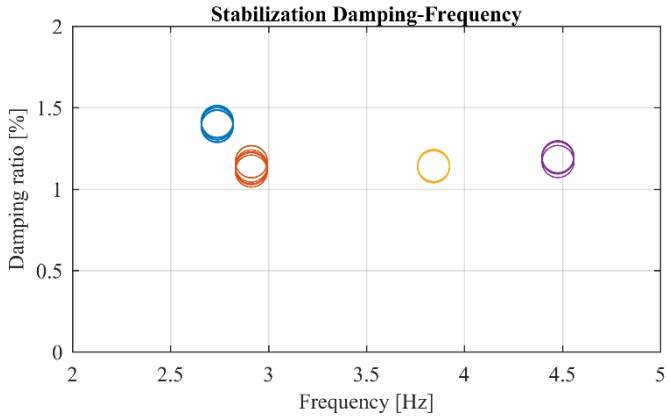

Figure 3.12 – Modal damping ratio estimates for the stable poles.

From all the stable poles available, the average values were computed and used as representative of the systems modal characteristics. Nevertheless, a specific model order, providing good results could have been chosen as representative instead, in which case very similar results would have been obtained. Both frequencies and damping ratios are presented in Table 3.3, along with the ones identified with Peak Picking and EFDD methods for comparison. The results obtained are coherent for all three applied methods.

Table 3.3 – Natural frequencies and damping ratios obtained with Peak Picking, EFDD and SSI-COV

Mode	Frequencies [Hz]			Damping ratios [%]	
	Peak Picking	EFDD	SSI - COV	EFDD	SSI - COV
1	2.731	2.734	2.738	1.32	1.41
2	2.921	2.917	2.913	1.16	1.17
3	3.833	3.845	3.842	1.13	1.15
4	4.504	4.492	4.477	1.20	1.20

The modal configurations of the four vibration modes, also obtained from the average of the configurations extracted from stable poles, are presented in Figure 3.13. Once again, as happened with the applications of Peak Picking and EFDD, the modal configurations achieved are respectively symmetric and antisymmetric.

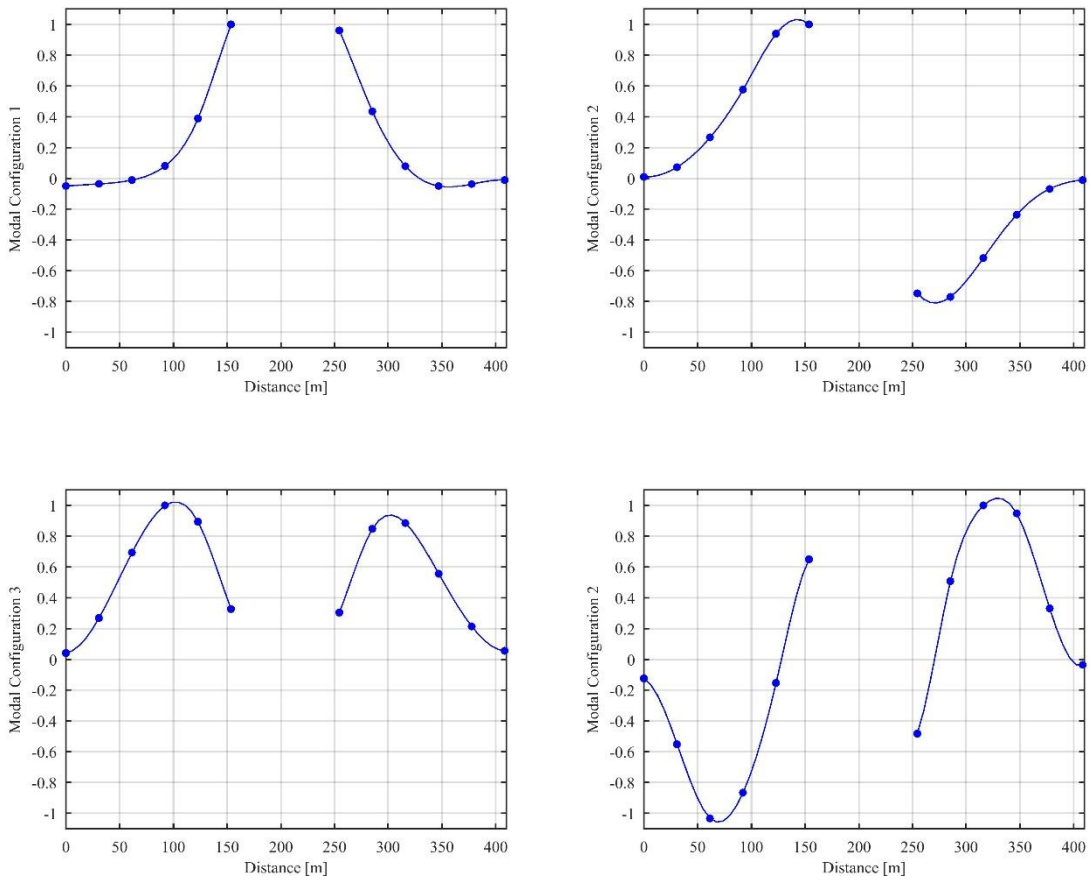

Figure 3.13 – Modal configurations obtained with SSI-Cov.

3.5.4. P-LSCF

The poly-reference Least Squares Complex Frequency Domain method (p-LSCF), also known as polymax, is a parametric, frequency domain method, which was initially developed in order to identify the modal characteristics of a system from frequency response functions (Guillaume et al., 2003). However, in this work, it will be presented an approach adapted by (B. Peeters & Van der Auweraer, 2005) to work with the output half-spectrum functions, thus becoming an output-only version of the method.

Right Matrix – Fraction Description

The right matrix-fraction description (RMFD) is a mathematical representation fitted by the p-LSCF method, that describes the relation between inputs and outputs of a dynamic system. The RMFD is used to parameterize the transfer function as a right division of two polynomial matrices, B^R and A^R:

$$H(s) = B^R \,.\, (A^R)^{-1} \tag{3.24}$$

With:

s	Complex variable

In the context of p-LSCF, the RMFD model is converted to a state-space model (Reynders, 2009). Assuming that matrices A^R e B^R have the same order (p) and that the degree of the polynomial of the determinant of $A(s)$ is equal to $p^R.n_o$ (being n_o the number of outputs), the matrices A, B, C and D from the state-space model are obtained through the following equations (dropping the subscript $*^R$ for simplification):

$$A = \begin{bmatrix} -{A_p}^{-1}.A_{p-1} & -{A_p}^{-1}.A_{p-2} & \cdots & -{A_p}^{-1}.A_1 & -{A_p}^{-1}.A_0 \\ I & 0 & \cdots & 0 & 0 \\ \vdots & \vdots & \ddots & \vdots & \vdots \\ 0 & 0 & \cdots & I & 0 \end{bmatrix} \tag{3.25}$$

$$B = \begin{bmatrix} {A_p}^{-1} \\ 0 \end{bmatrix}$$

$$C = \begin{bmatrix} B_{p-1} - B_p.{A_p}^{-1}.A_{p-1} & \cdots & B_0 - B_p.{A_p}^{-1}.A_0 \end{bmatrix}$$

$$D = B_p . A_p{}^{-1}$$

With:

I	Identity matrix

Half-Spectrum

For the p-LSCF algorithm to be applied, it is necessary to previously estimate the half spectrum matrix. Considering the input spectrum S_{uu} is constant and not dependent on frequency, as a result of a white noise excitation, the output spectrum is obtained by:

$$S_{yy}(\omega) = H(\omega) \, . S_{uu} \, . H(\omega)^H \tag{3.26}$$

In turn, the frequency response function may be expressed by the sum of the contributions of the dynamic system modes (Heylen et al., 2007),

$$H(\omega) = \sum_{k=1}^{n} \frac{\phi_k \, . l_k^T}{i . \omega - \lambda_k} + \frac{\phi_k^* \, . l_k^H}{i \, . \omega - \lambda_k^*} \tag{3.27}$$

With:

n	Number of vibration modes analysed
ϕ	Observable components of the mode shape configuration
l	Modal participation factor
λ	Poles ($\lambda_K, \lambda_K^* = -\xi_K \, . \omega_K \pm j . \sqrt{1 - \xi_k^2} \, . \omega_k$)

Combining equations (3.26) and (3.27), it is possible to define the output spectrum as a summation of the contributions of structural vibration modes (B. Peeters, 2000):

$$S_{yy}(\omega) = \sum_{k=1}^{n} \frac{\phi_k \, . g_k^T}{i . \omega - \lambda_k} + \frac{\phi_k^* \, . g_k^H}{i \, . \omega - \lambda_k^*} + \frac{g_k \, . \phi_k^T}{- i \, . \omega - \lambda_k} + \frac{g_k^* \, . \phi_k^H}{- i \, . \omega - \lambda_k^*} \tag{3.28}$$

With:

g	Operational reference vectors

From equation (3.28) four poles result for each mode, imposing the use of models with orders that are twice de modal order needed to model the transfer function of the same dynamic system. Thus, instead of equation (3.28), the Positive or Half-Spectrum is usually used:

$$S_{yy}{}^{+}(\omega) = \sum_{k=1}^{n} \frac{\phi_k \cdot g_k^T}{i.\omega - \lambda_k} + \frac{\phi_k^* \cdot g_k^H}{i \cdot \omega - \lambda_k^*} \tag{3.29}$$

In practical applications, since only discrete time signals are available, the Half-Spectrum may be estimated by the Correlogram approach, restricted to the positive time lags of the correlation function:

$$S_{yy}{}^{+}(\omega_j) = \frac{R_{yy}(0)}{2} + \sum_{k=1}^{j} R_{yy}(k.\Delta t)\, e^{-i.\omega_j.k.\Delta t} \tag{3.30}$$

With:

j	Number of time lags to analyse

To reduce the effect of leakage and the influence of the higher time lags, which have a larger variance (B. Peeters & Van der Auweraer, 2005), an exponential window should be applied to the correlations before the use of equation (3.30):

$$w_k = e^{-\beta.k.\Delta t}, for\ 1 \leq k \leq j \tag{3.31}$$

With:

β	Decay rate of the window

The application of the exponential window leads to biased values of damping for the computed poles, for which reason the damping value should then be corrected according to (Cauberghe, 2004):

$$\xi_{estimated} = \xi_{real} \frac{\beta}{\omega} \tag{3.32}$$

p-LSCF algorithm

The p-LSCF method models the half spectrum matrix using a right matrix-fraction description (RMFD) in the discrete-time frequency domain (Magalhães, 2010). Then, considering the use of matrices A^R and B^R, presented in equation (3.24), as polynomials of the same order p, the half-spectrum matrix is defined as:

$$S_{yy}{}^{+}(\omega_j) = B^R \,.\, (A^R)^{-1} = \left[\sum_{r=0}^{p} B_r \,.\, e^{i.\omega_j.\Delta t.r}\right] . \left[\sum_{r=0}^{p} A_r \,.\, e^{i.\omega_j.\Delta t.r}\right]^{-1} \tag{3.33}$$

The main goal of this method is to find the model parameters, matrices A^R and B^R, that lead to the minimum difference between the half-spectrum matrix estimated from the measured output time series ($\hat{S}_{yy}{}^{+}$) and the theoretical half-spectrum matrix given by equation (3.33). The nonlinear least squares problem can be simplified to a linear problem according to (Guillaume et al., 2003):

$$E^{LS}(\omega_j) = \left[\sum_{r=0}^{p} B_r \,.\, e^{i.\omega_j.\Delta t.r}\right] - \hat{S}_{yy}{}^{+}(\omega_j) \,.\, \left[\sum_{r=0}^{p} A_r \,.\, e^{i.\omega_j.\Delta t.r}\right] \tag{3.34}$$

Considering the polynomial basis functions evaluated at each frequency (ω_J) organized in one row with $(p+1)$ components:

$$\Omega\,(\omega_j) = \left[\Omega_0(\omega_j)\ \Omega_1(\omega_j)\ \cdots\ \Omega_p(\omega_j)\right] = \left[e^{i.\omega_j,\Delta t.0}\ \ e^{i.\omega_j,\Delta t.1}\ \ \ldots\ \ e^{i.\omega_j,\Delta t.p}\right] \tag{3.35}$$

then, equation (3.34) can be rewritten as:

$$E_o{}^{LS} = \Omega\,(\omega_j) \,.\, \begin{bmatrix} B_{0_o} \\ B_{1_o} \\ \vdots \\ B_{p_o} \end{bmatrix} + \left[\Omega_0(\omega_j).\hat{S}_{yy}{}^{+}{}_o\ \ \Omega_1(\omega_j).\hat{S}_{yy}{}^{+}{}_o\ \cdots\ \Omega_p(\omega_j).\hat{S}_{yy}{}^{+}{}_o\right] . \begin{bmatrix} A_0 \\ A_1 \\ \vdots \\ A_p \end{bmatrix} \tag{3.36}$$

With:

o	Line of the error matrix (which varies from 1 to the number of measured outputs)

Introducing the following definitions:

$$\alpha = \begin{bmatrix} A_0 \\ A_1 \\ \vdots \\ A_p \end{bmatrix} \tag{3.37}$$

$$\beta_o = \begin{bmatrix} B_{0_o} \\ B_{1_o} \\ \vdots \\ B_{p_o} \end{bmatrix}, with\ o = 1,2, \dots, n_o \tag{3.38}$$

With:

n_o	Number of measured outputs

Equation (3.36) can be written as:

$$\mathrm{E}_o{}^{LS}(\beta_{o,\alpha}) = [X_o \quad Y_o].\begin{bmatrix} \beta_o \\ \alpha \end{bmatrix} \tag{3.39}$$

Where:

$$X_o = \begin{bmatrix} \Omega\ (\omega_1) \\ \vdots \\ \Omega\ (\omega_{n_f}) \end{bmatrix} \tag{3.40}$$

$$Y_o = \begin{bmatrix} \left(\Omega_o\ (\omega_1) \cdots\ \Omega_p(\omega_1)\right) \otimes \hat{S}_{yy}{}^{+}{}_o(\omega_1) \\ \vdots \\ \left(\Omega_o\ \left(\omega_{n_f}\right) \cdots\ \Omega_p\left(\omega_{n_f}\right)\right) \otimes \hat{S}_{yy}{}^{+}{}_o(\omega_{n_f}) \end{bmatrix}, with\ o = 1,2, \dots, n_o \tag{3.41}$$

With:

$\otimes$	Kronecker product operator
ω_1, ω_{n_f}	Frequency interval limits

The expansion of the equation of the error matrix, with all parameters from matrices α and β_o, results in (the subscript $*^{LS}$ is dropped for simplification):

$$E_o(\beta_o, \alpha) = \begin{bmatrix} X_1 & 0 & \cdots & 0 & Y_1 \\ 0 & X_2 & \cdots & 0 & Y_2 \\ \vdots & \vdots & \ddots & \vdots & \vdots \\ 0 & 0 & \cdots & X_{n_o} & Y_{n_o} \end{bmatrix}.\begin{bmatrix} \beta_1 \\ \beta_2 \\ \vdots \\ \beta_{n_o} \\ \alpha \end{bmatrix} = J.\theta \tag{3.42}$$

As solving the identification problem through $J.\theta = 0$ would be too computationally demanding, the model parameters are usually obtained through a linear least squares cost achieved by adding all the squared elements of the matrix E_o, evaluated at each discretized frequency:

$$\varepsilon = \sum_{o=1}^{n_o} \sum_{r=1}^{n_r} \sum_{j=1}^{n_f} E_{o,r}(\omega_j) E_{o,r}(\omega_j)^* \tag{3.43}$$

With:

n_r	Number of reference outputs

From equations (3.40) and (3.41), (3.43) can be written as:

$$\varepsilon\,(\beta_o, \alpha) = \sum_{o=1}^{n_o} tr\{E_o(\beta_o, \alpha)^H . E_o(\beta_o, \alpha)\} = \sum_{o=1}^{n_o} tr\left\{\begin{bmatrix}\beta_o{}^T & \alpha^T\end{bmatrix} \cdot \begin{bmatrix}R_o & S_o \\ S_o{}^T & T_o\end{bmatrix} \cdot \begin{bmatrix}\beta_o \\ \alpha\end{bmatrix}\right\} \tag{3.44}$$

With:

$tr(*)$	Trace of matrix *
R_o	$Re\left(X_o{}^H . X_o\right)$
S_o	$Re\left(X_o{}^H . Y_o\right)$
T_o	$Re\left(Y_o{}^H . Y_o\right)$

Thus, the minimum of the cost function is obtained with:

$$\frac{\partial \varepsilon(\beta_o, \alpha)}{\partial \beta_o} = 2 \cdot (R_o . \beta_o + S_o . \alpha) = 0, with\ o = 1,2, \dots, n_o \tag{3.45}$$

$$\frac{\partial \varepsilon(\beta_o, \alpha)}{\partial \alpha} = 2 \sum_{o=1}^{n_o} \left(S_o{}^T \cdot \beta_o + T_o\right) = 0 \tag{3.46}$$

Eliminating the unknowns β_0, the size of the system of equations can be reduced:

$$2 \cdot (R_o . \beta_o + S_o . \alpha) = 0 \Leftrightarrow \beta_o = -R_o{}^{-1} \cdot S_o \cdot \alpha \tag{3.47}$$

Then, the α matrix is obtained through:

$$2\sum_{o=1}^{n_o}\left(T_o - {S_o}^T.{R_o}^{-1}.S_o\right)\alpha = 0 \Leftrightarrow M.\alpha = 0 \tag{3.48}$$

In order to avoid finding the trivial solution $\alpha = 0$, a constraint should be imposed on the parameters. In (Cauberghe, 2004) it is suggested to impose α_a (from the α matrix) as an identity matrix. Then, α is obtained with:

$$M.\alpha = 0 \Leftrightarrow \begin{bmatrix} M_{aa} & M_{ab} \\ M_{ba} & M_{bb} \end{bmatrix}\cdot \begin{bmatrix} \alpha_a \\ \alpha_b \end{bmatrix} = \begin{bmatrix} 0 \\ 0 \end{bmatrix} \Leftrightarrow M_{bb}.\alpha_b = -M_{ba} \Leftrightarrow \tag{3.49}$$

$$\Leftrightarrow \alpha_b = -{M_{bb}}^{-1}.M_{ba} \Rightarrow \alpha = \begin{bmatrix} I \\ -{M_{bb}}^{-1}.M_{ba} \end{bmatrix}$$

With:

M_{aa}	Contains the first n_r lines and columns of M
M_{ab}	Contains the first n_r lines and last p.n_r columns of M
M_{ba}	Contains the last p.n_r lines and first n_r columns of M
M_{bb}	Contains the last p.n_r lines and columns of M

Once α is defined, equation (3.47) is used to calculate matrix β_r and define the RMFD model. Thereupon, companion matrix is obtained as follows:

$$C_o = \begin{bmatrix} -{A_p}^{-1}.A_{p-1} & -{A_p}^{-1}.A_{p-2} & \cdots & -{A_p}^{-1}.A_1 & -{A_p}^{-1}.A_0 \\ I & 0 & \cdots & 0 & 0 \\ \vdots & \vdots & \ddots & \vdots & \vdots \\ 0 & 0 & \cdots & I & 0 \end{bmatrix} \tag{3.50}$$

The similarity between matrix A from equation (3.34) and equation (3.50) is easily detected. Thus, C_o represents the matrix A from the state-space model, the remaining model matrices may be obtained through equation (3.25).

With the state-space model defined, the dynamic system's modal parameters can be calculated using the same procedure presented for SSI-Cov, that is, from equation (3.20) to equation (3.23). Also in this case, the model order (p) that will produce the best results is unknown, so the computation of several orders and the presentation of the results in a stabilization diagram should be followed.

Application Example

The p-LSCF algorithm was applied considering all the sensors as references, and model orders between 1 and 20. The stabilization diagram presented in Figure 3.14 was achieved considering maximum variations of frequency and damping ratios between consecutive poles of 1%, and a minimum MAC value between consecutive poles of 95%. As in the previous example, four clear alignments of stable poles appear between the 2 and 5 Hz.

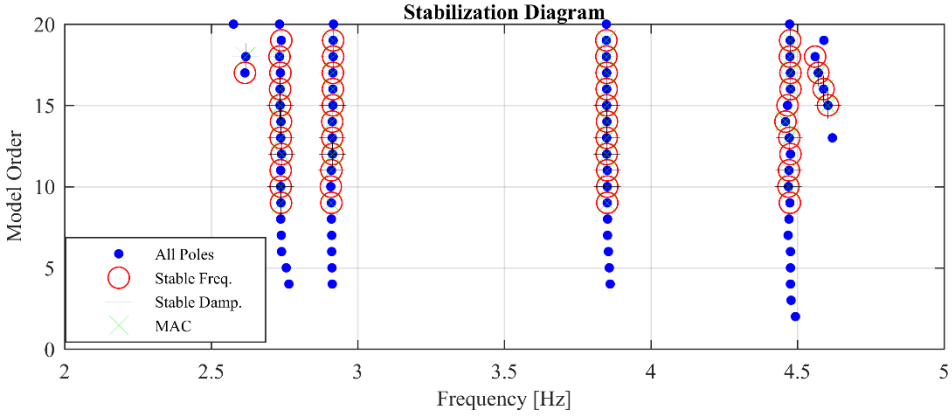

Figure 3.14 – Stabilization diagram obtained with the p-LSCF method.

In Figure 3.15 the damping ratios of the stable poles are presented as a function of the natural frequencies, and each colour represents a mode. All the four modes present good consistency, with a little more variability in the vertical direction, due to the variability of the damping values.

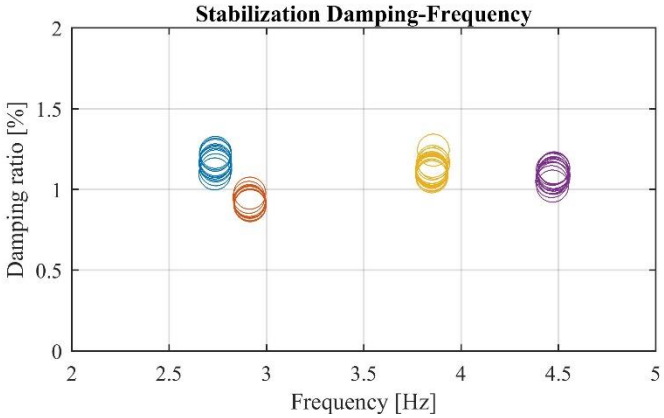

Figure 3.15 – Modal damping ratio estimates for the stable poles.

Such as in the case of the example using the SSI-Cov method, the modal estimates representative of the system's modal properties were chosen as the average values of the estimates provided by each stable pole. However, as indicated by the low data variability shown by Figure 3.15, good and

similar results would have been obtained if any of these stable poles had been chosen as representative. The values of both natural frequencies and damping ratios are presented in Table 3.4, along with the ones identified in the previous examples with the Peak Picking, the EFDD and the SSI-Cov methods, for comparison. While the values obtained for natural frequencies are coherent in all four application examples, with a maximum difference between estimates obtained with different methods of 0.031Hz, in the case of damping ratios higher variations between methods were obtained. However, the differences verified do not go over 0.25 %, which is acceptable taking into account the higher uncertainties associated with damping estimates. This will be further studied in the next section.

Table 3.4 – Natural frequencies and damping ratios obtained with Peak Picking, EFDD, SSI-Cov and p-LSCF

Mode	Frequencies [Hz]				Damping ratios [%]		
	Peak Picking	EFDD	SSI - Cov	p-LSCF	EFDD	SSI - Cov	p-LSCF
1	2.731	2.734	2.738	2.738	1.32	1.41	1.17
2	2.921	2.917	2.913	2.914	1.16	1.17	0.93
3	3.833	3.845	3.842	3.851	1.13	1.15	1.13
4	4.504	4.492	4.477	4.473	1.20	1.20	1.09

The average modal configurations of the four vibration modes (using only stable poles) identified with the p-LSCF method are represented in Figure 3.16. Once again, as happened with the previous examples, the modal configurations achieved are alternatively symmetric and antisymmetric.

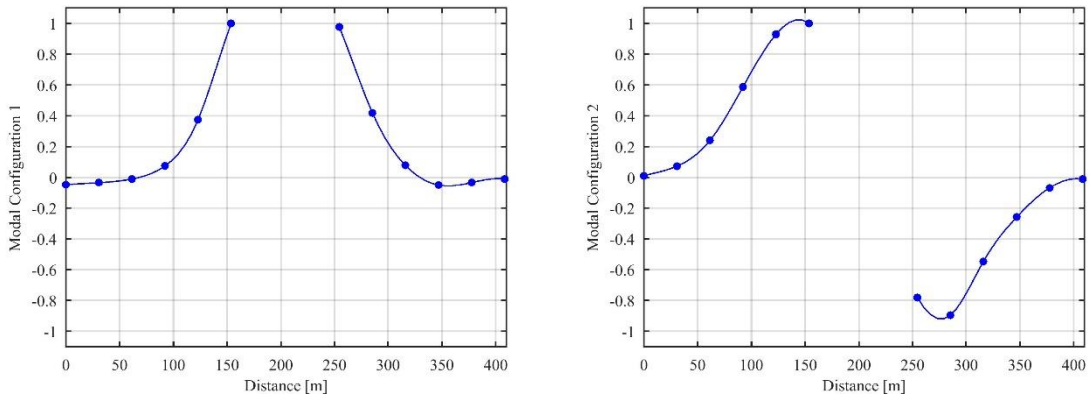

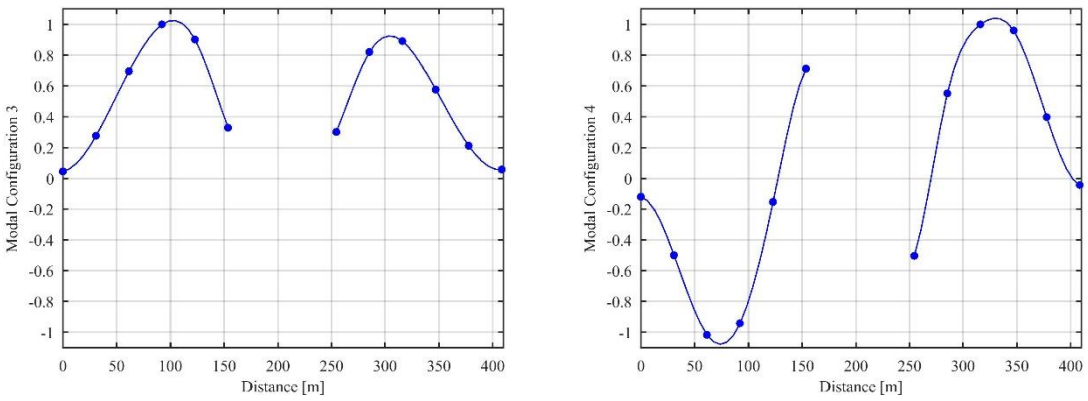

Figure 3.16 – Modal configurations obtained with p-LSCF.

In the next section, the topic of the uncertainty related with the estimates obtained from modal identification is addressed, together with procedures and mathematical tools to quantify and minimize it.

3.6. UNCERTAINTY IN MODAL PARAMETERS ESTIMATION

The modal parameters of a structure, estimated from ambient vibration measurements using identification methods such as those presented in the previous section, are always subject to bias and variance errors. Since identified modal characteristics are quite often used for calibration and validation of dynamic structural models, for structural control or for structural health monitoring, it becomes important to analyse the accuracy associated with the estimated parameters. Errors introduced in the identification process may be due to several reasons (Reynders et al., 2008). For instance: the use of a finite number of data samples; the inputs may not be a white noise; nonlinear distortions may be present in the data because of material or geometrical nonlinearities; non-stationary nature of structures activated by external factors such as temperature or wind; analog and/or digital filters introducing spurious poles; human induced errors.

Depending both on the identification method used and on the structure characteristics, each of the previous error causes may gain relevance over the others, and even different causes that were not mentioned may arise. Both the physical part of the problem, more strongly associated with the data collection, and the mathematical part, strictly related with the identification procedure, must be conducted with extreme care, in order to reduce the number of error sources and to mitigate the effects of those that cannot be completely supressed.

To mitigate bias errors, stabilization diagrams such as those presented earlier, along with the explanation of the SSI-Cov and the p-LSCF methods, are of good use. Constructed by choosing a wide range of model orders for the identification problem and by plotting all identified modal parameters in a *frequency versus model order* chart, these diagrams allow to remove the bias associated with both the model and the modes (Reynders et al., 2008):

- Bias of the model: spurious modes can be removed with the stabilization diagram, including noise modes that arise due to physical reasons, and mathematical modes that arise due to an over-estimation of the system order;

- Bias of the modes: due to an under-estimation of the system order, two different modes (true or noisy) can be wrongly identified as a single mode that results from the combination of the two. Both modes can be detected with a stabilization diagram if sufficiently high values of the model order are taken into account.

However, unlike bias errors, which can be mitigated, variance errors can only be estimated, they cannot be removed. In (Reynders et al., 2008) a detailed sensitivity analysis of the reference-based covariance-driven stochastic subspace identification method (SSI-Cov) yielded a novel expression for the covariance of the system matrices that are identified using this method, allowing the estimation of errors. Additionally, subsequent sensitivity analysis yielded expressions for the covariance of the modal parameters, allowing the estimation of uncertainty bounds. These expressions were applied to data obtained from a 30 meters high antennae and natural frequencies and damping ratios were estimated along with the related 2σ uncertainty bounds.

This strategy was also applied in (Reynders et al., 2014) to quantify the uncertainty of modal characteristics of a concrete bridge and a mid-rise building. Two validations of the procedure were performed for each structure. In the first one, the predicted uncertainty was compared to the variability of the natural frequencies and damping ratios obtained with different setups, whereas, in the second one, the estimation accuracy between different modes and setups was evaluated. In both cases it was concluded that the predicted variances were consistent with the experimental observations.

In (M. Döhler & Mevel, 2013), a computationally faster version of this algorithm is presented, along with a multi-order extended implementation that allows the calculation of uncertainty bounds for all elements of a stabilization diagram. The validation of the new algorithm, presented in (Michael Döhler et al., 2013), was executed on multi-setup ambient vibration data of the Z24 Bridge (B. Peeters, 2000)

A method to compute confidence intervals for the least-squares complex frequency-domain (LSCF) estimator algorithm is presented in (De Troyer et al., 2009), where an expression for the covariance matrix of estimated coefficients is derived. The same approach is also applicable for other frequency-domain modal parameters estimators, as for instance the iterative quadratic maximum likelihood. Even though a work using maximum likelihood to calculate uncertainty bounds, that became a reference in the subject, had already been presented by (Pintelon et al., 2007).

More recently, an application of a maximum likelihood algorithm, combined with the p-LSCF method, was presented by (Diord et al., 2017), where the uncertainties of the estimated modal parameters of a football stadium suspension roof are yield. The algorithm used to compute the uncertainties was first presented by (El-kafafy et al., 2015).

The computationally faster version (M. Döhler & Mevel, 2013) of the algorithm first presented in (Reynders et al., 2008) was implemented in Matlab and validated with routines provided by Professor Edwin Reynders, to yield standard deviation estimates associated with the estimates of natural frequencies and damping ratios provided by the SSI-Cov method. This algorithm is used in chapter 4 to perform the modal identification of a set of concrete dams where time-series of accelerations were recorded during ambient vibration tests. The method is used as well to perform the modal identification of Baixo Sabor and Foz Tua dams, respectively presented in chapters 6 and 7. Additionally, in the case of Baixo Sabor dam the standard deviation estimates associated with natural frequencies and damping ratios are also integrated in the procedures used for the continuous tracking of modal properties and for the mitigation of the effects of operational and environmental conditions.

Application Example

The time series used in the previous examples were used to quantify the uncertainties associated with the modal properties estimated with the SSI-Cov method. For each model order, besides the frequency and damping estimates, standard deviation estimates related to these modal parameters are obtained. In Table 3.5 the standard deviation estimates are presented for each mode natural frequency and damping ratio, obtained with the SSI-Cov. These estimates were computed as the average value of the estimates provided by the stable poles presented in Figure 3.11. Much higher values were obtained for the standard deviation of the damping ratios, when compared to the ones obtained for natural frequencies, as it was expected. Assuming normal distributions and 95 % of confidence intervals (~ 2σ), the results show that all the estimates presented in Table 3.4 with the different methods would fall inside the estimated confidence intervals.

Table 3.5 – Natural frequencies and damping ratios obtained with SSI-Cov and respective standard deviation values

Mode	f_{mean} [Hz]	f_{std} [Hz]	ξ_{mean} [%]	ξ_{std} [%]	Description
1	2.738	0.004	1.41	0.16	Symmetric
2	2.913	0.003	1.17	0.13	Antisymmetric
3	3.842	0.008	1.15	0.23	Symmetric
4	4.477	0.009	1.20	0.16	Antisymmetric

3.7. FINAL CONSIDERATIONS

Modal analysis provides important information about structures from a global perspective that can be very useful in the monitoring of the structure health condition, complementing the information that can be gathered from other destructive and non-destructive types of testing and inspection. Nevertheless, the identification of modal properties may also play an important role in the validation of structural design assumptions, in the calibration or updating of numerical models, in the development of mechanisms for vibration control and in the implementation of continuous monitoring systems.

In this context, in the first part of this chapter, experimental and operational modal analysis, the two main approaches to identify modal properties, were introduced along with the dynamic tests associated with both types of modal analysis, and particularities related with the application of OMA to dams were discussed. More specifically, on the one hand, the low levels of vibration that should be expected when performing ambient vibration tests in dams require the consideration of high-quality equipment, namely sensors and acquisition systems, and on the other hand, it should be taken into account that, in the case of a power plant operating nearby the dam, the data collected may be polluted with harmonics from the turbines rotation, whenever the plant is operating.

To obtain modal properties from structures subjected only to ambient vibrations, four well-established output-only identification methods such as Peak Picking, EFDD, SSI-Cov and p-LSCF were presented and their implementation was validated with experimental data collected in Baixo Sabor arch dam. The dam's first four vibration modes were identified and similar results were obtained with the application of the four methods. Additionally, the topic of the uncertainty related with the estimates obtained from modal identification was addressed, together with procedures and mathematical tools to quantify and minimize it, highlighting the importance of stabilization diagrams in the mitigation of bias errors. A tool that quantifies the uncertainty related with the modal estimates provided by the SSI-Cov method was implemented and applied to the same time-series used in the previous examples. As expected, higher uncertainties were found to be associated with damping ratios.

These tools will be used in chapter 4 to identify the modal properties of a set of Portuguese concrete dams, and in chapters 6 and 7 in the context of the vibration-based monitoring of Baixo Sabor and Foz Tua dams. The topic of automatic operational modal analysis is addressed in chapter 5.

4. DYNAMIC TESTING OF DAMS

4.1. INTRODUCTION

Historically, the dynamic testing of dams, performed with the aim of identifying the structure dynamic properties for numerical modelling and design updating and validation (Gauron et al., 2018), has been closely associated with the performance of forced vibrations tests, a field for which the National Laboratory for Civil Engineering (LNEC), in Portugal, most contributed from the beginning of the second half of the XX century to the present day.

As it was explained in the previous chapter, the performance of forced vibration tests as a mean for the application of experimental modal analysis, is a useful, accurate and well-established way of characterizing the dynamic behaviour of a structure, which has been successfully used not only on dams, but also on bridges, buildings and stadia. This approach presents, however, a few drawbacks, mostly related with the test procedure and equipment needed to perform it, namely the necessity of interrupting road traffic during the test, in the case of bridges and road crossed dams, and the considerable size and weight of the vibrators needed to excite such massive structures.

In this sense, the performance of ambient vibration tests has become more and more common in the past couple of decades, greatly benefiting from the technological evolution that occurred in the field of data acquisition. These are practical and economical dynamic tests that permit an accurate identification of modal parameters of civil engineering structures without disturbing their normal operation. Furthermore, the estimated modal properties are associated with normal operation conditions, and not artificially created loads. Ambient vibration tests are frequently performed right after the construction of important infrastructures for the validation of numerical models, before

rehabilitation works to better characterize the structure or in the context of inspection programs to evaluate the safety of existing structures. In addition to this, the information provided by these tests can be used for the design and tuning of devices for vibration control and for the configuration of dynamic monitoring systems (Magalhães, 2010).

Since the vibrations measured in a structure during an ambient vibration test are due only to the excitation provided by the environment, or to nearby human activity, (unless a strong external source of excitation, such an earthquake, occurs) the vibrations levels observed are many times smaller than those that would have been measured during a forced vibration test, which leads to the need of using high-quality sensors and data acquisition systems during the test. On the other hand, one can expect to achieve good results with medium-quality equipment when performing tests in more flexible structures, prone to be excited, such as towers or pedestrian bridges.

In the case of dams, however, generally very low levels of vibrations are expected to be measured, due to the remote locations of most structures of this type and to their massive nature, thus requiring top quality equipment to be successfully tested. Dynamic tests using ambient vibrations have already been conducted on dams in the past [(Deinum et al., 1982), (Clough et al., 1987), (Darbre et al., 2000; Hall, 1988) (Proulx et al., 2001)], often as an addition to forced vibration campaigns. In recent years, the performance of these tests on dams with the aim of calibrating and validating numerical models and structural assumptions became more common [(Baris Sevim et al., 2013), (Calcina et al., 2014), (García-Palacios et al., 2016), (Abdulamit et al., 2017)], even leading to the implementation of vibration-based monitoring systems relying solely in background excitation and trustworthy measuring and acquisition equipment.

In this context, this chapter focuses on a set of ambient vibration tests performed on six Portuguese concrete dams with different typologies, ages and stiffness characteristics, with the aim of getting better sensitivity to the problems raised by the very unfavourable signal-to-noise ratios verified during the dynamic testing of dams, as well as to better understand the level of accuracy that can be achieved in such applications. The tests were performed in four arch dams with different heights (Alto Lindoso dam – 110 m; Santa Luzia dam – 76 m; Bouçã dam – 63 m; Caldeirão dam – 39 m), in an arch-gravity dam (Castelo do Bode dam – 115 m) and in a multiple arch dam with three arches (Aguieira dam – 89 m). Most of these dams are located in central Portugal, as presented in Figure 4.1, while Alto Lindoso dam is located in the northern border with Spain.

1 - Alto Lindoso dam (heigth: 110m; crown length: 297m)

2 - Caldeirão dam (heigth: 39m; crown length: 122m)

3 - Santa Luzia dam (heigth: 76m; crown length: 178m)

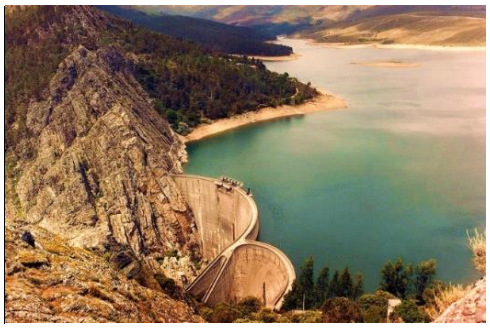

4 - Bouçã dam (heigth: 63m; crown length: 175m)

5 - Castelo do Bode dam (heigth: 115m; length: 402m)

6 - Aguieira dam (heigth: 89m; crown length: 400m)

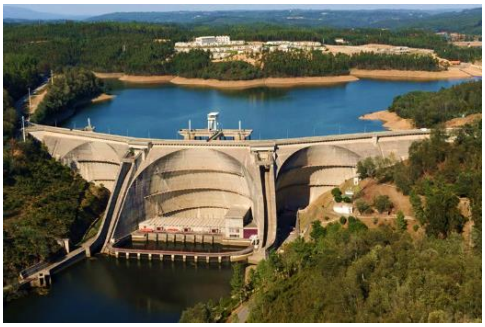

Figure 4.1 –Position of the whole set of tested dams in the map of Portugal (Google) followed by respective pictures (EDP).

In the next section, broad considerations are made about the procedure and equipment generally used in ambient vibration tests, and more specifically in the tested set of dams. Between sections 4.3 and 4.8 each of the six structures and test procedures are introduced separately and the databases collected during the ambient vibration tests are processed with the identification algorithms presented in chapter 3. Natural frequencies, damping ratios and respective standard deviation values, as well as mode shapes, are obtained for all the identified vibration modes.

In section 4.9, the data obtained from the ambient vibration tests performed in Alto Lindoso and Bouçã arch dams, in which force balance accelerometers were used to measure accelerations, will be numerically polluted with increasing levels of noise. A comparison between the results obtained from the modal identification of these structures through the analysis of the measured data and through the analysis of data simulating characteristic levels of noise associated with different types of accelerometers, such as piezoelectric and MEMS, is presented after the procedure used to simulate the added noise.

4.2. EXPERIMENTAL PROCEDURE AND EQUIPMENT

In the following section, general considerations are made about the procedure to use when performing ambient vibration tests. Additionally, specifications about the procedure and equipment used in the ambient vibration tests of the dams referred in the previous section are described.

Since no input is intentionally imposed on the structure when performing an ambient vibration test and there is no need to measure the input actually imposing on the structure the vibrations to be measured during the test, the experimental procedure to follow is a little simpler than the one used in forced vibration tests, using shakers or instrumented hammers (Santos, 2016).

In this sense, the test generally consists on measuring the structure response under ambient noise, using one or more reference sensors, at fixed positions, together with a set of moving sensors, placed at different measuring points along the structure, in different setups. The number of instrumented points is conditioned by the spatial resolution needed to appropriately characterize the shape of the most relevant vibration modes (which can be anticipated through numerical modelling or the study of similar structures tested before), while the reference points must be conveniently far from the corresponding nodal points. Furthermore, the number of sensors to distribute between the reference and moving sets depends on the size of the structure to be studied and on the number of sensors available to perform the test. For instance, if only two sensors were available, one of them must be used as reference, while the other moves along the structure. When performing tests on smaller structures, with no important constraints on the number of sensors available, it is sometimes possible to cover the entire measuring grid using all the sensors as references (no moving sensors), which may save an important amount of time.

The sampling frequency and the length of the time series collected represent very important characteristics of the test in terms of data acquisition, since they will limit the amount and quality of the information available in the recorded time series. In the case of the sampling frequency, for instance, if a value of 100 Hz is used, it means 100 measuring points are collected from each sensor during one second. The selected sampling frequency can be conditioned by the characteristics of the equipment adopted or by the characteristics of the studied structure. In order to avoid aliasing errors (Maia & Silva, 1997), it should be higher than at least two times the highest frequency captured by the sensors or the cutting frequency of analog low pass filters that might be included in the measuring chain. Also, since only the modes with a frequency lower than one half of the

sampling frequency are observable, the sampling frequency will limit the number of modes that can be identified and thus should be chosen accordingly.

On the other hand, the length of the time series collected in each setup may have an important influence on the estimates of modal parameters, especially relevant on the random error of modal damping ratio estimates. The optimal length depends on the lowest natural frequency of the structure, on the modal damping ratios, on the signal-to-noise ratio and also on the identification algorithm to be adopted during the processing of the collected data (parametric methods can provide better results with shorter time series than for instance the FDD method) (Magalhães, 2010). Consequently, the best length of the time series to collect, will always depend on the structure and equipment to be used during the test, but above all, it will depend on the time available to perform the test. In (Cantieni, 2005), a rule of thumb is suggested, stating the length of the time windows acquired should be 1000 to 2000 times the period of the structure's fundamental natural frequency. However, due to time constraints, lengths of about just 180 times the period of the mode with the lowest frequency have been used in (Magalhães, 2010) with very good results. In the present application, good results have been obtained with time windows 1800 to 7200 times the length of the period of the fundamental frequency, which are associated with time series durations from 15 to 60 minutes.

Regarding the equipment necessary to perform the test, the most important components are the sensors. Though displacements, velocities or even strains can be measured, sensors measuring accelerations are the most commonly used. Accelerometers based in many different working principles are available (MicroEletroMechanical, piezoelectric or capacitive) but force-balance ones are probably the most suited for civil engineering applications, since they present a measuring range starting at DC (meaning they are sensitive to very low natural frequencies, such as the 0.35 Hz presented in the wind turbine studied in (Oliveira et al., 2018)), they are conceived to be insensitive to high-frequency vibrations and their high sensitivity and low noise make them appropriate to measure the low levels of vibration usually observed during ambient vibration tests, especially the ones performed in dams, which are massive structures commonly located in remote places, far from main sources of vibration.

Traditionally, the continuous electrical signal produced by each sensor is transported by electrical cables to a central acquisition system (Figure 4.2), which comprehends analog-to-digital converters that transform the continuous signals into discrete sequences of numbers to be saved and later processed in a computer. The number of bits is the most important characteristic of the analog-to-

digital converter since it is directly related with the measurement resolution (the resolution is approximately equal to the measuring range divided by two to the power of the number of bits). Additionally, the acquisition system may also contain low pass filters or signal amplifiers to improve the quality of the digital signal.

An alternative to the use of central acquisition systems and long electrical cables is based on a set of portable autonomous recorders (Figure 4.2). These devices are constituted by a very sensitive internal or external tri-axial force balance accelerometer, an analog-to-digital converter with 24 bits, a rechargeable battery that enables autonomy for an entire day of tests, and an external GPS sensor to ensure that several units can work synchronously at different measuring points. Additionally, the recorded time series of accelerations are saved in a removable compact flash card that allows a fast download of the acquired data to a computer after the test (Cunha et al. 2007). The recorders must be programmed before the test to acquire a certain number of time series (one per recorder and setup) with defined length and time interval between consecutive setups, which are used to change the position of moving recorders, in the case there are any.

The ambient vibration tests that will be described in sections 4.3 to 4.8 were performed using either a central acquisition system or the portable recorders, depending on the characteristics of each structure and test. It should be mentioned that the central acquisition system range is limited to relatively short distances (maximum length: 150 meters) and that the portable recorders must be used open-air, for synchronization.

Figure 4.2 – Sensors positioned during tests: uniaxial accelerometer with cable (on the left); tri-axial recorder with GPS antenna (on the right).

4.3. ALTO LINDOSO DAM

4.3.1. DAM DESCRIPTION AND AMBIENT VIBRATION TEST

The Alto Lindoso arch dam, presented in Figure 4.3, is located in the north of Portugal, in the municipality of Ponte da Barca. This concrete double arch dam is embedded in a narrow valley zone, in the Lima river, allowing a useful storage of 347 million cubic meters of water (EDP), since 1992 when it started operating. The dam is 110 meters high and its crest, which is 297 meters long, constitutes a road link between the two banks of the river. A hydroelectric power plant was built 70 meters south from the dams left abutment. The plant has a total installed capacity of 630 MW, assured by two vertical Francis turbines that operate at 214.3 rpm (3.57 Hz).

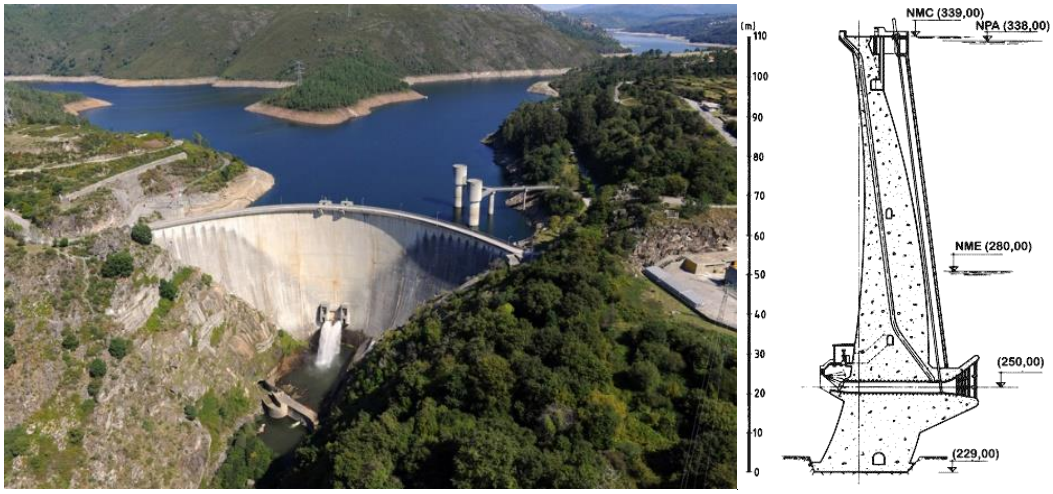

Figure 4.3 – Alto Lindoso arch dam: frontal view (EDP) and cross section (CNPGB).

The ambient vibration test of Alto Lindoso arch dam was performed on the 22nd of February 2017 and it was based on the use of ten GSR-24 recorders from Geosig equipped with internal tri-axial force-balance accelerometers. With the purpose of identifying as many vibration modes as possible, and taking into account the large dimensions of the structure, a test grid was prepared considering 21 measuring points, corresponding to the dam's 21 concrete blocks. To assure the measuring of accelerations in every point of the defined grid, four setups were considered, during which 6 accelerometers acted as references and the other 4 accelerometers as moving sensors. The six points marked with red dots in Figure 4.4 were used as references, while the other 15 points, marked with blue dots, were measured by the moving accelerometers.

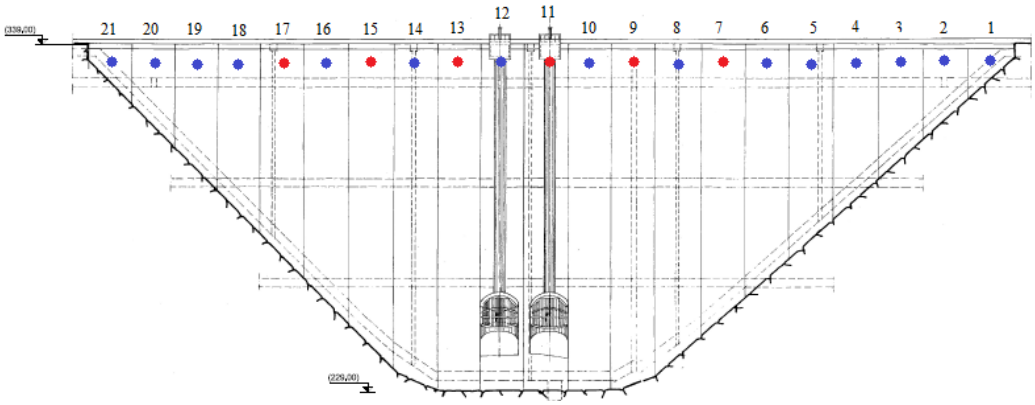

Figure 4.4 – Alto Lindoso dam: test layout.

Each setup had a duration of 58 minutes, after which a window of 2 minutes allowed for the redistribution of the moving accelerometers, summing four measuring hours. A sampling rate of 100 Hz was used during the acquisition which was later decimated to 50 Hz. The position of each accelerometer (S1 to S10) during each setup is presented in Table 4.1, using the numbering defined in Figure 4.4. In the fourth setup, the accelerometer S1 was positioned between blocks 11 and 12, thus this measuring point was called 11.5. During the test, the water level in the reservoir was 322 m (elevation from sea level).

Table 4.1 – Accelerometer disposition during each setup of the ambient vibration test

Setup	*S1*	*S2*	*S3*	*S4*	*S5*	*S6*	*S7*	*S8*	*S9*	*S10*
1	21	20	19	18	17	15	13	11	9	7
2	16	14	12	10	17	15	13	11	9	7
3	8	6	5	4	17	15	13	11	9	7
4	11.5	3	2	1	17	15	13	11	9	7

4.3.2. MODAL PARAMETERS IDENTIFICATION

The time series of accelerations measured during the ambient vibration test of Lindoso dam were processed with two of the modal identification algorithms that have been implemented in Matlab during the development of the present work (presented in Chapter 3). First, the Peak Picking method was used to have quick and rough estimates of the most relevant natural frequencies. The obtained averaged normalized power spectrum density function (ANPSD) is presented in Figure 4.5. The peaks corresponding to the identified vibration modes are marked with orange circles, while a black circle marks the peak corresponding to the first harmonic of the turbine rotation frequency (7.14Hz).

A considerable number of peaks are observed between 3 and 12 Hz, with the first natural frequency of the dam being located at around 3.55 Hz. Then the SSI-Cov method was applied to obtain more accurate estimates of natural frequencies and mode shapes, as well as damping values. This method was applied to each setup and model orders between 20 and 90 were considered. The stabilization diagram obtained from the third setup is presented in Figure 4.6, in which several vertical alignments of poles are clear. The alignments corresponding to the identified vibration modes were marked with blue dashed lines.

It is worth noting that all the peaks in the ANPSD function and all the alignments in the stabilization diagram were studied and the mode shapes obtained from each of them were analysed. The final set of identified vibration modes correspond to those presenting good agreement between the results obtained from both identification methods and presenting as well realistic mode shapes.

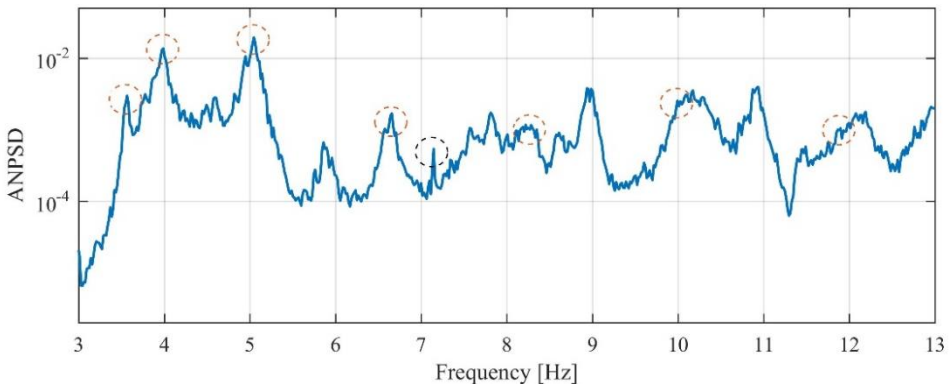

Figure 4.5 – ANPSD of Alto Lindoso arch dam ambient vibration test.

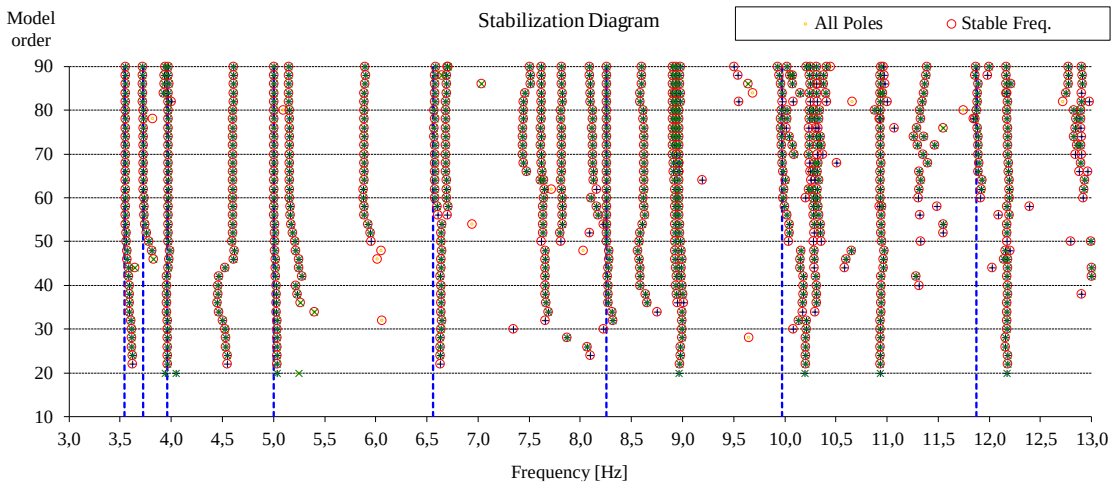

Figure 4.6 – Alto Lindoso arch dam stabilization diagram.

The first 7 vibration modes were identified and their modal properties, including natural frequencies and damping values, as well as the description of mode shapes, are presented in Table 4.2. These results correspond to the average of the values associated with the selected stable poles across the four setups. In the case of the first symmetric mode, two different frequencies that are associated with the same mode shape were identified (modes 2a and 2b), depending on the structure vibration level.

Table 4.2 – Modal parameters for Alto Lindoso dam first 7 vibration modes

Mode	f_{mean} [Hz]	f_{std} [Hz]	ξ_{mean} [%]	ξ_{std} [%]	Description
1	3.546	0.0045	1.19	0.12	Antisymmetric
2 a	3.752	0.0257	2.85	0.69	Symmetric
2 b	3.963	0.0105	2.16	0.28	Symmetric
3	5.008	0.0170	1.59	0.36	Symmetric
4	6.563	0.0094	1.31	0.17	Antisymmetric
5	8.255	0.0133	1.35	0.17	Symmetric
6	9.970	0.0279	1.30	0.27	Antisymmetric
7	11.873	0.0196	1.44	0.19	Symmetric

Table 4.2 presents also the standard deviation values for natural frequencies and damping, which were obtained using the method presented in (Reynders et al., 2008) and (Dohler& Mevel, 2013), allowing a better understanding of the accuracy achieved in the identification. For instance, while the first and fourth modes show the smaller standard deviation values associated with its frequency and damping estimates, the estimates associated with the third vibration mode, which was not identified in all the performed setups, seems to be the less accurate ones, presenting the highest standard deviation values.

Very clear and well-defined modal shapes were achieved for the 7 identified modes, which are presented in Figure 4.7. The first mode is antisymmetric and the second one is symmetric. From the third to the eighth mode, the configurations are alternatively symmetric and antisymmetric.

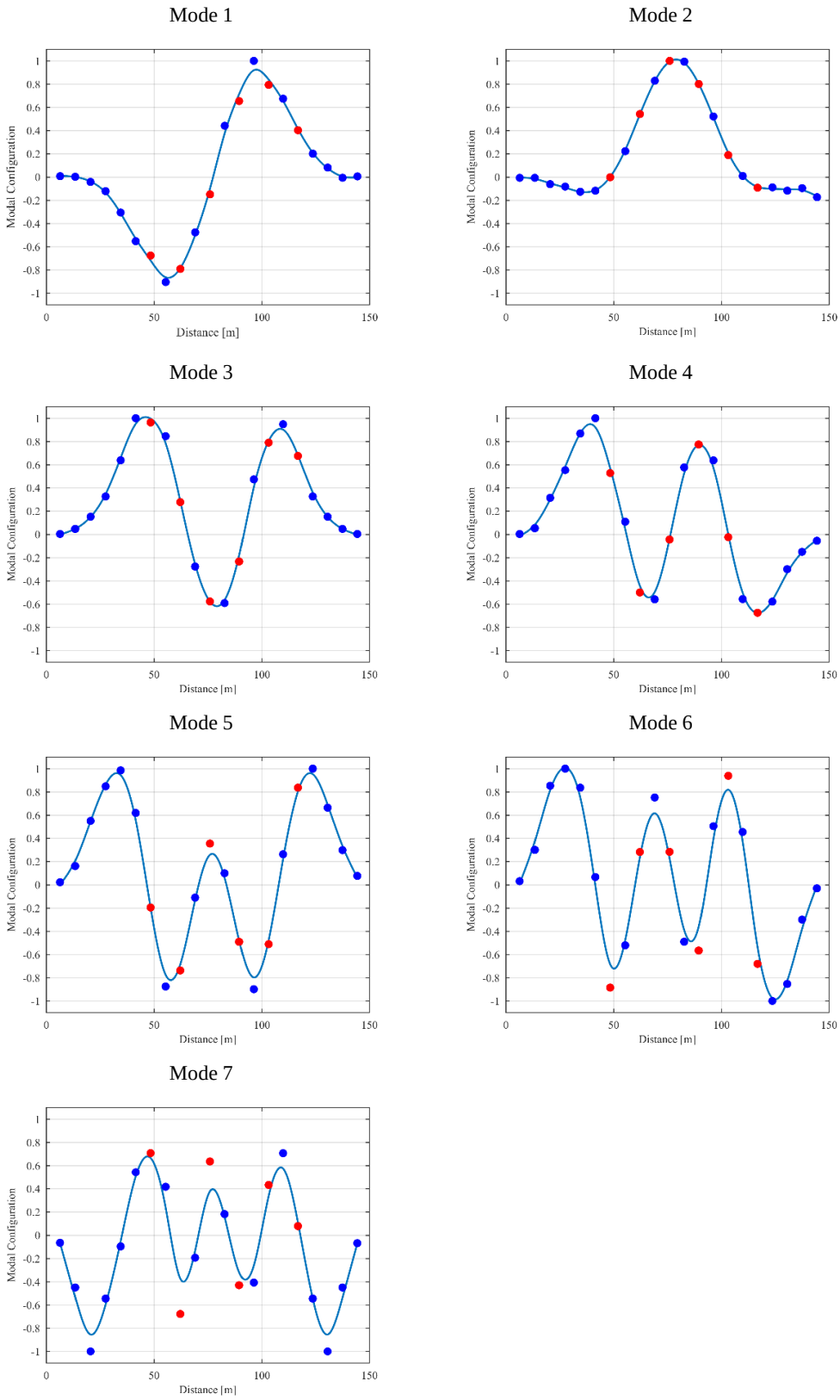

Figure 4.7 – Modal shapes of the first 7 modes of Alto Lindoso arch dam: curve fitted to the estimated modal coordinates.

4.3.3. COMPARISON WITH RESULTS FROM FORCED VIBRATION TEST AND NUMERICAL MODEL

In (Câmara et al., 1993) the forced vibration test performed in Alto Lindoso dam in 1992 is presented. When the test was performed, the level in the reservoir was 326 m (elevation from sea level), only 4 meters higher than the level registered during the ambient vibration test performed in 2017, presented above. Along with the forced vibration test, the results obtained from a finite element model of the dam are also presented by (Câmara et al., 1993). In this numerical model the concrete was assumed elastic, the rock mass foundation was also assumed elastic isotropic, the foundation was assumed massless and the effect of the reservoir on the dam was assumed to be given by the Westergaard added mass scheme (Westergaard, 1933). The natural frequencies obtained by the recent ambient vibration test, and the forced vibration test and numerical model developed in 1992 are presented in Table 4.3 for comparison. A close match was revealed between the natural frequencies and mode shapes obtained from both tests and the numerical modelling.

Table 4.3 – Natural frequencies obtained by: ambient vibration test (2017); forced vibration test (1992); numerical model (1992)

Mode	Ambient Vibration Test [Hz]	Forced Vibration Test [Hz]	Numerical Model [Hz]
1	3.55	3.45	3.43
2	3.75 / 3.96	3.80	3.93
3	5.01	5.30	5.03
4	6.56	6.60	6.51

4.4. BOUÇÃ DAM

4.4.1. DAM DESCRIPTION AND AMBIENT VIBRATION TEST

The Bouçã arch dam, presented in Figure 4.8, is located in central Portugal, in the municipality of Pedrogão Grande. This concrete double arch dam allows a useful storage of about 8 million cubic meters of water (EDP) in Zêzere river, a tributary of Tagus river. The dam, which started operating in 1955, is 63 meters high and its crest, which is 175 meters long, mostly constitutes the structure spillway. The hydroelectric power plant that was built downstream is installed with a capacity of 44 MW, assured by two Francis turbines that operate at 214.3 rpm (3.57 Hz).

The ambient vibration test of the Bouçã arch dam was performed on the 12th of June 2018 and it was based on the use of nine uniaxial force-balance accelerometers that were radially disposed along the dam's upper visit gallery. An acquisition system using cables was used, thus every measuring point had its own fixed sensor which may be used as reference during the processing of the measured data. The farthest sensor was nearly 65 m away from the acquisition system. The prepared test grid considered 9 measuring points on the dam's 9 central concrete blocks, which correspond to the group of blocks that are crowned by the spillway. The 9 measuring points are marked with blue dots in the scheme of the structure presented in Figure 4.9.

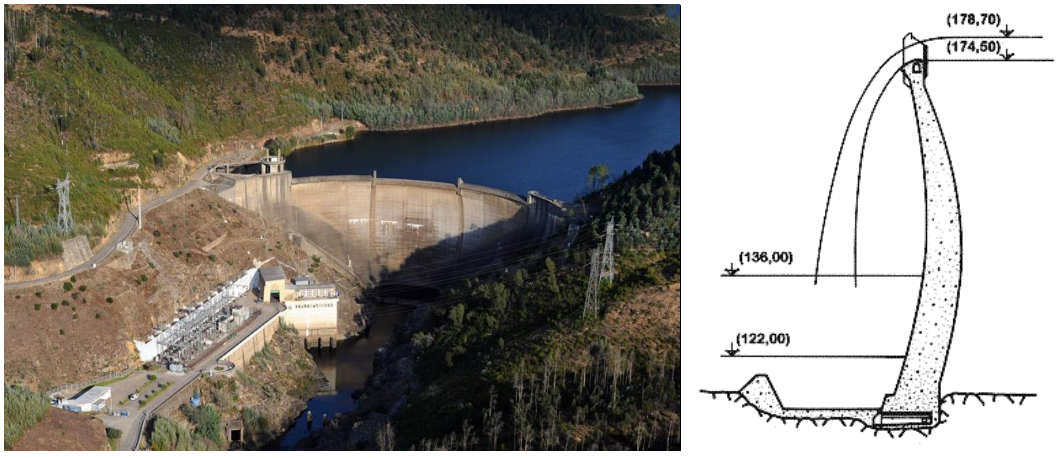

Figure 4.8 – Bouçã arch dam: frontal view (EDP) and cross section (CNPGB).

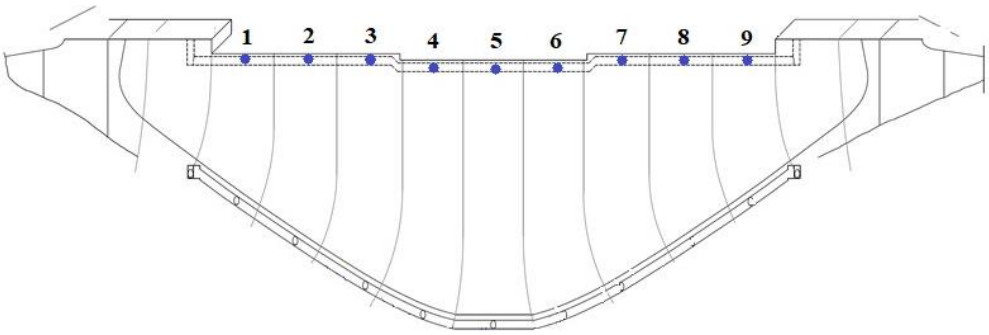

Figure 4.9 – Bouçã dam: test layout.

To assure a good characterization of the structure's dynamic behaviour 5 similar setups with a duration of 13 minutes were performed. A sampling rate of 100 Hz was used during the acquisition, which was later decimated to 50 Hz. The water level in the reservoir during the test was 174.7 m (elevation from sea level).

4.4.2. MODAL PARAMETERS IDENTIFICATION

The acceleration time series measured during the ambient vibration test of Bouçã dam were processed with two of the modal identification algorithms presented in Chapter 3. First, the Peak Picking method was used to have quick and rough estimates of the most relevant natural frequencies. The obtained averaged normalized power spectrum density function (ANPSD) is presented in Figure 4.10, where orange circles were used to mark the peaks corresponding to identified vibration modes. A considerable number of peaks are observed between 3 and 12 Hz, with the first natural frequency of the dam being located at around 3.30 Hz.

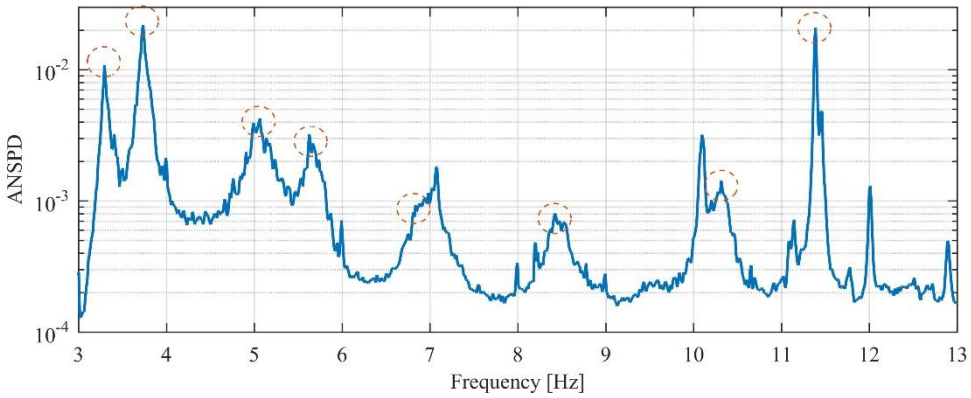

Figure 4.10 – ANPSD Bouçã arch dam ambient vibration test.

Then, the SSI-Cov method was applied to obtain more accurate estimates of natural frequencies and mode shapes, as well as damping values. This method was applied to each setup and model orders between 20 and 80 were considered. The stabilization diagram obtained from the third setup data is presented in Figure 4.11, in which vertical alignments of poles are clearly defined. The alignments corresponding to the identified vibration modes were marked with blue dashed lines.

The first 8 vibration modes were identified and their modal properties, including natural frequencies and damping values, as well as the description of mode shapes, are presented in Table 4.4. The presented results correspond to the average of the values associated with stable poles selected across the five setups.

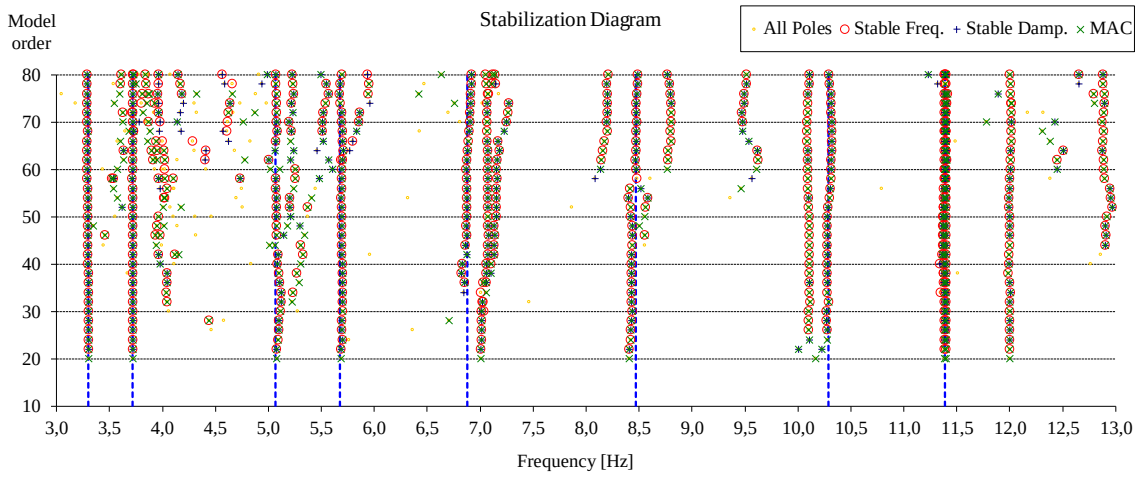

Figure 4.11 – Bouçã arch dam stabilization diagram.

Table 4.4 – Modal parameters for Bouçã dam first 8 vibration modes

Mode	f_{mean} [Hz]	f_{std} [Hz]	ξ_{mean} [%]	ξ_{std} [%]	Description
1	3.296	0.0069	1.464	0.206	Antisymmetric
2	3.733	0.0058	1.308	0.161	Symmetric
3	5.074	0.0342	3.203	0.605	Symmetric
4	5.676	0.0169	1.816	0.298	Antisymmetric
5	6.875	0.0342	1.782	0.504	Symmetric
6	8.452	0.0204	1.566	0.254	Antisymmetric
7	10.289	0.0236	0.999	0.256	Symmetric
8	11.394	0.0336	1.942	0.486	Antisymmetric

Table 4.4 presents as well the standard deviation values for natural frequencies and damping, which were obtained using the method presented in (Reynders et al., 2008) and (M. Döhler & Mevel, 2013), allowing a better understanding of the accuracy achieved in the identification. For instance, while the first and second modes show the smaller standard deviation values associated with its frequency and damping estimates, the estimates of the third vibration mode, which was not identified in all the studied setups, seems to be the less accurate ones, presenting the highest standard deviation values.

Very clear and well-defined mode shapes were achieved for the 8 identified modes, which are presented in Figure 4.12. Like in the case of Alto Lindoso dam, the first mode is antisymmetric and the second one is symmetric, and from the third to the eighth mode, the configurations are alternatively symmetric and antisymmetric.

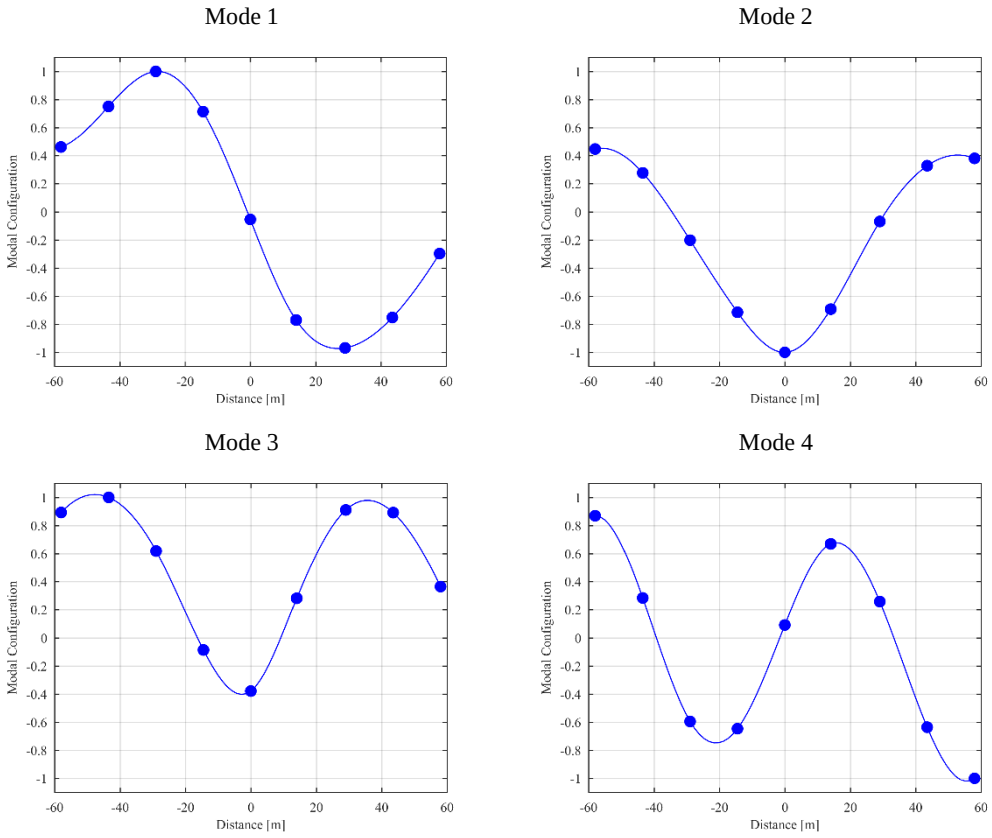

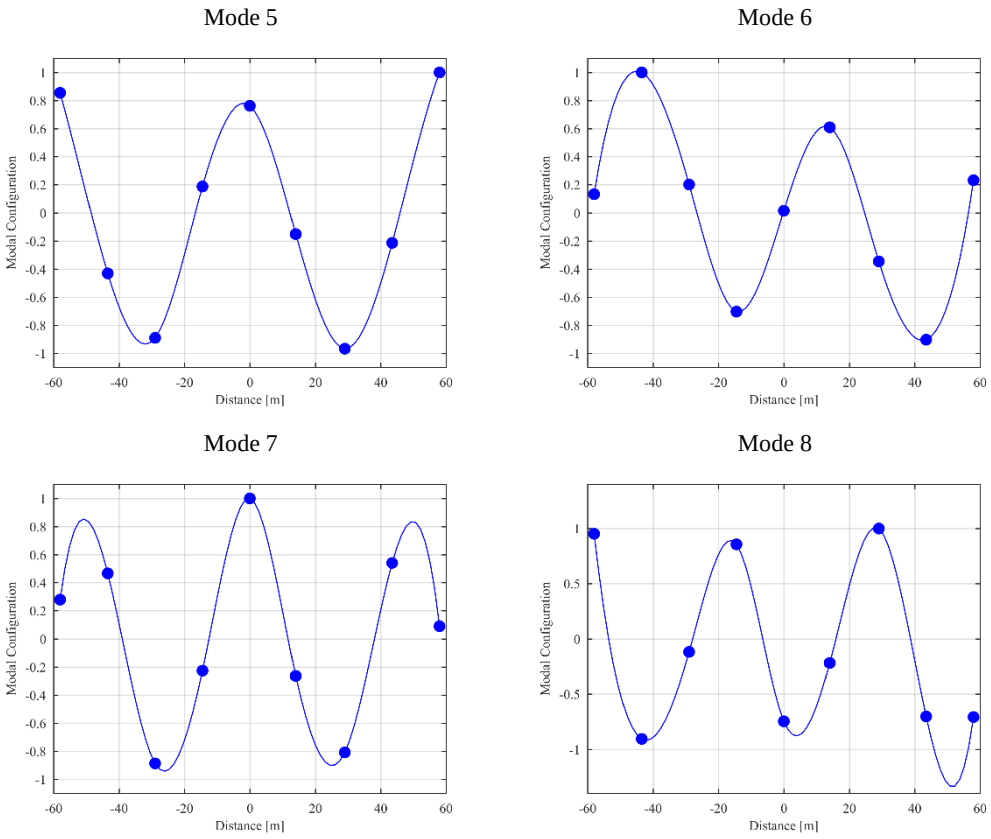

Figure 4.12 – Modal shapes of the first 8 modes of Bouçã arch dam.

4.5. CASTELO DO BODE DAM

4.5.1. DAM DESCRIPTION AND AMBIENT VIBRATION TEST

The Castelo do Bode dam, presented in Figure 4.13, is located in central Portugal, between the municipalities of Tomar and Abrantes. This concrete arch-gravity dam allows the storage of 902 million cubic meters of water (EDP) in the Zêzere river, downstream from Bouçã dam. The dam is 115 meters high and its 402 meters long crest constitutes a road link between the two banks of the river. This structure started operating in 1951 and nowadays is used for energy production, flood control, recreational events and water supply for Lisbon, the country's capital city. The hydroelectric power plant that was built downstream has a total installed capacity of 159 MW, assured by three vertical Francis turbines that operate at 214.3 rpm (3.57 Hz).

The ambient vibration test of Castelo do Bode dam was performed on the 17th of July 2018, when the water level in the reservoir was 116.60 m from sea level, and it was based on the use of ten GSR-24 recorders from Geosig equipped with internal tri-axial force-balance accelerometers. A test grid was prepared considering 10 measuring points, corresponding to the center of 10 concrete blocks, including the spillway blocks (measuring points 8 and 9). A single measuring layout was used, thus all the accelerometers acted as references, as represented by the red dots in Figure 4.14. The test had a total duration of two hours, divided in eight 13-minute setups. A sampling rate of 100 Hz was used during the acquisition, which was later decimated to 50 Hz. Between the fifth and sixth setups, and then between the seventh and the eighth setup, the recorder firstly positioned in measuring point "1" was moved to record accelerations in the upper visit gallery, respectively below positions "4" and "6".

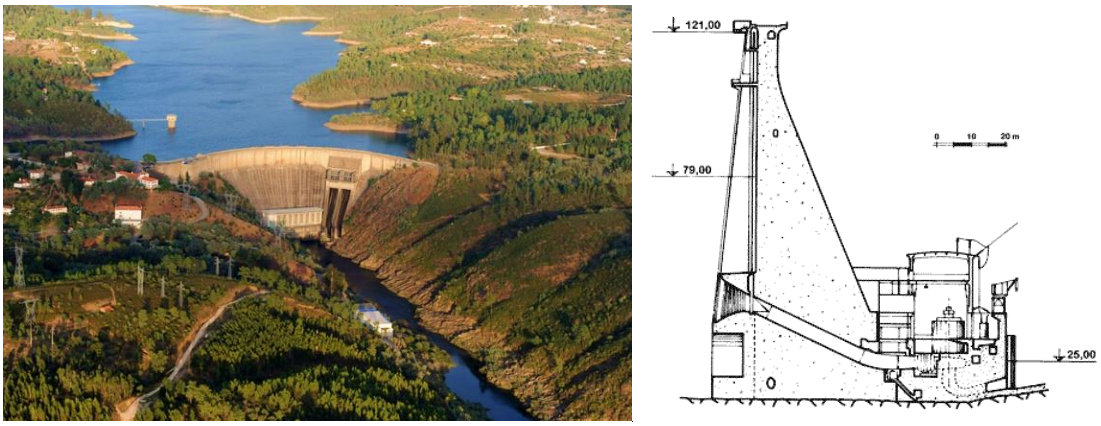

Figure 4.13 – Castelo do Bode dam: aerial view (EDP) and cross section (CNPGB).

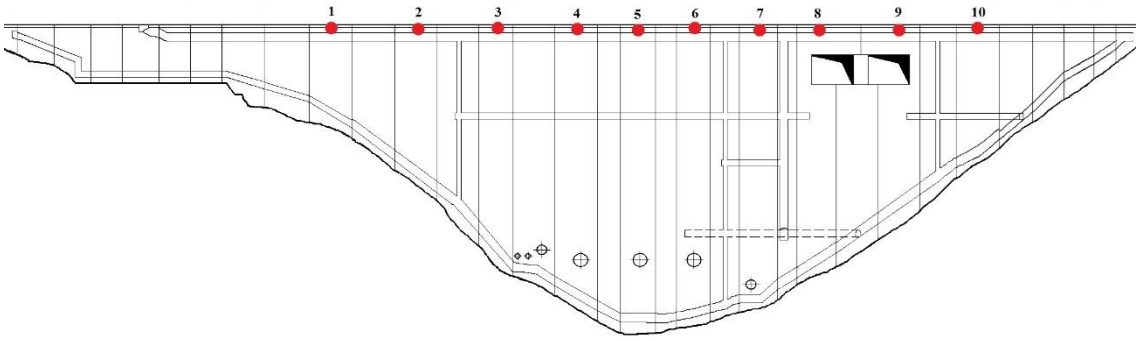

Figure 4.14 – Castelo do Bode dam: test layout.

4.5.2. MODAL PARAMETERS IDENTIFICATION

A first evaluation of the structure's natural frequencies was performed using the Peak Picking method. After the evaluation of the auto-spectra obtained from the time series measured in different points, an averaged normalized power spectral density (ANPSD) function was obtained. The ANPSD function is presented in Figure 4.15. The first few vibration modes of the structure appear between 3 and 10 Hz, with important frequency content appearing as well between 14 and 17 Hz. The first peak observable in the representation of the ANPSD function is very thin, since it corresponds to the rotation frequency of the turbines operating in the power production unity nearby (214 rpm ~3.57 Hz), mentioned in the previous section. The turbines operated during the entire test, so this parasite frequency and its harmonics are present in all the recorded setups. The first harmonic (7.14 Hz) is barely observable in Figure 4.15, but the third and fourth harmonics are easily distinguishable at 10.72 Hz and 14.29 Hz. Other thin peaks observable between 11 and 14 Hz are probably due to other machinery operating in the nearby power plant, which stands at the bottom of the dam (see left part of Figure 4.13).

After the first evaluation performed with the Peak-Picking method, the SSI-Cov method was applied to obtain more accurate estimates of natural frequencies as well as mode shapes and damping values. Similar stabilization diagrams were obtained from the time series recorded during the 8 setups. The stabilization diagram obtained from the third setup is presented in Figure 4.16. Excluding the first two modes, higher model orders were needed until clear and stable vertical alignments were achieved in this case, when compared to the applications presented in the previous sections. In this sense, model orders between 70 and 150 had to be considered. The alignments corresponding to the identified vibration modes were marked with blue dashed lines.

It is worth noting that all the peaks in the ANPSD function and all the alignments in the stabilization diagram were studied and the mode shapes obtained from each of them were analysed. The final set of identified vibration modes correspond to those presenting good agreement between the results obtained from both identification methods and presenting as well realistic mode shapes.

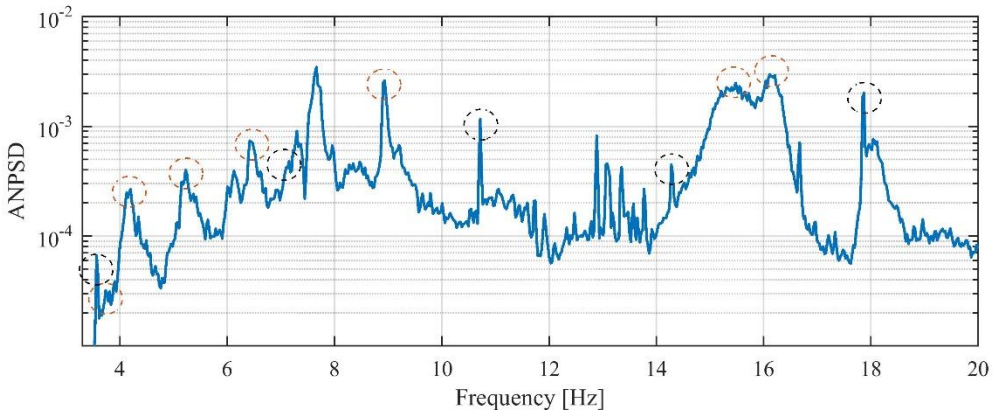

Figure 4.15 – ANPSD of Castelo do Bode dam ambient vibration test (orange circles marking the identified modes).

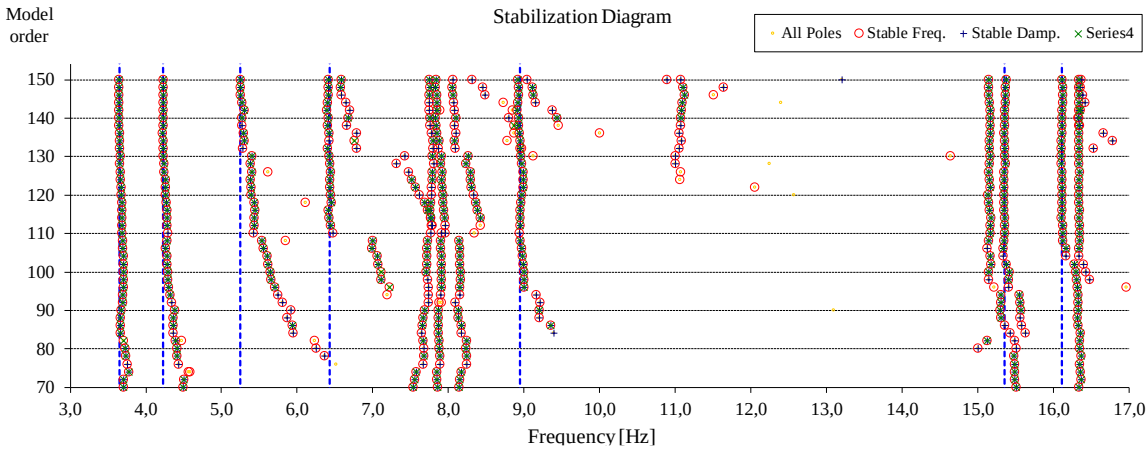

Figure 4.16 – Castelo do Bode arch dam stabilization diagram.

Seven vibration modes were identified and its modal properties, including natural frequencies and damping values, as well as the description of mode shapes, are presented in Table 4.5. The results correspond to the average of the values associated with the selected stable poles for the recorded setups. The first five vibration modes were identified between 3 and 10 Hz, as it had been anticipated by analysis of the ANPSD function and two more vibration modes were identified at 15.36 Hz and 16.11 Hz.

Table 4.5 – Modal parameters of Castelo do Bode dam first 7 vibration modes

Mode	f_{mean} [Hz]	f_{std} [Hz]	ξ_{mean} [%]	ξ_{std} [%]	Description
1	3.648	0.0204	6.415	0.621	Global
2	4.230	0.0145	3.273	0.313	Left side of the spillway
3	5.236	0.0326	3.069	0.639	Global
4	6.430	0.0409	2.188	0.648	Left side of the spillway
5	8.950	0.0289	1.300	0.418	Left side of the spillway
6	15.36	0.0224	1.778	0.171	Global
7	16.11	0.0203	1.145	0.151	Left side of the spillway

Table 4.5 presents as well the averaged standard deviation values for natural frequencies and damping ratios, which were obtained with the aim of better understanding the accuracy achieved in the identification. For instance, the third and fourth modes, which show the higher standard deviation values associated with natural frequencies, among the group of identified modes, correspond to the modes for which higher model orders were needed. On the other hand, the second vibration mode, whose alignment in the stabilization diagram is stable since the first model orders, presents the lower standard deviation associated with its natural frequency.

Due to the asymmetric characteristics of the structure and the extra localized stiffness provided by the two main spillways (see Figure 4.13 and Figure 4.14), a few local modes were identified, corresponding to configurations where the modal ordinates on positions around the spillway are very close to each other, while the other part of the configuration corresponds to a shape with rising number of concavities from one mode to the next. In the case of the global modes, the first two shapes identified for the other tested dams (see Figure 4.7), with one and two concavities respectively, were not identified. Additionally, a mode shape similar to the one presented by the first mode was identified around 8 Hz, which may correspond to a second order mode with the same configuration on the top, but different configurations at different height levels. Therefore, recordings synchronized with the ones performed in the crown would have to be made in the dam's galleries, to unmistakably identify this mode and its mode shape.

The mode shapes of the seven identified vibration modes are presented in Figure 4.20. The first, third and sixth modes corresponds to global modes, while the second, fourth, fifth and seventh correspond to modes associated with deflection of the left side of the dam.

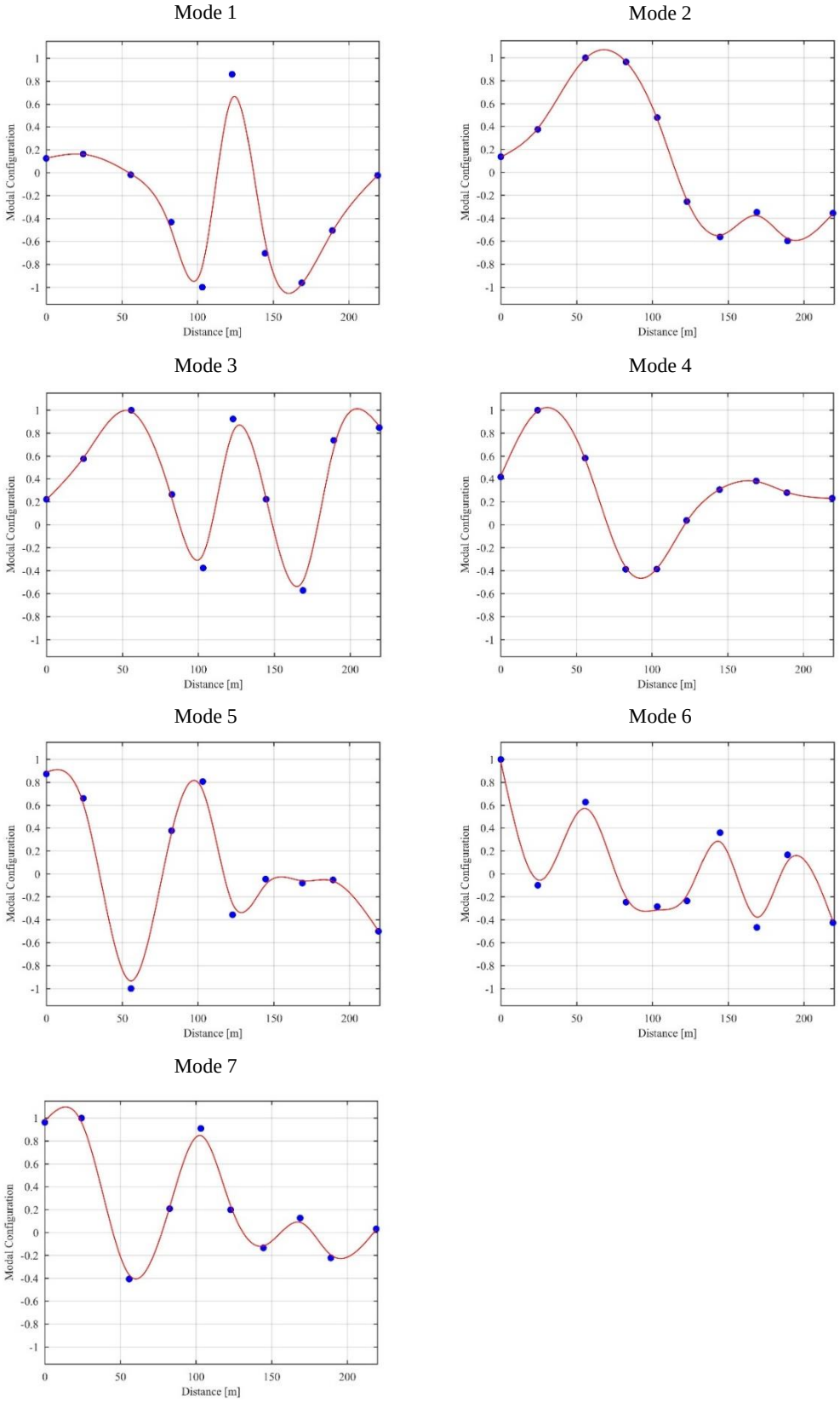

Figure 4.17 – Modal shapes of the 7 identified modes of Castelo do Bode dam.

4.6. CALDEIRÃO DAM

4.6.1. DAM DESCRIPTION AND AMBIENT VIBRATION TEST

The Caldeirão arch dam, presented in Figure 4.18, is located in the interior of Portugal, in the municipality of Guarda, just 50 km away from the border with Spain. This concrete double arch dam is operating since 1994 with the main purposes of energy production and to supply water to the region. The dam is just 39 meters high and its 122 meters long crest is mostly constituted by the dam spillway, even though there is a viaduct over the dam that allows to cross the Ribeira do Caldeirão river by car. The hydroelectric power plant associated with the Caldeirão dam has a total installed capacity of 40 MW, assured by vertical Francis turbines that operate at 333.3 rpm (5.56Hz).

Figure 4.18 – Caldeirão dam: aerial view (EDP) and cross section (CNPGB).

The ambient vibration test of Caldeirão dam was performed on the 2nd of June 2017 and it was based on the use of seven uniaxial force-balance accelerometers that were radially disposed along the dam's top viaduct. The acquisition system using cables was used, thus every measuring point had its own fixed sensor which may be used as reference during the processing of the measured data, and the farthest sensor was just 32 meters away from the acquisition system. The test grid considered 7 measuring points corresponding to the position of the laminar pillars supporting the viaduct. The position of the 7 measuring points is marked with blue dots in the picture of the structure presented in Figure 4.19.

To assure a good characterization of the structure's dynamic behaviour 3 similar setups were performed. Each setup had a duration of 19 minutes. A sampling rate of 100 Hz was used during the acquisition.

Figure 4.19 – Caldeirão dam: test layout.

Additional measurements were performed with four GSR-24 recorders from Geosig equipped with internal tri-axial force-balance accelerometers, which were disposed in the same seven recording positions over the viaduct, as well as in the dam's upper visit gallery.

4.6.2. Modal Parameters Identification

The data recorded with the seven uniaxial accelerometers disposed along the dam's top viaduct was pre-processed with high-pass filtering and decimation from 100 to 50 Hz. The pre-processed data was then used to identify the structures modal properties, namely natural frequencies, damping values and mode shapes. For this, both the Peak-Picking and the SSI-Cov methods have been used. In this context, an Averaged Normalized Power Spectral Density function (ANPSD) has been calculated and represented in Figure 4.20. The first peak is only found around 9 Hz, and a few others appear between 9 and 20 Hz. The peaks corresponding to identified vibration modes are marked with orange circles.

From the application of the SSI-Cov method results the stabilization diagram presented in Figure 4.21. Few well-defined vertical alignments appear between 9 and 16 Hz, according to the position of the peaks identified through the ANPSD function. From 16 to 20 Hz many disperse poles appear, creating some poorly-defined vertical alignments. The alignments corresponding to the identified vibration modes were marked with blue dashed lines.

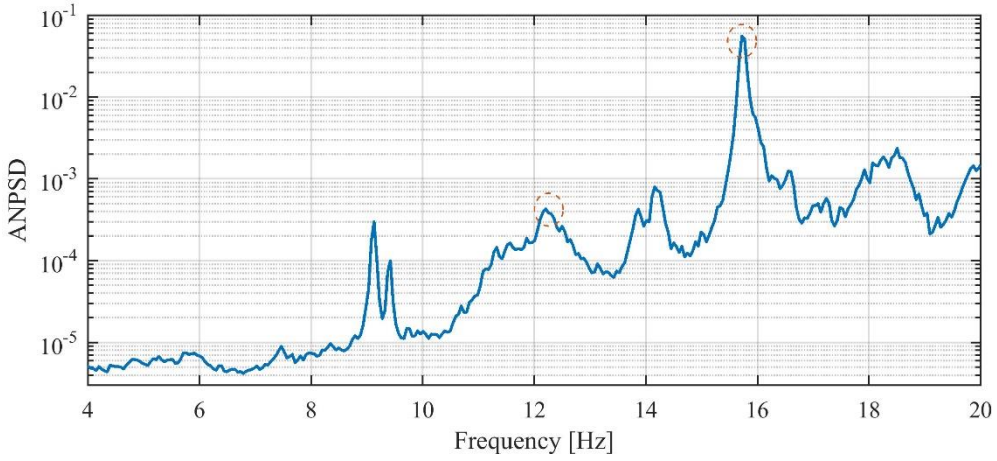

Figure 4.20 – ANPSD of Caldeirão dam ambient vibration test.

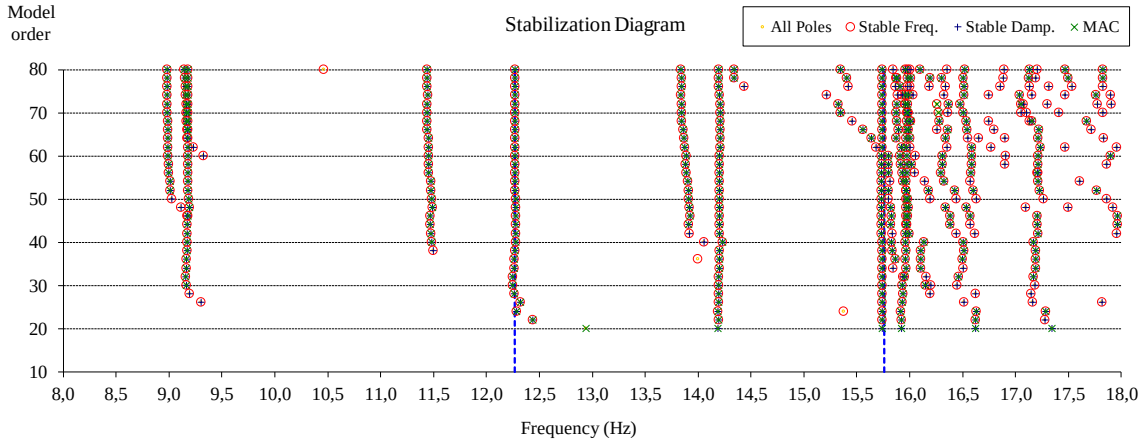

Figure 4.21 – Caldeirão dam stabilization diagram.

However, this analysis suggested that besides the vibration modes of the dam, vibration modes of the viaduct could be being identified as well, creating uncertainty in the identification process. In order to clarify which modes are really vibration modes of the dam, separating those of the viaduct, auto-spectra were calculated using time series measured by two sensors placed in the upper visit gallery, thus not suffering direct influence from the viaduct dynamic properties.

The two calculated auto-spectra are represented in Figure 4.22. Even though not being entirely clear, both auto-spectra obtained from the data recorded in the visit gallery show a couple of distinct peaks around 12.2 and 15.7 Hz, frequencies that were present in the stabilization diagram as well,

and therefore must correspond to vibration modes of the dam. Also around 14.1 Hz, a smaller peak may correspond to a different vibration mode. Nevertheless, this could still be due to the influence of the viaduct, thus this frequency ends up being discarded, along with all the other frequencies that had been previously identified, since neither of them may be assuredly associated with either the dam or the viaduct.

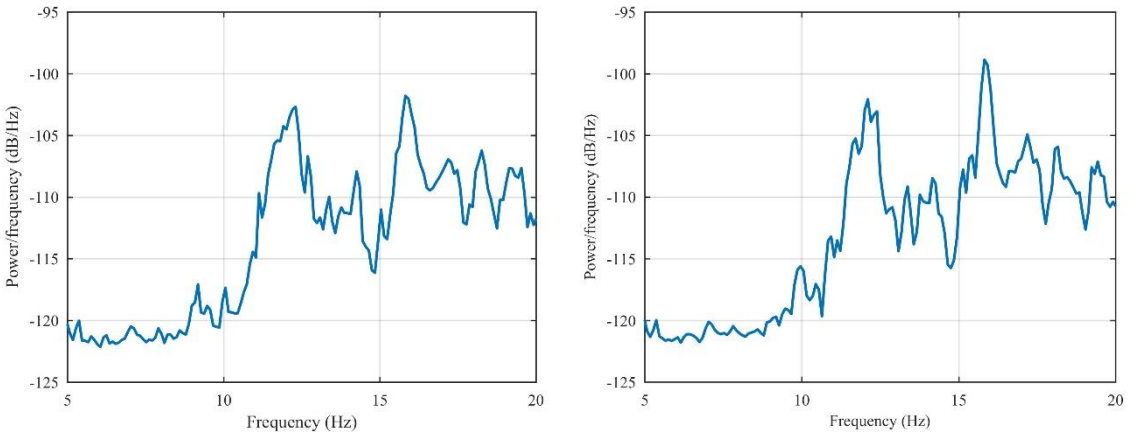

Figure 4.22 – Auto-spectra from time series recorded inside the upper visit gallery.

Finally, natural frequencies, damping values and respective standard deviation values associated with the two identified vibration modes are presented in Table 4.6. The * symbol used together with the ordering of these modes in Table 4.6 means to highlight these modes correspond to the first and second identified modes, but not necessarily to the dam's first and second modes. The mode shapes of the two identified modes are presented in Figure 4.23. These modes are antisymmetric and symmetric, respectively.

With these results, it was learned that besides the quite stiff connection between dam and viaduct, the majority of the sensors should have been placed in the dam's galleries

Table 4.6 – Modal parameters for Caldeirão dam first 2 vibration modes

Mode	f_{mean} [Hz]	f_{std} [Hz]	ξ_{mean} [%]	ξ_{std} [%]	Description
1*	12.265	0.0571	2.074	0.436	Antisymmetric
2*	15.759	0.0101	0.336	0.086	Symmetric

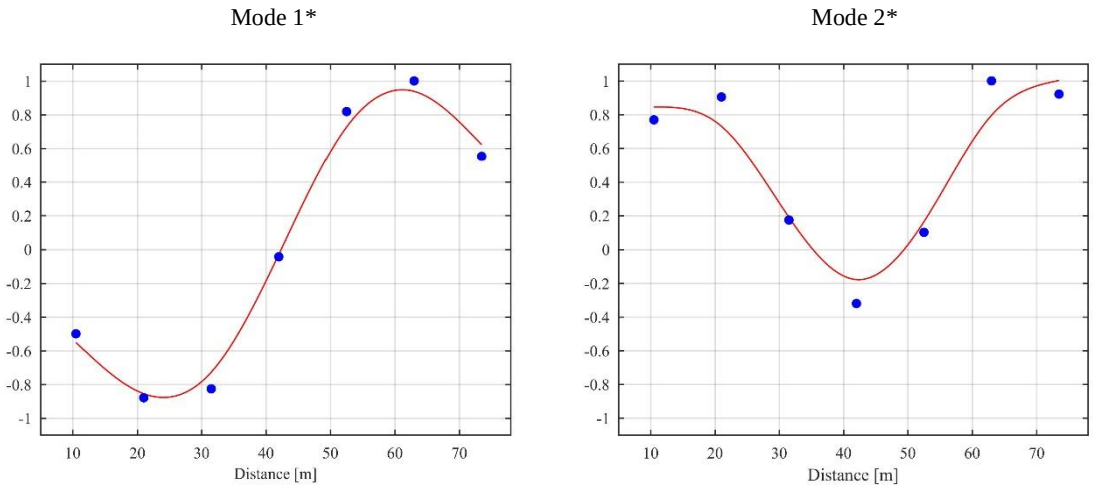

Figure 4.23 – Mode shapes of the identified modes of Caldeirão dam.

4.7. SANTA LUZIA DAM

4.7.1. DAM DESCRIPTION AND AMBIENT VIBRATION TEST

The Santa Luzia dam, presented in Figure 4.24, is an arch dam constituted by a main arch (on the left) and a second arch (on the right). This structure is located in central Portugal, in the municipality of Pampilhosa da Serra, allowing a storage of 50 million cubic meters of water (EDP) from Ribeira de Unhais river, in the hydrographic basin of Tagus river. This 76 meters high and 178 meters long dam is embedded in the canyon of a mountain and is operating since 1943. A hydroelectric power plant is working upstream with a total installed capacity of 24 MW, assured by four horizontal Pelton turbines that operate at 500 rpm (8.33 HZ).

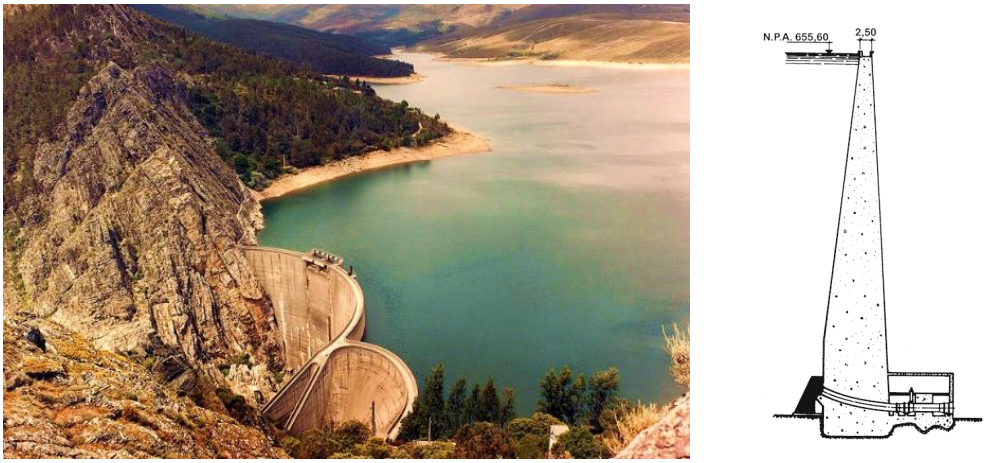

Figure 4.24 – Santa Luzia dam: aerial view (EDP) and (main arch) cross section (CNPGB).

The ambient vibration test of Santa Luzia dam was performed on the 10th of May 2018 and it was based on the use of seven uniaxial force-balance accelerometers that were radially disposed along the main arch crown. For this, the acquisition system using cables was used, thus every measuring point had its own fixed sensor which may be used as reference during the processing of the measured data, and the farthest sensor was about 43 meters away from the acquisition system. The test grid considered 7 measuring points corresponding to the center of the concrete blocks of the main arch. The position of the 7 measuring points are marked with blue dots in the scheme of the structure presented in Figure 4.25.

To assure a good characterization of the structure's dynamic behaviour 7 similar setups with the duration of 12 minutes were performed. A sampling rate of 100 Hz was used during the acquisition,

which was later decimated to 50 Hz. The level in the reservoir during the test was 655.08 meters (elevation from sea level).

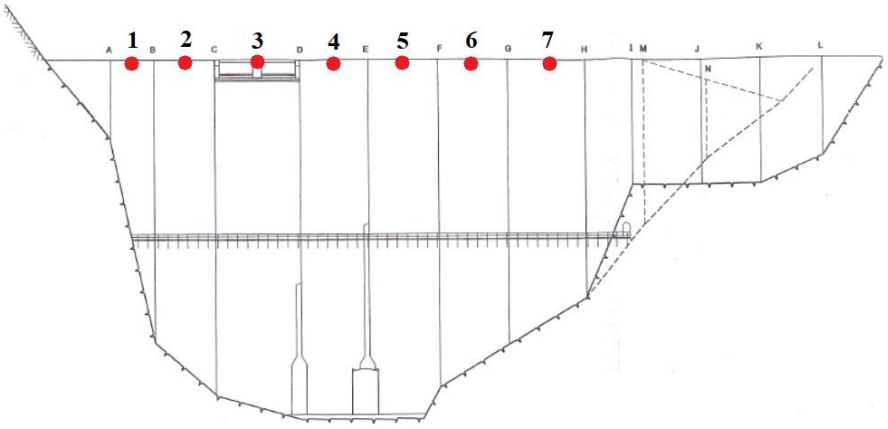

Figure 4.25 – Santa Luzia dam: test layout.

Additionally, GSR-24 recorders from Geosig, equipped with internal tri-axial force-balance accelerometers and synchronized through GPS, were disposed in the same recording positions, in order to complement the test previously described, by measuring the same data with different equipment.

4.7.2. MODAL PARAMETERS IDENTIFICATION

The time series recorded during the ambient vibration test of Santa Luzia dam, show that over the entire duration of the test the accelerations measured by both the sensors placed in position "3" (as defined in Figure 4.25) presented values substantially higher than the accelerations measured in any other point. This becomes clear through the representation of the time series obtained in every instrumented point during one setup (720 s), as presented in Figure 4.26.

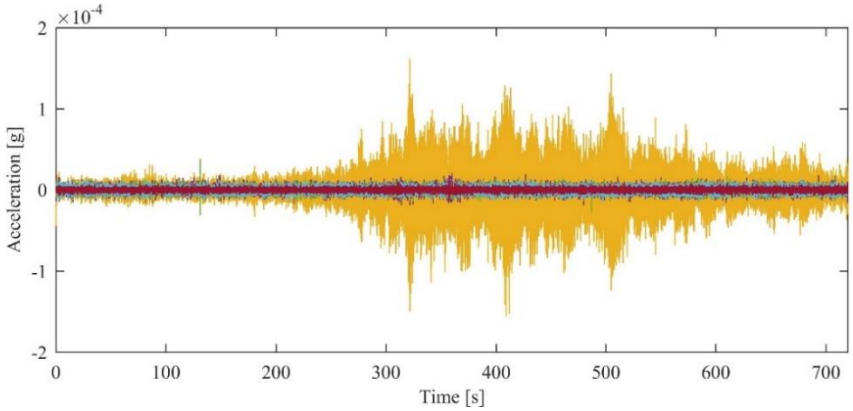

Figure 4.26 – Santa Luzia dam: time series of accelerations (sensor at position 3 is represented in yellow).

The abnormally high accelerations obtained in position "3" are probably due to the fact that this measuring point, unlike the others, does not correspond to the dam crown but to a concrete wall over the dam's spillway instead. This is the only point over the spillway where it was physically possible to install an accelerometer, but the obtained results seem to be polluted by local amplification effects, thus not allowing a precise identification of mode shapes.

Using the Welch method, auto-spectra were obtained for each of the time series presented in Figure 4.26, which are represented in Figure 4.27. The auto-spectra obtained from the time series measured in position "3" (in yellow) is clearly above all the others, presenting two well-defined peaks. Due to the local amplification, it becomes truly challenging to characterize the mode shapes associated with these well-defined peaks. However, other frequencies, such as the ones between 4 and 5 Hz and the one between 6 and 7 Hz, present peaks of similar amplitudes for all the channels, so the mode shapes can be identified.

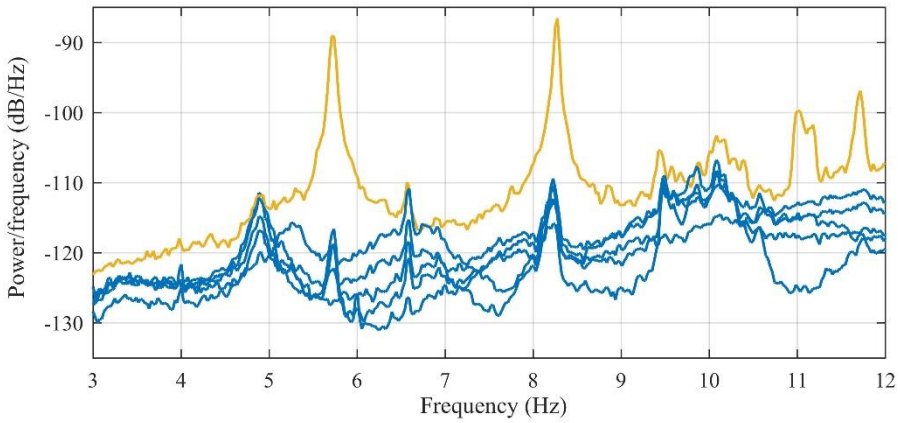

Figure 4.27 – Welch power spectral density estimates for each of the seven measuring sensors (spectra from sensor at position 3 is represented in yellow).

The SSI-Cov method was then applied to obtain accurate estimates of natural frequencies and mode shapes, as well as damping values. This method was applied to each setup and model orders between 20 and 80 were considered. A stabilization diagram obtained from one of the processed setups is presented in Figure 4.28.

Even though well-defined vertical alignments of poles appear around 5.7 Hz and 8.3 Hz, since it will not be possible to accurately identify the mode shapes associated with these frequencies, they will not be assumed as vibration modes frequencies. The same principle is applied to the alignment defined around 5.3 Hz and to the few alignments lying between 9.5 and 10.5 Hz.

On the other hand, mode shapes could be identified from the well-defined alignment around 4.9 Hz and from the poorly-defined alignment around 6.6 Hz, thus confirming the physical character of such poles.

Thus, the two vibration modes that were identified and their modal properties, including natural frequencies and damping values, as well as the description of mode shapes, are presented in Table 4.7. The presented results correspond to the average of the values associated with stable poles across the entire set of setups. The alignments corresponding to the identified vibration modes were marked with blue dashed lines.

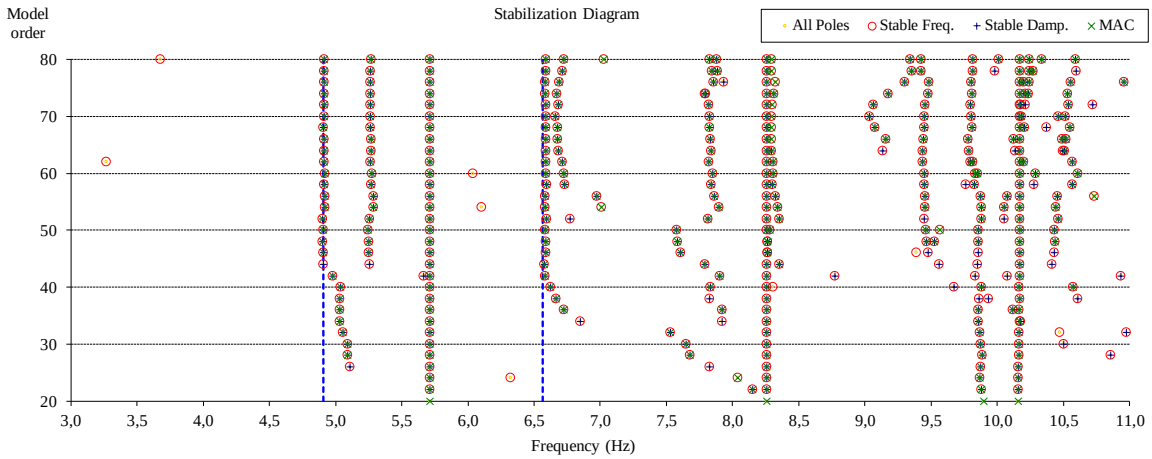

Figure 4.28 – Santa Luzia dam: stabilization diagram from the application of SSI-Cov.

Table 4.7 – Modal parameters for Santa Luzia dam two identified vibration modes

Mode	f_{mean} [Hz]	f_{std} [Hz]	ξ_{mean} [%]	ξ_{std} [%]	Description
1	4.910	0.0153	1.694	0.276	Antisymmetric
2*	6.596	0.0320	1.870	0.958	Symmetric

The standard deviation values of the identified natural frequencies and damping values are also presented in Table 4.7. These were obtained using the method presented in (Reynders et al., 2008) and (M. Döhler & Mevel, 2013), thus allowing a better understanding of the accuracy achieved in the identification. For instance, the standard deviation associated with the second identified vibration mode is higher than twice the value of the first mode standard deviation value, which

should be expected accounting to the shape of the alignment of poles presented in the stabilization diagram associated with this frequency. Additionally, it is worth noticing the high standard deviation presented by the damping of this second mode, leaving little confidence on the identified value.

The second mode was marked with a *, since it corresponds to the second mode that was identified, but not necessarily to the dam's second vibration mode. Clear mode shapes were achieved for the two identified modes, which are presented in Figure 4.29. The first mode is antisymmetric and the second one is symmetric.

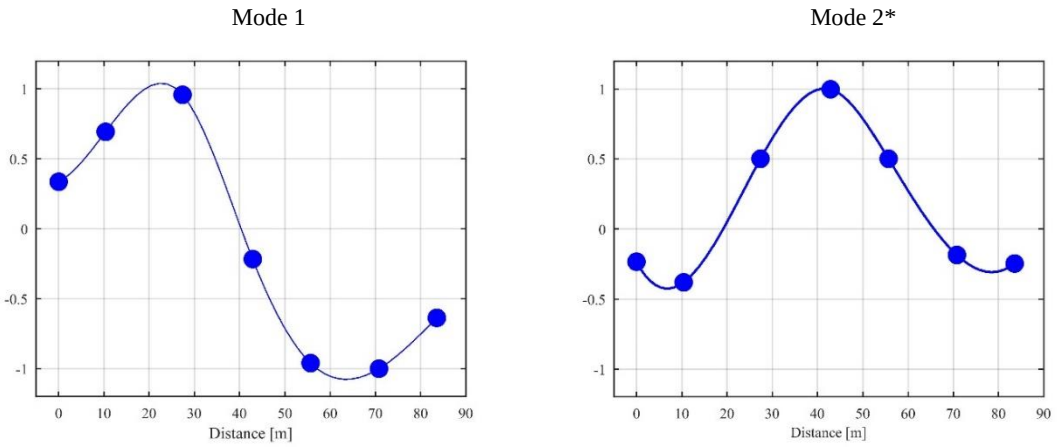

Figure 4.29 – Mode shapes of the two identified vibration modes of Santa Luzia dam.

4.8. AGUIEIRA DAM

4.8.1. DAM DESCRIPTION AND AMBIENT VIBRATION TEST

The Aguieira dam, presented in Figure 4.30, is a multiple arch dam constituted by three arches and two central abutments that work as well as spillways. This structure is located in central Portugal, between the municipalities of Mortágua and Penacova, allowing a storage of 216 million cubic meters of water (EDP) from Mondego river. The dam, which started operating in 1981, is 89 m high and its 400 m long crest constitutes a road link between the two banks of the river. A hydroelectric power plant was built downstream, below the central arch, and it is installed with a total capacity of 336 MW, assured by three vertical Francis turbines that operate at 125 rpm (2.08Hz).

The ambient vibration test of Aguieira dam was performed on the 26th of June 2018 and it was based on the use of ten GSR-24 recorders from Geosig equipped with internal tri-axial force-balance accelerometers. With the purpose of identifying as many vibration modes as possible and taking into account the large dimensions of the structure, a test grid was defined considering 17 measuring points in the dam's crest and 3 measuring points in the dam's upper visit gallery. To assure the measuring of accelerations in every point of the defined grid five setups were considered, during which 7 accelerometers acted as references, and the other 3 accelerometers as moving sensors. The 7 points marked with red dots in Figure 4.31 were used as references, while the other 13 points, marked with blue dots, were measured by the moving accelerometers.

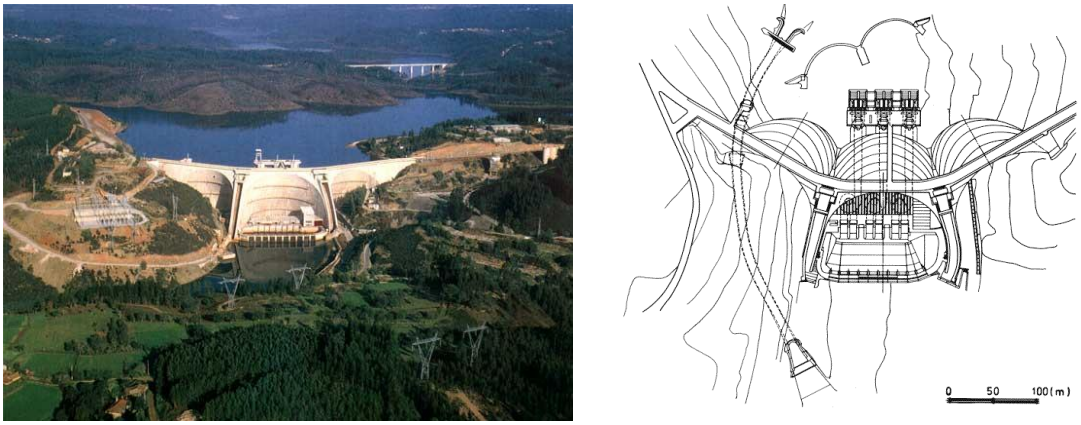

Figure 4.30 – Aguieira multiple arch dam: aerial view (EDP) and schematic top view (CNPGB).

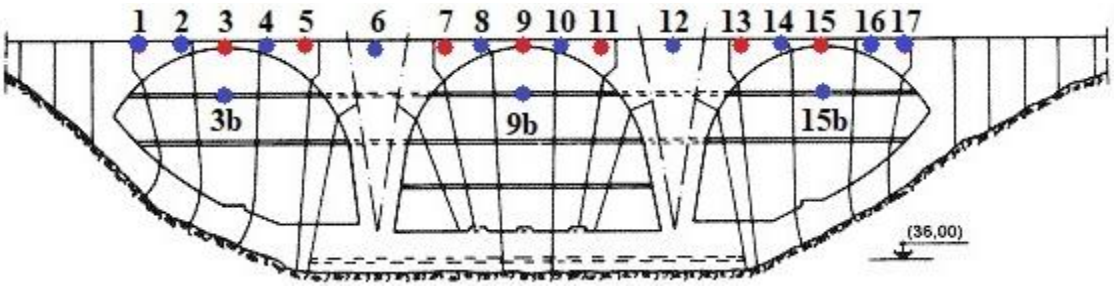

Figure 4.31 – Aguieira dam: test layout.

Each setup had a duration of 28 minutes, after which a window of 2 minutes allowed for the redistribution of the moving accelerometers. A sampling rate of 100 Hz was used during the acquisition, which was later decimated to 50 Hz. The position of each accelerometer (S1 to S10) during each setup is presented in Table 4.8, using the numbering defined in Figure 4.31. The measuring in the dam's gallery was assured by the sensor S4 and started with the second setup. The water level in the reservoir was 123.6 m (elevation from sea level).

Table 4.8 – Accelerometer disposition during each setup of the ambient vibration test

Setup	*S1*	*S2*	*S3*	*S4*	*S5*	*S6*	*S7*	*S8*	*S9*	*S10*
1	1	17	3	-	7	15	5	9	11	13
2	2	16	3	3b	7	15	5	9	11	13
3	4	14	3	9b	7	15	5	9	11	13
4	6	12	3	15b	7	15	5	9	11	13
5	8	10	3	-	7	15	5	9	11	13

4.8.2. *Modal Parameters Identification*

The hydroelectric power plant was fully operating during most of the test, inducing high levels of vibration on the dam. Only during the last setup the turbines from the power plant stopped operation. Therefore, the intensity of the accelerations measured are much higher during the first four setups than those measured during the last setup. This becomes clear through the analysis of Figure 4.32, where the time series of accelerations recorded by the entire set of sensors during the first and last setups are represented together. When the turbines stop operation the intensity of the measured accelerations decreases more than ten times.

However, higher levels of vibration do not necessarily mean better quality results when applying modal identification methods to such data. In this case, since the main source of excitation is due to turbine operation and these turbines operate at a steady frequency, the results get polluted with its rotating frequency (125 rpm – 2.083 Hz) and its multiples. This is clear on the left part of Figure 4.33 where the ANPSD function obtained from setup 1 is represented, showing very sharp peaks at 2.08 Hz, 4.17 Hz, 6.25 Hz, 8.33 Hz and 10.42 Hz, that difficult the identification of natural modes of the structure whose frequencies lay close to these harmonics. Having this problem in mind, an ANPSD function obtained from setup 5, when the turbines were not operating, was represented in the right side of Figure 4.33. If on the one hand, the absence of harmonics allows the identification of peaks that were hidden otherwise, on the other hand, the lower levels of vibration produce less clear spectra. Therefore, time series recorded during both types of operating conditions must be carefully analysed.

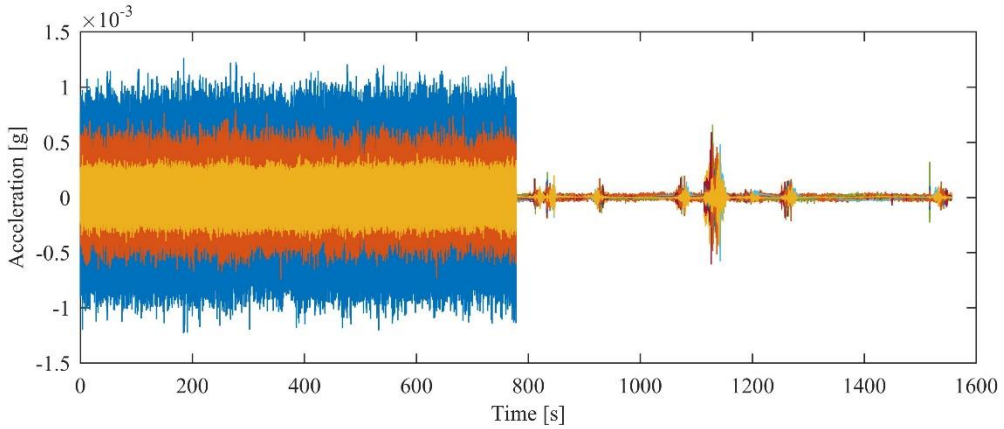

Figure 4.32 – Concatenation of the time series of acceleration recorded by all sensors during the first and the last setups.

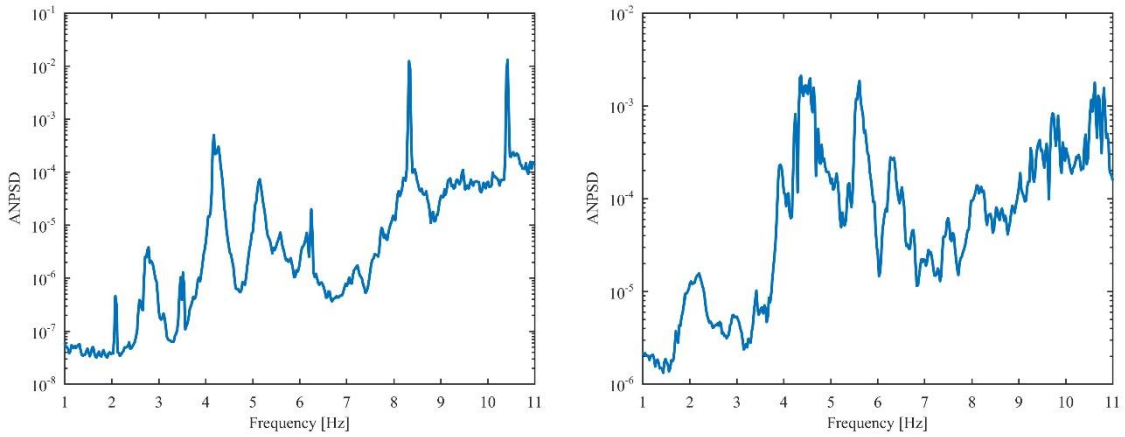

Figure 4.33 – ANPSD of Aguieira dam ambient vibration test: setup1 (on the left) and setup5 (on the right).

The SSI-Cov method was then applied to the recorded time series of accelerations, and the stabilization diagrams obtained from setups 1 and 5 are presented in Figure 4.34. In the first case the diagram is dominated by alignments associated with the turbines rotation frequency and its harmonics, thus only one vibration mode could be identified. In the bottom diagram, however, since the turbines were not operating during setup 5, other alignments appear and four more modes could be identified.

Natural frequencies, damping and standard deviation values were obtained for the five identified modes. Since most of the setups are polluted with the turbines rotation frequencies and its harmonics, it is possible that not all natural vibration modes of the structure have been identified. Therefore, the identified modes and its properties are presented in Table 4.9 and their order is presented together with a * symbol since the first identified mode may not correspond to the dam first natural mode, and so on. Mode shapes are presented in Figure 4.35 for the full extent of the dam, thus representing the three arches separated by the two central abutments. The classical classification of vibration modes in symmetric or antisymmetric shapes is not easily used in this specific case, since in most modes each arch presents its own shape and the global mode comprehends the concatenation of the three parts.

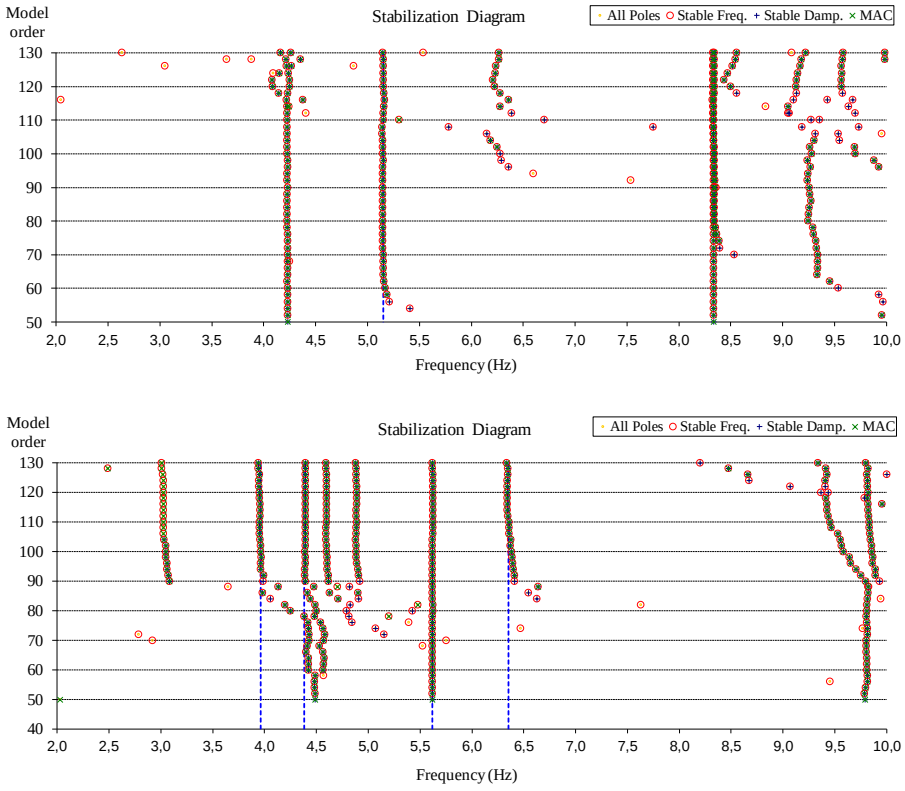

Figure 4.34 – Aguieira dam: stabilization diagram from setup1 (top) and setup5 (bottom).

Table 4.9 – Modal parameters of Aguieira dam five identified vibration modes

Mode	f_{mean} [Hz]	f_{std} [Hz]	ξ_{mean} [%]	ξ_{std} [%]
1*	3.956	0.0149	1.910	0.680
2*	4.368	0.0351	1.886	0.928
3*	5.148	0.0082	0.585	0.124
4*	5.620	0.0027	0.866	0.058
5*	6.345	0.0348	1.434	0.913

Small differences may exist between consecutive mode shapes. For instance, while in mode 1* the central and right arches present a somewhat symmetric shape and the left arch does not seem to be activated, in mode 2* all three arches present a roughly symmetric shape. The same occurs with mode 3*, but in this case all three arches' shapes are in phase, while in mode 2* the central arch vibrates out of phase when compared to the lateral arches. In turn, in modes 4* and 5* individual arches present already antisymmetric shapes, and the global mode results once again from the concatenation of the different parts.

Mode 1*

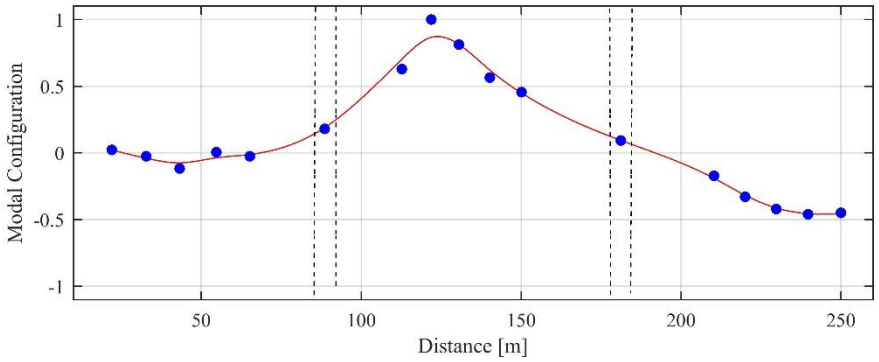

Mode 2*

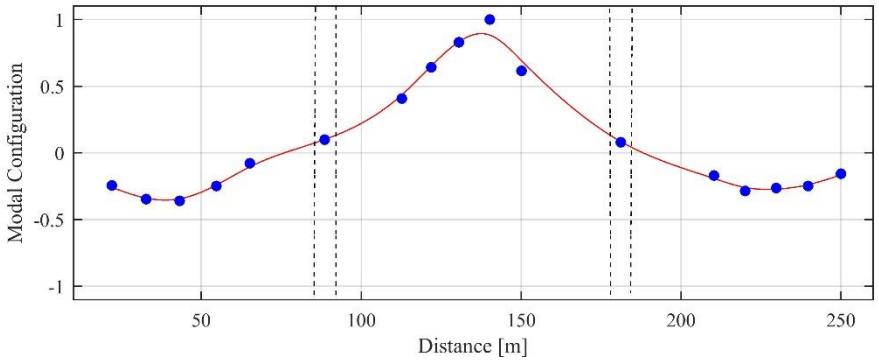

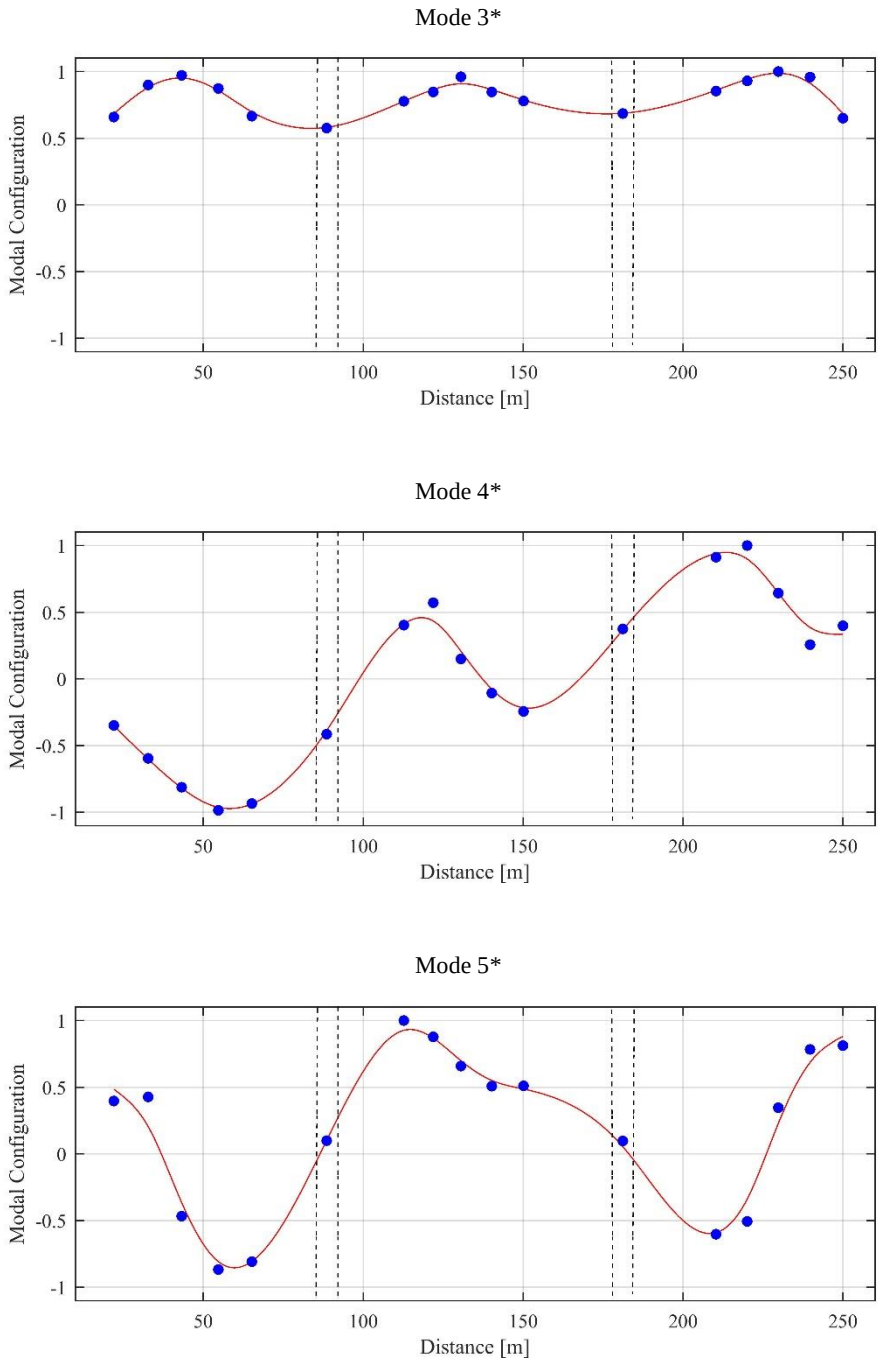

Figure 4.35 – Mode shapes of vibration modes of Aguieira dam.

Finally, it is important to note that, following the procedure used in the previous applications, all the peaks in the ANPSD function and all the alignments in the stabilization diagrams were studied and the mode shapes obtained from each of them were analysed, thus the final set of identified vibration modes correspond to those presenting good agreement between the results obtained from both identification methods and presenting as well realistic mode shapes.

4.9. EFFECT OF SENSOR NOISE ON MODAL PROPERTIES IDENTIFICATION

When compared to forced vibration tests, much lower levels of vibration and much lower signal to noise ratios should be expected under natural excitation (Pereira et al., 2018), therefore very sensitive sensors and high-resolution digitizers are required to obtain good results. However, top quality equipment is generally associated with high costs, so it may not be always available. To overcome this, more economical solutions, with lower capabilities, may arise as an alternative in certain situations. Consequently, it is important to explore the accuracy of the results achieved with different types of accelerometers (Pacheco et al., 2018) when performing operational modal analysis.

In this context, the data obtained from the ambient vibration tests performed on Alto Lindoso and Bouçã arch dams, in which force balance accelerometers were used to measure accelerations, will be numerically polluted with increasing levels of noise. A comparison between the results obtained from the modal identification of these structures through the analysis of the measured data and through the analysis of data simulating characteristic levels of noise associated with different types of accelerometers, such as piezoelectric and MEMS, is presented in the next sections. But first, the procedure used to simulate such noise is explained.

4.9.1. NOISE SIMULATION

To complement the data obtained with force balance sensors (FB) during the ambient vibration tests and investigate on the feasibility of sensors with different functioning basic principles, such as Piezoelectric and MicroElectricalMechanical Systems (Evans et al., 2014) accelerometers, being used to test arch dams, the noise floor expected for regular sensors was ascertained.

Through the performance of laboratory measurements with four different conventional sensors, including two piezoelectric accelerometers (PE1 and PE2) and a medium-quality (MEMS 2) and a high-quality (MEMS1) MicroElectricalMechanical Systems accelerometers, it was possible to assess typical noise levels of these types of sensors. Numerically generated white noise time series were tuned with different amplitudes in order to simulate the spectral noise levels assessed in laboratory for each of the four tested sensors. The four numerically generated noise floors are presented in Figure 4.36 and, taking into account that the vertical scale is logarithmic, the quality difference between piezoelectric and MEMS accelerometers is clear. While both the considered

piezoelectric sensors present a noise floor well below 10^{-11} [g^2 / Hz], in the case of MEMS this values are close to 10^{-9} and 10^{-10} [g^2 / Hz] respectively.

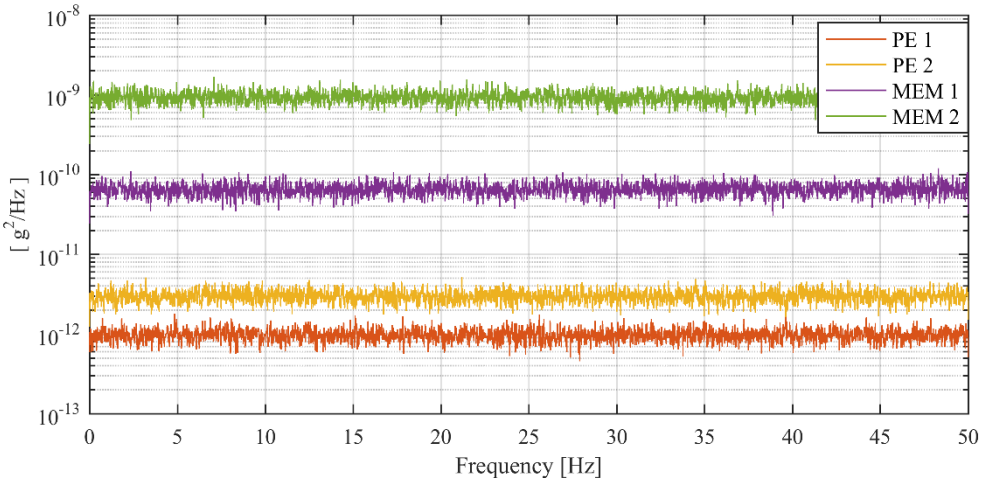

Figure 4.36 – Numerically generated noise spectra.

4.9.2. APPLICATION TO ALTO LINDOSO DAM

The ambient vibration test of Alto Lindoso arch dam has been presented in section 4.3. In this section, the spectra of the noises previously simulated are compared to spectra obtained from the time series measured during the test. Afterwards, the numerically simulated time series of noises are added to the measured data and the results obtained in the five studied cases (FB, PE1, PE2, MEMS1 and MEMS2) are compared.

In the upper part of Figure 4.37, the considered noise floors are compared to different auto-spectra obtained from real data measured by two accelerometers positioned in different points during the ambient vibration test. In the case of the considered piezoelectric noise floors, while PE1 is constantly below the peaks of the real spectra, PE2 is below most of the peaks, but eventually crossing one or other peak. In turn, for MEMS the opposite is verified, since MEMS2 is constantly over the top of the peaks and the position of MEMS1 generally lays between going through the peaks and over the top of the peaks.

Finally, the simulated band-limited white noise time series were added to the originally measured acceleration time series. Therefore, it was assumed that the spectral noise is constant in the frequency range under analysis. Since the noise time series were added to the measured data, new

time series were obtained that simulate the data that would have been measured if the piezoelectric or the MEMS accelerometers had been used during the ambient vibration test.

The lower part of Figure 4.37 shows the auto-spectra obtained from real data measured by the same force balance accelerometers (in blue) and the auto spectra obtained from the piezoelectric and from the MEMS simulated time series. Whereas most of the peaks in the spectra obtained from the real measured time series (FB) are reproduced in the spectra obtained from simulated piezoelectric time series (PE1 and PE2), the same does not apply to the 'MEMS' derived spectra which, depending on the time series used to compute the spectra, may hide the peaks under the noise floor.

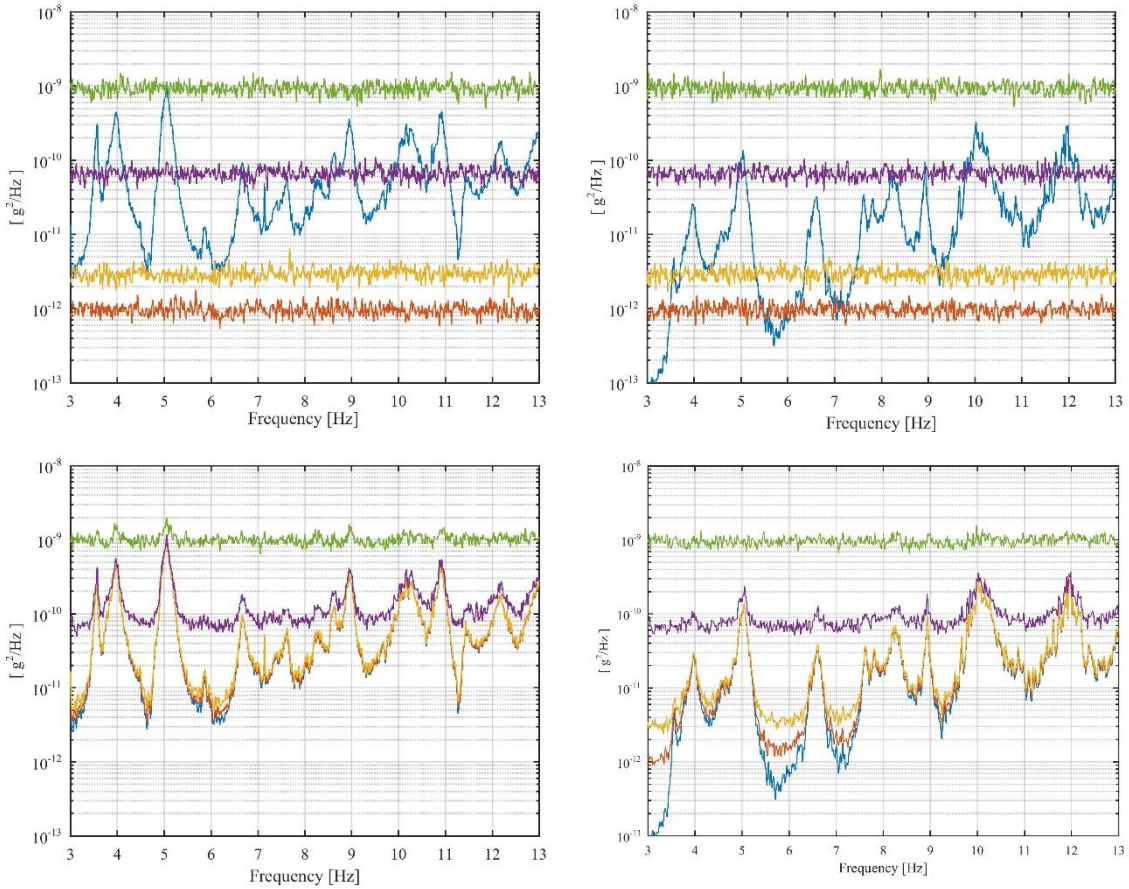

Figure 4.37 – Upper figures: auto-spectra from real measuring points (blue) and auto-spectra of numerically generated noise floors; Lower figures: auto-spectra from real data polluted with numerically generated noises.

An automatic modal identification was performed, applying the SSI-Cov method to the time series of acceleration measured during the ambient vibration test first (FB) and then to the time series polluted with the numerically simulated noises. Natural frequencies and damping ratios were obtained, as well as the standard deviation associated with each estimate. A comparison between

the modal properties and standard deviations obtained in the five studied scenarios, for the first and second vibration modes, is presented in Table 4.10. Generally, the standard deviations associated with both natural frequencies and damping ratios increase with the amplitude of the noise added to the measured time series of accelerations, though in the case of the two piezoelectric scenarios (PE1 and PE2) only small differences are found in the results, when compared to the original ones. Considerably higher uncertainties are associated with the modal properties identified from the MEMS time series, as it was expected. When using MEMS2 time series, the first mode was not even identified, which is also the case with other modes that were not presented here.

Table 4.10 – Comparison between the modal properties, and respective standard deviations, obtained in the five studied scenarios, for vibration modes 1 and 2 (Alto Lindoso arch dam)

Scenario	f_{mean} [Hz]	f_{std} [Hz]	ξ_{mean} [%]	ξ_{std} [%]
		Mode 1		
FB	3.546	0.0045	1.194	0.123
PE1	3.546	0.0046	1.278	0.136
PE2	3.545	0.0064	1.054	0.212
MEMS1	3.563	0.0165	1.340	0.457
MEMS2	-	-	-	-
		Mode 2		
FB	3.963	0.0105	2.164	0.280
PE1	3.962	0.0106	2.159	0.280
PE2	3.964	0.0106	2.139	0.284
MEMS1	3.960	0.0175	2.375	0.466
MEMS2	3.947	0.0302	2.084	0.708

4.9.3. APPLICATION TO BOUÇÃ DAM

The ambient vibration test of Bouçã arch dam has already been presented as well, in section 4.4. Just like in the case of Alto Lindoso in the previous section, the spectra of the noises previously simulated are compared to spectra obtained from the time series measured during the ambient vibration test of Bouçã dam and the results obtained in the five studied scenarios (FB, PE1, PE2, MEMS1 and MEMS2) are compared once again.

In the left part of Figure 4.38, the considered noise floors are compared to auto-spectra obtained from real data measured during the ambient vibration test. Contrary to the verified with the test performed in Alto Lindoso dam, in Bouçã dam the spectra obtained from time series measured

during the same setup but in different positions do not present considerable amplitude differences, mostly due to the much shorter length of the crown (when compared to Alto Lindoso) and to the fact that all the measuring points are located at a fair distance from the abutments.

In this case, the considered piezoelectric noise floors (PE1 and PE2) are above many of the peaks of the real spectra, crossing many of them as well. In turn, both MEMS1 and MEMS2 are constantly over the top of the peaks.

Once again the simulated band-limited white noise time series were added to the originally measured acceleration time series and it was assumed that the spectral noise is constant in the frequency range under analysis. The new time series obtained simulate the data that would have been measured if the piezoelectric or the MEMS accelerometers had been used during the ambient vibration test of Bouçã dam.

The right part of Figure 4.38 shows the auto-spectra obtained from real data measured by the same force balance accelerometers (in blue) and the auto spectra obtained from the piezoelectric and from the MEMS simulated time series. In this case, just a few of the peaks in the spectra obtained from the real measured time series (FB) are reproduced in the spectra obtained from simulated piezoelectric time series (PE1 and PE2). The 'MEMS' derived spectra, however, do not clearly reproduce any of the peaks in the spectra obtained from the real measured time series, which are hidden under the noise floors.

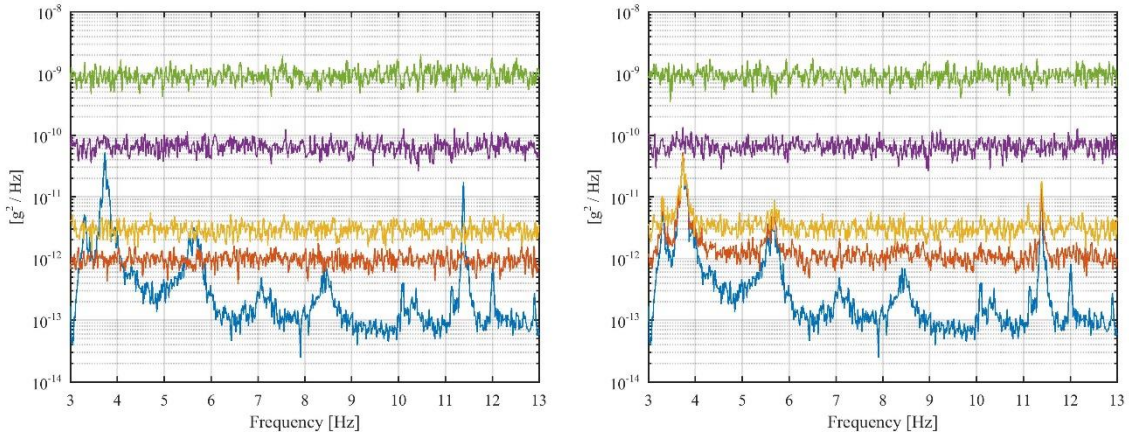

Figure 4.38 – Left part of the figure: auto-spectra from real measuring points (blue) and auto-spectra of numerically generated noise floors; Right part of figure: auto-spectra from real data polluted with numerically generated noises.

The automatic modal identification performed with the Alto Lindoso test, applying the SSI-Cov method, was repeated. The time series of acceleration measured during the ambient vibration test

of Bouçã dam (FB) and the time series polluted with the numerically simulated noises were used. Natural frequencies, damping ratios and respective standard deviation values were obtained for the same five scenarios, and the results for the first and second vibration modes are presented and compared in Table 4.11. The increase in standard deviations associated with both natural frequencies and damping ratios obtained from the two piezoelectric scenarios simulated (PE1 and PE2) when compared to the results obtained in the force balance scenario is clear. When using MEMS1 and MEMS2 time series, the first two modes were either not even identified or modal properties identified are associated with extremely high uncertainties, which is the case of the second mode, identified in the MEMS1 scenario.

Table 4.11 – Comparison between the modal properties, and respective standard deviations, obtained in the five studied scenarios, for vibration modes 1 and 2 (Bouçã arch dam)

Scenario	f_{mean} [Hz]	f_{std} [Hz]	ξ_{mean} [%]	ξ_{std} [%]
		Mode 1		
FB	3.296	0.0069	1.464	0.206
PE1	3.301	0.0157	1.544	0.438
PE2	3.291	0.0185	1.554	0.528
MEMS1	-	-	-	-
MEMS2	-	-	-	-
		Mode 2		
FB	3.733	0.0058	1.308	0.161
PE1	3.735	0.0082	1.228	0.283
PE2	3.738	0.0113	1.340	0.383
MEMS1	3.747	0.1281	1.942	2.687
MEMS2	-	-	-	-

4.10. FINAL CONSIDERATIONS

Ambient vibration tests have been successfully performed in a group of six concrete dams located in Portugal, with distinct characteristics and typologies, which during the tests were submitted to different operational and ambient excitations, periodically including the rotation of electricity production turbines, since all the dams are part of hydroelectric developments, thus showing the suitability of operational modal analysis in concrete dams. The studied group of structures included four arch dams with very different heights (Alto Lindoso dam, Santa Luzia dam, Bouçã dam and Caldeirão dam), an arch-gravity dam (Castelo do Bode dam) and a multiple arch dam (Aguieira dam).

Two distinct acquisition systems were available to perform the tests and each of them was used depending on the characteristics and geometry of the structure. Though a few measurements have been conducted in visit galleries, the bulk of the tests were performed in the dam's crowns, which are generally accessible and mostly consist of road connections between the two river margins. The exception was Bouçã dam, whose crown constitutes the dam main spillway, in which the test was performed inside the upper visit gallery. Different test layouts and durations had to be considered for each case, but all the tests were successfully executed and time series of accelerations were collected for the whole set of dams.

Quite diverse vibration levels were measured. The intensity of the recorded accelerations mainly varies according to the operation conditions, namely the rotation of turbines in power plants whose operation may increase vibration levels by a factor of 100 to 1000, therefore, vibration levels could go from few micro g to few milli g, depending on the proximity of the plant to the dam. Apart from Santa Luzia dam, whose respective power plant is not located in its vicinity, the effect of the production complex operation on vibration levels was felt in every dam during the entire test or just part of it, depending on the case.

In order to compare the vibration levels measured in the whole set of tested dams, time series of accelerations recorded by the sensors positioned in the central part of each of the tested structures are presented in Figure 4.39. Time series were chosen taking into account operation conditions, so that electricity production turbines were stopped, and only ambient vibration was exciting the dams during these periods. In the case of Castelo do Bode dam, the power plant was operating during the entire test, thus it was not possible to record any period during which the dam was being excited solely by ambient vibration. Generally, the vibration levels recorded go from a few micro g in quiet

conditions to many tens of micro g when traffic crosses the dam or human activities with machinery occur nearby. In the case of Castelo do Bode, which had the power plant fully operating, vibration levels are constantly close to milli g. To complement this analysis, the time series presented in Figure 4.39 were used to obtain auto-spectra, which are represented in Figure 4.40 with the same colour codes. Figure 4.40 is very interesting in the sense that it exposes the minimum signal amplitude needed to assure adequate characterization of the auto-spectra from the whole set of tested dams, which is between 10^{-13} and 10^{-14} g^2/Hz.

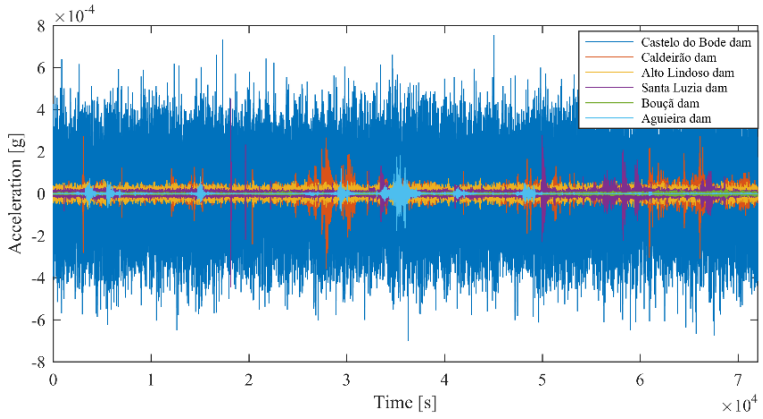

Figure 4.39 – Time series of accelerations collected in the whole set of tested dams.

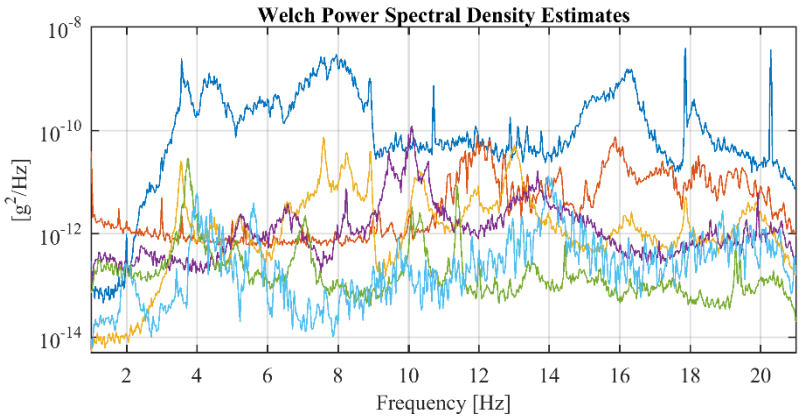

Figure 4.40 – Auto-spectra obtained from each of the time series presented in Figure 4.39.

Concluding, in this chapter the suitability of the application of operational modal analysis to concrete dams is evaluated and good results were obtained for structures with quite different stiffness, such as Alto Lindoso and Castelo do Bode dams. Additionally, though very similar results were obtained for natural frequencies and damping ratios when analysing the time series obtained by both the measuring system using uniaxial accelerometers and electrical cables, and the system using portable recorders, it was concluded that synchronization problems may occur when

performing ambient vibration tests using portable recorders synchronized by GPS, thus affecting the quality of mode shapes. If a problem like this occurs only once during a test it can be mitigated through manual synchronization. On the other hand, if GPS problems are verified constantly during the test, the quality of the identified mode shapes may be seriously affected.

Synchronization problems are not expected to occur when performing tests using a central acquisition system connected to the accelerometers through electrical cables, but this system is limited in range to about 150 m.

Finally, it was concluded that, generally, MEMs accelerometers are not yet suited for dynamic testing of dams based on ambient vibrations, while piezoelectric accelerometers may be used for this purpose, though not providing results as good as the ones provided by force-balance sensors.

5. CONTINUOUS DYNAMIC MONITORING

5.1. INTRODUCTION

In order to confidently maintain large civil infrastructures, such as dams, with high levels of performance and safety, decisions should be supported by integrated monitoring systems considering real continuous data, directly obtained from the structures. The Portuguese regulations for dams safety (RSB, 2018) actually recommends the implementation of equipment to characterize seismic actions in structures with high risks (class I) and the performance of in situ dynamic tests.

The main idea behind continuous monitoring and the installation of structural health monitoring systems consists of accumulating data while a system or structure is operating in normal conditions which is used to construct a reference model. During subsequent operation of the system, new data is compared to the reference and any significant deviations are taken to indicate novel behaviour that may correspond to structural damage. This approach has potential problems if the structure is embedded in a changing environment and the reference model is only characteristic of a limited range of external conditions, since in this case measurements in an undamaged condition, but from a different environmental state, may falsely register novelty and infer deterioration (Worden et al., 2002). However, this problem can be easily solved guaranteeing that a correct amount of data, from a diverse set of characteristic operational and environmental conditions, is used to build the reference model, and considering processing tools that permit to minimize the effects of such conditions, thus normalizing data and creating features insensitive to external factors.

Structural health monitoring systems are historically associated with static data. This is the case of dams, which are classically equipped with systems capable of measuring displacements, stresses,

relative movements between joints or temperatures, with the aim of studying the structural static behaviour. A few examples of implemented continuous monitoring systems based on static data measurements being used to evaluate the health condition of dams can be found in (Loh et al., 2011), (Mata, 2011) and (Hu & Wu, 2019).

Nevertheless, vibration-based health monitoring systems are nowadays becoming quite common as well, and have also already been successfully implemented in many different large civil structures such as bridges (Magalhães et al., 2012), wind turbines (Oliveira et al., 2016), stadia roofs (Martins et al., 2014) or bell-towers (Ubertini et al., 2016).

Though the sporadic dynamic testing of dams has been common and very useful in the past, through the performance of forced vibration tests (Gomes & Carvalho, 2014) (Gomes & Lemos, 2016b), which provide accurate and trustworthy results, the installation of vibration-based health monitoring systems on dams is still very uncommon. A continuous ambient vibration programme was carried out in Mauvoisin dam (Darbre & Proulx, 2002), recording twice a day during 180 days, with the main purpose of studying the effect of the reservoir water level on the structure natural frequencies. Similar works were later developed in Hitotsuse dam (Okuma et al., 2008) in Japan, and in Cabril dam (Mendes, 2010) in Portugal. The main goal of both applications was to follow the evolution of natural frequencies over time and for this the first three or four vibration modes of these structures were tracked for about one year, respectively in the Japanese and in the Portuguese case.

In this context, the next few sections are used to address first the main stages of structural health monitoring and its particularities, from in situ data acquisition to model developing and damage detection, and then the automation of operational modal analysis, necessary to process the enormous amount of data provided by vibration-based monitoring systems and continuously track the modal parameters of a structure. Moreover, an overview on different techniques used to remove the effects of operational and environmental conditions on modal properties is presented and the peculiarities related with damage detection using control charts are addressed as well.

5.2. STRUCTURAL HEALTH MONITORING BASED ON MODAL PARAMETERS

Civil engineering structures are generally supposed to have long operation life spans. During this long-term operation lifetime, they are submitted to many factors, both environmentally and human induced, that degrade their condition and performance capacity, gradually leading to the occurrence of damage and, in last instance, to collapse. Safety, operation and sustainability requirements must always be met during the structure operation lifetime, which implies that maintenance and rehabilitation actions should be executed periodically, as a preventive measure, and punctually when essential intervention is needed to maintain the structure capacity above a minimum performance threshold. Figure 5.1 presents a theoretical profile evolution of the performance of a structure over time and the effects that the referred maintenance measures may inflict.

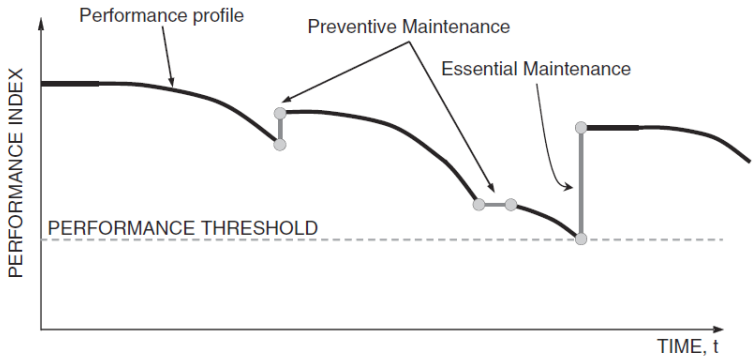

Figure 5.1 – Effects of different maintenance types on the structural performance (Frangopol & Soliman, 2016).

Thus, the implementation of a Structural Health Monitoring (SHM) system is generally envisaged to: (1) validate the modification to an existing structure with the potential benefit of improving design specifications; (2) detect the external loading and response, and predict the possible deterioration to assess the safety of a structure; (3) provide the evidence for planning structure inspection, rehabilitation, maintenance, retrofit and repair works; (4) acquire a vast amount of in situ data for further study on structural engineering, such as earthquake-resistant designs, novel structural types and smart material applications (Brownjohn, 2007).

A system capable of monitoring and assessing structural performance automatically, is highly desirable. Over the last few decades, many different SHM systems, with distinct features, background and purposes have been developed and successfully implemented in major civil engineering structures, such as bridges, buildings, towers, dams, stadiums or tunnels. A state-of-the-art work presenting a few examples may be found in (Li et al., 2016). However, even though

many different assemblies and techniques have been proposed, (Farrar et al., 2001) describes structural health monitoring as a statistical problem that mostly consists of the three main steps, presented in Figure 5.2.

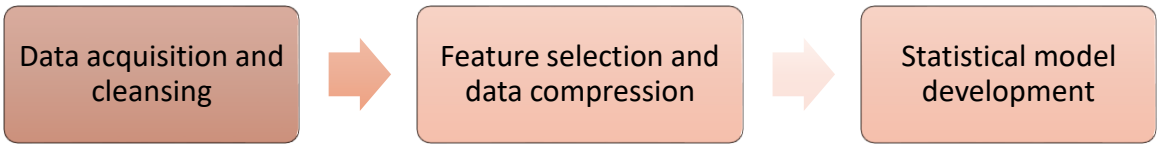

Figure 5.2 – Stages of Structural Health Monitoring.

A major SHM focus in recent years has been vibration-based health monitoring, because vibration measurements can be used to detect damage invisible or hidden within the internal areas of the structure before it can be observed by visual inspection. The main idea behind vibration-based SHM is that damage usually modifies structural characteristics such as stiffness which are manifested in the measured vibration response of the structure (Amezquita-Sanchez & Adeli, 2016). Thus, extracted features from periodically sampled dynamic responses, properly submitted to continuous statistical evaluation over time, can serve as indicators of the structural condition of the evaluated system (Magalhães, 2010).

Continuous vibration-based SHM applied in civil engineering structures is particularly suitable for the extraction of features that are adequate to be used as damage indicators, since it permits the identification of the structures modal parameters under operational conditions. Moreover, these features may be automatically identified with the help of the output-only modal analysis methods presented in chapter 3, which provide accurate estimates of natural frequencies, modal damping ratios and mode shapes, using only the ambient and operation induced vibration as excitation. The identification of these modal parameters, from continuously acquired acceleration time series, allows the characterization of their evolution over time and therefore the detection of anomalous variations, which may indicate the occurrence of damage.

Additionally, features can be extracted from data recorded in situ through the use of a wide variety of models. The work (Amezquita-Sanchez & Adeli, 2016) presents a review of recent articles on alternative signal processing techniques usually used for vibration-based SHM, such as Auto Regressive Moving Average (ARMA) models, Kalman filters or wavelet transform, along with some new approaches proposed in the past few years as potential candidates for future SHM research.

Damage detection is generally organized in four levels according to Rytter's classification (Rytter, 1993), presented in Figure 5.3. The first level relies on a qualitative assessment that damage is, or not, present in the structure; the second level consists on the identification of the probable location of the damage; the third one defines the type of damage that is being identified; and the fourth, and last level, dwell on the assessment of the damage extension, evaluating its severity. An additional fifth level was later introduced by (Worden & Dulieu-Barton, 2004), about the structure's safety and the prediction of its remaining lifetime.

Although it is possible to go beyond, depending on many factors such as the comprehensiveness of the data acquired, the structure's complexity or the type of damage involved (Santos, 2014), normally only level 1 is achieved with a permanent dynamic monitoring system. Nonetheless, the main goal of a monitoring system is usually to give an alert that should then trigger more detailed investigations that may then reach the upper levels (Magalhães, 2010).

For instance, when using modal parameters for this purpose, it is possible to detect damage without having any measuring point in the vicinity of the damaged zone, which is a major advantage, but not localize or quantify it. However, it is also worth noting that while a damage occurrence implies a structural novelty, and consequently different modal parameters, the reverse is not true, that is, the identification of structural novel behaviour does not necessarily imply that the structural system is damaged. A brief literature review on novelty identification is presented in (Santos, 2014).

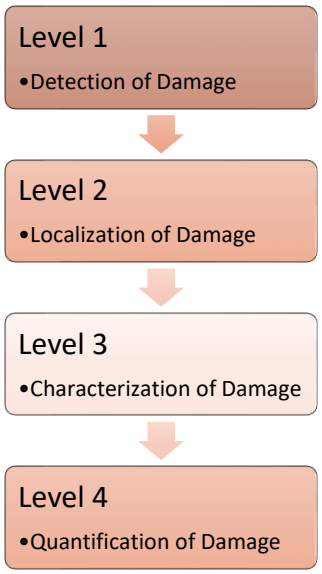

Figure 5.3 – Rytter's levels in damage assessment.

According to (Fan & Qiao, 2011), vibration-based damage identification methods may be categorized attending on the extracted features they use, citing natural frequency-based methods, mode shape-based methods, curvature/strain-based methods and other methods based on modal parameters. Natural frequencies are commonly used for damage detection since they are usually less contaminated by experimental noise and therefore accurate estimates are easily obtained. This is not the case with mode shapes, since identification procedures accurate enough for the detection of damage require the use of a dense measuring grid. In turn, modal damping ratios, frequently present high levels of uncertainty that difficult the detection of anomalous variations associated with damage.

However, it is unlikely to identify structural novelties directly from natural frequencies obtained from continuous modal identification since these data are contaminated by the influence of both environmental and operational effects. In the case of environmental effects, natural frequencies values may be highly altered by temperature, humidity and wind, whereas traffic intensity, blade's rotation speed or reservoir water level are examples of operational conditions that may disturb the identification process respectively in bridges, wind turbines and dams. Consequently, it becomes essential to separate the effects produced by these factors in the modal estimates. Alternatively, features that are not strongly affected by external conditions, such as mode shapes, could be used. Nevertheless, as it was already addressed in this text, the identification of accurate enough mode shapes to be considered as damage indicators would require the use of an extremely complex and expensive monitoring system.

Though many sporadic ambient vibration tests have been successfully performed on dams over the years, continuous dynamic monitoring in this kind of structure is not a common practice yet. An example of the implementation of a dynamic monitoring system on a dam is presented by (Mendes, 2010). In this work a series of tests previously performed on Cabril arch dam, in Portugal, as well as a numerical model are first presented. Then the author presents the monitoring system that was installed on the dam and the data acquired during almost a year. The evolution of natural frequencies over time are shown, along with a model that aims to separate the effects of reservoir water level, temperature and time from the frequencies estimates.

In the following section, tools and concepts related with the automatic tracking of modal properties and quantification of their uncertainties are introduced.

5.3. AUTOMATED OPERATIONAL MODAL ANALYSIS

5.3.1. INTRODUCTION

As discussed in the previous sections of this chapter, operational modal analysis allows to obtain modal characteristics of a particular structure, such as natural frequencies, damping ratios and modal configurations, in a real operating context. The evaluation of these parameters, in particular through the analysis of their general evolution and local variations over time, can be used to ascertain the health condition of a structure, taking into account that changes in its dynamic behaviour, reproduced in its modal properties, may be associated with the occurrence of structural damage.

It is therefore important to develop and implement tools that, based on the modal identification methods presented in chapter 3, or similar ones, allow the referred modal parameters to be automatically and systematically extracted from time series of in loco measured data. These tools must be carefully and properly tuned in order to provide results similar to those that would be obtained if the process resulted from greater intervention of the operator, or even better results, taking into account that an automated process may reduce the occurrence of systemic errors introduced by the analyst.

Therefore, in the case of multi-order parametric identification methods such as SSI-Cov and p-LSCF, after the construction of stabilization diagrams, an algorithm must be able to automatically determine a set of parameters from the poles of the diagram, distinguishing between the physical and the spurious modes, and excluding the second ones. For this, two different approaches may be considered, either using just the stable poles in the diagram and immediately reducing the noise caused by unstable poles, or skipping the stabilization procedure and directly using all the poles obtained from the modal identification method. Good results can be achieved with both procedures, as demonstrated in (Magalhães et al., 2009). The extraction of modal properties related to physical modes from the entire set of poles in stabilization diagrams can be achieved through several methods, and (Reynders et al., 2012) points out the three main types: histograms analysis, partitioning methods and hierarchical clustering.

In the case of histogram analysis, the frequency axis in the stabilization diagram is divided into narrow bins and the number of stable poles in each bin is counted. This procedure was studied by (Scionti et al., 2003) which presented an algorithm based on this procedure, successfully tested it

with in-flight data from an aircraft. Both the other types, partitioning methods (non-hierarchical clustering) and hierarchical clustering, represent branches of clustering analysis, thus these statistical multivariate methods are addressed in the next section. On the other hand, Fuzzy C means clustering (Carden & Brownjohn, 2008) and Least Squares Support Vector Machines algorithms (LSSVM) (Goethals et al., 2004) are examples of approaches using current knowledge of the system to improve the future identifications, which can be beneficial when dealing with a large number of datasets (Soal et al., 2018). However, these techniques are suited for modal tracking, but not for modal parameters estimation from individual data records (Reynders et al., 2012).

Summarizing, operational modal analysis is comprehended by four main sequential and dependent stages, defined in the diagram presented in Figure 5.4. The first three stages, from data collection to signal processing and lastly to system identification, were already addressed in chapter 3, where state-of-the art methods were presented. The next sections concentrate on the fourth and last of these stages, the automatic determination of a validated set of modal parameters, which is the key to vibration-based structural health monitoring systems.

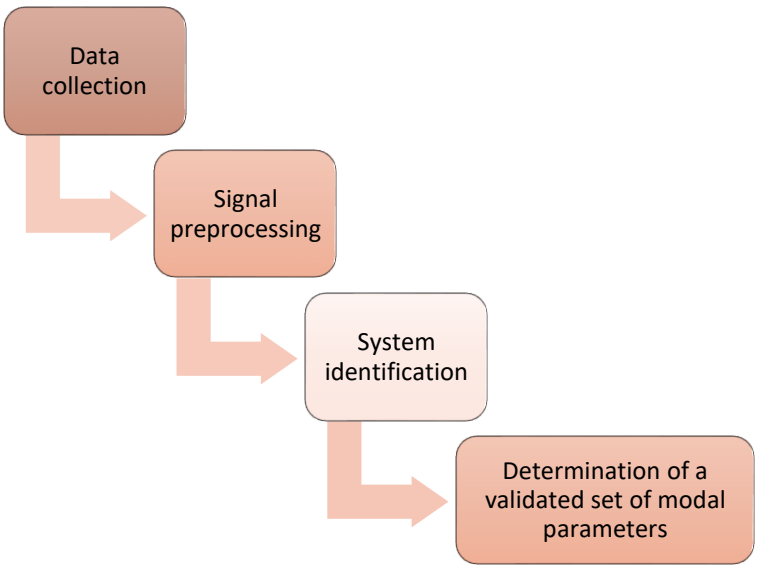

Figure 5.4 – Stages of operational modal analysis.

5.3.2. CLUSTER ANALYSIS

Cluster analysis is an exploratory method that consists of grouping elements into classes in such a way that each class is constituted by elements similar to each other, and that all classes are as heterogeneous as possible in relation to each other. That is, each individual belonging to a particular group is similar to all others belonging to the same group, and different from those belonging to the other groups.

In the context of modal identification methods using multi-order models, such as SSI-Cov and p-LSCF, the main objective is to group modal estimates that represent the same physical mode. For this, it is possible to use hierarchical or non-hierarchical classification methods.

Non-hierarchical methods are characterized by the definition of a number of classes to be obtained, which in the context of operational modal analysis may be considered a drawback. These methods involve grouping elements into a number of groups, previously determined, that will be as heterogeneous as possible among each other and as homogeneous as possible within each group. For this, initial seeds are defined by the user, around which the clusters will be created. In relation to hierarchical methods they have the advantage of being easily applied to large data matrices. Moreover, these methods are capable of regrouping individuals into clusters, other than those in which they were initially placed, if this leads to greater intra-group homogeneity and intergroup heterogeneity, which is not the case with hierarchical methods, where inclusion in a group is definitive (Johnson & Wichern, 2007). Examples of the application of this type of algorithms in the automatic classification of poles resulting from modal identification methods are presented in (P. Verboven et al., 2002) and (Scionti & Lanslots, 2005). A general scheme of the application of this algorithm is illustrated in Figure 5.5.

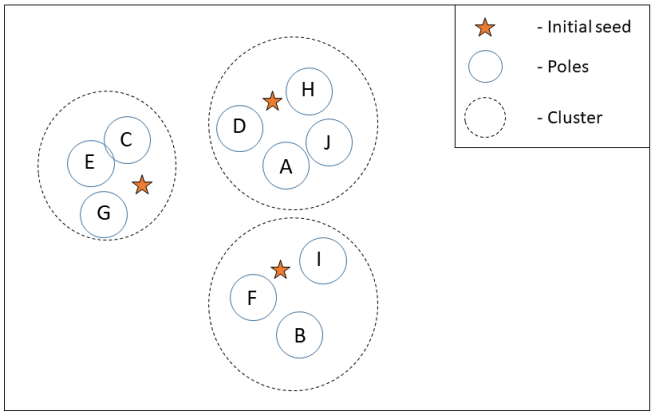

Figure 5.5 – Simple scheme of non-hierarchical clustering.

Hierarchical methods, in turn, resort to successive steps of individual aggregation. These methods may be agglomerative or divisive. In agglomerative hierarchical methods, there are initially a number of groups equal to the number of individuals under study, and these are grouped according to their neighborhood until a single group is obtained. On the other hand, in divisive hierarchical methods there is a single group where all individuals are included, and these are distributed in subgroups according to their distance measures, until all individuals are isolated (Johnson & Wichern, 2007). The end result of the application of hierarchical methods is often presented in the form of a tree representation (dendrogram). The dendrogram allows to understand the evolution of aggregations between variables from the most branched zone, where each variable corresponds to a class, to the top of the tree in which all the variables belong to a single class. It is up to the analyst to assess where the dendrogram should be cut to obtain a suitable number of classes. Some typical dendrograms are shown in Figure 5.6. Summing up, the algorithm of hierarchical clustering methodology complies the following four main steps:

1) Calculation of the similarity between every pair of poles, which measures the distance between poles.

2) Calculation of the similarity between every cluster, using adequate criteria as single linkage, complete linkage, average linkage or centroid method (Branco, 2004);

3) Linking the clusters in a hierarchical tree;

4) Definition of a rule to cut the hierarchical tree, which will define the final number of clusters.

Pappa et al. (Pappa et al., 1998) is said to be the first work to report the consideration of this type of strategy for automatic system identification. In this case, modal properties of a space shuttle were being identified, and the Modal Assurance Criterion (MAC) and differences between natural frequencies values were used as distance measures (Reynders et al., 2012). Examples of application using the LSCF and the SSI-Cov methods are presented, respectively in (Peter Verboven et al., 2003) and (Magalhães et al., 2009).

In the next section, a specific hierarchical clustering methodology following the previous four steps is presented. This methodology was implemented and applied in the tracking of natural frequencies obtained in the context of the continuous monitoring of Baixo Sabor and Foz Tua arch dams, which will be presented in chapters 6 and 7.

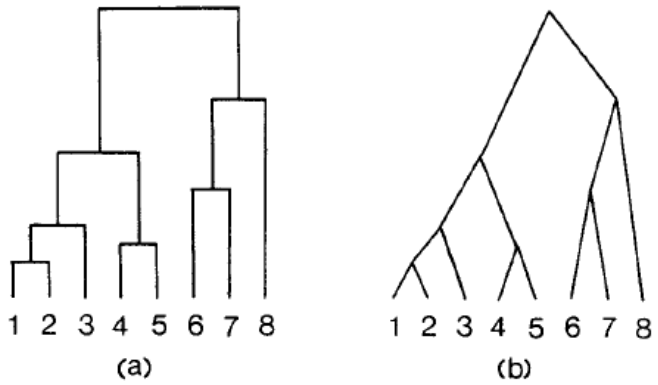

Figure 5.6 – Typical dendrogram configurations (Gordon, 1999).

5.3.3. ADOPTED HIERARCHICAL CLUSTER ANALYSIS

In the context of the continuous dynamic monitoring of dams, a methodology for automatic identification of modal parameters was adopted and implemented. This methodology, which was first proposed and implemented by (Magalhães, 2010) to continuously track the natural frequencies of a long span arch bridge, is based on a hierarchical cluster algorithm that may be applied to parametric system identification methods, such as SSI-Cov and p-LSCF, with the aim of separating physical modes from spurious ones.

As stated in the last section, the hierarchical cluster analysis starts with the calculation of the similarity between every pair of poles. Estimates of modal damping are not appropriate to distinguish modes of vibration, since two distinct modes may have the same damping value, and also because their estimates present a high scatter, as illustrated with Figure 3.15. Thus, natural frequency values and mode shapes are used for this purpose. In this case, the distance between two poles is calculated using equation (5.1):

$$d_{i-j} = \left|\frac{f_i - f_j}{f_j}\right| + (1 - MAC_{i,j}) \tag{5.1}$$

With:

f_i	Natural frequency of modal estimate i
f_j	Natural frequency of modal estimate j
$MAC_{i,j}$	Modal Assurance Criterion between modal configurations of estimates i and j
ϕ_i	Modal configuration i

ϕ_j	Modal configuration j

Short distances between two poles mean that they represent similar frequencies and modal configurations and that they probably represent the same vibration mode, so they should be included in the same cluster. It is worth noting that each application of an automated algorithm requires a training period to accurately tune it, before it can be used without any human interaction. In this case, for instance, weighting factors may be used in order to accentuate either the frequency or the MAC part of the equation.

Once the first step is concluded, the similarity between clusters must be calculated. In the implemented strategy the single linkage was considered, so the shortest distance between two poles belonging to the two clusters (one pole from each cluster) is used to represent the distance between clusters. Distances are calculated through equation (5.1) once again.

After the tree diagram is constructed a rule must be defined to find the cutting level. Since the number of clusters containing spurious poles that will be formed is unknown, it is necessary to choose a criterion that do not exclude physical modes. In this case, the maximum distance among the distances between any pole and its closest pole inside the cluster was the chosen rule, to guarantee homogeneous clusters. However, the maximum distance value must be carefully assessed since too short distances may lead to similar poles falling into different clusters and too large distances may induce the aggregation of different poles into the same cluster (Magalhães, 2010).

The identification process ends with the distinction between physical and spurious poles clusters, from the entire set of clusters. Taking in mind that poles referring to physical modes are normally consistent along the different orders of identified systems, thus producing much more populated clusters, most of the spurious poles clusters may be detected, and consequently abandoned, for presenting a reduced number of poles. In some applications, if the number of physical modes (n_m) expected in the frequency range of analysis can be anticipated (by a preliminary analysis), then the n_m clusters with more elements may be selected (Magalhães, 2010). However, it is worth noticing that in the case of the existence of external sources of noise, such as rotating machines working close to the structure, the recorded time series of accelerations will be polluted with very specific frequencies which, though not corresponding to a physical mode of the structure, may later generate populated clusters that may be mistaken for one (Pereira et al., 2018). In this sense, it is recommendable to choose the first (n_m + s) most populated clusters, where "s" corresponds to a safety net adequate to each application.

Then, the remaining (n_m + s) clusters are compared to a set of reference modal properties of the vibration modes intended to be tracked, defined during a training period, and the relevant clusters are finally selected. To perform this comparison between clusters and references, average values of the modal parameters associated with the poles inside the selected clusters are computed and then used as representative of their cluster. Nevertheless, before computing the cluster representative averages, it is important to eliminate poles associated with extreme values of modal damping ratios. For this an outlier analysis (Johnson & Wichern, 2007) is performed within each cluster, which consists on eliminating poles with damping ratios respectively below or above the limits defined by the inequations in (5.2):

$$Dr < Q1 - 1.5\,IQR \qquad (5.2)$$

$$Dr > Q3 + 1.5\,IQR$$

With:

Dr_i	Damping ratios estimate
$Q1$	Lower quartile: 25 % of values are below this limit
$Q3$	Upper quartile: 25 % of values are above this limit
IQR	Interquartile: Q3 – Q1

Finally, each cluster representative values are compared to the reference properties in two consecutive stages. First, every cluster natural frequency average is compared to the reference natural frequency of the first vibration mode and the clusters that present differences below a predefined limit are selected. Then, to differentiate modes with close frequency values, the MAC values between the representative mode shapes of the selected clusters and the reference mode shape of the first vibration mode is computed and the cluster with the highest MAC value is selected as the modal estimate of the first vibration mode, if the corresponding MAC is above a predefined limit. This procedure is then repeated for the other vibration modes until a complete set of modal estimates is obtained.

Though this technique is generally very efficient, some aspects should be taken into account when dealing with specific monitoring scenarios. For instance, when the structure being monitored is subjected to intense operational and environmental effects leading to large frequency variations over time, higher frequency differences between reference and cluster frequencies must be admitted when performing the modal tracking, since the reference value is fixed but the value of the natural

frequency to be tracked is oscillating over time and the intensity of this oscillation is not necessarily known. This scenario may lead to an increase in the number of misidentifications or, in extreme cases, to the impossibility of accurately tracking one or more modes. To overcome this drawback, instead of fix frequency references, moving references can be used. The frequency reference value of each vibration mode varies over time, accompanying the variation of the natural frequency true value, based on estimates provided by the study of the operational and environmental conditions affecting the structure. This will be used in the application presented in chapter 7.

5.3.4. Improving Modal Tracking with the Estimation of Uncertainties

Using the methodology presented in the previous section for automatic operational modal analysis, a group of clusters is obtained after the application of SSI-Cov to a 30-minute set of recorded accelerations. Moreover, each cluster is composed by a group of poles and, if the version of SSI-Cov presented in (Reynders et al., 2008) and (M. Döhler & Mevel, 2013) is used, besides the three regular quantities obtained from the common application of SSI-Cov, two more are obtained with this version, thus five different quantities are associated with each pole:

- Natural frequency (f [Hz]);
- Damping ratio (d [%]);
- Mode Shape;
- Standard deviation of natural frequency (f_{std} [Hz]);
- Standard deviation of damping ratio (d_{std} [%]).

With this implementation, it would be possible to obtain as well the standard deviations associated with each modal ordinate, which would indicate the uncertainty related to the final mode shape. However, this was not considered in this work. Additionally, relative values of standard deviations may be computed, dividing each standard deviation value by its natural frequency ($f_{std\text{-}relative}$) or damping ratio ($d_{std\text{-}relative}$). In the end, the estimates of modal properties and respective standard deviation values are calculated as the mean value of all the poles integrating the cluster, eventually disregarding estimates with high uncertainty.

An example using real data from the dynamic monitoring system of Baixo Sabor is presented in Table 5.1, comprehending five poles, which for the purpose of this example were selected from all the poles belonging to the same cluster, thus resulting from the same set of 30 minutes acceleration time series. Most of the five poles present natural frequencies close to 3.52 Hz, and damping ratios

around 1.5 %. It is worth noticing that the frequency value of pole 3, the only one in the group closer to 3.51 than to 3.52 Hz, shows the highest standard deviation, indicating that higher uncertainty is associated with this pole. The same is observed with the standard deviation of its damping ratio, which is so high that it leads to a relative standard deviation of 101.7 %. In this sense, the estimates of modal properties for this cluster were calculated considering both the mean of the five poles and the mean of four poles, excluding pole 3. Even if small differences were obtained, it is worth pointing out that the uncertainty associated with the modal properties was minimized in the second case, which gives the analyst more confidence in the results obtained and prospects better chances of successfully building damage detection models in the future.

Table 5.1 – Pole quantities example

Pole	f [Hz]	f_{std} [Hz]	$f_{std\text{-}relative}$ [%]	d [%]	d_{std} [%]	$d_{std\text{-}relative}$ [%]
1	3.522	0.0041	0.117	1.488	0.110	7.4
2	3.521	0.0053	0.152	1.503	0.229	15.2
3	3.513	0.0419	1.194	1.540	1.566	101.7
4	3.524	0.0086	0.245	1.624	0.335	20.6
5	3.520	0.0113	0.321	1.585	0.500	31.6
$Mean_{all}$	3.520	0.0143	0.406	1.548	0.548	35.3
$Mean_{[1,2,4,5]}$	3.522	0.0073	0.209	1.550	0.294	18.7

The following section of this chapter presents different methods that allow performing a separation and removing the effects of environmental and operational conditions on features extracted from identification methods, permitting an adequate continuous monitoring of structures.

5.4. REMOVING OF ENVIRONMENTAL AND OPERATIONAL EFFECTS

5.4.1. INTRODUCTION

In the context of structural health monitoring, it is common for environmental and operational effects, such as temperature, humidity, wind, road traffic or turbines rotation to generate data variability large enough to hide anomalies produced by novel structural behaviour that, in this sense, must be distinguished and eliminated.

The process of removing this parasite effects provoked by environmental and operational conditions, also known as *data normalization*, generally follows one of two main approaches (J. P. Santos et al., 2013). The first approach relies on the use of environmental and operational actions as inputs to establish regression models with the structural responses (system outputs), whose parameters are tuned using a large number of observations. In turn, the second one is based on statistical algorithms that do not consider the referred inputs, not needing the measurement of the mentioned external factors.

Analogously to the nomenclature used for system identification algorithms, methods associated with the first approach, that is, methods adopting the measurements of external factors as inputs, will be designated input-output methods, while methods related with the second approach, which does not rely on external factors measurements, will be labeled output-only methods. Alternatively, these methods may also be called regression-based normalization methods and latent-variables based normalization methods, respectively.

5.4.2. INPUT-OUTPUT METHODS

As it was addressed before, natural frequencies are commonly used as monitoring features, since they are usually less contaminated by experimental noise than other modal properties and therefore accurate estimates are easily obtained. A straightforward way of establishing relations between environmental and operational factors and the estimated natural frequencies consists on the construction of linear regression models. In spite of being able of assuming only linear relations between inputs and outputs, the fact is that most of this physical relations have a linear nature, and the input might also be manipulated to present linear relations. Therefore, multivariate linear regression models, based on computationally undemanding algorithms, will be presented in this section.

Different methods, more complex and appropriate to model nonlinear relations, are based on Neural Networks, such as the Multi-Layer Perceptron (MLP), used by (Ni et al., 2009) to describe the relation between temperature and natural frequencies on a bridge, or methods based on statistical learning, such as the Support Vector Regression (SVR).

Multiple Linear Regressions

Multiple Linear Regression (MLR) models main goal is to predict response values (dependent variable) based on the evaluation of a collection of predictor (independent variable) data (Johnson & Wichern, 2007). The model may initially be used to interpret the influence of the predictor variable on the dependent one and then, once this relation is established, to treat predictor values in order to forecast dependent data that is not available.

In the context of Structural Health Monitoring, environmental or operational factors are used as predictors for modal parameters, namely natural frequencies. Generally, a model is constructed with a set of data which then allows to predict natural frequencies values based on the evaluation of an independent external factor, such as temperature, and finally these predicted values are compared to the ones directly obtained from modal identification algorithms. This method is applied to a real scenario in chapter 6, with the aim of removing the effect of reservoir water level, temperature and concrete hardening with time on a dam's natural frequencies. Additionally, it is applied once again in chapter 7 to predict the best reference that should be used in the modal tracking of a particular vibration mode of a second concrete arch dam.

The method will first be addressed to the situation of a single dependent variable being used, and then will be generalized to a version with multiple response variables. The mathematical definition of a Multiple Linear Regression Model is provided by (Johnson & Wichern, 2007):

$$y = Z.\beta + \varepsilon \tag{5.3}$$

With:

y	Vector with n observations of the dependent variable Matrix dimension: $(n \times 1)$
Z	Matrix with the n values of the predictors (for p environmental effects) Matrix dimension: $(n \times (p+1))$

β	Vector with weight parameters of the p predictor variables Matrix dimension: $((p+1) \times 1)$
ε	Vector with the values of the random error Matrix dimension: $(n \times 1)$

Random errors, due to measurement issues and the existence of variables not explicitly considered in the model, are represented with vector ε and present the following properties:

$$E[\varepsilon] = 0 \tag{5.4}$$

$$Cov[\varepsilon] = E[\varepsilon . \varepsilon^T] = {\sigma_\varepsilon}^2 . I \tag{5.5}$$

With:

$E[*]$	Expected value operator

It is important to mention, on the one hand, that in equation (5.3) the first column of Z is filled by ones, which is the reason why there are $(p+1)$ columns in this matrix, and on the other hand, that a normalization is usually performed on Z, being each element subtracted from the mean values and then divided by the variable's standard deviation:

$$Z_i' = \frac{Z_i - E[Z_i]}{\sigma_{Z_i}} \tag{5.6}$$

With:

Z'	Normalized value of Z
σ	Standard deviation

However, the previous matrices should only be defined after the evaluation of the influence that each predictor has on the response variable. This influence may be assessed with the calculation of correlations, which may be computed with Pearson's product-moment correlation coefficient (Johnson & Wichern, 2007) presented by equation (5.7) for the calculation of the correlation between two variables x and y:

$$r_{xy} = \frac{Cov(x,y)}{\sigma_x . \sigma_y} \tag{5.7}$$

Predictors that present high correlation values with the response variable and low correlation values with other predictors should be selected (Magalhães, 2010). Pearson's correlation values close to zero represent low linear correlations, while values close to one (in absolute value) might indicate a good correlation. Nonetheless, since this tool only analyses linear correlations, a correlation equal to zero means only that no linear relation exist between the two variables, but the possibility of a non-linear relation must not be excluded.

The next step consists on the estimation of matrix β (named as $\hat{\beta}$), which is obtained through the application of the least squares method and defined as:

$$\hat{\beta} = (Z^T.Z)^{-1}.Z^T.y \tag{5.8}$$

The random error, vector ε, should now be evaluated. In that sense, an estimation of the residual random errors is given by the difference between real and estimated response variable (Johnson & Wichern, 2007):

$$\hat{\varepsilon} = y - \hat{y} = (I - Z.(Z^T.Z)^{-1}.Z^T).y \tag{5.9}$$

The quality of the model adjustment may be assessed through the computation of the estimation of the variance of $\hat{\varepsilon}$:

$$\hat{\sigma}_\varepsilon{}^2 = \frac{1}{n}.\sum_{k=1}^{n} \varepsilon_k{}^2 \tag{5.10}$$

However, since this indicator depends on the absolute values of y variable, a second path that includes the calculation of the coefficient of determination, may be used to avoid this inconvenience:

$$R^2 = 1 - \frac{\sum_{k=1}^{n} \varepsilon_k{}^2}{\sum_{k=1}^{n}(y_k - \bar{y})^2} = \frac{\sum_{k=1}^{n}(\hat{y}_k - \bar{y})^2}{\sum_{k=1}^{n}(y_k - \bar{y})^2} \tag{5.11}$$

The coefficient R^2 represents a ratio between variances that quantifies how much of the responses' variance is explained by the predictor variables. It varies from one, associated with situations where the adjustment passes exactly through all data points, to zero, which represents a total independence

between response and predictor variables. Once a good model is obtained, it can be used to predict future values of the response variable ($\hat{y}_0$), designated forecasts, based on predictors not considered for its definition (z_0). :

$$\hat{y}_0 = z_0 \,.\hat{\beta} \tag{5.12}$$

Since it is not expected for forecasted and observed values to exactly match, it is essential to calculate confidence intervals to account for the existent uncertainty. In that sense, if errors (ε) are considered as normally distributed, a confidence interval of $100 \cdot (1-\alpha)$ per cent is given for the forecasted values ($\hat{y}_0$) by (Johnson & Wichern, 2007):

$$\hat{y}_0 \pm t_{n-p-1}\left(\frac{\alpha}{2}\right).\sqrt{\hat{\sigma}_\varepsilon[1 + z_0{}^T (Z^T.Z)^{-1}.z_0]} = \hat{y}_0 \pm I(z_0) \tag{5.13}$$

With:

$t_{n-p-1}(\frac{\alpha}{2})$	The upper $100(1-\alpha)$th percentile of a t-distribution with n-p-1 degrees

With equation (5.13) a range is defined within which the estimated natural frequencies should lay in. Taking into account the considerations about how the first column of Z is filled with ones and the elements of the other columns are normalized, the confidence interval can be written as (Magalhães, 2010):

$$\bar{y} - I(z_0) < \tilde{y}_0 \sum_{j=2}^{p} \beta_j z_{0j} < \bar{y} + I(z_0) \tag{5.14}$$

With:

$\tilde{y}_0$	New response variable value (which was not considered for the definition of β)

Frequencies outside this interval are generally explained as a result of an incorrect identification or by the occurrence of a novel structural behaviour. In the context of structural health monitoring, these regression models should be built using as training period the data collected from an entire year, so that seasons influence in the identification output are well characterized. It is worth noting that regression models are not valid for extrapolations, so forecasted values must always be associated with input data within the interval used to construct the model.

The presented method may be easily generalized for a set of several dependent variables, by formulating the previous methodology as many times as response variables there are, or through the following matrix equation:

$$Y = Z.B + E \tag{5.15}$$

With:

Y	Matrix with n observations of the m dependent variables Matrix dimension: $(n \times m)$
Z	Matrix with the n values of the p predictors (for p environmental effects) Matrix dimension: $(n \times (p+1))$
B	Matrix with weight parameters of the p predictor variables Matrix dimension: $((p+1) \times m)$
E	Vector with the values of the random error Matrix dimension: $(n \times m)$

Dynamic Regression Models

The previously presented regression model is considered a static model, since it forecasts response values for a certain instant k using only data from predictor variables collected with the same time instant k. However, there are models classified as dynamic, that besides correlating the timely correspondent information, take into account that dependent variables may also be influenced by the model inputs of previous time instants. A good example of this impact would be the effect of response variables with a large inertia to predictor's variation, such as temperature on natural frequencies, since the process characteristics of heating and cooling of materials would justify the use of dynamic regression models.

The implementation of dynamic regression models may follow the same formulation presented for static models, adding to this one predictors consisting of observations of the independent variables according to a predefined time lag with respect to the dependent variables.

5.4.3. OUTPUT-ONLY METHODS

Alternatively to input-output methods, the removing of environmental and operational effects on modal parameters may be achieved using methods that do not need the measurement of these external factors. However, these methods can be used in combination with the previously presented ones with the aim of producing an even cleaner time evolution of extracted features.

Principal Components Analysis (PCA) and Factor Analysis (FA) are two multivariate statistical tools that try to explain the variance of the set of extracted features variables, whose algorithms are based on the decomposition of the covariance matrices (Johnson & Wichern, 2007). PCA is applied with good results to the monitoring of bridges in (Yan et al., 2005a), (Magalhães et al., 2012) and (Comanducci et al., 2016), using the method by itself or in combination with Multiple Linear Regressions. Additionally, in (Bellino et al., 2010) PCA is used in the monitoring of a railway bridge that was considered a time-varying system, due to the passage of trains. On the other hand, the use of Factor Analysis for structural health monitoring is demonstrated in (Kullaa, 2004) and (Deraemaeker et al., 2008) using data generated by numerical models.

Furthermore, Auto Associative Neural Networks (AANN) is a latent-variable method known as the nonlinear counterpart of the PCA method, which aims to define the optimal mapping between a set of original variables and a newly obtained set of uncorrelated variables (Santos, 2014). Also, the Multilayer Perceptron (MLP) is a neural network technique that has been used to reproduce the horizontal displacement recorded by a pendulum in a Portuguese large concrete dam (Mata, 2011).

Additionally, the Second Order Blind Identification (SOBI), a source separation technique that exploits the time coherence of the source (Belouchrani et al., 1997), has been used to separate the effects of operational and environmental conditions from the tracked natural frequencies of a steel cable and of a concrete arch bridge (Rainieri et al., 2019), with results and computation needs similar to those of PCA.

In the following subsection the PCA method is presented in more detail. This method will be used in chapter 6, by itself and in combination with MLR, to remove the effect of operational and environmental conditions from the natural frequencies obtained with the continuous monitoring of a concrete arch dam

Principal Components Analysis

Principal Components Analysis (PCA) is a multivariate statistical method used for reduction and simplification of the information contained in the variables under study through the explanation of its variance or covariance structure. Most of this structure, obtained from the evaluation of m variables, may then be explained through the linear combination of a smaller set of p independent and orthogonal variables, called principal components, hence reducing the problem's dimension. However, even though the majority of the problem's variance may be explained by the new set of p variables, the explanation of the entire variance of the whole set of original variables is only achievable if $p = m$.

Algebraically, PCA transforms the initial set y of variables into a new z coordinate system (Johnson & Wichern, 2007):

$$z = T.y \tag{5.16}$$

With:

z	Matrix with n principal components
	Matrix dimension: ($m \times n$)
T	Orthogonal matrix that computes the linear transformation
	Matrix dimension: ($m \times m$)
y	Vector with n observations of the m dependent variables
	Matrix dimension: ($m \times n$)

The main goal of PCA is to define a matrix T that allows the calculation of a z matrix with explained variance of the original set of variables in descending order, that is, the upper principal components explain the most system's variance.

The normalization presented in equation (5.6) may be applied in this method, as well. One important property of matrices y and z is presented by the next equation (Magalhães, 2010):

$$\Sigma = E[y.y^T] = E[T^T.z.z^T.T] = T^T.\Lambda.T \tag{5.17}$$

With:

Σ	Covariance (or correlation, if the normalization of equation (5.6) is applied) matrix of y

Λ	Covariance matrix of z (diagonal matrix)

The PCA methodology starts with the singular value decomposition of matrix Σ:

$$\Sigma = U.S.U^T \tag{5.18}$$

With this decomposition, and taking into account equations (5.17) and (5.18), one may conclude that matrices T ($T = U^T$) and Λ ($\Lambda = S$) are obtained. At this point, a suitable number of principal components should be chosen looking both at equation (5.19), that gives the cumulated percentage of variance contained in the selected p components, and to the differences between the variance explained by consecutive principal components. When these differences are close to zero, it means that the gain between using or not the next principal component is not significant and thus, depending on the application, a smaller number of components may be chosen.

$$\mathrm{I} = \frac{\sum_{i=1}^{p} s_i}{\sum_{i=1}^{m} s_i} \tag{5.19}$$

With:

Σ	Covariance (or correlation, if the normalization of equation XX is applied) matrix of y

Once p components are chosen, a matrix $\hat{T}$ is automatically defined by the first p columns of U, and the new reduced $\hat{z}$ matrix is obtained with equation (5.16). Even though the main objective of the dimension reduction is already achieved, it is still possible to redirect the z components to the original space and to compute an estimation of $\hat{y}$ (Magalhães, 2010):

$$\hat{y} = \hat{T}^T.\hat{z} = \hat{T}^T.\hat{T}.y \tag{5.20}$$

Therefore, the residual error (ε) between the real observations and the estimations obtained after the transformation results from the following difference:

$$\varepsilon = y - \hat{y} \tag{5.21}$$

Similarly to what was exposed about regression models, the application of PCA to eliminate the effects of environmental and operational conditions must take in consideration a training period

long enough to contain a full range of variations of these external factors as well as a period relative to the structure's healthy state.

The dimension reduction imposed by the method's first phase eliminates minor errors such as the random errors that arise during the identification process (to obtain, for instance, natural frequencies), but not the effects due to relevant factors, such as temperature. These external conditions act as major influencers that are only excluded with the computation of the difference between observed values and the estimates obtained from equation (5.20). Therefore, these residues may be used to detect abnormal variations that may be associated with novel structural performance. Moreover, the number of components retained should be equal to the number of independent variables producing the largest contribution to the variance in the data and whose effects have to be removed (Comanducci et al., 2016).

The fact that PCA assumes linear correlations between output variables is a main limitation in the cases when the relation between such variables is not linear. In order to overcome this limitation, the Local PCA approach, proposed by (Kambhatla & Leen, 1997) may be considered. Local PCA consists of a local approach, where the original n-dimensional space is properly partitioned and linear principal components are locally defined in each sub region, which is known to be more computationally efficient when compared to other non-linear methods (Yan et al., 2005b). A geometric interpretation of both PCA and Local PCA in a generic bivariate case, considering two sub regions, is presented in Figure 5.7.

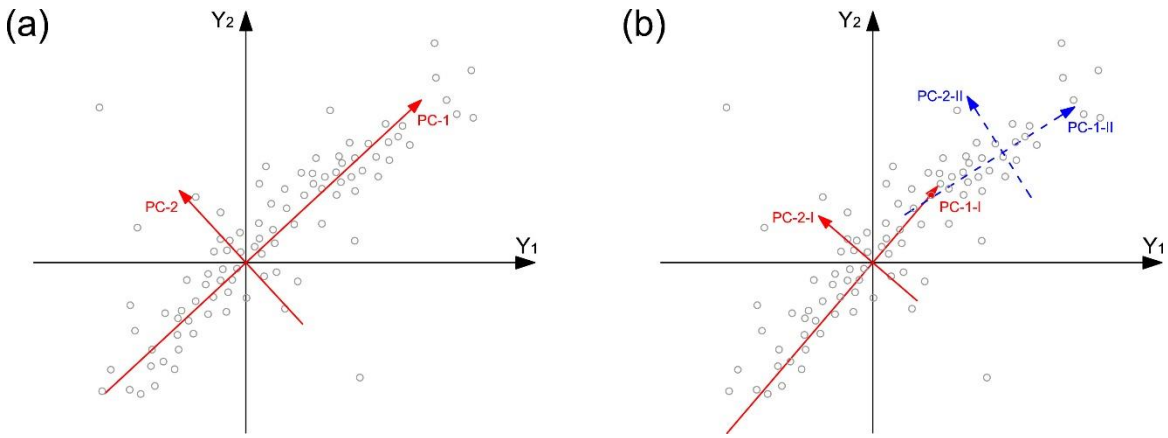

Figure 5.7 – (a) Geometric interpretation of principal components analysis (PCA and (b) local PCA (L-PCA) (Comanducci et al., 2016).

5.5. DAMAGE DETECTION – CONTROL CHARTS

Control charts are a technique used for statistical process control that is applied to perform a global evaluation on whether the development of one or more variables is kept within predefined limits. In the context of structural health monitoring, features insensitive to environmental and operational factors should be used, otherwise very large limits would be needed to keep the process under control, thus hiding the emergence of novel behaviour due to structural causes. In this context, the time evolution of a structure's natural frequencies, after the minimization of the effects of external factors, becomes an interesting feature to evaluate the emergence of damage using this tool. A control chart consists in the representation of observations over time, along with horizontal lines, called control limits that mark the boundaries of acceptable data variation due to common causes. When associated with structural health monitoring, observations outside this region are considered out-of-control events, which suggests the possibility of damage occurrence. Examples of control charts being used to perform damage detection are presented in (Soo Lon Wah et al., 2019).

A common example of control charts is the Shewhart $\bar{X}$-chart, which is constructed by plotting individual observations, or the mean of groups of observations, over time along with a central line, that represents the mean, and two other lines representing the upper (UCL) and lower (LCL) control limits. For this type of chart, these limits are defined as (Montgomery, 2009):

$$\mathrm{UCL} = \bar{\bar{x}} + R.\sigma \tag{5.22}$$

$$\mathrm{LCL} = \bar{\bar{x}} - R.\sigma$$

With:

$\bar{\bar{x}}$	Mean value from all observations.
σ	Standard deviation (when single observations are controlled).
R	"Distance" between the control lines and the central line.

In the case the mean of subsamples with size r is being controlled, σ is equal to the sample standard deviation divided by $\sqrt{r}$. Additionally, if $R = 3$, and a normal distribution is assumed, the control limits correspond to a confidence level of 99,7%.

However, in the presence of a process characterized by more than one feature (for instance, m vibration modes), multivariate control charts, as T^2 control chart, can be applied to set a control

region for future observations, based on the data collected during the training period. These charts use a statistical test named T^2 and the LCL is always assumed as zero.

Similarly to what was presented for $\bar{X}$-chart, T^2 control charts may be applied both to individual observations and to subgrouped data. In the case of each future individual observation x being checked, the expressions for the T^2 - statistic and the UCL are computed as defined next:

$$T^2 = \frac{n}{n+1}.(\mathrm{x} - \bar{\bar{x}})^T.S^{-1}.(\mathrm{x} - \bar{\bar{x}}) \tag{5.23}$$

$$\mathrm{UCL} = \frac{(n-1).m}{n-3}.F_{m,n-m}(\alpha)$$

With:

n	Number of observations collected during the reference period
x	Individual observation (vector with m components)
S	Covariance matrix
$F_{m,n-m}(\alpha)$	α percentage point of the F distribution with m and $n-m$ degrees of freedom

On the other hand if, instead of individual observations, subsamples grouping r observations are controlled, the T^2 - statistic and the UCL follow the expressions:

$$T^2 = \mathrm{r}.(\bar{\mathrm{x}} - \bar{\bar{x}})^T.S^{-1}.(\bar{\mathrm{x}} - \bar{\bar{x}}) \tag{5.24}$$

$$\mathrm{UCL} = \frac{m.(s+1).(r-1)}{s.r-s-m+1}.F_{m,s.r-s-m+1}(\alpha)$$

With:

$\bar{\mathrm{x}}$	Subgroup average
$\bar{\bar{x}}$	Process average
R	Number of groups collected during the reference period

In the context of structural health monitoring it is important to define performance criteria that help the user to analyse the charts and the occurrence of damage. Therefore, three parameters are introduced for investigating the damage detection capabilities of a determined SHM application. The first two are the relative frequencies of outliers in the reference (or observation) period and in the control (or damaged) period, denoted by $\mathrm{Out}_{\mathrm{ref}}$ and $\mathrm{Out}_{\mathrm{control}}$, respectively. The control period

consists in the period that will be checked for the occurrence of damage, or when damage is introduced in the data, in the case of numerically simulated damages used to test damage detection tools. Thus, Out_{ref} and $Out_{control}$ are computed as:

$$Out_{ref} = \frac{n_{out_{ref}}}{n_{T^2_{ref}}} \tag{5.25}$$

$$Out_{control} = \frac{n_{out_{control}}}{n_{T^2_{control}}}$$

With:

n_{out}	Number of outliers, during the reference (ref) or the control periods
n_{T^2}	Total number of control points, during the reference (ref) or the control periods

In order to detect damage, $Out_{control}$ should be maximized and its optimal value is 100 %, though damage can be detected with lower percentages. When the UCL is statistically computed in the reference period as the value of T^2 corresponding to a cumulative frequency of 95 %, the objective value of Out_{ref} is 5 %. However, when using short periods, or group averages from a large number of elements, resulting in a reduced number of points, values significantly different from 5 % can be observed. A performance indicator, J_R is thus introduced to better quantify the damage detection capabilities of the considered techniques (Comanducci et al., 2016), which is defined as:

$$J_R = \frac{\overline{T^2}_{control}}{\overline{T^2}_{ref}} \tag{5.26}$$

With:

$\overline{T^2}_{ref}$	Average T^2 value during the reference period
$\overline{T^2}_{control}$	Average T^2 value during the control period

A larger value of J_R indicates a clearer increase in T^2 in comparison with the normal conditions, thus highlighting a higher capability of the considered technique in revealing the occurrence of damage.

Finally, a prompt way of first detecting small damages (which do not lead to a percentage of outliers above the UCL close to 100 %), consists in considering the occurrence of damage only if a number "n" of outliers is consecutively found above the UCL.

5.6. FINAL CONSIDERATIONS

Besides the punctual occurrence of major external actions, such as earthquakes or accidents, the normal subjection to time and operational and environmental factors will inevitably slowly deteriorate structures. In this way, to keep structures within high levels of safety and performance, and extend their life spans as long as possible, maintenance and rehabilitation programs are imperative. For this, information about the structure should be gathered as frequently as possible. In the case of dams, though structural health monitoring systems are historically associated with the gathering of static data such as displacements, stresses or relative movements between joints, dynamic testing in the shape of forced vibration tests are common as well, mostly to validate design assumptions and calibrate and update numerical models. However, vibration-based monitoring systems have been successfully installed in many different structures in the past, and a few cases of this type of programs running in concrete dams have been reported to provide promising results.

In this context, tools and concepts that should be taken into account when using automatic operational modal analysis to perform modal tracking were addressed in this chapter. Good results can be achieved using cluster analysis. The procedure that was adopted in the processing of the data recorded in the case studies that will be presented in chapters 6 and 7 was also described. Additionally, it was introduced the possibility of including the uncertainties associated with natural frequencies and damping ratios in the algorithm used for modal tracking, with the aim of minimizing the number of misidentifications and thus obtain monitoring features associated with higher confidence levels.

Besides assuring the tracking of modal properties, to efficiently monitor a structure, it is necessary to study the influence of external factors in such properties. In this sense, a short overview on different techniques used to remove the effects of operational and environmental conditions on modal properties was presented. Techniques such as multiple linear regressions (MLR) and principal components analysis (PCA) that will be used in chapter 6, were described with more detail. Finally, control charts were introduced and the particularities related with the performance of damage detection using this tool were addressed, including the presentation of few performance criteria. It is worth mention, that the quality of both the minimization of the effects of external factors and damage detection tools is strictly related with the correct characterization of the variables affecting the structure, thus accurate measurements and large monitoring periods are imperative.

6. CONTINUOUS DYNAMIC MONITORING OF BAIXO SABOR DAM

6.1. INTRODUCTION

The continuous dynamic monitoring of Baixo Sabor dam is being carried out by the Laboratory of Vibrations and Structural Monitoring (ViBest) of the Faculty of Engineering of the University of Porto (FEUP) and by the Concrete Dams Department of the National Laboratory of Civil Engineering (LNEC), in the scope of the research project (DAM_AGE, 2016-2018), in order to identify the dam dynamic characteristics and their evolution over time, taking into account the variation of ambient and operational conditions, as well as the possible evolution of the materials mechanical properties (LNEC et al., 2015).

In this chapter, Baixo Sabor arch dam and the dynamic monitoring system installed on the structure are introduced. Afterwards, it is presented the data obtained during the first three years of continuous monitoring, between 01/12/2015 and 30/11/2018, which comprehends a major part of the reservoir filling period. The dams first 10 vibration modes are identified using SSI-Cov method, and automatic operational modal analysis is used to track the modal properties of these modes during the monitoring period. The uncertainties associated with natural frequencies and damping ratios are quantified and used to improve the quality of the results produced by the tracking routines.After this, multiple linear regression models and principal components analysis are used to minimize the effects of operational and environmental factors on the estimated natural frequencies. Lastly, the corrected natural frequencies are used, along with damages numerically simulated, to test the suitability of the present system and methodologies on the detection of novel structural behaviour, through the use of control charts.

6.2. DESCRIPTION OF THE STRUCTURE

The Baixo Sabor hydroelectric power plant is located in the municipality of Torre de Moncorvo, north-east of Portugal. Its construction started in 2008 and the dam came into service in 2016. Its reservoir extends 60 km north along the Sabor River, a tributary of the Douro River whose watershed comprises a large part of the district of Bragança, allowing a useful storage of 630 million cubic meters of water (EDP). This is a strategic location since there are four other power plants located downstream (Crestuma-Lever; Carrapatelo; Régua; Valeira) that can be supplied by Baixo Sabor reservoir in case of need. Figure 6.1 shows the location of the power plant, marked with a red symbol, on a map of northern Portugal.

Figure 6.1 – Location of Baixo Sabor hydroelectric power plant in the north-east of Portugal (Google).

This project included the construction of two dams located about 12.6 km from each other. However, in this work, only the upstream step will be approached. This is constituted by a concrete double-curvature arch dam, embedded in a narrow valley zone, installed with 189 MW of capacity. The dam is 123 m high and its crest, with a width of 6 m, is 505 m long. Thirty-two concrete vertical blocks, separated by vertical contraction joints, compose the arch, which is crossed by six horizontal visit galleries and one general gallery for drainage that contacts with the foundation all along the upstream side of the structure. The dam is endowed with a spillway composed by four floodgates, 16 m long each. The full storage level is at 234 meters above sea level and the turbines in the power plant adjacent to the dam rotate at 214 rpm. Figure 6.2 shows an aerial view of the dam and the reservoir and a closer picture of the spillway, referring to May of 2016 after the monitoring had started. In the aerial photography, it is possible to observe that the powerhouse containing the turbines for electricity production is quite close to the dam, which influences the results, as it will be concluded in the next sections of this chapter.

Figure 6.2 – Baixo Sabor arch dam (EDP).

Besides the more common static monitoring, which includes the measuring of water pressures, temperatures, movements of joints and concrete strains, among others (A. L. Batista & Matos, 2016), the dam is also equipped with a geodesic system to measure absolute and relative displacements, a seismic monitoring system to evaluate the behaviour of the structure when subjected to seismic actions and a dynamic monitoring system to continuously characterize its dynamic properties.

6.3. PRELIMINARY EXPERIMENTAL AND NUMERICAL STUDIES

When preparing the instalation of a continuous dynamic monitoring system in a structure it is important to study both the structure and its dynamic properties, in order to guarantee the monitoring system will be adequate to the task and provide good results. This study may be accomplished experimentally, through the performance of forced or/and ambient vibration tests, or/and numerically, through the development of a numerical model. Additionally, similar works developed in similar structures should be investigated. In this sense, this section presents the forced vibration tests performed in Baixo Sabor dam by the Concrete Dams Department of the Portuguese National Laboratory for Civil Engineering (LNEC) and the numerical model of the dam developed by the same institution (J. Gomes & J. V. Lemos, 2016a), which were important tools in the preparation and validation of the continuous dynamic monitoring system of Baixo Sabor dam.

6.3.1. FORCED VIBRATION TESTS

Two forced vibration tests were performed in Baixo Sabor arch dam by the National Laboratory for Civil Engineering (LNEC) to assess the dynamic characteristics of the structure. The first test (FVT 1) was conducted in January 2015, when the construction of the structure was finishing and the water level in the reservoir was 195.5 meters above sea level, which was considered as representing an empty reservoir. The second test (FVT 2) was executed in May 2016 when the reservoir was completely full, with the water level reaching 234 meters above sea level (Jorge Gomes et al., 2018).

The results of the first test were particularly important when preparing the installation and configuration of the continuous dynamic monitoring system, which started operating in December 2015, as well as to calibrate the numerical model developed in LNEC. On the other hand, the second vibration test contributed to evaluate the variation of modal properties taking into account the variation in the level of water in the reservoir between the two tests and to validate the results obtained by the continuous monitoring system.

The eccentric mass vibrator presented in Figure 6.3 a), which has been developed at LNEC, was used to apply horizontal forces with different amplitudes and frequencies. This vibrator was designed to apply a maximum force of 160 kN in a range of frequencies between 1 and 30 Hz. In turn, Figure 6.3 b) and c) present the velocity transducers and accelerometers used during these tests.

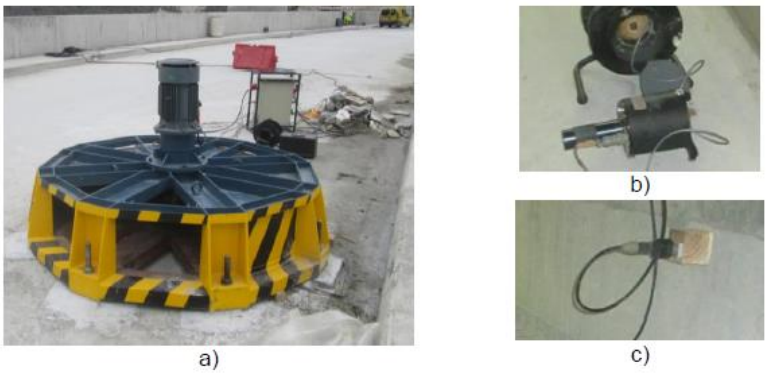

Figure 6.3 – Field equipment: a) eccentric mass vibrator, b) velocity transducer, c) accelerometer.

Both tests were performed by continuous scanning (sine sweep), which consists of applying a sinusoidal load, continuously varying frequency between two predefined values. In this case, the frequencies of imposed loads varied between 1.5 Hz and 9.6 Hz. In order to ensure a better excitation of the dam, and consequently more reliable results, various mass configurations placed on the vibrator were used, concretely large masses for lower excitation frequencies, and small masses that allow higher frequencies to be applied. Figure 6.4 presents the position of the vibrator (yellow dot) and the accelerometers (red dots) during the performed tests.

Figure 6.4 – Vibrator and accelerometers position during forced vibration tests.

Based on the response functions determined from the experimental results, the modal parameters of the dam were identified, namely natural frequencies, modal configurations and modal damping ratios. The structure natural frequencies and damping values obtained for the two tests can be compared by analysing Table 6.1.

Table 6.1 – Modal properties obtained with FVT 1 and FVT 2

	FVT 1 (water level 195.5 m)		FVT 2 (water level 234 m)	
Mode	Frequency [Hz]	Damping Ratio [%]	Frequency [Hz]	Damping Ratio [%]
1	2.75	1.0	2.44	1.23
2	2.95	1.0	2.57	1.02
3	3.87	1.1	3.34	1.18
4	4.46	0.6	3.93	0.40
5	5.26	0.6	4.78	1.20
6	6.22	1.4	5.37	1.15

Comparing the results from FVT 1 and FVT 2, the values of natural frequencies decreased considerably for all the identified vibration modes, while the values of damping rations have both decreased and increased, depending on the mode. The decrease of frequency values is related to the higher water level in the FVT 2. The mode shapes identified for the first six vibration modes are presented in Figure 6.5. The representation of mode shapes corresponding to the two upper visit galleries is done in red, while the original shape of the dam is represented in blue and grey.

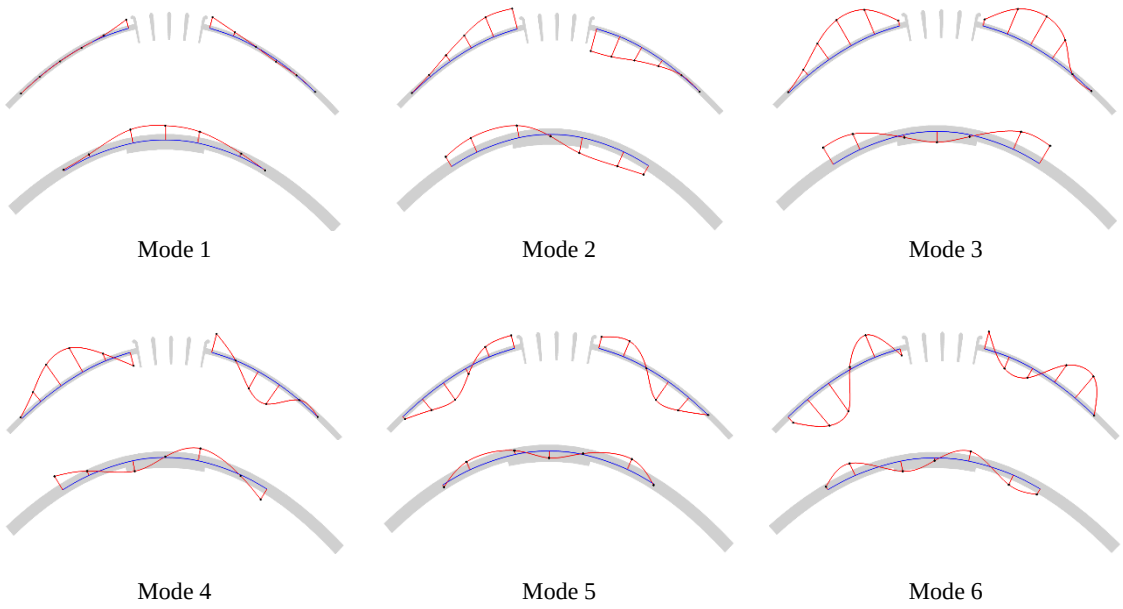

Figure 6.5 – Modal configurations of the first six modes of Baixo Sabor arch dam obtained with forced vibration tests (Jorge Gomes et al., 2018).

6.3.2. NUMERICAL MODEL OF BAIXO SABOR DAM

A numerical model of Baixo Sabor dam was developed by the Concrete Dams Department of the National Laboratory for Civil Engineering (LNEC), in order to study the structure static and dynamic behaviour. This model, based on discrete and finite elements, takes into account the dam's contraction joints, the deformability of the foundation and the reservoir (J. Gomes & J. V. Lemos, 2016a). To model the dam, 32 vertical blocks were discretized in isoparametric 20-node brick finite elements. Though a more elaborate model considering the discretization of the reservoir was developed by LNEC, a simplified representation of the reservoir and foundation was used in the context of this work, which was intended to allow a preliminary comparison with the experimental data. The dynamic dam-reservoir interaction was simulated with Westergaard's added mass technique, for the nodal points of the model located in the upstream face below the reservoir level. It is known that in arch dams, Westergaard's method overestimates the hydro-dynamic effects, so the masses had to be scaled (Priscu et al., 1985). In this case, a scaling factor of 0.525 was used to match the first natural frequency estimated with the first forced vibration test (FVT 1). The deformability of the foundation was also achieved through an elastic joint on the dam's surface of insertion, with stiffness parameters calibrated to provide a deformability approximate to that of a rock mass with Young's modulus of 35 GPa, obtained from field tests. The adopted material parameters are presented in Table 6.2 and two views of the numerical model are presented in Figure 6.6.

Table 6.2 – Main parameters of the numerical model

Concrete		Dam contraction joints		Foundation joint	
Young's modulus	35.0 GPa	Normal stiffness	50.0 GPa/m	Normal stiffness	12.5 GPa/m
Poisson ratio	0.20	Shear stiffness	20.8 GPa/m	Shear stiffness	5.2 GPa/m
Density	2400 kg/m^3				

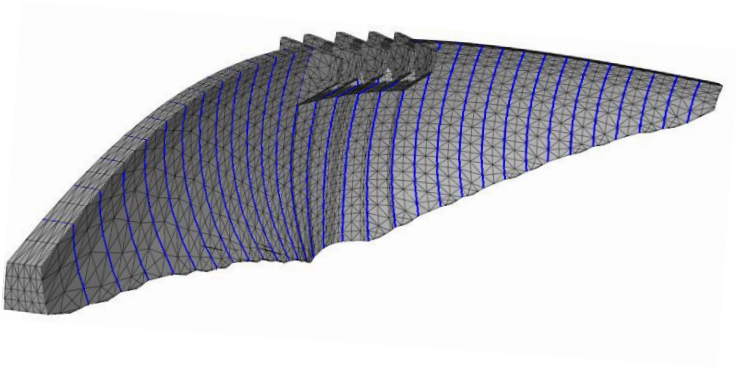

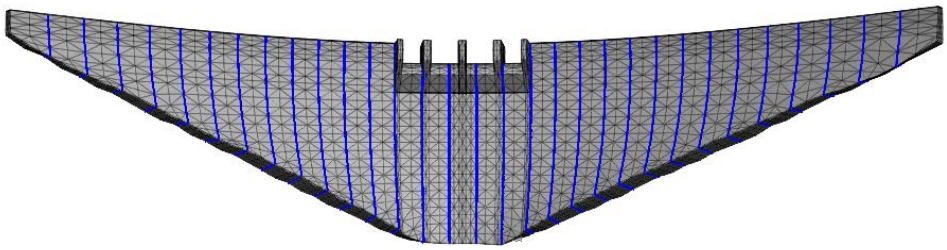

Figure 6.6 – Two views of the numerical model of Baixo Sabor dam; representation of blocks separated by contraction joints.

The natural frequencies obtained both through the first forced vibration test (FVT 1) and through the numerical model, when the reservoir water level was 195.5 meters above sea level, are presented together for comparison in Table 6.3, along with the value for the MAC between the mode shapes obtained for each mode in the two approaches. Close results were achieved for the natural frequencies obtained with the forced vibration test and the numerical model, in spite of the simplifications of this model. The frequencies of the first mode are identical, given the scaling factor of the added masses, but accurate matches were achieved as well for the other modes, even though higher differences occur for higher orders modes. Numerical mode shapes also approximate fairly well the experimental results.

Table 6.3 – Comparison of results from FVT1 and the numerical model

Mode	FVT 1 [Hz]	Numerical Model [Hz]	MAC
1	2.75	2.75	0.77
2	2.95	2.96	0.95
3	3.87	3.96	0.90
4	4.46	4.46	0.79
5	5.26	5.39	0.88
6	5.88	6.07	0.86

6.4. DYNAMIC MONITORING SYSTEM DESCRIPTION

When monitoring large civil engineering structures, it is advantageous to have digitizers distributed over the monitored structure in order to reduce cable length and thus electrical interferences that can corrupt the signals (Magalhães, Cunha, et al., 2008). Therefore, the dynamic monitoring system installed in Baixo Sabor arch dam is divided into three subsystems connected by optical fibre. Subsystem 1 and subsystem 2 are composed by 6 uniaxial force balance accelerometers and a digitizer each, and both subsystems are connected to a field processor which is, in turn, linked to a computer (NUC). The two groups of accelerometers are radially installed over the upper gallery, disposed on each side of the spillway. Subsystem 3 is composed of 8 uniaxial force balance accelerometers, radially installed over the second and third upper galleries, and two digitizers that are connected to a computer, which is responsible for running the acquisition. To perform modal analysis a good synchronization of the data recorded by all digitizers must be assured, which required the installation of GPS antennas. In addition, the field computer is connected to the optical fibre network between the dam and the plant allowing remote access. A scheme representing the monitoring system main elements is presented in Figure 6.7, while the position of the total 20 accelerometers is characterized in Figure 6.8 by red and blue marks in both a scheme and a picture of the structure.

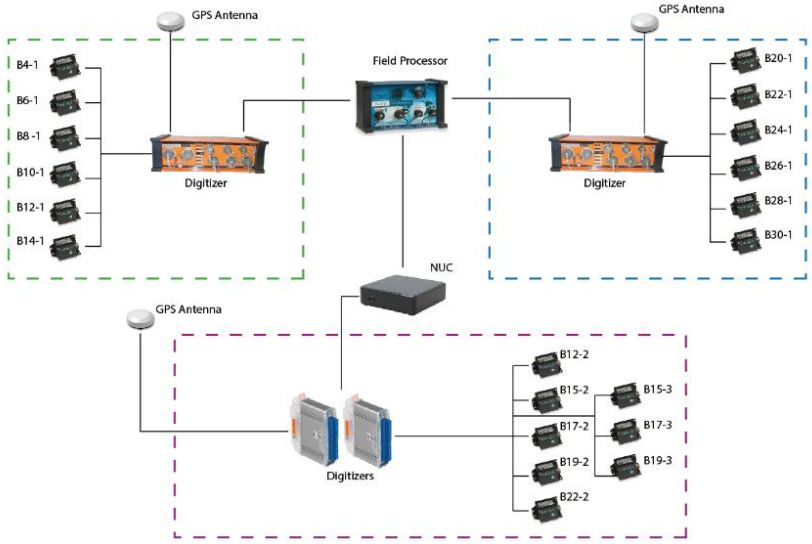

Figure 6.7 – Scheme of the monitoring system (Gomes & Magalhães,2015).

The force balance accelerometers used (FBA ES-U and FBA ES-U2 from Kinemetrics) have a dynamic range of 140 dB and 155 dB, respectively, and a frequency bandwidth that goes from DC to 200 Hz. These accelerometers can measure up to 4 g, but in this application they were configured

to measure in the range -0.25 g / +0.25 g, in order to allow the accurate characterization of very low acceleration signals.

The dynamic monitoring system is configured to continuously record acceleration time series with a sampling rate of 50 Hz and a duration of 30 minutes at all instrumented points, thus producing 48 groups of time series per day. This data is automatically stored in the field computer and then transferred remotely both to FEUP and LNEC, with an FTP connection, where they are stored and processed.

Additionally, in order to better characterize eventual seismic actions acting on the dam, a seismic monitoring system has also been implemented. This seismic system, which is working independently from the dynamic monitoring system previously described, is presented in (Pereira Gomes et al., 2018).

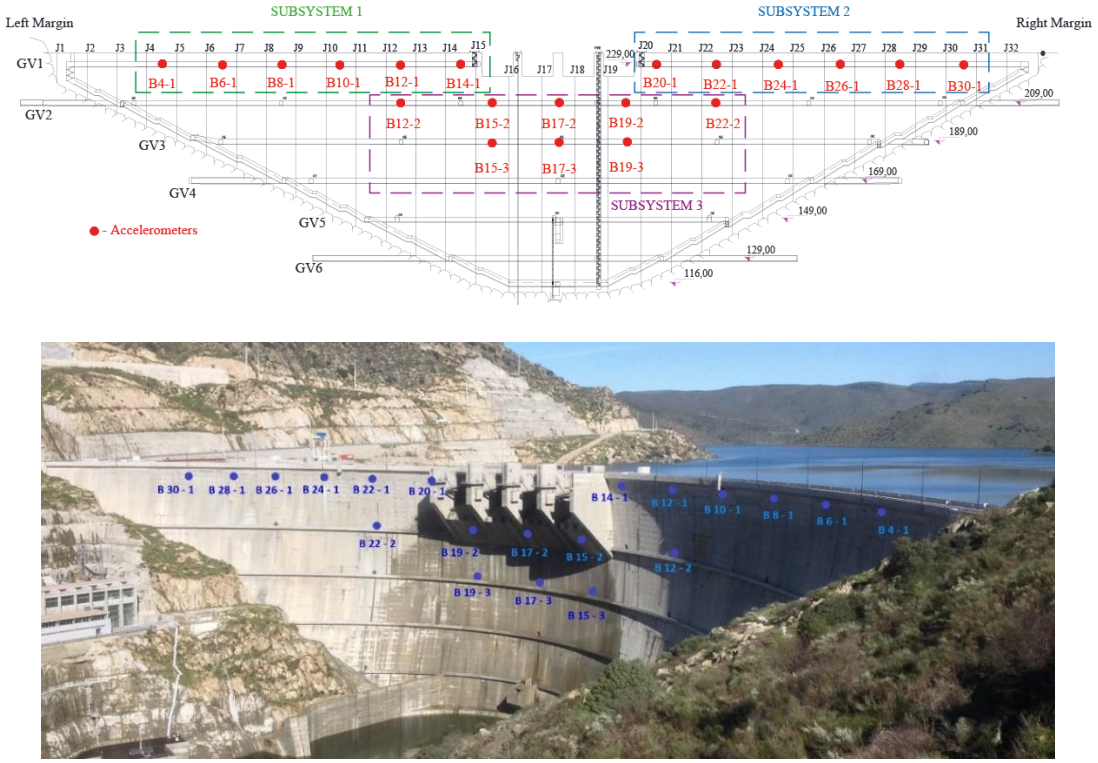

Figure 6.8 - Position of measuring points and subsystems components of Baixo Sabor dynamic monitoring system.

6.5. MONITORING RESULTS

6.5.1. INTRODUCTION

The Baixo Sabor dam continuous dynamic monitoring system is configured to record time series of accelerations with a duration of 30 minutes at all instrumented points. The duration was defined according to the techniques used in its data processing, and it can be adjusted if needed. In a first stage, the data processing is accomplished through the application of the following tasks to every set of 30 minutes of data:

- storage in database with the original data;
- pre-processing of the acceleration time series, including the elimination of offsets, filtering with an eighth-order low-pass Butterworth filter (Mathworks, 2016) and re-sampling with a frequency of 25 Hz (the first 10 modes are below 10 Hz);
- characterization of acceleration amplitude by maxima and root mean squares values (RMS), and characterization of energy distribution across the analysed frequency range over time through the construction of colour maps in the frequency domain;
- identification of modal parameters (natural frequencies, modal damping ratios and modal configurations), based on the dam's response under operation conditions, using state of the art output-only modal identification algorithms;
- storage of all the obtained results in a database.

For the most important and challenging task, the continuous automated identification of the modal parameters, alternative output only algorithms (Magalhães & Cunha, 2011) were tested, and it was concluded that good results could be achieved through the combination of the Covariance Driven Stochastic Subspace Identification (SSI-Cov) with a routine for automated interpretation of the obtained results based on clusters analysis.

The characterization of acceleration by amplitude and root mean square values is particularly relevant during the three weeks presented in Figure 6.9, since it allows the identification of three different types of operating conditions. The distinctive accelerations measured on each sensor, around January 12th, correspond to a period of flood generated by intense rain, during which the spillway gates were open, thus producing abnormal levels of vibration. Right after this event, a period ending on January 15th also presents well-defined accelerations, but with much lower intensity, which in this case was mainly caused by the continuous operation of the turbines for

energy production. The third and last type of operating conditions is the most common one and the one that results in the lowest values of measured accelerations, which happens when the structure is just under natural excitation, such as traffic and wind.

Another extraordinary event occurred during the second week of May, resulting in the greatest effective vibration levels of the three year period of monitoring, as may be observed in Figure 6.10, where the vibration levels measured during the first six months of monitoring are presented. This case corresponded to the execution of a forced vibration test. On the other hand, lower levels of vibration correspond to excitation produced by ambient vibration, traffic or by the turbine operation. It should also be noticed that the maximum values observed for the vibration levels reach intensities almost 10 times higher than those of quadratic means, which shows that the excitation conditions are not constant, reaching sharp variations within the same 30-minute period.

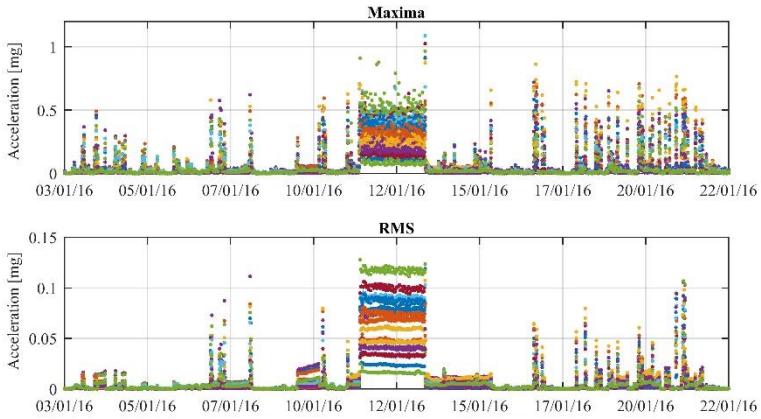

Figure 6.9 - Maximum and RMS accelerations measured between 03/01/2016 and 22/01/2016.

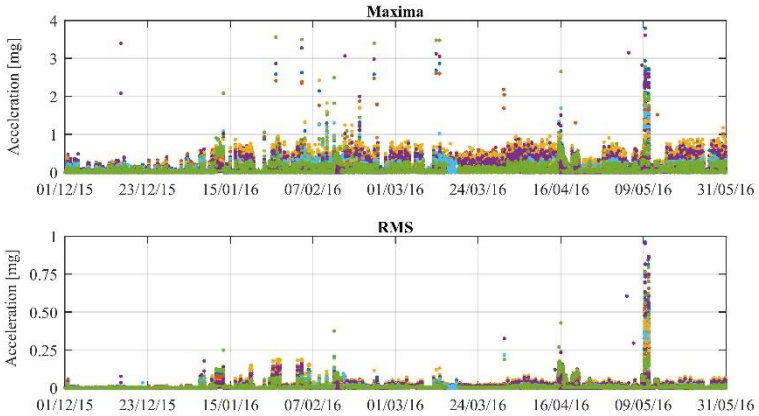

Figure 6.10 - Maximum and RMS accelerations measured between 01/12/2015 and 31/05/2016.

6.5.2. MODAL PARAMETERS IDENTIFICATION

From the acceleration samples, it is possible to obtain modal parameters estimates using methods such as those presented in section 3. Different analysis stages require different approaches; in particular, when starting to analyse a set of data, it is important to apply simple methods granting good, solid results that allow preparing other deeper and more detailed analyses.

A straightforward methodology to identify different vibration modes and get rough estimates of natural frequencies, allowing as well to perform a simple evaluation of its evolution during a period of time, consists on the application of the singular value decomposition to the spectra matrix of each acceleration sample. The assembly of first singular value spectra allows the construction of a colour map like the one shown in Figure 6.11. Colours are a function of intensity, with warm colours (red) associated with higher values. The red zones indicate the existence of more energy in the frequency bands to which they are associated, thus providing approximate estimates of the natural frequencies of the structure and the harmonics present in the excitation motivated by the operation of the turbines. Therefore, following the large red spots from the beginning to the end of the colour map, one identifies the natural frequencies and the way they vary along time. On the other hand, the thin and well-defined red lines present at frequencies 3.57 Hz and 7.14 Hz correspond to the turbine rotation frequency and its first multiple. The periods where these lines appear in the colour map in Figure 6.11 are in total agreement with the periods corresponding to the second type of operating conditions in Figure 6.9. During such periods, the minor intensity associated with natural frequencies, compared to turbine rotation frequencies, makes them harder to identify.

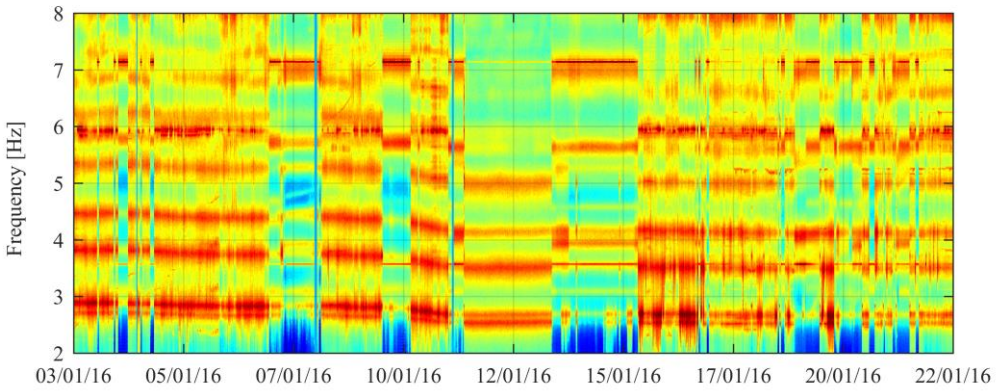

Figure 6.11 – Colour map with the frequency evolution between 03/01/2016 and 22/01/2016.

After this first rough analysis using colour maps, the modal identification of the structure was performed using the SSI-Cov method. The first ten modes of vibration were identified and natural frequencies, damping values and modal configurations were obtained. The mode shapes of the ten identified modes are presented in Figure 6.12. The contribution of the accelerometers located in each of the three instrumented visit galleries was represented with a different colour and symbol. Therefore, the modal ordinate of the accelerometers located in the upper visit gallery (GV1) were marked with blue "*" symbols, the ones from the second gallery (GV2) were marked with red "o" symbols, and finally the modal ordinates obtained from the accelerometers positioned in the third visit gallery (GV3) were marked with black "+" symbols. Then, the function "spline" from Matlab was used to interpolate the mode shapes. All the mode shapes are clear and well-defined, with increasing complexity from the first to the tenth mode. Mode shapes are alternatively symmetrical and anti-symmetrical, thus the first, third, fifth, seventh and ninth modes are symmetrical and the second, fourth, sixth, eighth and tenth modes are anti-symmetrical modes of vibration.

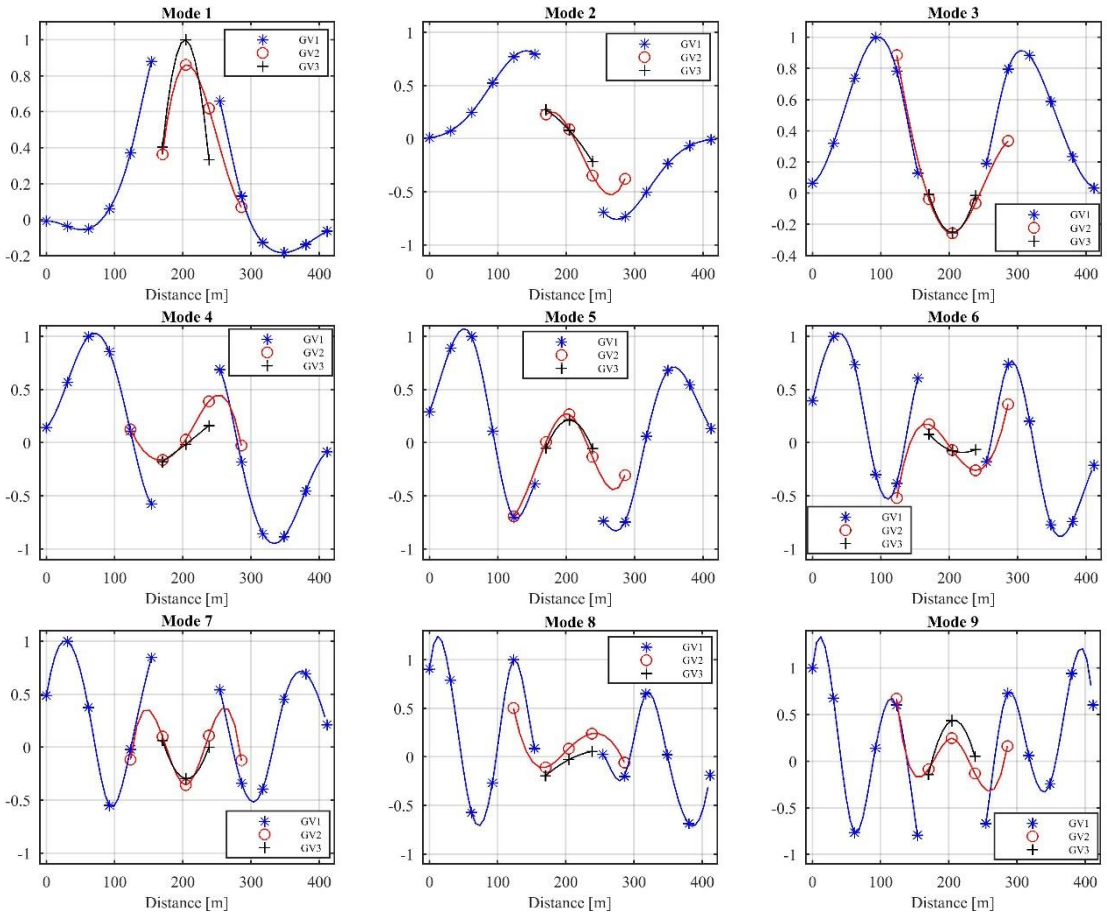

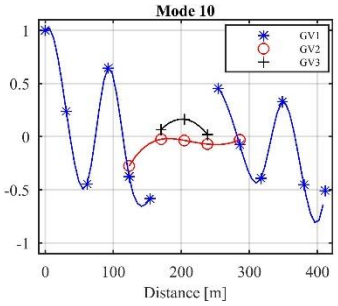

Figure 6.12 – Modal configuration of the first ten modes of Baixo Sabor arch dam.

The natural frequencies and damping ratios, with respective standard deviation values, identified from the time series of accelerations measured during the first day of monitoring (01/12/2015), between the 00:00 and 00:30, are resumed in Table 6.4. It is important to notice that the first ten vibration modes are found between 2 and 10 Hz, generally presenting damping ratios between 1.1 and 1.6 % (being the fifth mode the only exception). The standard deviations associated with the natural frequencies of most modes present values around 0.02 Hz, though these values vary from 0.011 Hz in the case of the second mode, to 0.054 Hz in the case of the eighth mode. As expected, the values of damping ratios present higher uncertainty, and the standard deviations associated with their estimates vary from 0.189 to 0.857 %.

Table 6.4 – Modal parameters for the structure's first ten modes (00:00 – 01/12/2015)

Mode	f_{mean} [Hz]	f_{std} [Hz]	ξ_{mean} [%]	ξ_{std} [%]	Description
1	2.739	0.020	1.291	0.585	Symmetric
2	2.917	0.011	1.413	0.383	Antisymmetric
3	3.852	0.026	1.332	0.702	Symmetric
4	4.475	0.021	1.381	0.476	Antisymmetric
5	5.299	0.045	2.081	0.857	Symmetric
6	6.210	0.024	1.541	0.444	Antisymmetric
7	6.886	0.019	1.116	0.323	Symmetric
8	8.033	0.054	1.434	0.714	Antisymmetric
9	8.773	0.021	1.547	0.304	Symmetric
10	9.686	0.020	1.854	0.189	Antisymmetric

6.5.3. AUTOMATED OPERATIONAL MODAL ANALYSIS

In the context of continuous dynamic monitoring, it is crucial to automate the modal analysis, in order to process the enormous amount of produced data more easily and to obtain results in real time. It is therefore important to implement tools that, based on the identification methods previously presented, allow the referred modal parameters to be extracted automatically from the acquired time series. These tools should also be properly tuned in order to provide similar or better results than those that would be obtained if the process was conducted manually.

In this work the SSI-Cov method was adopted. When working with parametric identification methods, such as the SSI-Cov (or the p-LSCF) it is not possible to predict the model order that better characterizes the dynamic behaviour of the structure. So the best way to estimate the modal parameters is to use models with multiple orders within a previously determined interval. In this case, after some preliminary experiments considering the characteristics of the stabilization diagrams obtained with different time series and the time needed to perform the computation, this interval was set to consider model orders between 40 and 140. Additionally, stabilization diagrams with good quality were achieved considering as references just the six measuring points in Subsystem 1, as defined in Figure 6.8, which allows saving computation time. Also, correlation functions with 100 points (100/25 = 4 seconds → 4 x 2.74 = 10.9 periods of the lower frequency) were adopted. Finally, taking into account the ten modes identified in the previous section, the algorithm was configured to ignore poles with natural frequencies outside the interval [2 ; 10.5] Hz.

The hierarchical algorithm used for automatic interpretation of stabilization diagrams is applied to all the poles in the diagram, using a limit for the distance between modes of the same cluster equal to 0.01 (calculated with equation (5.1)). The results illustrated in Figure 6.14 show that the poles belonging to the 10 physical modes within the analysed frequency range are grouped together.

Instead of using all the poles in the diagram, the clustering could have been applied just to the stable poles, however, since unstable poles form their own clusters, which can be easily eliminated for being composed by just a few elements, no significant gains would have been achieved with this process. Therefore, using all the poles in the diagram avoids the classification of stable poles thus reducing the number of input parameters of the method while maintaining its efficiency (Magalhães et al., 2009).

In order to remove extreme values of modal damping estimates (not taken into account in the clustering process), an outlier analysis can be performed within each cluster. The mode estimates with a modal damping ratio below the lower quartile minus 1.5 times the interquartile range or above the upper quartile plus 1.5 times the interquartile range are eliminated. Figure 6.15 presents the effects of this statistical approach in the modal estimates derived from the stabilization diagram presented in Figure 6.13.

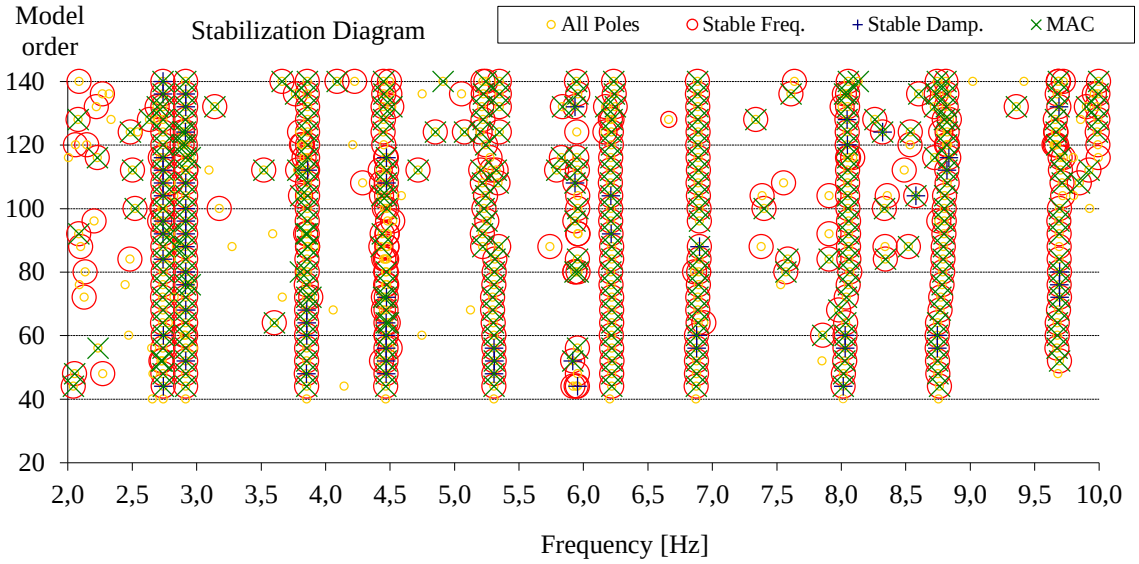

Figure 6.13 – Stabilization diagram obtained for the analysis of the time series collected at 2016/05/08 13:00.

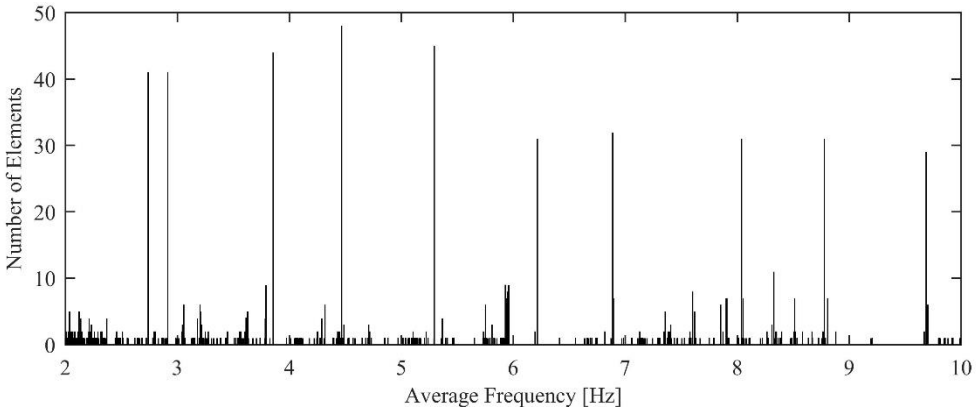

Figure 6.14 – Number of elements of the formed clusters with all the poles of the stabilization diagram.

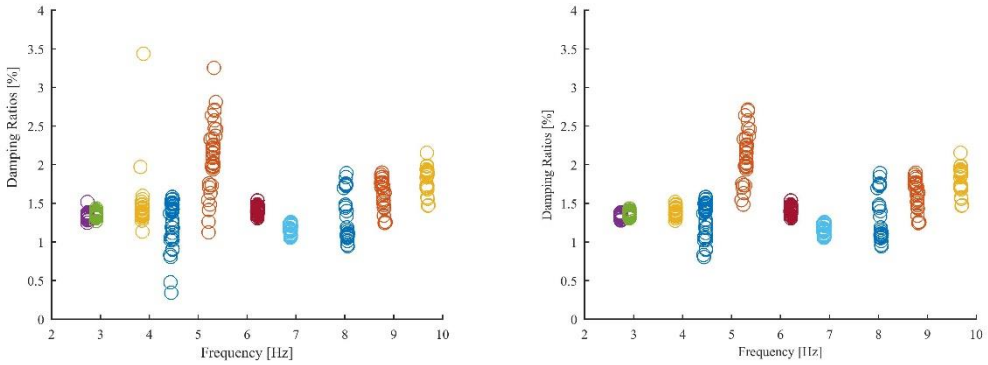

Figure 6.15 – Damping vs Frequency diagram of the mode estimates that belong to the clusters with more elements, before (on the left) and after (on the right) the outliers elimination.

After this step, the final modal estimates associated with the dataset under analysis are defined as the mean values of the poles included in each cluster, thus there are one frequency and damping estimates for each of the 25 clusters that were previously chosen. The ten vibration modes identified in the previous section are likely to lie among these 25 clusters, which also comprehend spurious modes and may comprehend as well parasite frequencies provoked by nearby sources of noise, such as rotating machines.

The frequency estimates (cluster averages) obtained from all the clusters in each dataset during the first six months of monitoring are represented in Figure 6.16. The absence of results in a few areas of the figure corresponds to periods of system failure or maintenance for which no data was available. Though there are many estimates dispersed all over the figure, generally corresponding to spurious modes, the evolution of the first four vibration modes is clear and well-defined. In the case of the fourth mode, for instance, its natural frequency varies from 4.5 Hz in December to around 4 Hz in May, presenting an abrupt decrease in value in mid-January, which is common to the other modes. In this sense, Figure 6.16 results to be very helpful, allowing the analysis a general view on all the frequencies that are relevant enough to lead to the formation of clusters, which may or not correspond to vibration modes, before the identification process is concluded, serving as well as future reference to check the quality of the final results.

The thin, but clearly defined, alignment present at 3.57 Hz in Figure 6.16, pointed at with a blue arrow, corresponds to the turbine rotation frequency that had been previously identified in the colour map in Figure 6.11. This alignment is located inside the range of variation of the third vibration mode and it presents mode shapes that are similar to that of this physical mode, which has the closest natural frequency, leading many times to the incorrect classification of the turbine rotation frequency as a dam vibration mode and thus introducing a significant bias in the results.

This tracking challenge, due to the presence of the turbine rotation frequency and its harmonics, will be explored in the next section. Two other alignments, not so clearly defined and of unknown source, are present around 3.1 and 4.6 Hz.

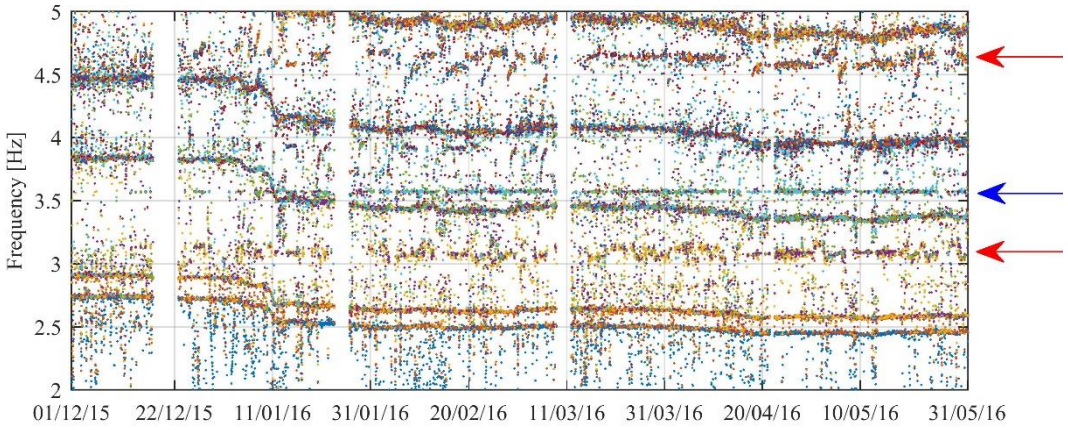

Figure 6.16 – Natural frequencies identified with the SSI-Cov method; a blue arrow pointing to turbine rotation frequency; red arrows pointing to other parasite frequencies.

To conclude the identification process, the modal estimates obtained in each setup have to be compared with the ones identified in previous setups. In other words, a tracking procedure is needed to link the modal parameters identified from each dataset that are associated with the same physical mode.

In the present application, the algorithm searches between the entire set of estimates to find the ones that correspond to true vibration modes, which was first achieved by comparing each new group of estimates with a set of reference values, that were obtained from selected datasets with very clear stabilization diagrams. Each new set of modal properties would only be accepted if the MAC (Modal Assurance Criterion) (Allemang & Brown, 1982) between the estimated mode shape and the reference mode shape was higher than 0.55 and the variation between the estimated frequency and the reference frequency value was lower than 10%. However, though acceptable results were achieved with this procedure, the high 10 % limit for frequency variation needed to cover the large range of frequency values assumed by each mode during the monitored period, leads to several misidentifications. Therefore, instead of a fix reference for each mode natural frequency, a set of variable frequency references (one per mode per dataset) was used, which were obtained as functions of reservoir water level. Consequently, a 3 % limit for frequency variation could then be used, eliminating many misidentifications.

The evolution over time of the natural frequencies of the 10 tracked vibration modes during the three years of continuous monitoring is characterized in Figure 6.17, where each point corresponds to a 6-hour average and each vibration mode is represented using a different colour. Averaged parameters were considered in order to achieve a visually cleaner figure, more suitable to represent the 10 modes at once without losing much precision, which becomes evident since the abrupt variation of frequency that occurred in early January 2016 is still noticeable, as it was in Figure 6.16. All the modes show significant frequency variation during the three years of monitoring, which is clearer when observing modes 7 to 10 that present higher variability.

Damping ratios were tracked as well and its evolution during the monitoring period is presented in Figure 6.18, using 6-hour averages once again and the same colours used to represent natural frequencies. In this case, all the modes present values in the same range, roughly between 0.5 and 2.5 %, which difficult the perception of each modes evolution. Individual analyses are presented in the next section.

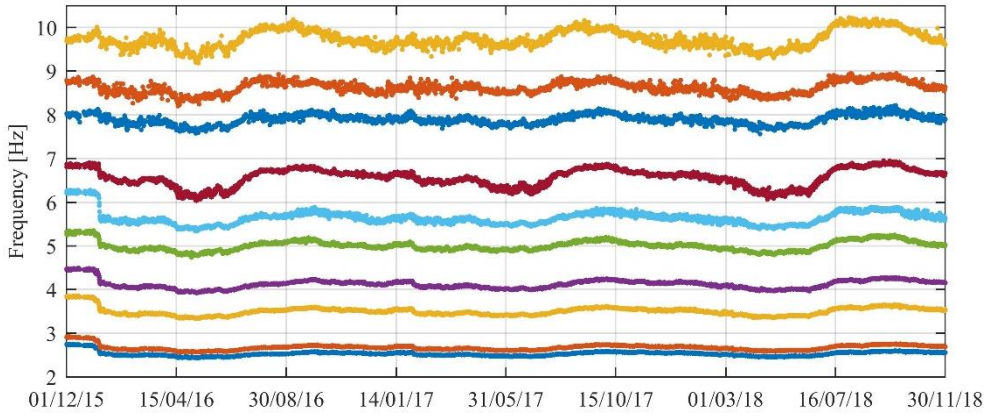

Figure 6.17 – Time evolution of 6-hour average natural frequencies (first ten vibration modes).

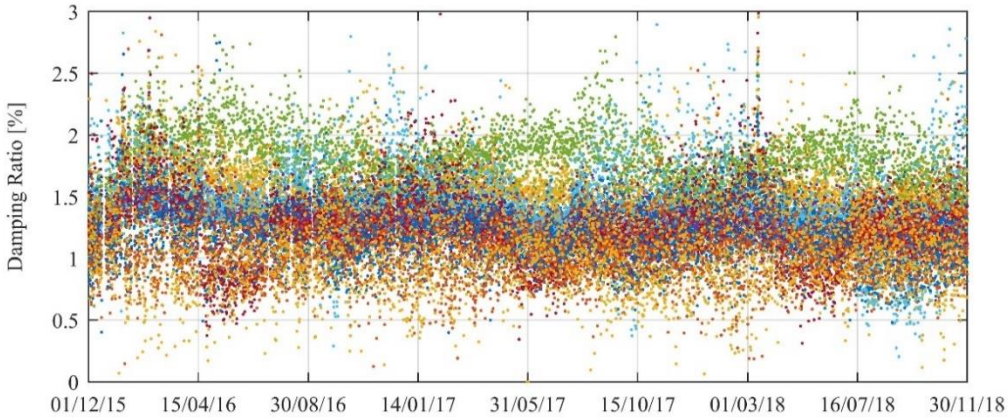

Figure 6.18 – Time evolution of 6-hour average damping ratios (first ten vibration modes).

To better understand the evolution of natural frequencies a zoom on the first two vibration modes is presented in Figure 6.19. In this case all the available data was used, thus each point corresponds to the frequency estimate obtained from each 30 minutes dataset. After a first sudden decrease in value, the frequency of both modes presents slow seasonal fluctuations inside a large and more or less stable range. However, the thickness of the representation suggests daily variations are important as well.

These important variations during the monitoring period are probably due to operational and environmental factors, such as temperature and reservoir water level, and are verified in all the tracked modes with similar patterns. This explains the high values assumed by the standard deviation of each vibration mode frequency during this period, which are presented in Table 6.5 along with their mean values. Still, higher modes present higher variability, being the standard deviation of the first two modes about 0.1 Hz, while in the case of the ninth and tenth modes it assumes values around 0.4 Hz. On the other hand, the variability of damping ratios does not seem to be directly related to the order of their specific vibration mode, though the second mode presents the lower standard deviation during the monitoring period. Additionally, mean damping ratios vary from 1.1 % (ninth mode) to 1.8 % (fifth mode).

Finally, it is worth noting that, with the exception of the first mode, the number of missing values (datasets in which a certain mode was not identified) generally increases with the order of the mode. Modes 2 to 4 present the highest success rates (between 96 and 97 %), and most of their missing values do not correspond to any failure in the identification process, but to lack of data measured in that period instead, due to system failure or maintenance. In turn, modes 8 to 10 present the lowest success rates (between 49 and 64 %), which does not prevent the characterization of these modes evolution over time, but may preclude their use as part of damage detection routines.

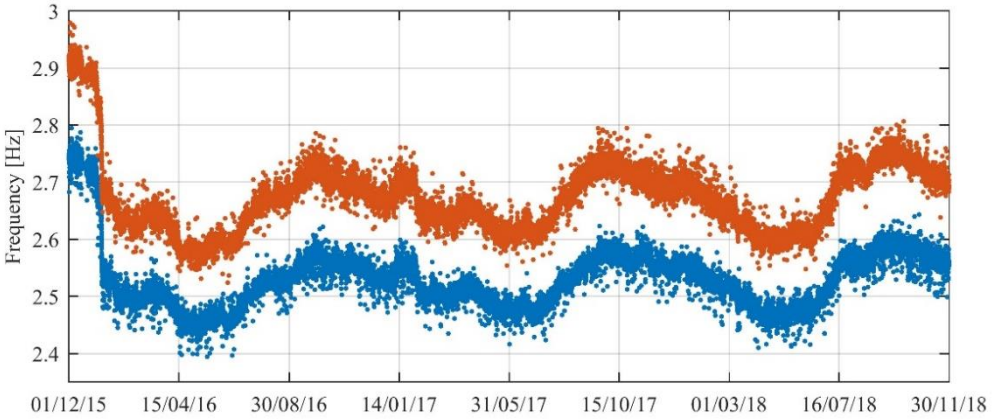

Figure 6.19 – Time evolution of 12-hour average natural frequencies.

Table 6.5 – Modal parameters of the structure's first ten modes during the first three years of monitoring

Mode	Missing values [%]	f_{mean} [Hz]	f_{std} [Hz]	ξ_{mean} [%]	ξ_{std} [%]	Description
1	10.19	2.527	0.097	1.401	0.411	Symmetric
2	3.16	2.700	0.103	1.252	0.288	Antisymmetric
3	3.25	3.499	0.143	1.484	0.471	Symmetric
4	3.66	4.118	0.164	1.327	0.369	Antisymmetric
5	10.11	5.001	0.199	1.810	0.458	Symmetric
6	17.70	5.623	0.250	1.440	0.531	Antisymmetric
7	13.43	6.572	0.294	1.244	0.462	Symmetric
8	35.99	7.896	0.340	1.148	0.455	Antisymmetric
9	39.39	8.633	0.384	1.091	0.488	Symmetric
10	50.81	9.761	0.485	1.300	0.557	Antisymmetric

6.5.4. USING UNCERTAINTIES ON MODAL TRACKING

To evaluate the advantage of considering uncertainties in the algorithm used for modal tracking, the results obtained with the processing presented in the previous section will be used as a baseline for comparison. In the methodology presented in the previous section the uncertainty of modal estimates was quantified but not included in any step of the tracking algorithm. For reference in this work, this processing will be named Processing A.

In this sense, the natural frequencies and damping ratios obtained with Processing A for the first seven modes are represented independently in Figure 6.20 and Figure 6.21, to provide a closer evaluation of their evolution over time. However, in this case, the colour of each modal estimate was represented as a linear function of its standard deviation. Therefore, natural frequencies were represented in blue if their standard deviation values were close to 0 Hz, and they were represented in yellow if they were close to 0.05 Hz, or higher than this value. For the modal damping ratios estimates, relative standard deviations were used to choose the colour of each estimate. Thus, damping ratios were represented in blue if their relative standard deviation values were close to 0 %, and they were represented in yellow if they were close to 50 %, or higher than this value.

The value of 0.05 Hz represents a substantial uncertainty that for the structure under consideration should not be accepted. Furthermore, the 50 % limit for the relative standard deviation results from the consideration that values higher than 50 % would mean negative damping ratios, assuming a normal distribution and a 95% confidence interval, which is not physically possible.

Figure 6.20 shows that the frequency estimates of the first modes are generally associated with lower standard deviation values, indicating higher uncertainties are associated with higher modal orders. However, all the seven modes show many estimates represented in yellow that clearly diverge from the main tracking line. Additionally, in the figure that corresponds to the evolution of mode 3, a thin blue horizontal alignment seems to be defined between 3.55 and 3.60 Hz, indicating a specific frequency that always presents very low standard deviations.

The damping ratios of all seven modes present as well many estimates represented in yellow, indicating a considerable number of estimates associated with relative standard deviations higher than 50 %. Furthermore, besides the normal variability around the mean, mode 3 presents a significant number of estimates with low damping, between 0 and 1 %, which do not seem to be

season related. The vast majority of estimates with seemingly abnormal damping values present high relative standard deviations, as indicated by its yellow colour.

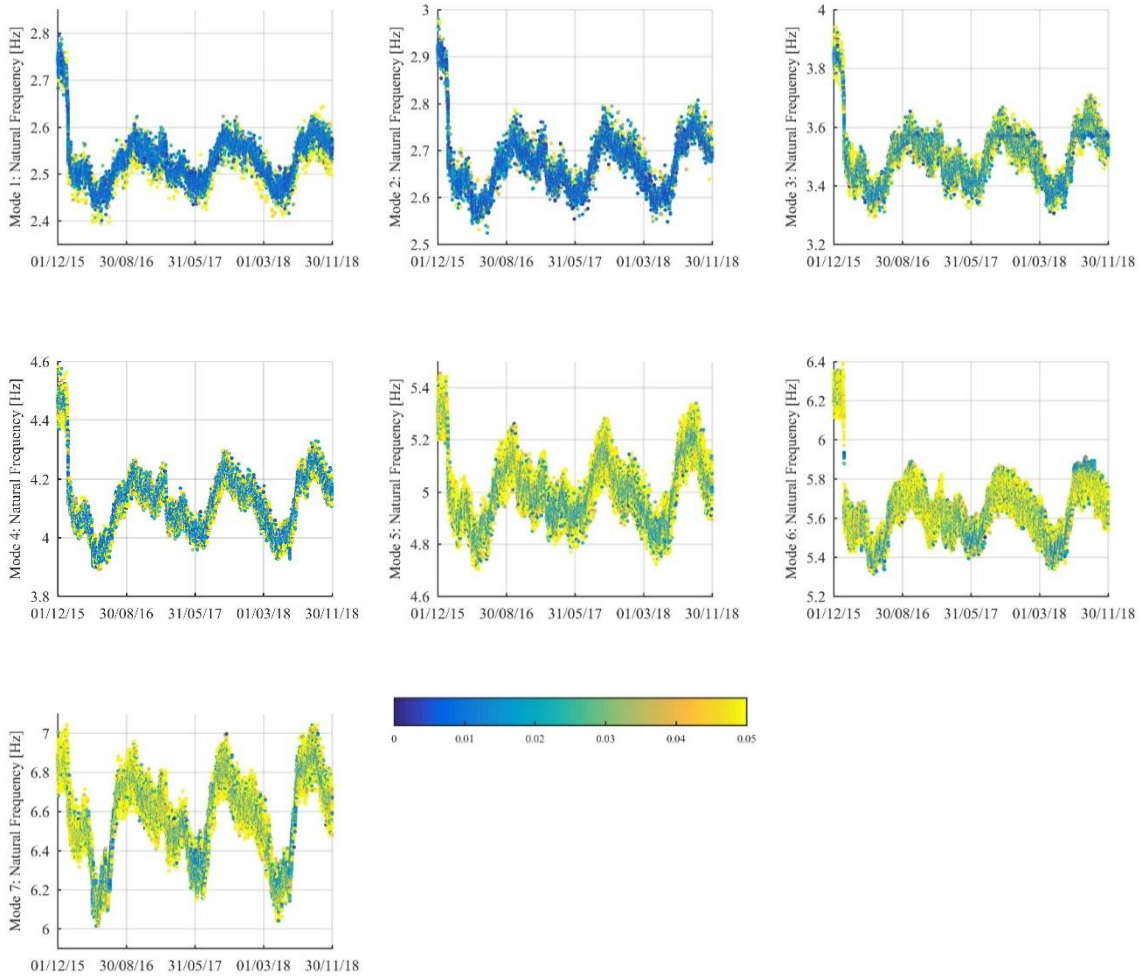

Figure 6.20 – Natural frequencies with colour as a function of standard deviation (Processing A).

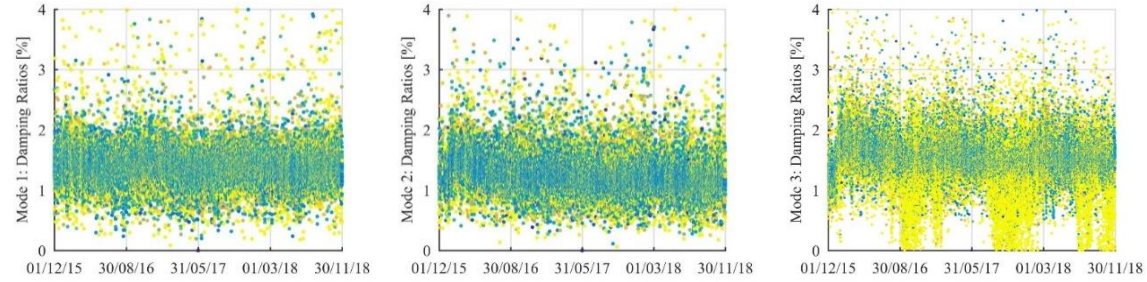

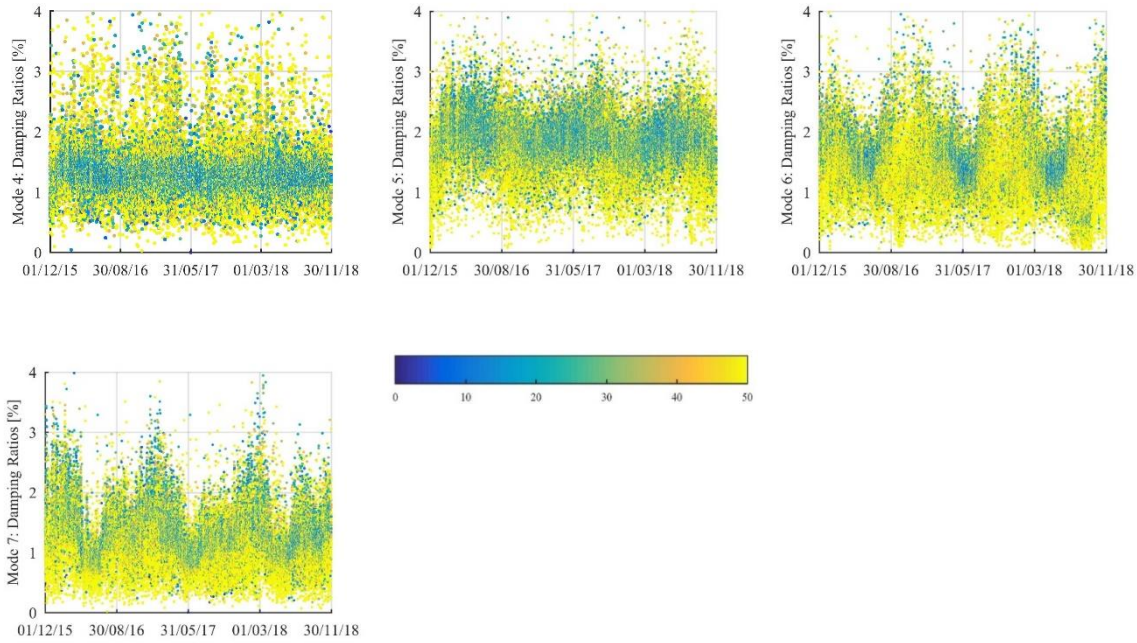

Figure 6.21 – Damping ratios with colour as a function of relative standard deviation (Processing A).

After the analysis of the results provided by processing A, a new tracking strategy was put through, yet this time, before the comparison between each new set of modal properties estimates and the previously defined references, all the clusters obtained from the application of SSI-Cov to each 30 minutes time series of accelerations were analysed considering the uncertainties of each pole estimate. This analysis, which will be referenced as Processing B, consisted on the evaluation of standard deviations and, consequently, all the poles whose frequency standard deviation was equal or higher than 0.05 Hz and all the poles whose relative damping standard deviation was equal or higher than 50 % were eliminated. In conclusion, most clusters became more homogeneous, and many clusters that were composed mainly of poles associated with high standard deviations disappeared. However, the number of setups for which one or more modes were not tracked increased, diminishing the number of successful identifications.

From the perspective of most modes, this strategy turned out to be profitable, and the good results obtained will be presented hereafter. However, in a first stage, in the case of the third mode, it had negative consequences. Figure 6.22 presents the distribution of frequencies and damping ratios identified for the third mode with Processing B. On the one hand, there is an abnormal number of identifications between 3.55 and 3.60 Hz, and on the other, there is an abnormal number of identifications with damping close to 0 %. This indicates that the elimination of poles with higher

uncertainty was favourable to a systematic identification of the turbine rotation frequency (3.57 Hz) as the frequency of mode 3, increasing the number of misidentifications.

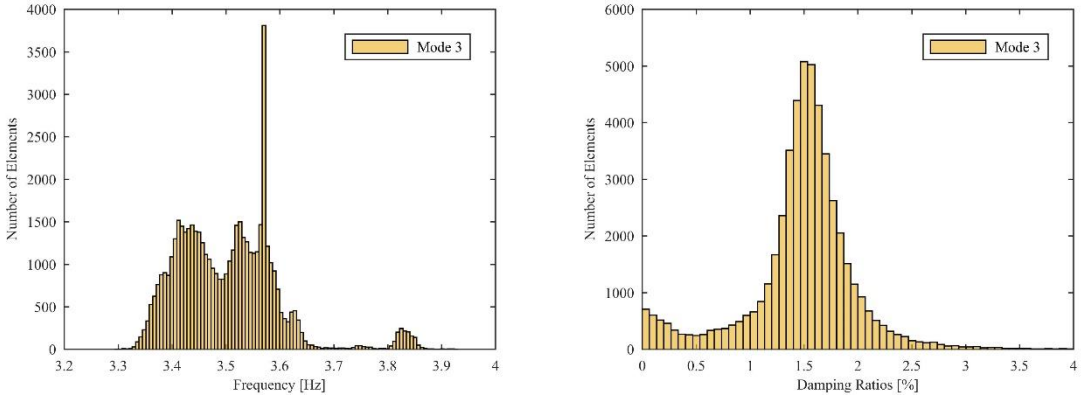

Figure 6.22 – Histograms of frequency and damping of mode 3 (Processing B).

In order to minimize the number of times the turbine rotation frequency is identified as mode 3 natural frequency, the characteristics of the estimates associated with this parasite frequency were studied. Thus, besides presenting modal damping ratios close to 0, these estimates systematically present very low standard deviation values for both frequency and damping. In this sense, all the frequency estimates identified for mode 3 which presented frequency standard deviations lower than 0.005 Hz were represented in yellow in Figure 6.23, while all the other frequency estimates were represented in black. The vast majority of yellow points correspond to frequencies very close to 3.57 Hz, therefore associated with the turbine rotation frequency.

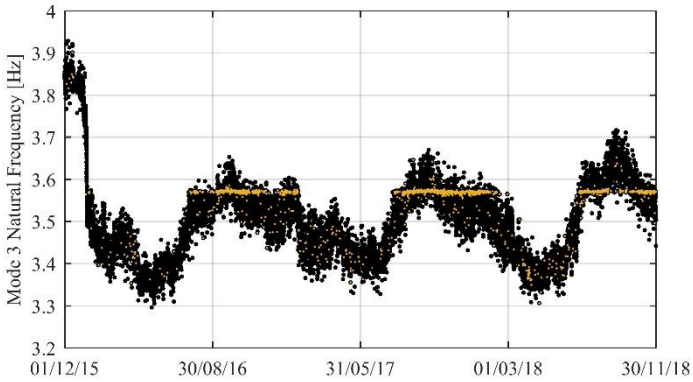

Figure 6.23 – Misidentifications of the third mode after Processing B.

Taking into account previous considerations, Processing C was put through, combining the conditions used in Processing B with the elimination of poles with frequency standard deviations lower than 0.005 Hz, in the range between 3.566 Hz and 3.576 Hz. This time, good results were

achieved for the third mode. The colour of natural frequency (Figure 6.24) and damping (Figure 6.25) estimates was once again represented as a function of their respective standard deviation values, using the same limits used in Figure 6.20 and Figure 6.21.

In the case of natural frequency, there are still some outliers in the seven modes, but its number reduced considerably. Moreover, the seven figures generally present darker colours, indicating a significant reduction in the value of standard deviations, thus increasing the confidence level of individual estimates. Though mode 3 still presents a few estimates with high uncertainty, the thin blue horizontal alignment associated with the turbine frequency is not clearly distinguishable anymore.

The general level of accuracy of damping ratios increased as well, though there are still many estimates with high uncertainty. In the case of the third mode, which presented several damping ratio estimates with values close to 0, related to the turbine rotation frequency, the number of low damping estimates decreased considerably. Most of the low damping estimates with high uncertainty that were not eliminated present damping values between 0.5 and 1 %, indicating that in some cases the SSI-Cov algorithm was not capable to separate the third mode estimate from the turbine harmonic.

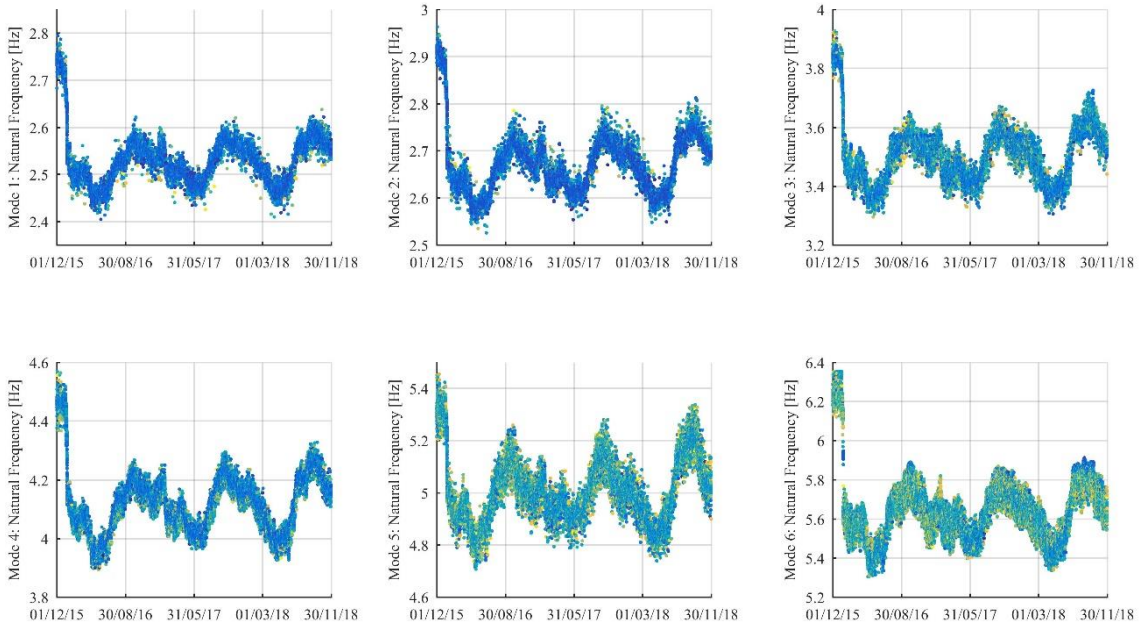

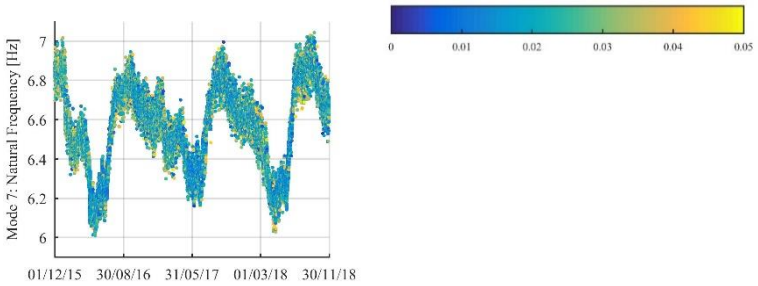

Figure 6.24 – Natural frequencies with colour as a function of standard deviation (Processing C).

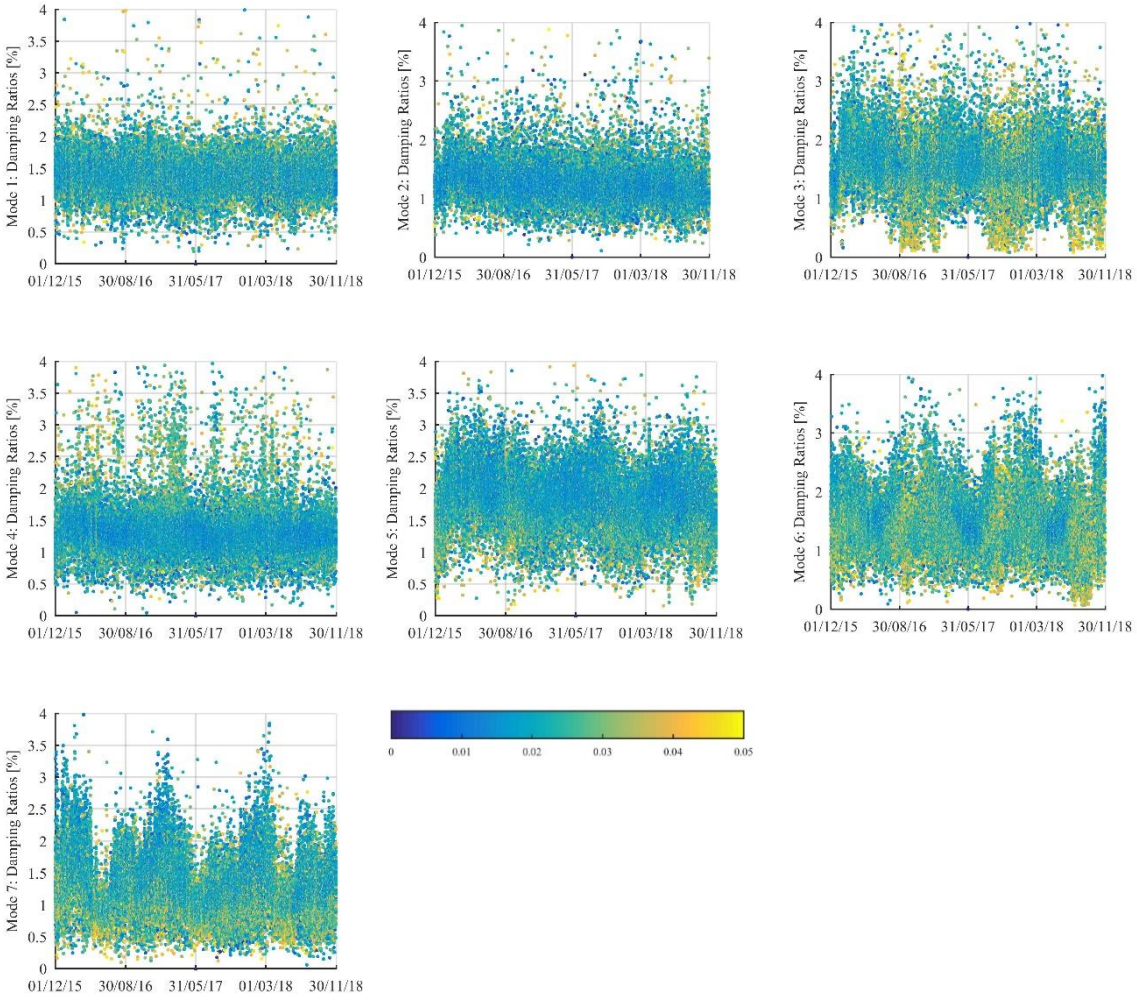

Figure 6.25 – Damping ratios with colour as a function of relative standard deviation (Processing C).

Finally, the results obtained with Processings A and C, the first and last ones, are summarized in Table 6.6 for comparison. For each vibration mode, means and standard deviations of the estimates

obtained for the entire analysed period were calculated for four parameters: natural frequencies (mean (f) and std (f)), damping ratios (mean (d) and std (d)), frequency standard deviations (mean (f_{std}) and std (f_{std})) and relative damping standard deviations (mean ($d_{std\text{-}relative}$) and std ($d_{std\text{-}relative}$)).

In the case of natural frequencies, the mean and standard deviation for the whole studied period did not present considerable changes from Processing A to C, which was expected, since the effect of operational and environmental conditions on natural frequencies is predominant when compared to the effect of random errors. The elimination of estimates associated with the turbine frequency, however, led to a decrease of the third mode natural frequency mean. On the other hand, the mean and standard deviation of frequency standard deviations decreased substantially for the seven modes, indicating a more accurate set of estimates.

Considerable variations were observed in the means of damping ratios of third and fourth modes. The third mode damping ratio mean for the studied period increased in agreement with the elimination of turbine rotation generated poles, and the fourth mode damping ratio mean decreased in agreement with the elimination of outliers with high uncertainty, which presented high damping values as well. Estimates that are more accurate were achieved also in the case of damping ratios, as shown by the clear reduction of the relative standard deviation values of damping.

Table 6.6 – Results comparison between Processing A and C

Processing	mean (f)	std (f)	mean (d)	std (d)	mean (f_{std})	std (f_{std})	mean ($d_{std\text{-}relative}$)	std ($d_{std\text{-}relative}$)
Mode 1 – A	2.527	0.097	1.401	0.411	0.012	0.014	34.7	45.5
Mode 1 – C	2.528	0.097	1.388	0.287	0.008	0.004	20.7	7.5
Mode 2 – A	2.670	0.103	1.251	0.288	0.011	0.011	34.2	45.7
Mode 2 – C	2.670	0.103	1.256	0.282	0.007	0.004	18.1	6.9
Mode 3 – A	3.499	0.143	1.484	0.471	0.026	0.025	73.8	98.9
Mode 3 – C	3.491	0.146	1.566	0.414	0.013	0.007	22.4	8.5
Mode 4 – A	4.118	0.164	1.327	0.370	0.021	0.023	42.4	60.3
Mode 4 – C	4.119	0.164	1.324	0.341	0.011	0.006	18.5	6.6
Mode 5 – A	5.001	0.199	1.810	0.458	0.040	0.035	53.1	79.2
Mode 5 – C	5.001	0.199	1.833	0.415	0.018	0.007	20.1	7.4
Mode 6 – A	5.623	0.250	1.440	0.531	0.048	0.044	72.1	105.6
Mode 6 – C	5.616	0.252	1.452	0.479	0.020	0.009	23.9	8.4
Mode 7 – A	6.572	0.294	1.244	0.462	0.047	0.042	71.3	99.6
Mode 7 – C	6.574	0.296	1.270	0.435	0.020	0.008	23.2	8.3

6.5.5. ANALYSIS OF THE MODAL PARAMETERS VARIATION

After the application of automatic operational modal analysis to the time series of accelerations measured by the dynamic monitoring system of Baixo Sabor arch dam, and the elimination of high uncertainty and harmonic related estimates, the time evolution of the modal parameters observed during three years (from 01/12/2015 to 30/11/2018) is analysed.

As it was acknowledged in previous sections, the natural frequencies of the structure varied largely during the monitoring period. The first modes frequency, for instance, though presenting a mean value of 2.53 Hz, decreased from around 2.75 Hz in December 2015 to 2.45 Hz in May 2016, and continued to present large variations through the entire monitoring period. These variations are mostly due to operational and environmental conditions, such as temperature and reservoir water level.

In this sense, the evolution of the first vibration mode natural frequency over time and that of the level of water in the dam's reservoir are presented together in Figure 6.26 for comparison, in which the value of water level corresponds to the difference above sea level. From the analysis of this figure it becomes obvious that a straight relation exists between natural frequency and water level, since the value of frequency always decreases when the water level rises, and vice-versa. This is particularly clear during the first six months of monitoring, when the first filling of the dam was taking part, especially during a period of intense rains in January 2016 during which a sudden rise of more than 10 meters in the water level led to the fastest decrease in the values of natural frequencies being monitored.

The natural frequencies of the first seven modes were represented in Figure 6.27 as a function of the reservoir water level, with the same colour scheme used in previous sections. For this, the first year of monitoring was used and the same type of relation was found for every mode, confirming the inverse relation between the two variables. The reduced number of points between 222 and 227 meters of water level are due to the intense rains and fast-rising waters during the filling period, referred before. It is worth noting that for every mode, the evolution of the first group of points, between 210 and 212 m of water level, presents a low slope, close to the horizontal, indicating the less important effect of water on natural frequencies for lower levels, thence supporting the assumption that was taken when the first forced vibration was performed, which considered the water level of 195.5 m as representative of an empty reservoir.

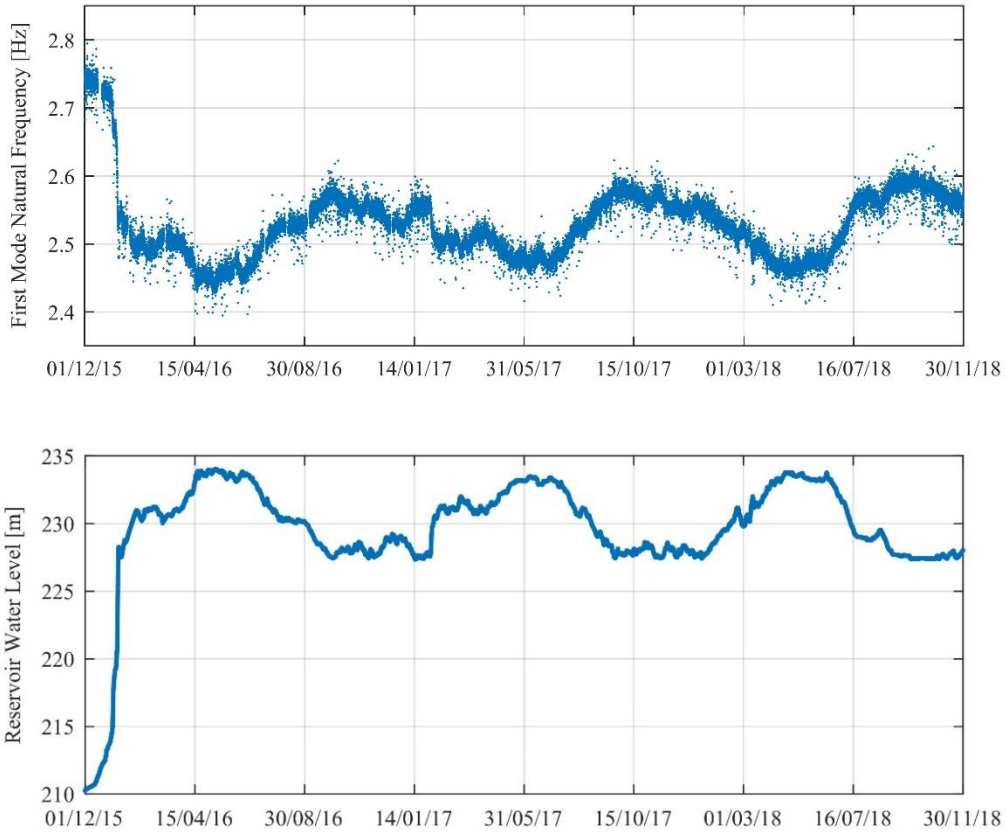

Figure 6.26 – Comparison between the time evolution of the first mode natural frequency and that of the level of water in the dam's reservoir.

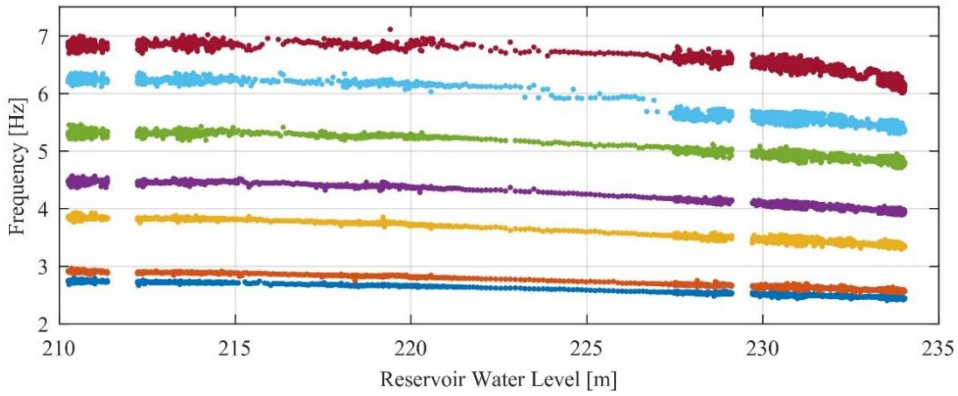

Figure 6.27 – Natural frequency as a function of reservoir water level (first 7 modes).

The relation between each modal frequency and water level was studied independently and quadratic regressions were found to reproduce the results obtained with high determination coefficients for all the seven modes. The quadratic functions determined for the first two vibrations modes are presented in Figure 6.28 as examples. In these cases, determination coefficients around

0.99 were obtained, result to which largely contributed the removal of outliers previously achieved with both the moving references and the uncertainty analysis performed during modal tracking.

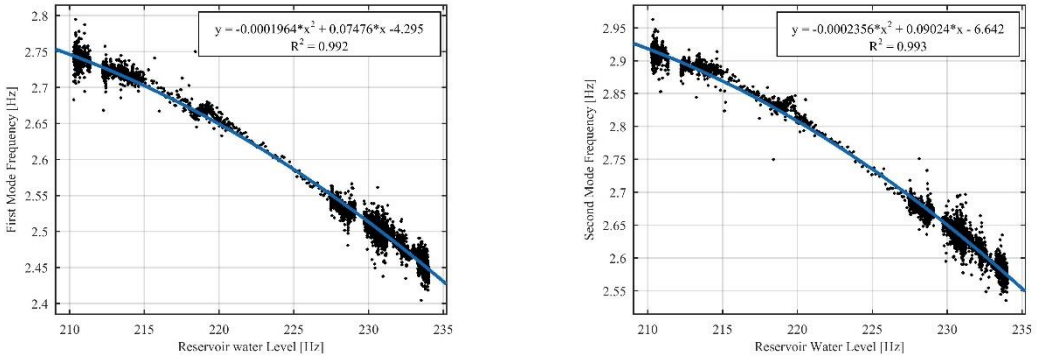

Figure 6.28 – Correlation between the first natural frequency and reservoir water level (on the left); correlation between the corrected first natural frequency and ambient temperature.

Besides the major influence of water level on natural frequencies, other factors play an important role in their evolution over time. A zoom in the evolution of the natural frequencies of modes 6 and 7 during the summer days of 2017 shows daily fluctuations that resemble those of air temperature. The dam is located about 200 km from the sea, in a region where air temperature may present daily amplitudes of more than 20 ºC, which is not expected to occur during the winter, that is characterized by moderate amplitudes. This can be observed in Figure 6.30, where the evolution of air temperature measured in the hydroelectric complex over the three years of monitoring is presented. Although considerable temperature amplitudes are verified during the winter as well, the highest amplitudes, represented by a wider thickness, occur during the summer. Furthermore, important seasonal variations are also verified. Ambient temperature may vary from 0 ºC in the winter to around 40 ºC in the summer, influencing the dam dynamic behaviour.

Additionally, the abundant solar radiation also characteristic of the region during summer may play a significant role in this physical system by warming the dam's downstream surface, as well as the first layer of still waters in the reservoir. However, this effect will be indirectly considered through temperature measurements.

To better understand the effect of ambient temperature on natural frequencies the relation between the two variables was studied. However, since the effect of water level is generally predominant, first the quadratic regressions previously obtained between frequency and water level were used to

minimize this effect and thus expose variations on frequency due to other effects, such as temperature. Consequently, the values of natural frequencies corrected of the effect of water level were represented as a function of ambient temperature. The representations of the first two modes are presented in Figure 6.31, where rough linear regressions with determination coefficients around 0.5 were obtained, indicating a linear relation between natural frequency and temperature.

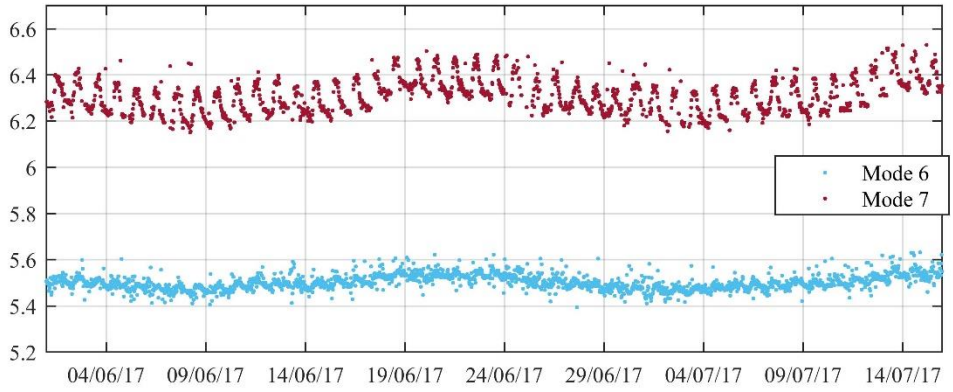

Figure 6.29 – Daily fluctuations of the natural frequencies of modes 6 and 7 during the summer.

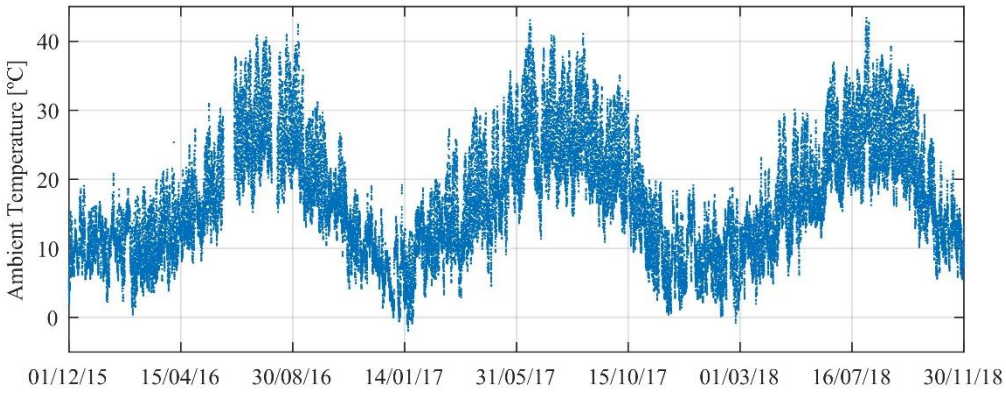

Figure 6.30 – Air temperature evolution during the monitoring period.

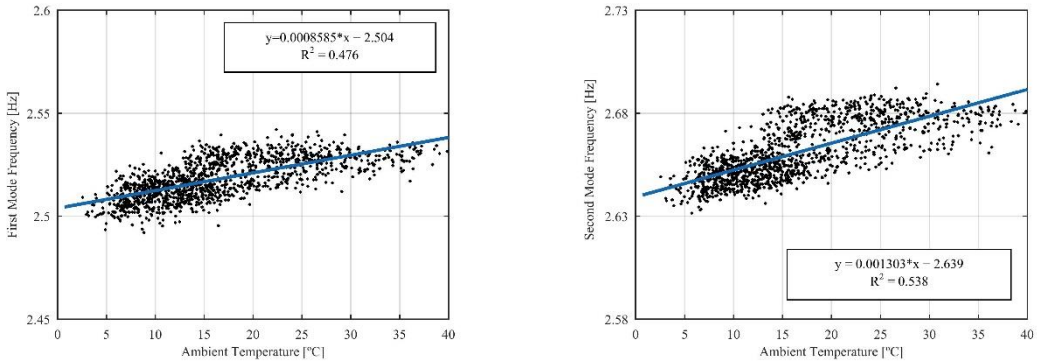

Figure 6.31 – Correlation between ambient temperature and the first two natural frequencies after correction of the effect of reservoir water level.

6.6. MINIMIZATION OF ENVIRONMENTAL AND OPERATIONAL EFFECTS ON NATURAL FREQUENCIES

The characterization of the variation of the dam modal parameters presented in the previous section has shown that, though other factors may play an important role, these are essentially influenced by reservoir water level and temperature. In turn, this section aims to establish a model to minimize the effects of these environmental and operational factors on the estimated natural frequencies. The different approaches that can be followed to achieve this goal have already been described in chapter 5.

In the present application, a multiple linear regression model will be adopted in the first instance. The data collected during the first year of the continuous dynamic monitoring, from 01/12/2015 to 30/11/2016, is used to establish the model and then, data collected during the second and third years of monitoring, from 01/12/2016 to 30/11/2018, are used to validate the quality of the forecasts provided by the regression model. For this purpose, the natural frequencies of the dam's first seven vibration modes obtained from the application of Processing C in section 6.5.4. are used.

The first step when building a regression model consists of the selection of the predictors. Taking into account the analyses performed in the previous section and the high determination coefficients presented in Figure 6.28, reservoir water levels emerge as the main candidates. Since 30-minute datasets have been used to perform modal identification, but only hourly measurements of water levels were available, linear interpolations between consecutive points have been used to duplicate the number of predictors in accordance with the number of frequency estimates, which is acceptable taking into the account both the slow variations on water level and the short period of time considered to perform the interpolations. Additionally, provided that a linear model is being considered and that the relation between natural frequency and water level has been shown to be better represented by a quadratic curve, two predictor variables are built from the values of water levels. The first, hereafter known as W1, consists on the whole set of water level values without any change, whereas the second variable, W2, consists on the square values of the levels present in W1, disposed exactly by the same time order.

It was shown in the previous section that temperature influences natural frequencies as well, and a linear relation between the two was observed, which is in accordance with state-of-the-art works (Magalhães, Cunha, et al., 2012). To better characterize the structure behaviour, instead of the ambient temperature measurements used in the previous section, concrete temperatures should be used. The concrete temperature of the dam is being measured in more than 50 sections, as depicted

by Figure 6.32. Since the downstream surface of the dam is in contact with the atmosphere, and exposed to sunlight, while the upstream surface is mostly covered with reservoir water, whose temperature does not suffer wide variations throughout the year, it is expected for the dam to present different concrete temperatures through its depth, from upstream to downstream. In this sense, each section was instrumented with (at least) three thermometers: the first positioned closer to the upstream surface, the second positioned in the centre of the section (in some sections more than one thermometer are positioned in the centre of the section) and finally the third thermometer positioned closer to the downstream surface.

However, only man-operated measurements of concrete temperatures are available, which are performed roughly every two weeks. Since these timely distanced measurements were not suitable to use as predictors, a curve was adjusted to the data available during the three-years period of monitoring (using Matlab's function "fit"), allowing to obtain 30-minute estimates of concrete temperature in every instrumented point. Though a few outliers are present, good fitting results were obtained using the sum of Fourier functions.

To show the wide differences that may be found in concrete temperatures measured between the upstream and downstream surfaces, data from section "10-11-12", which is located between visit galleries GV1 and GV2 was represented in Figure 6.33. The relative position of each instrumented section to the dam's surfaces are defined by the colour in which the data is represented, which varies between orange, blue and yellow depending weather upstream, internal or downstream measurements are considered. Manually obtained measurements are represented by points and the curves fitted to estimate unavailable data are represented by full lines in the respective colour. Ambient temperature is represented as well, in light blue, for comparison purposes. As it was expected, analysing Figure 6.33 it becomes clear that concrete temperatures measured near to the downstream surface (represented in yellow) present the closest evolution over time to ambient temperature, though exhibiting lower amplitudes between maximum and minimum temperatures. On the other hand, temperatures measured in the internal instrumented section show the highest time gap between their relative maxima and minima and the ones presented by ambient temperature, indicating the effect of this external factor takes months to reach the dams internal concrete, even if the thinnest part of the dam is considered. It is also worth referring that the sinusoidal form of the evolution of concrete temperature measured near the upstream surface, with roughly 10 ºC of seasonal amplitude, is characteristic of the sections instrumented at the same elevation, but not of the rest of the instrumented upstream sections, which present much flatter evolutions over time,

with smaller amplitudes. This is probably due to the proximity of the first layer of instrumented sections to the water surface of the reservoir, where water temperature is influenced as well by ambient temperature and radiation, while deep waters present a more stable temperature throughout the year.

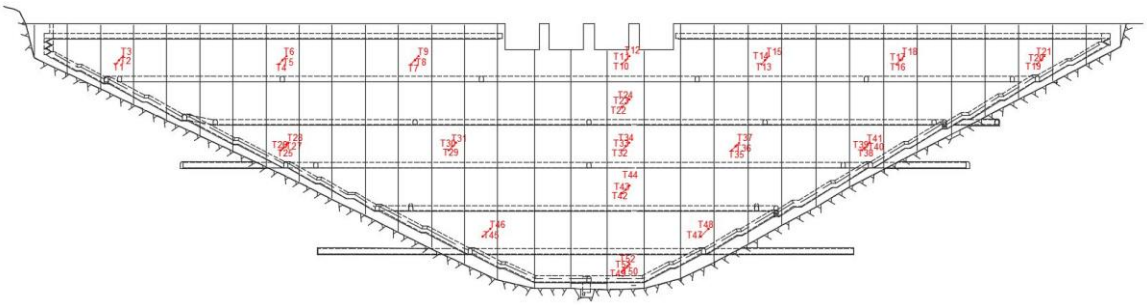

Figure 6.32 – Sections instrumented to measure concrete temperature.

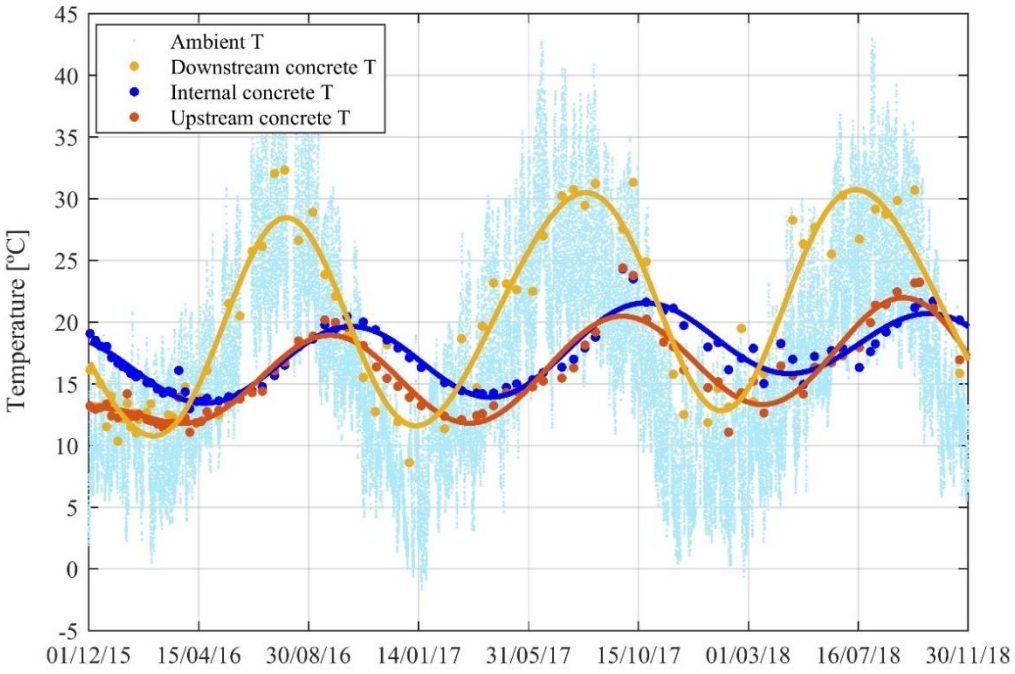

Figure 6.33 – Comparison between ambient temperature and concrete temperatures measured at different concrete depths of the same dam section.

Although concrete temperatures should proportionate better results when used as predictors in the regression model, provided that they actually represent a physical state of the structure, since only sporadic concrete temperature measurements are available and the curves that were fitted to these data do not account for short term variations such as the ones that occur daily, or even between consecutive weeks, ambient temperature should be considered as predictor as well, to complement concrete temperature data.

As it was studied before, daily frequency variations seem to be linearly related to ambient temperature, especially during summer when daily thermal amplitudes are greater. In this case, 10-minute measurements were available, so three-point means were used to build the predictor variable (TA) with the same number of elements of natural frequencies, without losing accuracy in ambient temperature evolution, as shown in Figure 6.34 where it is represented between 01/06/2017 and 15/07/2017, using the same period used in Figure 6.29.

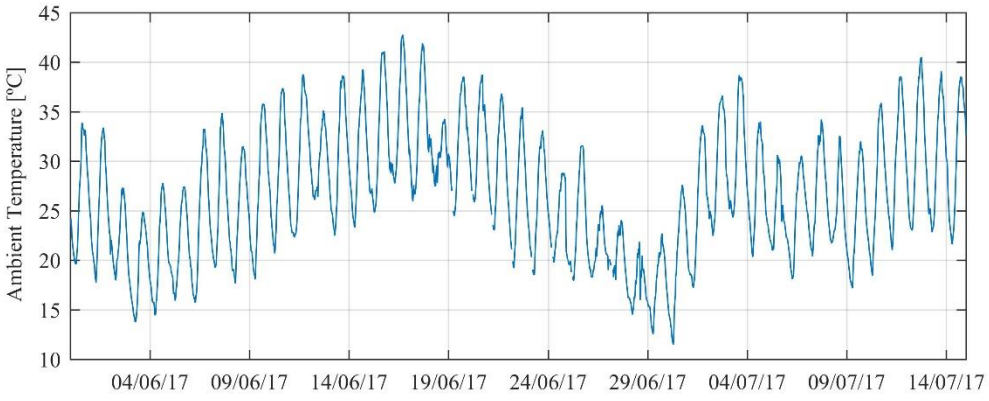

Figure 6.34 – Ambient temperature variation between 01/06/2017 and 15/07/2017 – 30.minute averages.

Finally, the influence of the concrete hardening on natural frequencies may assume a significant role in such a massive structure, especially during the first years after the last pouring, so it should not be neglected. To simulate this slow non-linear process, whose increase rate diminishes with time, a simple model is used considering a logarithmic function. This variable will be considered as a possible predictor and it will be hereafter designated as "H" (concrete Hardening).

After the preliminary selection of possible predictor variables based on correlation coefficients and also taking into account the physics of the problem, alternative regression models should be considered. In the first step, five static models (SM1 to SM5) with an increasing number of predictors were tested. The predictors considered were the two water level variables (W1 and W2), ambient temperature (Ta), concrete temperature (Tc_13 and Tc_14) and the variable modelling

concrete hardening (H). The predictors used in each model are discriminated in Table 6.7. The accuracy of the forecasts obtained with each static model is quantified in Table 6.8 by the coefficient of determination R^2_{for}, calculated through the first equality of equation (5.10) (chapter 5) using the values of the natural frequencies estimated from the acceleration time series (and tracked with Processing C) for the period between 01/12/2016 and 30/11/2018 (which was not considered in the construction of the regression models) and the values forecasted by the regression models.

Generally, the addition of each new predictor improved the ability of the model to perform forecasts. The obtained results show that the best models are SM4 and SM5, which present the highest coefficients of determination depending on the mode considered, which shows that using concrete hardening as a predictor does not necessarily improve the quality of the model. Static model 3 (SM3) presents already high coefficients of determination (above 0.87 for the first 5 modes) using just reservoir water level, ambient temperature and downstream concrete temperature (instrumented point 14), indicating the value of natural frequency mostly depends on these variables. This is corroborated through the addition of internal concrete temperature (instrumented point 13) in model SM4 and concrete hardening in model SM5 which, though increasing the determination coefficients, proportionated only minor gains. Additionally, the analysis of the weight of each predictor also indicates the major contribution to the regression model comes from the reservoir water level, followed by ambient temperature. However, it is not possible to draw conclusions about the relative importance of each temperature predictor, due to the existence of correlations between them, and even between reservoir water level and temperature variables, since seasonal variations of water level go along with those of ambient temperature. Upstream concrete temperature variables were considered as well, but the results obtained were as not as good.

Table 6.7 – Static regression models: used predictors

	SM1	SM2	SM3	SM4	SM5
W 1	x	x	x	x	x
W 2	x	x	x	x	x
Ta		x	x	x	x
Tc 14			x	x	x
Tc 13				x	x
H					x

Table 6.8 – Static regression models: coefficients of determination

	SM1 R^2_{for}	SM2 R^2_{for}	SM3 R^2_{for}	SM4 R^2_{for}	SM5 R^2_{for}
F1	0.853	0.906	0.933	0.935	0.950
F2	0.808	0.893	0.943	0.943	0.951
F3	0.759	0.891	0.928	0.930	0.915
F4	0.819	0.902	0.938	0.938	0.947
F5	0.565	0.829	0.876	0.878	0.872
F6	0.595	0.754	0.775	0.809	0.736
F7	0.741	0.867	0.873	0.881	0.896

Figure 6.35 presents the evolution of the dam's first seven modes natural frequencies obtained from the application of operational modal analysis to three years of data (from 01/12/15 to 30/11/2018) as well as the values of frequency forecasted with regression model SM5. Each mode is represented in the colour previously used, while all the forecasts are represented in black. The evolution of the seven sets of forecasts follows the evolution of natural frequency estimates obtained from OMA, in accordance with the good results presented in Table 6.8, though small deviations are observable even with this low accuracy scale, especially for the modes of higher order.

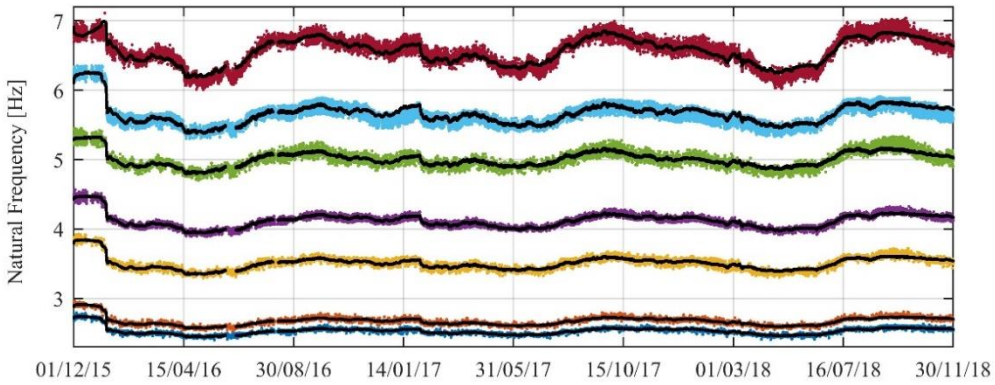

Figure 6.35 – Estimated with OMA vs predicted with regression model SM5 natural frequencies: first seven modes.

To verify the quality of the forecasts, a zoom of the previous figure is represented in Figure 6.36, thus showing the evolution of vibration modes 1 and 2 frequency estimates and forecasts. The evolution of the forecasts of these two modes, the two whose regression models presented the highest determination coefficients, almost perfectly follows the evolution of frequency estimates, even if presenting a few flaws. On the one hand, even using ambient temperature as predictor the regression model is not able to produce forecasts with the same short-term variability presented by natural frequency estimates, indicating the true variability of the mentioned estimates due to operational and environmental conditions is most times overgrown by the uncertainty associated

with the identification process. On the other hand, the model shows inability to accurately follow the evolution of frequency estimates in a couple of periods, namely between October and November 2017 and during the same period of 2018.

The ability of the regression model to represent frequency estimates is better understood through the analysis of Figure 6.37, where the evolution of the natural frequency of the first two vibration modes after the minimization of operational and environmental effects with the static regression model SM5. Much more stable evolution of natural frequencies around their means was achieved. The effects of the variability issue mentioned before and the sporadic inability of the regression model to produce forecasts as accurate as it generally does become clearer. The gaps in the corrected frequencies are due to gaps in the predictor variables (mainly ambient temperature).

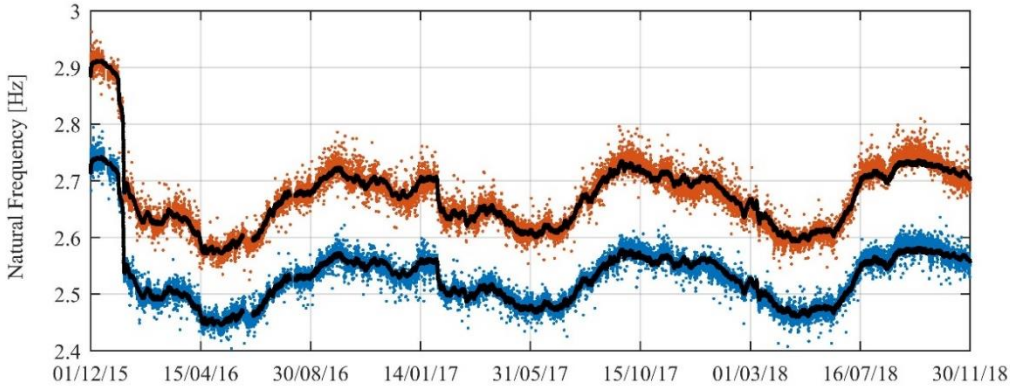

Figure 6.36 – Estimated with OMA vs predicted with regression model SM5 natural frequencies: first two modes.

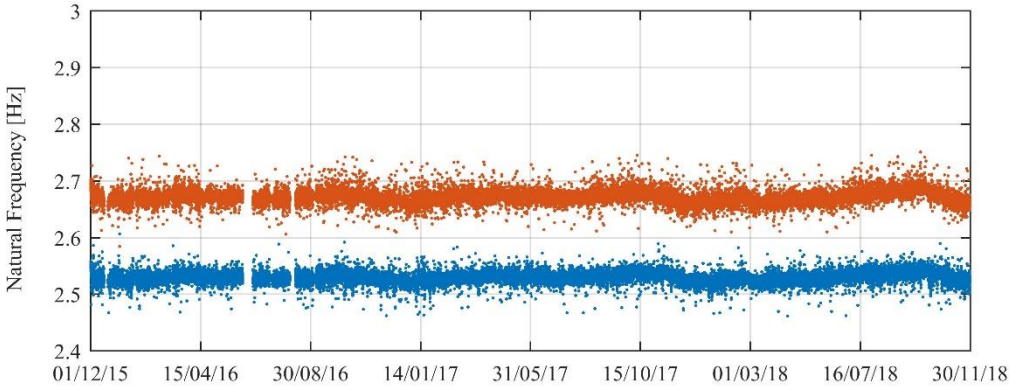

Figure 6.37 – Natural frequency evolution of the first two modes after the application of regression model SM5.

Histograms may be used to evidence the reduction of the range of variation of natural frequencies after their correction with SM5. In this sense, Figure 6.38 presents the histogram of the natural

frequencies of the first three vibration modes during the period adopted for validation of the regression models (from 01/12/2016 to 30/11/2018), before and after the correction. It is clear that after the application of regression model SM5, the values of natural frequencies are concentrated in a much narrower interval and their histograms present shapes that resemble those of normal distributions.

Additionally, the standard deviations of each modes frequencies during the two-year validation period were calculated and presented in Table 6.9. In the case of the first four modes, standard deviations reductions of more than 70 % were achieved, proving once again the quality of regression model SM5. In turn, with modes five to seven good results were achieved as well, but standard deviations reductions ranged only between 54 and 68 %, with mode 6 presenting the lowest reduction. Moreover, though important reductions were achieved, modes 6 and 7 still present significantly high standard deviations, around 0.06 Hz, that can hide frequency variations due to small damages that may eventually affect the structure.

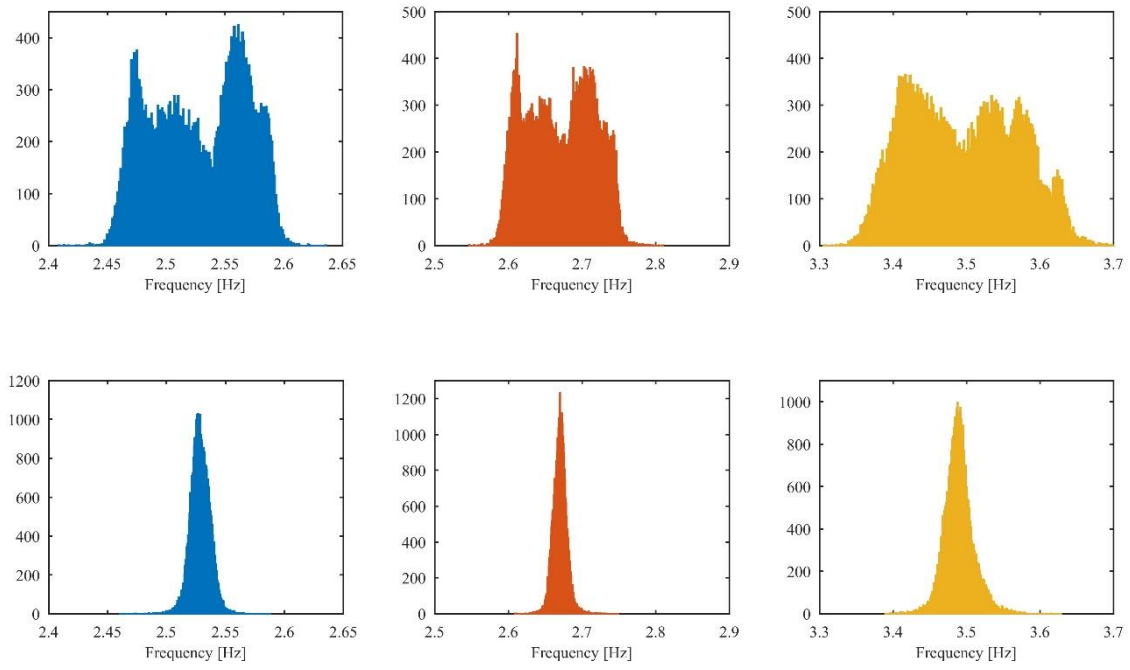

Figure 6.38 – Histograms of the natural frequencies of the first three modes, before (top figures) and after (bottom figures) the minimization of environmental and operational effects (regression model SM5, data from 01/12/2016 to 30/11/2018).

Table 6.9 – Standard deviation of the first seven modes natural frequency (30-minute) estimates over a two-year period (from 01/12/2016 to 30/11/2018) before (old) and after (new) the minimization of operational and environmental effects

	Two-years standard deviation [Hz]	
	Before correction	After correction
F1	0.0398	0.0089
F2	0.0458	0.0101
F3	0.0742	0.0209
F4	0.0816	0.0186
F5	0.1046	0.0372
F6	0.1215	0.0554
F7	0.1929	0.0618

To conclude the analysis of the quality of the adopted regression model and its capability to minimize the effects of operational and environmental factors on natural frequencies, the correlation coefficients between natural frequencies before and after correction were calculated, since high correlations between two natural frequencies would mean they are influenced by common factors.

Therefore, the correlation coefficients between the first seven modes' natural frequencies identified between 01/12/2016 and 30/11/2018 are presented in Table 6.10. The coefficients obtained using frequencies before correction are presented on the left, whereas the coefficients obtained using frequencies after correction provided by regression model SM5 are presented on the right. Each coefficient is represented with a shade of blue which depends on its own value: values closer to 1 are represented in dark blue; values closer to 0 are represented in light blue.

It can be observed that before correction all the frequencies presented a high correlation between each other, being the lowest correlation coefficient obtained, between the first and the fifth mode, equal to 0.88. The right part of Table 6.10 presents much lighter shades of blue, suggesting the correlation between variables after the correction provided by the regression model largely decreased. However, though a few correlation coefficients decreased to values lower than 0.2, there are still many coefficients around 0.3 and 0.4, which consists in a significant correlation between variables, indicating the model could still be improved.

Table 6.10 – Correlation coefficients between frequencies before and after the application of regression model SM5 (data from 01/12/2016 to 30/11/2018)

	F1	F2	F3	F4	F5	F6	F7
F1	1.00	0.97	0.95	0.96	0.88	0.88	0.92
F2	-	1.00	0.96	0.97	0.91	0.89	0.93
F3	-	-	1.00	0.96	0.93	0.90	0.93
F4	-	-	-	1.00	0.91	0.89	0.93
F5	-	-	-	-	1.00	0.89	0.90
F6	-	-	-	-	-	1.00	0.89
F7	-	-	-	-	-	-	1.00

	F1	F2	F3	F4	F5	F6	F7
F1	1.00	0.41	0.32	0.34	0.30	0.30	0.12
F2	-	1.00	0.36	0.40	0.36	0.31	0.17
F3	-	-	1.00	0.36	0.47	0.28	0.24
F4	-	-	-	1.00	0.43	0.23	0.18
F5	-	-	-	-	1.00	0.25	0.31
F6	-	-	-	-	-	1.00	0.13
F7	-	-	-	-	-	-	1.00

Dynamic regression models could be used to try to reduce the differences between frequency observations and predictions even further. However, temperature is the only predictor whose effect on the structure may be delayed, since heat transfer depends on time, and temperature is already quantified in regression model SM5 by three different predictor variables, consisting on temperature measurements in three concrete depths levels: ambient temperature, downstream concrete temperature and internal concrete temperature. In this sense, dynamic regression models were not considered.

Nevertheless, the static models previously presented were tested once again, this time considering the uncertainty associated with each natural frequency estimate as weights (weighted static models: SM_W). These uncertainties were studied and quantified in section 6.5. The weights were considered as the inverse of the variance associated with each frequency estimate, thus as the uncertainty decreases, the weight of each estimate increases.

The first five weighted static models correspond exactly to the five static models previously used, this time using uncertainties. Generally, similar results were obtained, yet this time the coefficients of determination were slightly lower for most modes. Only with the seventh mode an increase in the coefficient of determination was verified, when using SM5_W. Additionally, many other models were considered and two of them produced very specific improvements, namely with modes 4 and 5. The predictors used in each model are systematized in Table 6.11. Weighted static model SM6_W was built by taking SM5_W and adding the upstream concrete temperature measured in point 12 (Tc 12) as a predictor. In turn, in SM7_W only ambient temperature and downstream concrete temperature (Tc 14) were used as temperature related predictors. The coefficients of determination obtained for each mode with each model are presented in Table 6.12. The values of determination coefficients that correspond to improvements from the results previously obtained with regular static models were highlighted with light blue.

Table 6.11 – Weighted static regression models: used predictors

	SM1_W	SM2_W	SM3_W	SM4_W	SM5_W	SM6_W	SM7_W
W 1	x	x	x	x	x	x	x
W 2	x	x	x	x	x	x	x
Ta		x	x	x	x	x	x
Tc 14			x	x	x	x	x
Tc 13				x	x	x	
H					x	x	x
Tc 12						x	

Table 6.12 – Weighted static regression models: coefficients of determination

	SM1_W R^2_{for}	SM2_W R^2_{for}	SM3_W R^2_{for}	SM4_W R^2_{for}	SM5_W R^2_{for}	SM6_W R^2_{for}	SM7_W R^2_{for}
F1	0.853	0.902	0.927	0.930	0.948	0.917	0.948
F2	0.807	0.890	0.939	0.938	0.948	0.946	0.949
F3	0.733	0.880	0.926	0.917	0.916	0.855	0.928
F4	0.476	0.900	0.931	0.928	0.933	0.953	0.941
F5	0.568	0.826	0.881	0.875	0.866	0.834	0.886
F6	0.587	0.734	0.749	0.791	0.658	0.774	0.741
F7	0.740	0.871	0.871	0.897	0.903	0.894	0.890

Table 6.13 summarizes the regression models best suited for the forecasting of each vibration mode, along with the respective coefficients of determination and the standard deviations of the residuals that result from the difference between natural frequency observations and forecasts. Four static models and three weighted static models using uncertainties as weights were used, demonstrating once again the important role the quantification of uncertainties may assume in the fields of operational modal analysis and structural health monitoring. With the exception of mode 6, all the regression models present coefficients of determination above 0.88. However, when standard deviations of residuals are analysed, three groups may be formed: the corrected natural frequencies of the first four modes present low standard deviations, all below 0.020 Hz; modes 6 and 7 still present high standard deviations, around 0.055 Hz; mode 5 natural frequency presents a significant standard deviation of 0.035 Hz. These divisions may play an important role when selecting the modes used for damage detection, since high data variability may hinder the detection of small frequency variations.

Finally, the new correlation coefficients between each modes natural frequency after correction of operational and environmental factors with the models reported in Table 6.13 are presented in the

right part of Table 6.14, while the left part of the table is used for the presentation of the correlation coefficients previously obtained using just regression model SM5. The same blue scale is used for comparison. A significant reduction was achieved for modes 4, 5 and 6, indicating there is less correlation between variables and thus better minimization of the effect of external factors on natural frequencies. Slight improvements are verified as well with mode 3, while mode 7 presents both reductions and slight increases in the correlations with the other modes. Generally, better results were achieved using different regression models for each vibration mode and considering weighted models in the process.

Table 6.13 – Best correlation model for each natural frequency: Coefficients of determination and residuals standard deviation

	Regression model	R^2_{for}	Residuals std
F1	SM5	0.950	0.0089
F2	SM5	0.951	0.0101
F3	SM4	0.930	0.0181
F4	SM6_W	0.953	0.0174
F5	SM7_W	0.886	0.0351
F6	SM4	0.809	0.0528
F7	SM5_W	0.903	0.0576

Table 6.14 – Correlation coefficients between frequencies after the application of regression model SM5, on the left, and after the application of models reported in Table 6.13, on the right (data from 01/12/2016 to 30/11/2018)

	F1	F2	F3	F4	F5	F6	F7
F1	1.00	0.41	0.32	0.34	0.30	0.30	0.12
F2	-	1.00	0.36	0.40	0.36	0.31	0.17
F3	-	-	1.00	0.36	0.47	0.28	0.24
F4	-	-	-	1.00	0.43	0.23	0.18
F5	-	-	-	-	1.00	0.25	0.31
F6	-	-	-	-	-	1.00	0.13
F7	-	-	-	-	-	-	1.00

	F1	F2	F3	F4	F5	F6	F7
F1	1.00	0.41	0.30	0.20	0.27	0.27	0.12
F2	-	1.00	0.34	0.27	0.36	0.29	0.18
F3	-	-	1.00	0.25	0.38	0.21	0.21
F4	-	-	-	1.00	0.30	0.12	0.12
F5	-	-	-	-	1.00	0.18	0.30
F6	-	-	-	-	-	1.00	0.16
F7	-	-	-	-	-	-	1.00

6.7. PRINCIPAL COMPONENTS ANALYSIS AND CONTROL CHARTS

After the application of multiple linear regressions (MLR) to the vibration modes of the dam that are being tracked, which was performed in the previous section with the aim of minimizing the effects of operational and environmental conditions on modal properties, statistical tools may be used to detect shifts in natural frequencies that correspond to the effect of damages on the dynamic behaviour of a structure. The control charts introduced in chapter 5 are especially adequate to the present application since they allow to detect changes on processes characterized by several variables, such as the natural frequencies of the different tracked vibration modes.

Since the structure under study is very recent and has been submitted neither to major seismic activity nor other extraordinary conditions, nor to long-term deterioration processes, damage is not expected to be detected. Instead, damages will be numerically simulated in the next section, where the ability of control charts to detect such damages will be tested. In this sense, the purpose of this section is to guarantee the quality of the minimization of the effect of the operational and environmental conditions thought the production of clean control charts that may be later used as baseline for damage detection.

At a first instance, Shewhart control charts based on the 7 monitored natural frequencies were tested, using the corrected values obtained after the combined application of regression models SM4, SM5, SM5_W, SM6_W and SM7_W, as described in Table 6.13. Data from 01/12/2016 to 30/11/2017 was used as reference data to calculate the values of x and S adopted in the expression of T^2 (equation (5.22)), whereas observations between 01/12/2017 and 31/05/2019 were used to build the control part of the chart and assure and verify the quality of the chart associated with the non-damaged situation.

Since the higher number of missing values in modes 6 and 7, when compared to the first five modes, would considerably decrease the data available to build the control charts, the analysis proceeded with the natural frequencies of the first 5 vibration modes.

Mathematical expressions for the upper control limit (UCL) were defined in chapter 5 with equations (5.22) and (5.23) when control charts were first introduced. Theoretically, when the process is under control, which in the present application corresponds to the period when the structure is not damaged, the values of T^2 should lay between 0 and the UCL. However, this limit is exceeded by a large number of points during both the reference and control periods, which is probably caused by the fact that the data used in this application does not respect all the assumptions

adopted for the definition of the limit, such as the independence between consecutive observations. Consequently, the definition of the UCL had to be accomplished through the evaluation of the distribution of the T^2 values during the reference period. In this sense, the UCL was defined as the sum of the average T^2 with two times the T^2 standard deviation (during the reference period), so that approximately 95% of T^2 values would be below the UCL. This approach is only possible as long as the reference period is large enough to confidently define the UCL.

Many different Shewart control charts were tested considering groups from 1 to 96 elements, and finally the ones resulting from the consideration of groups with 6 and 96 points, corresponding respectively to 3-hour and 2–day data, are represented in Figure 6.39 for comparison. The reference period (from 01/12/2016 to 30/11/2017) is represented in blue and the control period (from 01/12/2017 to 31/05/2019) is represented in orange, while the UCL is represented by a red horizontal line.

While just a few disperse outliers appear above the UCL during the reference period, many more disrespect the limit during the control period. Moreover a clear peak appears between May and December 2018, indicating a structural behaviour that had not been considered during the period used to build the model (01/12/2016 – 30/11/2017). This peak found between May and December 2018 may be explained by the fact that for the first time, due to a long period with reduced precipitation and thus lower reservoir water level, the upstream concrete temperature rose above the internal concrete temperature (see Figure 6.33), motivating a set of structural conditions that had not occurred during the period used to build the model. Additionally, the general high variability observed for the T^2 values is attributed to the lack of accuracy of the predictors related with concrete temperature, which were estimated from isolated data with low confidence levels, especially during the last months of monitoring for which a lower number of measurements is available. The control charts obtained after the application of MLR to natural frequencies are not suited for damage detection since they would lead to false identifications of damage.

Therefore, in order to achieve control charts suited for damage detection, five new procedures were considered for the minimization of the effects of operational and environmental conditions on modal properties, through the combined application of MLR with PCA (principal components analysis) and through the application of PCA by itself.

After the procedure presented before (MLR), the second procedure tested corresponded to the application of PCA to the residuals obtained from the application of MLR to natural frequencies.

This second approach will be named MLR+PCA. Since most of the data variability had been already removed through the application of MLR, four components had to be considered when using PCA to obtain at least 95 % of variance of the observed data, as it is presented in Table 6.15, where the number of components finally selected in each procedure considering PCA is marked in bold.

Since there are two major external sources of data variability affecting the dam's modal properties (reservoir water level and concrete temperature), two other procedures were tested, considering the direct application of PCA to natural frequencies. In the first, PCA1, the method was applied using only one principal component, while in the second, PCA2, two principal components where considered.

Finally, taking into account that the evolution of water level is very well characterized with accurate data and that most the of the flaws of the MLR model are due to lack of accuracy in the characterization of concrete temperature, a regression model considering just the reservoir water level ($MLR_{Water\ Level}$) was built and tested. In the end, the principal component analysis was applied to the residuals of the application of the $MLR_{Water\ Level}$ model to natural frequencies. In this last procedure, three components were needed to reach the threshold of 95 % of accumulated variance.

The control charts obtained for these five procedures are represented as well in Figure 6.39. Once again, both groups with 6 and 96 elements were considered and tested.

Table 6.15 – Accumulated variance explained (%) by the first n components in each procedure using PCA

Number of Components	MLR + PCA	PCA1	PCA2	$MLR_{Water\ Level}$ + PCA
1	67.0	**97.7**	97.7	87.1
2	82.5	99.5	**99.5**	94.0
3	93.1	99.8	99.8	**97.5**
4	**97.1**	99.9	99.9	99.0
5	100.0	100.0	100.0	100.0

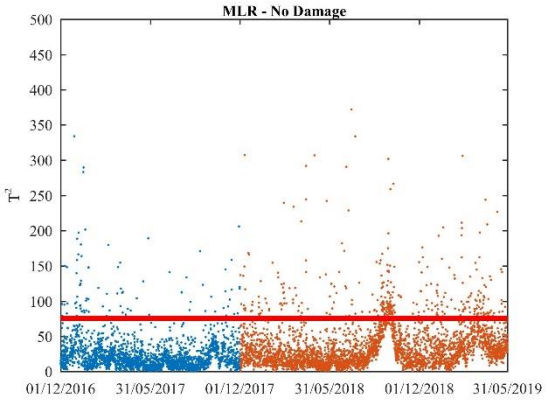
MLR - No Damage
T^2
0
50
100
150
200
250
300
350
400
450
500
01/12/2016
31/05/2017
01/12/2017
31/05/2018
01/12/2018
31/05/2019

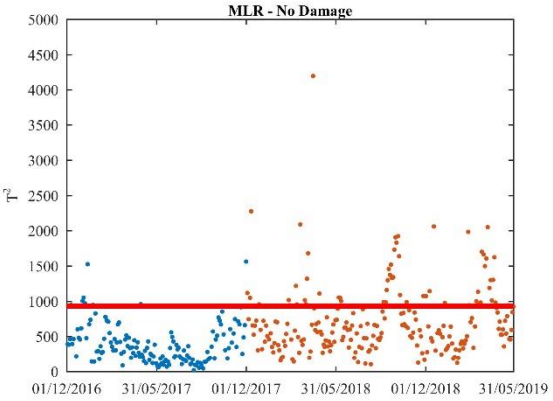
MLR - No Damage
T^2
0
500
1000
1500
2000
2500
3000
3500
4000
4500
5000
01/12/2016
31/05/2017
01/12/2017
31/05/2018
01/12/2018
31/05/2019

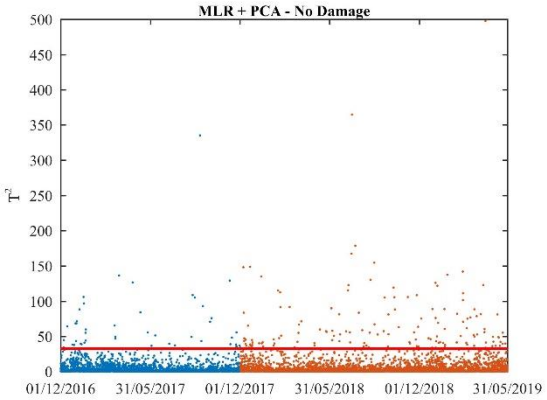
MLR + PCA - No Damage
T^2
0
50
100
150
200
250
300
350
400
450
500
01/12/2016
31/05/2017
01/12/2017
31/05/2018
01/12/2018
31/05/2019

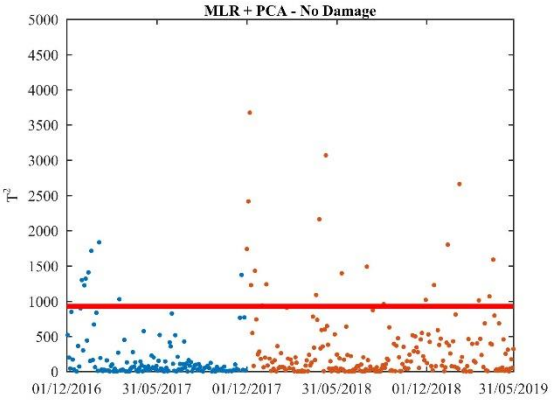
MLR + PCA - No Damage
T^2
0
500
1000
1500
2000
2500
3000
3500
4000
4500
5000
01/12/2016
31/05/2017
01/12/2017
31/05/2018
01/12/2018
31/05/2019

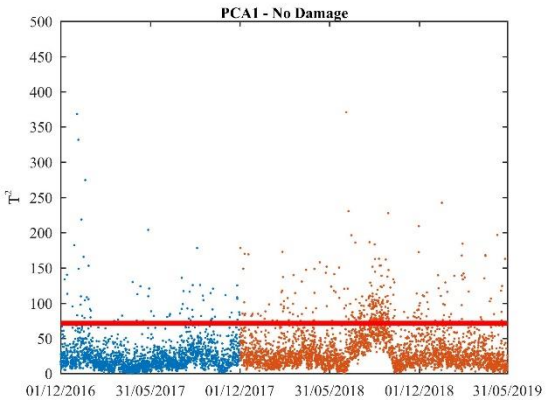
PCA1 - No Damage
T^2
0
50
100
150
200
250
300
350
400
450
500
01/12/2016
31/05/2017
01/12/2017
31/05/2018
01/12/2018
31/05/2019

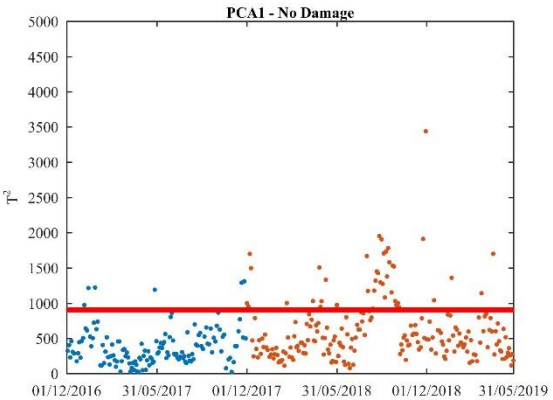
PCA1 - No Damage
T^2
0
500
1000
1500
2000
2500
3000
3500
4000
4500
5000
01/12/2016
31/05/2017
01/12/2017
31/05/2018
01/12/2018
31/05/2019

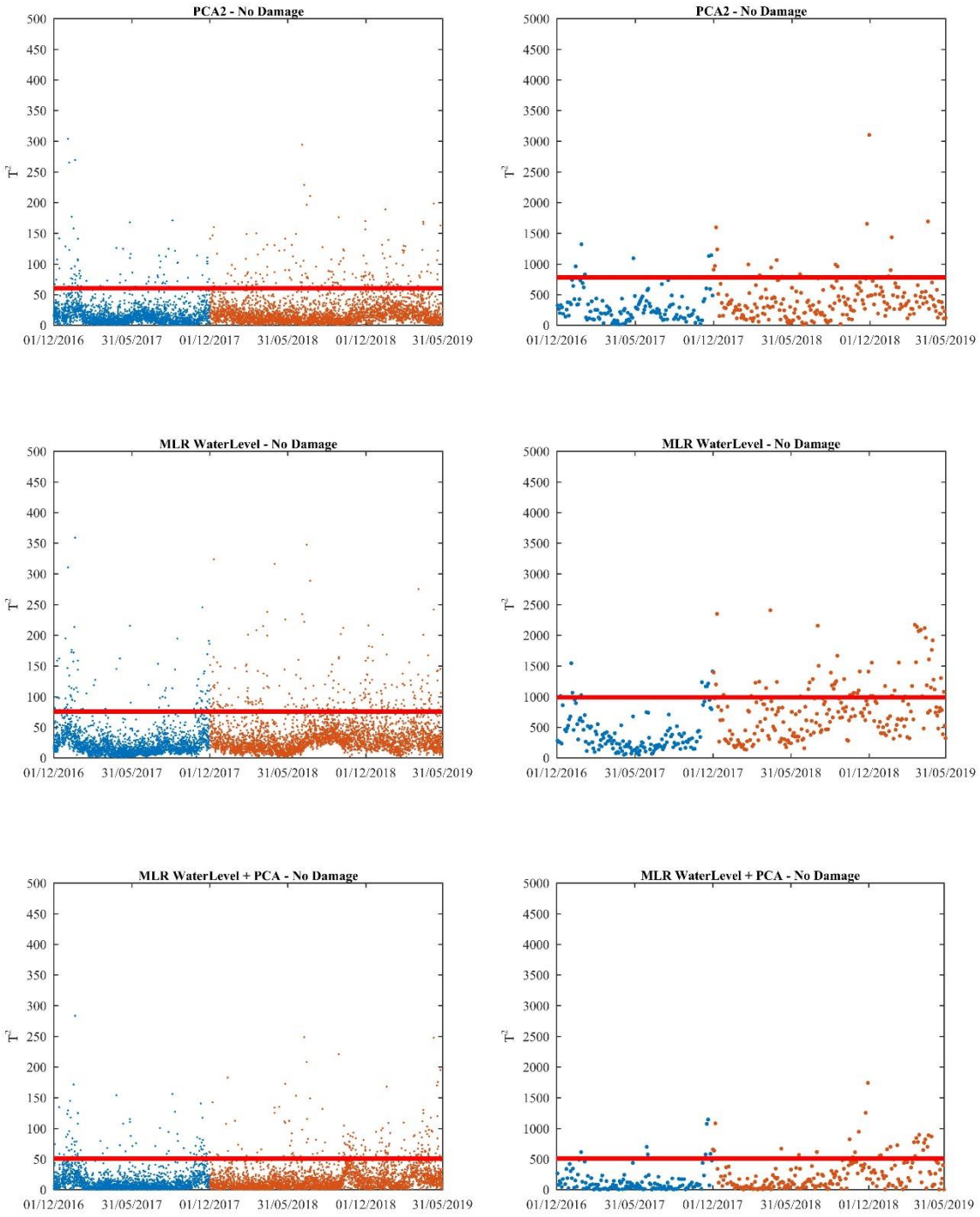

Figure 6.39 – Baseline control charts (no damage) obtained for the six procedures considered to minimize operational and environmental conditions: 6-points groups on the left; 96-points groups on the right.

The combined application of MLR and PCA resulted in a stable control chart, with just a few disperse outliers. In turn, major differences were found when direct PCA was used with one and two components. While a stable control chart was obtained with PCA2, it is clear that using just one principal component (PCA1) is not enough to completely eliminate the effects of concrete temperature variation on modal properties. In turn, with $MLR_{Water\ Level}$ and $MLR_{Water\ Level}$ + PCA, the effects of concrete temperature variation are still visually detectable.

To choose which procedures should be used in the next section to test the ability of control charts on the detection of damages, the values of the indexes introduced in Chapter 5 (J_R, Out_{ref} and $Out_{control}$) were calculated for each of the tested procedures and presented in Table 6.16. The values presented correspond to the scenarios with groups of 96 elements, which produce much better results detecting damage, when compared to the charts using groups with just 6 elements, as it will be shown in the next section. In the case of the J_R index, which represents the ratio between the average T^2 value during the control period and the average T^2 value during the reference period, values between 1.3 and 2.0 are obtained, which indicates that generally higher T^2 values are obtained during the control period of every procedure. Since values close to 1.0 should be expected, the best results are presented by the MLR+PCA and the PCA2 procedures, respectively with J_R = 1.31 and J_R = 1.37.

Out_{ref} and $Out_{control}$ represent the percentage of T^2 values above the UCL limit during the reference and the control periods. While in the case of Out_{ref} the results lie between 5.04 and 6.76 %, in accordance with the fact that the UCL was established as leading to 95 % of values below it, assuming a normal distribution to the T^2 values. On the other hand, in the case of $Out_{control}$ the results obtained vary from 7.44 to 26.34 %. Once again, the MLR+PCA and the PCA2 procedures present the best results, being the only two procedures that present a number of outliers lower than 10 % during the control period.

Slightly higher values of J_R and outlier counting during the control period do not mean novel structural behaviour is being detected. Therefore, even if the previous indexes are important to evaluate the charts (and their ability to detect damage) it is imperative to ensure that no false detections will occur. In this sense, another index is used corresponding to the number of times that five consecutive points are found above the UCL, either during the reference ($Alert_{ref}$) and the control periods ($Alert_{control}$). To ensure no false detections of damage occur, both $Alert_{ref}$ and $Alert_{control}$ should be equal to zero. In the present application five consecutive points correspond to 10 days (5 x 2 days), which is considered an acceptable time window for the monitoring system to

produce an alert for the possibility of the detection of small damage, not compromising the dam safety. Different applications may require other type of alerts.

Procedures MLR+PCA and PCA2 are the only ones with no alerts during both the reference and the control periods, in accordance with the good results presented for the other indexes evaluated. In the next section, numerically simulated damages will be introduced in the data to test the ability of the control charts produced by these two procedures in detecting such damages.

Table 6.16 – Control Charts quality: indexes obtained for the control charts with groups of 96 elements, after the application of each procedure used to mitigate the effects of operational and environmental conditions

Model	J_R	Out_{ref} *[%]*	$Out_{control}$ *[%]*	$Alert_{ref}$	$Alert_{control}$
MLR	1.89	5.48	25.56	0	21
MLR + PCA	1.31	5.11	7.44	0	0
PCA1	1.64	5.04	19.53	0	19
PCA2	1.37	5.04	8.37	0	0
$MLR_{Water\ Level}$	2.02	6.76	26.34	0	5
$MLR_{Wate\ rLevel}$ + PCA	1.87	5.76	13.49	0	1

6.8. DAMAGE DETECTION

As it was presented in Table 6.9, the lowest standard deviation for the evolution of the observed natural frequencies among the first seven vibration modes, during the second and third years of monitoring, was presented by the first mode and it roughly corresponded to 0.040 Hz, whereas many modes presented standard deviations close to 0.100 Hz and even above this value. These high standard deviation values result from the effect of operational and environmental conditions and suggest that regular data variability imposed by common operating conditions is large enough to hide frequency variations that can occur due to small damages, and thus hinder their detection.

However, it was demonstrated in the last section that the effects of operational and environmental conditions on natural frequencies may be largely reduced with the correct post-processing. In this sense, in this section it is evaluated if the control charts presented in chapter 5 are suitable to detect small shifts of the natural frequencies. For this, the natural frequencies corrected by the MLR+PCA and PCA2 models presented in the previous section and damages simulated with the finite element model presented in section 6.3.2 are used.

6.8.1. DAMAGE SIMULATION

Damage in dams may stem from a diversity of occurrences, as for instance vibrations due to an earthquake, foundation sliding or concrete deterioration due to cracking or chemical reactions. The accurate numerical modelling of damage scenarios directly motivated by the referred causes would require the development of very complex non-linear models and a large number of assumptions. As these models would provide only approximate results, and the construction of very sophisticated models is not the main focus of this work, a simpler approach was followed. The likely consequences of extreme events or of structural ageing are modelled in a simplified manner by reductions of stiffness in a few dam components, such as part of concrete blocks or the contraction joints.

In this manner, four different damage scenarios were considered, D1, D2, D3 and D4. The location and extent of each considered damage are presented in Figure 6.40. The first damage scenario (D1) corresponds to the decrease of Young's modulus value in a group of 11 elements in the central part of the dam, at an elevation of 200 m above sea level. Only elements in the most upstream layer were considered, which corresponds to a part of the structure that is stress sensitive and may be subjected to cracking. The second damage scenario (D2) is equivalent to the first one, with similar

extent, though only 5 elements were damaged in this case, and it is located between the abutment and the central part of the dam, also at 200 m above sea level. The third scenario (D3) corresponds to more confined damage in the central part of the structure, but it goes from upstream to downstream, through the three layers of elements of the dam model, between 185 and 205 m above sea level. In this case, 18 elements were used to introduce damage. Finally, in the fourth damage scenario (D4) both the normal and shear stiffness of the six central contraction joints were reduced. Damages D1, D2 and D3 were represented in Figure 6.40 with light blue and damage D4 was represented with red.

Damage scenario D1

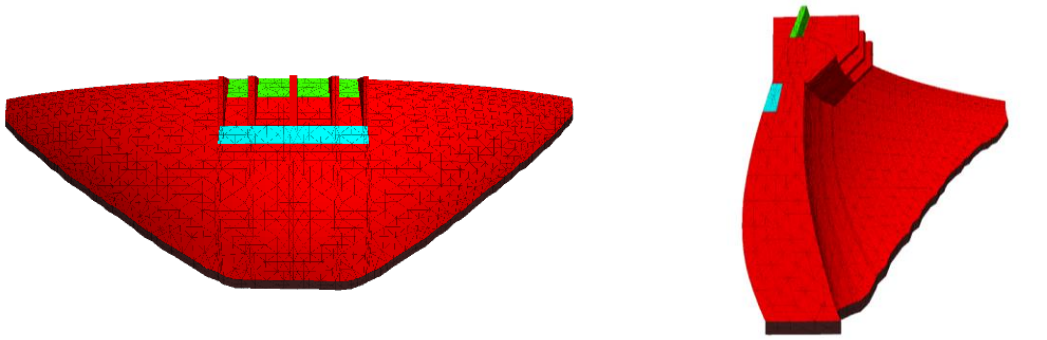

Damage scenario D2

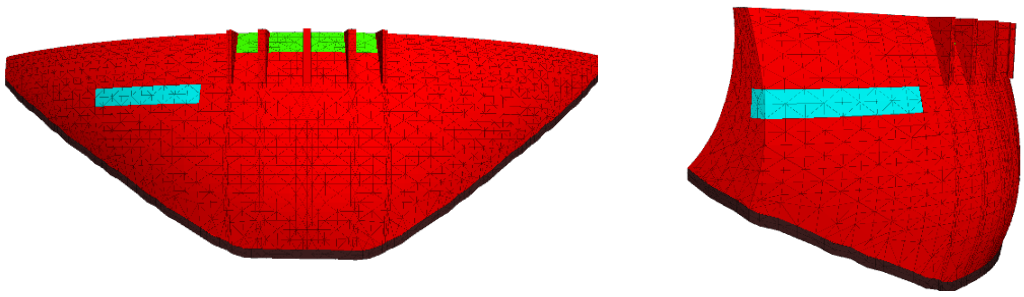

Damage scenario D3

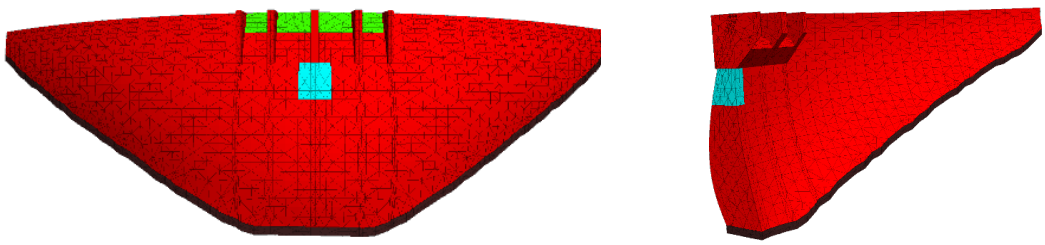

Damage scenario D4

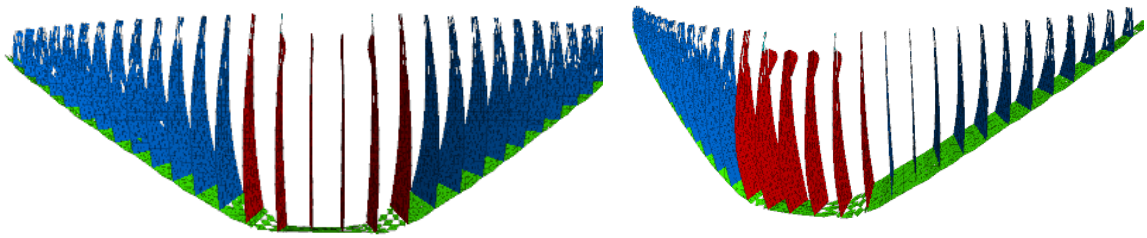

Figure 6.40 – Location, extent and type of simulated damage scenarios.

The natural frequencies obtained with the numerical model for the first seven vibration modes were used as reference values for comparison with the natural frequencies obtained after the introduction of each damage. Results were obtained for several reservoir water levels between 210 and 234 m (heights between which the water level varied during the monitoring period), but small differences were found between them. Moreover, five levels of damage intensity were considered, which consisted in the reduction of Young's modulus of selected elements (or normal and shear stiffness in the case of joints) in 10, 30, 50, 70 or 90 %. Major differences were observed between the results obtained with the five damage intensities.

The different damage intensities were considered keeping in mind that a monitoring system should be able to alert for the occurrence of novel structural behaviour, which may lead to inspections in the structure and ultimately to maintenance or rehabilitation works. However, since damages may result from slow continuous deterioration processes or from extreme actions that can originate or accelerate such deterioration processes, it is important to detect them while they are still not very relevant and the safety of the structure is not significantly reduced. In this sense, it is worth studying if the monitoring system is just able to detect damages in an advanced stage or already when they are still starting to develop.

The results obtained with a level of water in the reservoir of 234 m and damage intensities of just 10 %, which is the most challenge scenario to test the damage detection tools, are presented in Table 6.17. Additionally, the results obtained with the same level of water in the reservoir and damage intensities of 50 %, which correspond to intermediate damage intensities, are presented in Table 6.18. While in the first case most modes presented frequency reductions between 0.02 and 0.08 %, in the intermediate case roughly 10 times higher frequency reductions were verified. The higher minimum and maximum frequency reductions were achieved with 90 % damage intensities, assuming values between 0.3 % and 4 %. Furthermore, in each damage scenario, different frequency

reductions were verified for each vibration mode, indicating the possibility of locating damage through the study of the relation of the effect of damages between modes.

Table 6.17 – Natural frequencies (in Hz) associated with damage scenarios D1, D2, D3 and D4 (10% of damage intensity) compared with the numerical reference values (Ref) with a water level of 234 m

		D1		D2		D3		D4	
Mode	Ref	Freq [Hz]	Δ Freq. [%]	Freq [Hz]	Δ Freq. [%]	Freq [Hz]	Δ Freq. [%]	Freq [Hz]	Δ Freq. [%]
1	2.45372	2.44928	-0.181	2.45337	-0.014	2.45065	-0.125	2.45186	-0.076
2	2.68436	2.68276	-0.059	2.68297	-0.052	2.68235	-0.075	2.68259	-0.066
3	3.58254	3.58199	-0.015	3.57815	-0.122	3.58189	-0.018	3.58085	-0.047
4	4.05438	4.05196	-0.060	4.05131	-0.076	4.05312	-0.031	4.05269	-0.042
5	4.84020	4.83624	-0.082	4.83665	-0.073	4.83662	-0.074	4.83820	-0.041
6	5.52693	5.52433	-0.047	5.52355	-0.061	5.52549	-0.026	5.52460	-0.042
7	6.34223	6.33806	-0.066	6.33836	-0.061	6.34034	-0.030	6.33918	-0.048

Table 6.18 – Natural frequencies (in Hz) associated with damage scenarios D1, D2, D3 and D4 (50% of damage intensity) compared with the numerical reference values (Ref) with a water level of 234 m

		D1		D2		D3		D4	
Mode	Ref	Freq [Hz]	Δ Freq. [%]	Freq [Hz]	Δ Freq. [%]	Freq [Hz]	Δ Freq. [%]	Freq [Hz]	Δ Freq. [%]
1	2.45372	2.42677	-1.098	2.45147	-0.092	2.43333	-0.831	2.43773	-0.652
2	2.68436	2.67441	-0.371	2.67476	-0.358	2.67128	-0.487	2.66941	-0.557
3	3.58254	3.57904	-0.098	3.55280	-0.830	3.57845	-0.114	3.56818	-0.401
4	4.05438	4.03907	-0.378	4.03449	-0.491	4.04641	-0.197	4.04002	-0.354
5	4.84020	4.81165	-0.590	4.81732	-0.473	4.82077	-0.401	4.82318	-0.352
6	5.52693	5.51091	-0.290	5.50577	-0.383	5.51818	-0.158	5.50735	-0.354
7	6.34223	6.31616	-0.411	6.31771	-0.387	6.32875	-0.213	6.31623	-0.410

The introduction of damages in the experimental data was based on the presented relative reductions of natural frequencies (Δ Freq.). It was assumed that each damage scenario occurred on the 1st of December of 2017, so the natural frequency estimates obtained from data measured after this date were automatically multiplied by the coefficient 1+(Δ freq.)/100, where Δ Freq. assumes the values presented in Table 6.17 and in Table 6.18, when the water level is 234 m. However, since the frequency variations due to the simulation of damages obtained with the numerical model are dependent on water level, instead of fixed frequency reductions, the Δ Freq. considered to insert the damage in each natural frequency estimate was a function of the water level verified during the 30-minute time series of acceleration used to identify such natural frequency estimate. In this sense, for each vibration mode, the damage introduced is not the same during the studied period, so the frequency reduction introduced varies in time, both in percentage of the mode natural frequency and in absolute value in Hz.

6.8.2. Application of Implemented Tools

After the introduction of the damages presented in the previous section in the data obtained from the continuous monitoring, through (water level dependent) frequency reductions, the ability of control charts to detect the presence of such damages is tested. In section 6.7 two baseline control charts were defined, based on the application of the MLR+PCA and PCA2 procedures to mitigate the effects of operational and environmental conditions on natural frequencies. Since the results obtained with the control charts after the application of the PCA2 procedure showed a much stronger ability to detect damage, when compared to the control charts obtained after the application of the MLR+PCA procedure, only the first (PCA2) are analysed in the present section.

In Figure 6.41 a) ("No Damage") the T^2 calculated between 01/12/2016 and 31/05/2019, without considering any type of damage, are represented. The reference period (from 01/12/2016 to 30/11/2017) is represented in blue and the control period (from 01/12/2017 to 31/05/2019) is represented in orange. Only a few isolated outliers can be found above the UCL, marked with a red horizontal line. The same is verified during the control period (before damage is considered), proving the model does not produce false identifications of damage, if the existence of damage is only considered after the occurrence of a few consecutive points above the UCL. Since averages of 96 elements were adopted, new points resulting from the collection of new data are only marked in the control charts every two days.

Besides the undamaged situation mentioned before, Figure 6.41 presents as well three control charts related with the detection of damage, more specifically, in Figure 6.41 b), c) and d) the control charts obtained considering damage scenario D3 with 10, 30 and 50 % of stiffness reduction are respectively presented. The introduction of damages clearly leads to higher values of T^2, which subsequently increase with the intensity of the damage introduced. In the case of 50 % of stiffness reduction, almost the entire set of T^2 values obtained after the introduction of damage are found above the UCL, thus damage would be unequivocally detected only a few days after its occurrence. Though it was not represented, the same is verified with damage intensities of 70 and 90 %, only with even higher T^2 values. A similar situation occurs with the scenario of 30 % of stiffness reduction, which presents the majority of T^2 values clearly above the UCL. Once again, damage would be detected soon after its occurrence, using the rule of assuming damage existence only after a few consecutive points (5 or more) are found above the UCL.

On the other hand, with the 10 % of stiffness reduction scenario, the most challenging one for the detection algorithms, though a few points are found above the UC, the average T^2 value increased only marginally and the majority of points is found below the UCL and never during the entire test period is it possible to find 5 consecutive points above the UCL In this sense, it would not be possible to detect damage D3 with such low intensity, even if evaluated for several weeks. Although damage D3 seems to be the hardest one to identify for very low damage intensities, similar difficulties occur on the identification of the novel behaviour introduced with the other types of damage simulated when so low intensities (10 %) are considered, as it will be shown later.

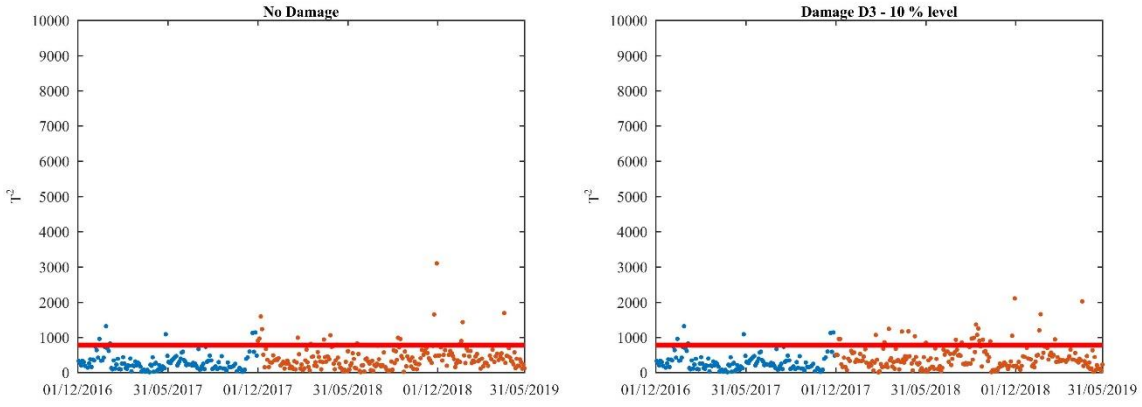

a) b)

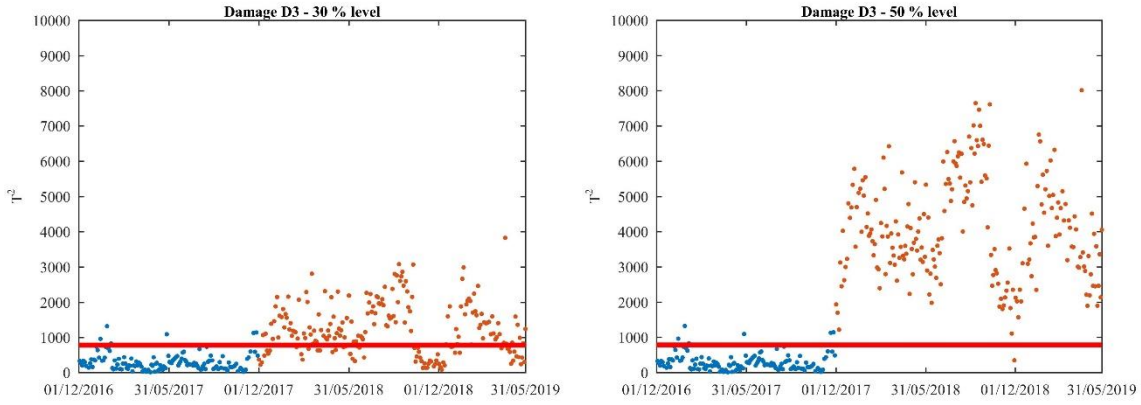

c) d)

Figure 6.41 – Damage scenario D3: from 0 to 50 % of stiffness reduction.

This analysis of the ability of the presented methodology to detect the same type of damage with different intensities was repeated with the other three damage scenarios. Similar results were obtained, thus the four control charts with the 50 % of stiffness reduction for the four damage scenarios were represented in Figure 6.42. This damage intensity was chosen to be represented since it corresponds to the intermediate intensity considered in the simulations, though in the majority of the studied cases damages can be unequivocally detected just a few days after its occurrence even for 30 % intensities. In turn, as it was said before, damages resulting from 10 % of stiffness reduction may require several weeks, or even a few months to be detected. On the other hand, damages resulting from 70 % of stiffness reduction, or higher, could be easily detected a few days after its occurrence as well, using this methodology, or even just one day after its occurrence, using averages with just 6 points.

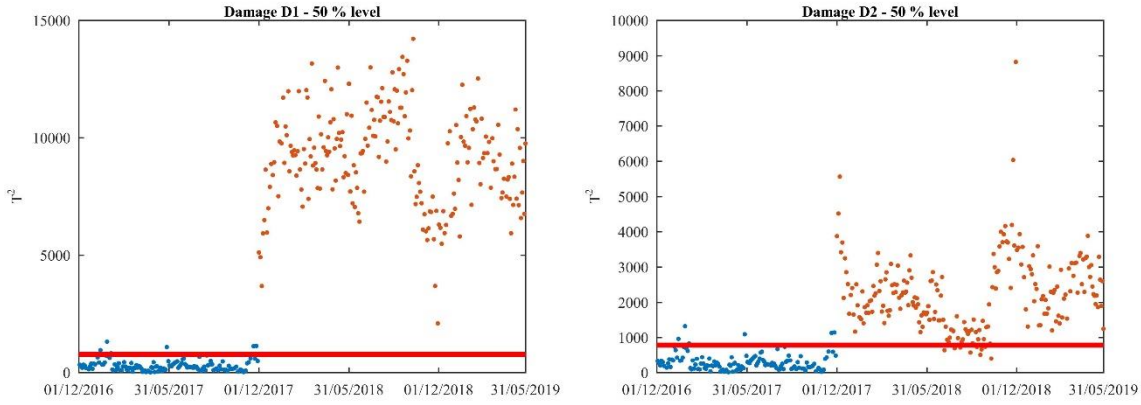

a) b)

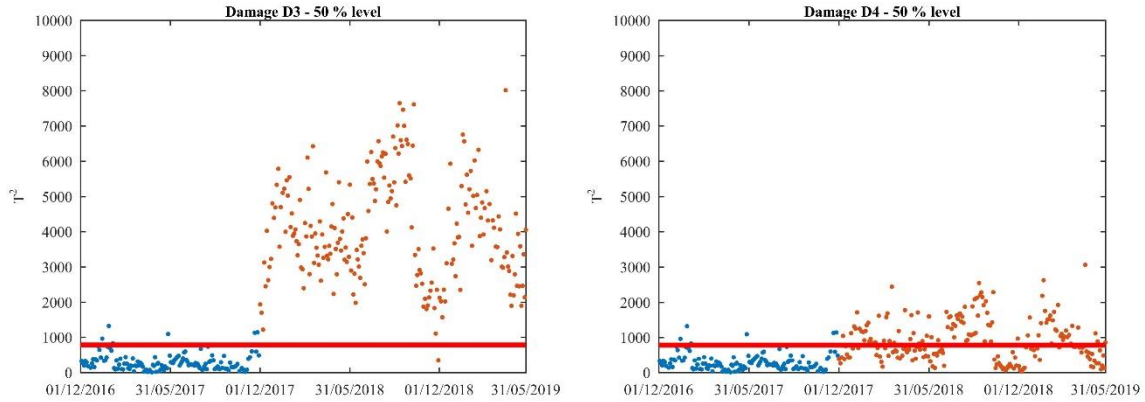

c) d)

Figure 6.42 – Location, extent and type of simulated damage scenarios.

Some tendencies are observable in the control charts, probably due to the correlation between natural frequencies and the frequency reduction introduced with damages, which results from the dependency of frequency reductions on water level variation.

The indexes used in section 6.7 to evaluate the quality of control charts were used once again, this time to help in the detection of damage. The value of each index is presented in Table 6.19 for the different damage scenarios and damage intensities. The baseline indexes relative to the undamaged situation are presented in the top of the table for comparison. After the visual inspection presented before, these indexes provide an important tool to quantify the ability of the charts to detect each type of damage simulated.

For 10 % of damage intensity similar results are obtained for the four types of damages, with just one alert, or no alerts at all, during the entire control period and J_R values close to the undamaged situation. Only through a continuous evaluation of the number of outliers during the control period, which rises to values from 12 to 19 %, could one suspect about the presence of damage. The 30 % of damage intensity scenarios, on the other hand, can be clearly identified with damages D1, D2 and D3, which present more than 50 alerts and more than 50 % of outliers during the control period. In the case of damage D4, however, though the J_R value rises to 1.76 and the number of outliers to 21 %, only a few alerts are verified during the entire control period, therefore, the 50 % intensity scenario would be needed to produce consecutive alerts.

For higher damage intensities, more than 90 % of outliers are found through the whole set of simulated damages and alerts would occur consecutively, almost every two days.

Table 6.19 – Damage detection: indexes obtained for the control charts with groups of 96 elements, after the introduction of the 4 simulated damages scenarios with different damage intensities

Damage Scenario	J_R	Out_{ref} [%]	$Out_{control}$ [%]	$Alert_{ref}$	$Alert_{control}$
No Damage	1.37	5.04	8.37	0	0
D1 - 10 % level	1.74	5.04	19.1	0	1
D1 - 30 % level	9.05	5.04	97.2	0	196
D1 - 50 % level	31.1	5.04	100	0	211
D2 - 10 % level	1.65	5.04	13.5	0	1
D2 - 30 % level	3.20	5.04	54.9	0	53
D2 - 50 % level	4.54	5.04	94.9	0	173
D2 - 70 % level	18.6	5.04	100	0	211
D3 - 10 % level	1.42	5.04	12.1	0	0
D3 - 30 % level	4.22	5.04	66.8	0	88
D3 - 50 % level	13.8	5.04	99.5	0	206
D3 - 70 % level	38.6	5.04	100	0	211
D4 - 10 % level	1.74	5.04	19.1	0	1
D4 - 30 % level	1.76	5.04	21.9	0	7
D4 - 50 % level	3.12	5.04	52.1	0	60
D4 - 70 % level	10.9	5.04	99.1	0	204
D4 - 90 % level	136	5.04	100	0	211

Finally, it is important to mention the aptitude of the monitoring system to detect novel structural behaviour is directly connected with the amount of data collected during the reference period. Therefore, although this damage detection system could probably have been constructed successfully with shorter periods of monitoring, in particular, the ones used to build the regression models and the control charts references, it is expected that the larger the history of data acquired the higher the accuracy of the model. In this sense, the accuracy of the damage detection system is presumed to improve with the new data being collected.

Additionally, it is worth mention as well that the main purpose of monitoring and damage detection systems, such as the one presented, is to detect abnormal behaviour in early stages, so that maintenance or retrofitting operations can be adequately studied and planned, thus it is not relevant that damages simulated and tested in this section can only be detected a few days after its occurrence. On the contrary, these timings are perfectly adequate for the detection of small early stage damages. Furthermore, as it was previously mentioned, high-intensity damages capable of considerably affecting the structures safety condition can be detected in less than a day.

6.9. FINAL CONSIDERATIONS

This chapter started with the description of Baixo Sabor arch dam and the forced vibration test performed by the Concrete Dams Department of the Portuguese National Laboratory for Civil Engineering (LNEC) in the structure, which was used to calibrate the numerical model of the dam, developed by LNEC as well. Both the forced vibration test and the numerical model were used to study the dam's dynamic behaviour and thus essential to design the dynamic monitoring system that was then installed in the structure for continuous monitoring.

After this, the dynamic monitoring system installed in the dam was presented, including its architecture and the disposition of the accelerometers in the dam. The system has been functioning properly, being able to characterize both very low vibrations levels (in the order of micro g) and high vibration levels provoked by small earthquakes, water discharges or forced vibration tests. The main source of vibrations in the structure comes from the rotation of the electricity production turbines, in the nearby power plant. The reduced number of lost setups after the initial period that succeeded the installation demonstrates the robustness and reliability of the monitoring system.

Using the time series of accelerations recorded by the monitoring system during its first day of monitoring and the SSI-Cov method, the dams modal properties were identified, namely the natural frequencies, damping ratios and mode shapes of the first 10 vibrations modes. The modal properties identified were in total accordance with the results provided by the numerical model and the forced vibration test. The natural frequencies of the 10 modes can be found between 2 and 10 Hz, and their damping ratios present values between 1 and 2 %. The turbines rotation frequency and its harmonics pollute the measured data, being commonly and easily identified. The tools implemented for automatic operational modal analysis, described in chapter 5, were then used to continuously identify the modal properties from the data collected by the monitoring system.

The dams first 10 vibration modes, whose modal properties had been identified, have been successfully tracked during full three years of monitoring. This period included the first filling of the dam's reservoir, which makes this application the first to continuously record the dynamic behaviour of a concrete dam during its first filling, to the best of the author's knowledge. The values of natural frequencies presented high variability during the monitoring period, thus moving references have been used within the tracking algorithms to improve the quality of the tracking and decrease the number of misidentifications. With the exception of the first vibration mode, the

number of missing values generally increased with the modal order, from 3 % in the second mode to 50 % in the tenth.

The uncertainty associated with each natural frequency and damping ratio identified was ascertained, using a modified version of the SSI-Cov method. The evolution of this uncertainties was studied along with the evolution of modal properties. Afterwards, the uncertainty values were used to improve the quality of the modal tracking once again, through the elimination of the poles resulting from the SSI-Cov method that were associated with high uncertainty, on the one hand, and through the minimization of misidentifications related to the turbine rotation frequency and harmonics, on the other.

The study of the evolution of the structure modal properties unveiled a straight inverse relation between natural frequencies and the level of water in the reservoir, which is due to the enormous amount of mass that is added to the system dam-reservoir. This effect overlaps the increase in stiffness due to the dam's contraction joints closing when the weight of the water grows, which should lead to a decrease in natural frequency values. The effect of both seasonal and daily air temperature variations on natural frequencies was studied as well. While in most modes only the seasonal variations seem to produce detectable shifts in natural frequencies, modes 6 and 7 seem to be meaningfully affected by air temperature on a daily basis also, which is clearer during summer, when daily temperature amplitudes are greater.

After the study of the influence of environmental and operational effects on natural frequencies, multiple linear regression models aiming to explain the observed variations were built. For this, reservoir water level, air temperature, concrete temperature and concrete hardening were the factors used to define the variables adopted as predictors. The effect of using the uncertainties associated with natural frequencies estimates as weights in regression models was tested with positive results. The selected regression models (one per mode) permitted to largely minimize the effects of environmental and operational factors on the values of natural frequencies, opening the possibility of identifying small frequency shifts due to abnormal occurrences.

However, it was demonstrated that using residuals from the difference between natural frequency estimates and predicted natural frequencies obtained from the regression models did not produce stable control charts that could be used for damage detection. In this sense, principal components analysis was used as well in the mitigation of operational and environmental effects, both in combination with multiple regression models and by direct application to natural frequency

estimates. Six models were tested and the two that produced stable control charts and guaranteed no false identifications would occur, were chosen to be used for damage detection.

The numerical model of the dam developed by LNEC was used to simulate damages that may occur in the dam after strong earthquakes or as the result of long term material deterioration through ageing and chemical processes. These simulations allowed to ascertain the intensity of the frequency shifts that would be verified in the dam if such damages occurred. For a broad analysis, different damage intensities and different water levels were tested. Afterwards, data from the continuous monitoring was polluted with these frequency shifts and the control charts previously built were used to try to detect such damages. In the end, it was demonstrated that the construction of control charts with residuals from the application of principal components analysis allows the detection of small frequency shifts due to the numerically simulated damage scenarios. Furthermore, the time needed to detect the damage is inversely proportional to the damage extent.

Concluding, it was demonstrated that a dynamic monitoring system like the one installed at Baixo Sabor arch dam allows not only to better understand the dynamic behaviour of concrete arch dams and accurately calibrate numerical models, but also to closely monitor the instrumented structure, preventing the proliferation of small damages through the detection of abnormal structural behaviour, guaranteeing timely maintenance procedures and thus prolonging the structure life span with high safety standards.

7. CONTINUOUS DYNAMIC MONITORING OF FOZ TUA DAM

7.1. INTRODUCTION

The continuous dynamic monitoring of Foz Tua dam is being carried out by the Laboratory of Vibrations and Structural Monitoring (ViBest) of the Faculty of Engineering of the University of Porto (FEUP) and by the Department of Dams of the National Laboratory of Civil Engineering (LNEC), in the scope of the research project (DAM_AGE, 2016-2018), in order to identify the dam dynamic characteristics and their evolution over time, taking into account the variation of ambient and operational conditions, as well as the possible evolution of the materials mechanical properties.

In this chapter, Foz Tua arch dam and the dynamic monitoring system installed in the structure are introduced. The data obtained during the first year of continuous monitoring, between 08/12/2017 and 07/12/2018, is presented afterwards. First, the vibration levels measured with the dynamic monitoring system are characterized. Then, the dam's first six vibration modes are identified using the SSI-Cov method and the natural frequencies, damping ratios and mode shapes obtained with the time-series recorded during the first day of monitoring are presented.

Finally, automatic operational modal analysis is used to track the dam's modal properties during the first year of continuous monitoring, and the influence of operational and environmental effects on natural frequencies and damping ratios is studied. Since the main goal of this application is to test the modal tracking tools with a second example, the study developed about Foz Tua dam is not as extended as the one presented for Baixo Sabor dam.

7.2. DESCRIPTION OF THE STRUCTURE AND THE MONITORING SYSTEM

The Foz Tua hydroelectric complex is located in the north of Portugal at the mouth of the Tua river, a tributary of the Douro river, between the municipalities of Alijó and Carrazeda de Ansiães. The power plant, located in the right bank of the river, is equipped with 270 MW of power capacity, making it a very important asset in the country's energy production capacity. Its 27 km long reservoir, with 106 million cubic meters of capacity, is accomplished through a 108 m high concrete arch dam (Tua, 2016) whose construction was concluded by the end of 2016. The complex is equipped with a pumping system that allows recovering water from downstream, contributing to optimize the hydroelectricity production managing of the Douro basin.

The structure corresponds to a concrete double-curvature arch dam, embedded in a narrow valley zone. The 275 m long arch (crest length) is composed by concrete 18 blocks, separated by vertical contraction joints, and includes visit galleries at six different levels, besides the general gallery for drainage. The full storage level is at 172 m. Figure 7.1 shows pictures of the dam and its reservoir taken from downstream, from above and from upstream, referring to November 2016, right before the start of the exploration period.

Figure 7.1 – Foz Tua arch dam (EDP).

To ensure a good characterization of the dynamic behaviour of the dam, the arch dam has been equipped with a vibration-based structural health monitoring system. This equipment is composed by a set of 12 accelerometers that were radially disposed along the two upper visit galleries, 4 in the upper visit gallery (GV1), being half of them on each side of the dam spillway gates, and the other 8 accelerometers in the second visit gallery (GV2). All the accelerometers are connected to a set of digitizers, and the synchronization of the data is assured by GPS and ethernet connections. The system is continuously recording data with a sampling rate of 50 Hz, and every 30 minutes a data file is compiled and saved, thus 48 data files are obtained every day.

Figure 7.2 characterizes the position of the accelerometers, marked in blue in a scheme of the dam. There is one more accelerometer on the left side of the structure, following the dam geometry, which is not entirely symmetric.

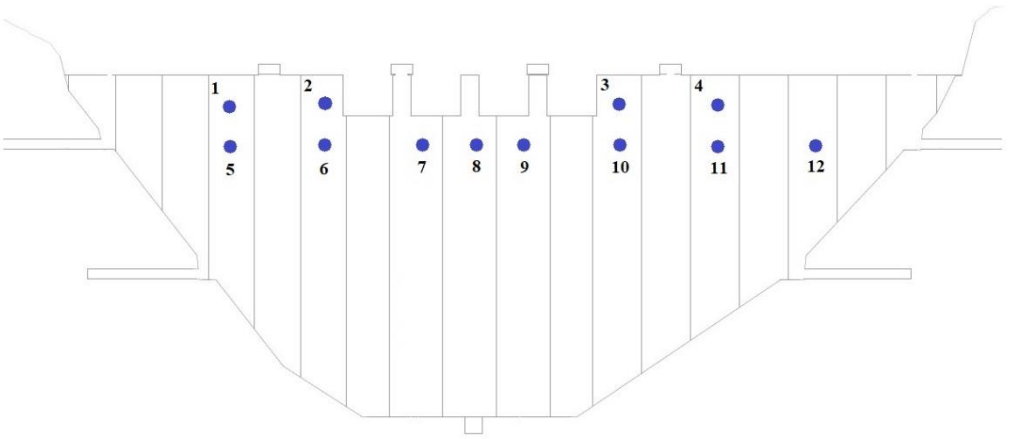

Figure 7.2 – Distribution of the accelerometers in the scheme of Foz Tua dam.

7.3. CONTINUOUS DYNAMIC MONITORING

The Foz Tua dam continuous dynamic monitoring system is configured to record time series of accelerations with a duration of 30 minutes at all instrumented points, which is an adequate duration for the application of the techniques used in their processing, even though this can be adjusted if necessary. The recorded samples are pre-processed, which includes the conversion to engineering units, the elimination of offsets, the application of an eighth-order low-pass Butterworth filter (Mathworks, 2016) and re-sampling with a frequency of 25 Hz. After this step, the automatic processing performed evaluates each 30 minutes data set individually in order to obtain modal parameters and features characterizing the vibration levels. Every day 48 values are obtained for each parameter.

In the next few sections, the dam's vibration levels are evaluated and its modal properties are identified, and tracked over the first year of continuous monitoring.

7.3.1. CHARACTERIZATION OF VIBRATION LEVELS

During the monitoring period the dam has been subjected only to ambient vibration, that is, no excitation was purposely induced in the structure with the intention of performing modal identification. In this sense, the vibrations in the structure were caused solely by the conditions in the surrounding natural environment, such as the wind, small seismicity or nearby road traffic, among others, and by the normal operation of the hydroelectric plant underlying the dam. In the specific case of the power plant, besides everyday human activities the main source of excitation would come from the energy production circuit, therefore it is expected to find the turbine rotation frequency (185.5 r.p.m.) as a predominant frequency in the measured time series.

For each time series of 30 minutes the maximum acceleration measured by each sensor and the root mean square (RMS) of its accelerations during this period were respectively identified and calculated, allowing to characterize the intensity of the measured vibrations. Even though this processing was performed for the entire monitoring period, the representation of its evolution over time, presented in Figure 7.3, comprehends just a two months period between January 20th and March 20th, in order achieve a clearer figure, which can be more easily analysed. Each of the 10 measuring channels is represented by a different colour and short periods with no data refer to situations of system failure or maintenance.

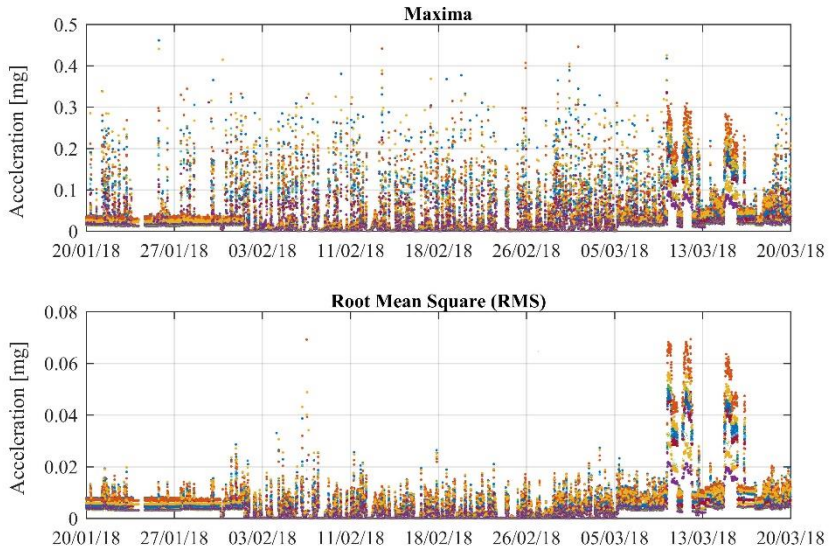

Figure 7.3 – Maxima and effective values (RMS) evolution between 20/01/2018 and 20/03/2018.

The top and the bottom parts of Figure 7.3 complement each other. While the information about the maximum accelerations measured by each sensor enables the verification of the suitability of the monitoring system to the studied application, as well as to check for abnormal activity around the sensors or any malfunction, the root mean square values give the analyst a more precise view on the general vibration level of the structure during each recorded period.

The analysis of the evolution of the RMS presented in Figure 7.3 suggests that the operational conditions may be divided in three different stages:

a) From January 20th to the end of January (left part of the figure) medium to high vibration levels are obtained, with clear and constant differentiation of the accelerations measured on each sensor, indicating an uninterrupted operation of the energy production system;

b) From February 3th to March 5th (central part of the figure) much lower vibration levels are recorded along with sparsely distributed higher accelerations, suggesting pure ambient vibration as the main source of structural excitation, occasionally complemented with excitation from the operation of the energy production system;

c) Around March 13th (right part of the figure) very high vibration levels are continuously measured during short periods. This massive source of energy probably corresponds to the opening of the dam's spillway gates, during periods of intense rains and consequent flood.

A zoom on the transition from the operational conditions described in a) to the conditions described in b) is presented in Figure 7.4. It is clear that the vibration levels variation largely depends on the operational situation. The RMS of the measured accelerations decrease from a few micro *g* to 10 times smaller intensities when the turbines stop operating. Additionally, the dominance of the excitation coming from the energy production system becomes obvious when considering that an almost constant acceleration intensity is registered by each sensor during a period of many consecutive days, implying the same vibration source is present.

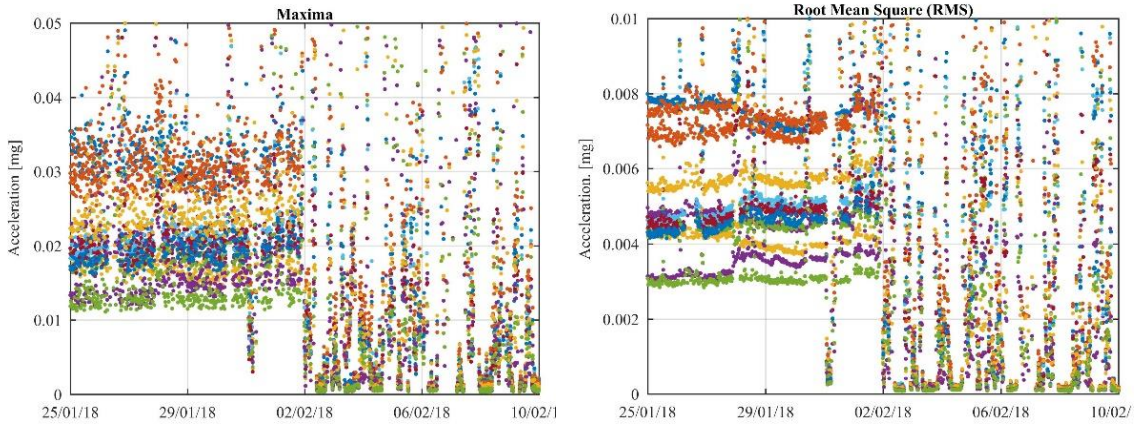

Figure 7.4 – Maxima and effective values (RMS) evolution between 25/01/2018 and 10/02/2018.

7.3.2. MODAL PARAMETERS IDENTIFICATION

From the time series of accelerations modal parameters estimates can be obtained, using state of the art identification methods such as those presented in chapter 3. Different analysis stages require different approaches; in particular, when starting to analyse a set of data, it is important to apply simpler methods that provide preliminary results, solid enough to allow preparing other deeper and more detailed analysis.

A straightforward methodology to identify different vibration modes and get rough estimates of natural frequencies, allowing as well to perform a simple evaluation of its evolution over time, consists on the application of the singular value decomposition to the spectra matrix estimated from each acceleration dataset. The assembly of each dataset first singular value allows the construction of a colour map such as the one shown in Figure 7.5. Colours are a function of intensity, with warm colours (red) associated with higher values. The red zones indicate the existence of more energy in the frequency bands to which they are associated, thus providing approximate estimates of the

natural frequencies of the structure and the harmonics present in the excitation motivated by the operation of the energy production turbines.

Figure 7.5 is related to the first 10 days of continuous dynamic monitoring, between 08/12/2017 and 18/01/2018. There are two evident horizontal red alignments, very close to each other, between 2 and 4 Hz, which probably correspond to the dam's first two vibration modes, and two more red alignments between 4 and 6 Hz, potentially indicating the third and fourth vibration modes. A few other alignments seem to exist between 6 and 10 Hz, however they present considerable frequency variations during the analysed period, not being possible with this preliminary analysis to distinctly identify how many vibration modes would be hidden in this blurred interval of frequencies. Additionally, very well-defined dark red horizontal lines appear occasionally between the first two alignments and near the top of the figure, probably corresponding to the turbine rotation frequency (185.5 r.p.m. – 3.09 Hz) and its second harmonic (9.27 Hz).

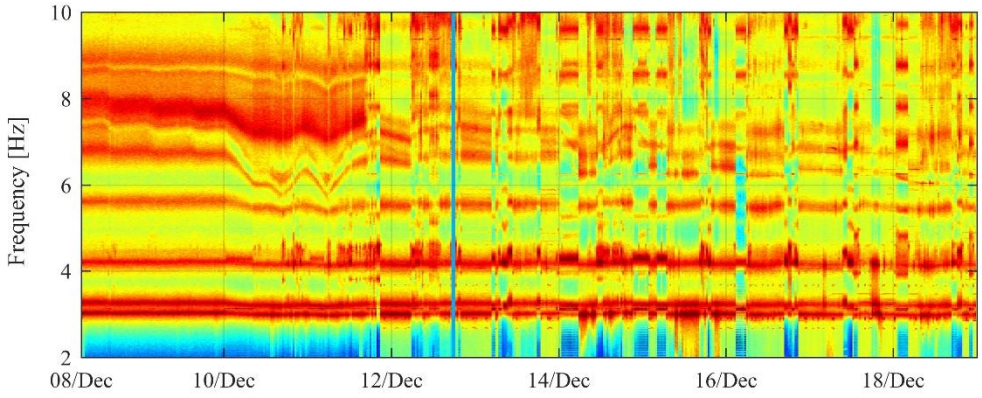

Figure 7.5 – Colour map with the frequency evolution between 08/12/2017 and 18/12/2017.

After this first analysis, a modal identification was performed using the SSI-Cov method. The first six modes of vibration were identified from time series recorded in December 8th, the first day of monitoring, and natural frequencies, damping values and modal configurations were obtained. A two-dimensional representation of the modal configurations is presented in Figure 7.6. The modal ordinates obtained from the modal identification are represented with blue dots and the full modal configuration was obtained using interpolations. Only sensors between number 5 and number 11 (see Figure 7.2) were used in this representation to facilitate the distinction between symmetrical and anti-symmetrical shapes, and all the obtained configurations are clear and unequivocal. The first, fourth and sixth modes are approximately anti-symmetrical and the second, third, and fifth are approximately symmetrical modes of vibration.

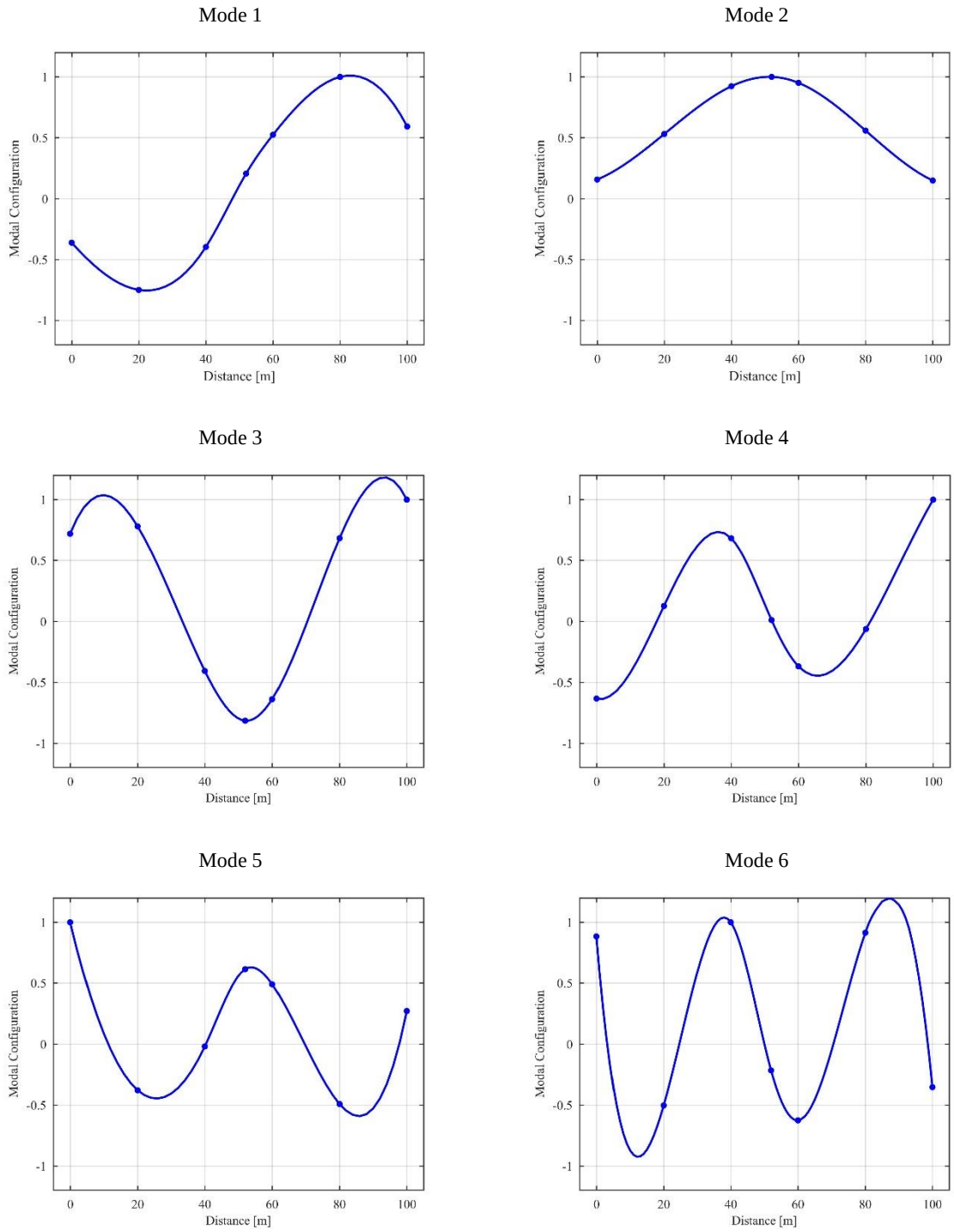

Figure 7.6 – Modal configuration of the first six modes of Foz Tua arch dam.

The natural frequencies and damping ratios obtained for the first six modes with the time series measured during December 8th are resumed on Table 7.1, along with the description of their mode shape, presented before. The identified natural frequencies fit in the intervals defined through the

evaluation of the colour map, demonstrating the relevance of this simple tool in preliminary analysis. Additionally, the damping ratios of the six modes present values between 1 and 2 %, which is common for this type of structure.

The identification of other modes, even though possible, is conditioned by the number of sensors available in the same horizontal alignment (GV2), making it harder to correctly identify the mode shape of superior mode orders.

Table 7.1 – Modal parameters for Foz Tua dam first six modes

Mode	Frequency [Hz]	Damping ratio [%]	Description
1	3.03	0.95	Antisymmetric
2	3.26	1.47	Symmetric
3	4.19	1.37	Symmetric
4	5.61	1.36	Antisymmetric
5	6.72	1.98	Symmetric
6	7.32	1.12	Antisymmetric

7.3.3. MODAL PROPERTIES EVOLUTION

To better understand the dynamic behaviour of a structure it is important to study the way its modal properties vary over time. In this sense, the SSI-Cov method was applied to the entire set of data recorded during the first year of monitoring, from December 8th to December 7th and a routine based on cluster analysis, introduced in chapter 5 and applied as well in chapter 6, was used to automatically identify the structure's first vibration modes. The automatic identification relies in the comparison between the whole set of modal properties identified by the SSI-Cov method and a set of reference modal properties corresponding to the dam's vibration modes. For this, in a first stage fix reference natural frequencies were used, associated with intervals between which it is expected for the modes natural frequencies to oscillate. In the great majority of applications, this procedure grants excellent results with high identification rates. However, in the case of Foz Tua dam, unusually high frequency variations occur in the matter of just a few hours, which leads to target frequency intervals superposition and hinders the modal tracking process. These unusual frequency variations are made clear in Figure 7.7, where the whole set of natural frequency estimates identified with the SSI-Cov method (before modal tracking) during the first four days of monitoring is presented. Even with just four days of monitoring, alignments of points corresponding to the evolution of vibration modes natural frequencies are easily found. Nevertheless, while the

values of the first four modes natural frequencies are quite stable during this small period (around 3.00 Hz, 3.25 Hz, 4.20 Hz and 5.50 Hz), in the case of the fifth and sixth modes large variations of about 1.0 Hz are verified, (see inside the red circle in Figure 7.7). Additionally, when the Modal Assurance Criterion (MAC) between the identified and the reference mode shapes of the fifth and sixth modes is low, it is possible for one of these modes to be mistakenly identified as the other.

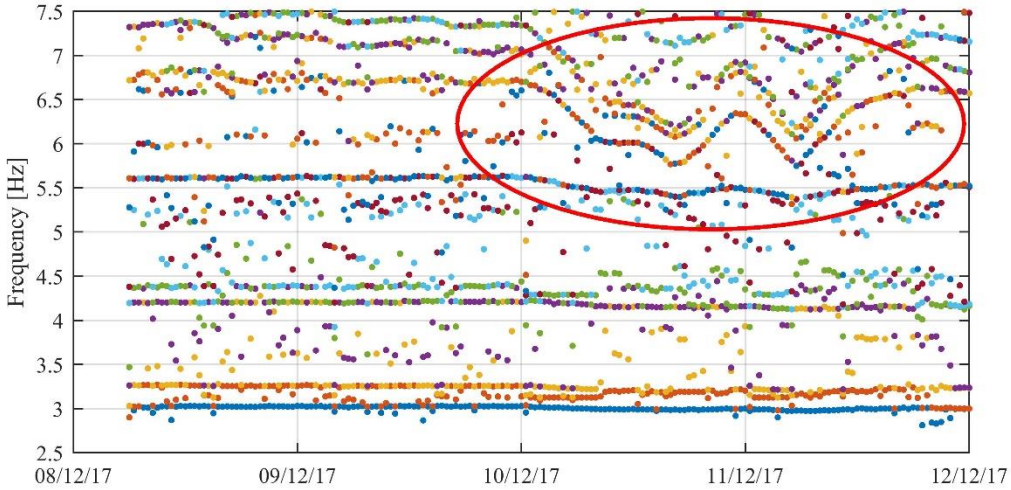

Figure 7.7 – Whole set of natural frequency estimates identified with the SSI-Cov method (before modal tracking) during the first four days of monitoring.

In this sense, to properly track the natural frequency of the dam's fifth mode and reduce the number of misidentifications, a moving reference is needed. However, to choose a rule suitable to define the evolution of such moving reference it is indispensable to understand why natural frequencies vary in such a way. Taking in consideration the monitoring of Baixo Sabor arch dam and the study of the operational and environmental conditions affecting the dam dynamic behaviour (Pereira et al., 2018), the evolution of the tracked natural frequencies during the first four days of monitoring of Foz Tua dam were represented in Figure 7.8 a), side by side with the evolution of the dam's reservoir water level during the same period (Figure 7.8 b)). It is clear that an inverse relation exists between natural frequencies and water level, as it was expected, since the rising of water in the reservoir consists in an addition of mass to the "dam-reservoir" system, which leads to a decrease in the values of natural frequencies. Though the frequencies of all the vibration modes are affected by the evolution of water level, the fifth mode natural frequency is much more affected. Even so, in the case of the fourth mode the effect of water level is clear as well, even without zooming to its evolution.

Taking this relation in consideration, the values of the fifth mode natural frequency were represented as a function of the reservoir water level, which is presented in Figure 7.8 c). A quadratic curve was almost perfectly fitted between the two with a very high coefficient of determination of about 0.99.

This curve was then used in the modal tracking process to predict the fifth mode natural frequency, transforming reservoir water level measurements into frequency estimates that are then used as references. Since the reference used to track the fifth mode is now dependent of the value of water level and for each water measurement there is a correspondent frequency estimate, a moving reference is obtained.

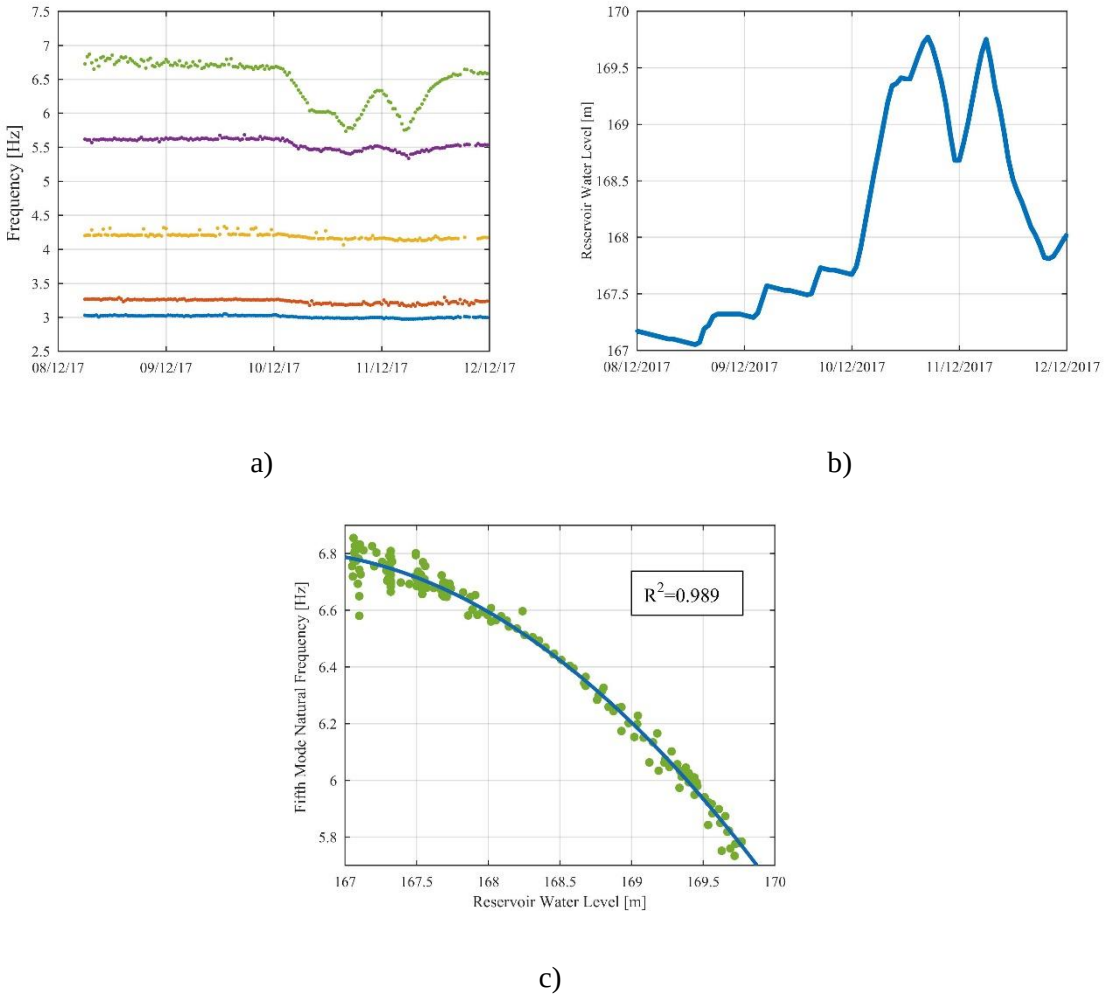

Figure 7.8 – a) Four-day zoom of natural frequencies evolution; b) Four-day zoom of reservoir water level evolution; c) relation between water level and the fifth mode natural frequency.

Moreover, the modal tracking was applied to the entire set of preprocessed data, using fixed frequency references for modes between the first and the fourth, and the previously mentioned moving reference in the case of the fifth mode. The first five vibration modes were successfully identified in more than 80 % of the datasets, with the first two vibration modes being identified in more than 95 % of the available datasets. In order to achieve clear data representation, the evolution of the first five vibration modes natural frequencies is presented in Figure 7.9 using a different colour for each mode and 12-hour moving averages. In turn, the evolution of the level of water in the reservoir is presented in Figure 7.10. During this period, the water level varied between 167 and 170 m, remaining quite stable over time, taking into consideration the total height of the dam. The inverse relation between water level and natural frequencies becomes clear by observing the figures together.

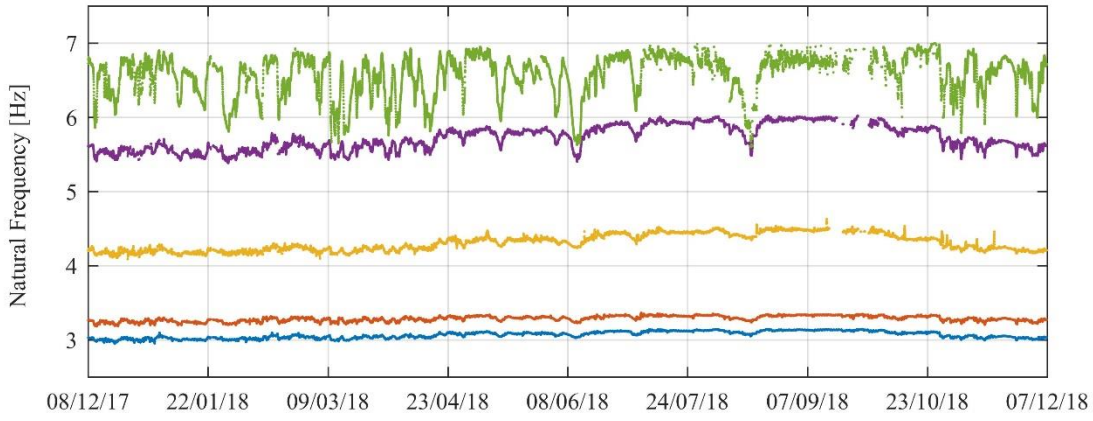

Figure 7.9 – Time evolution of 12-hour moving average of natural frequencies (from 08/12/2017 to 07/12/2018).

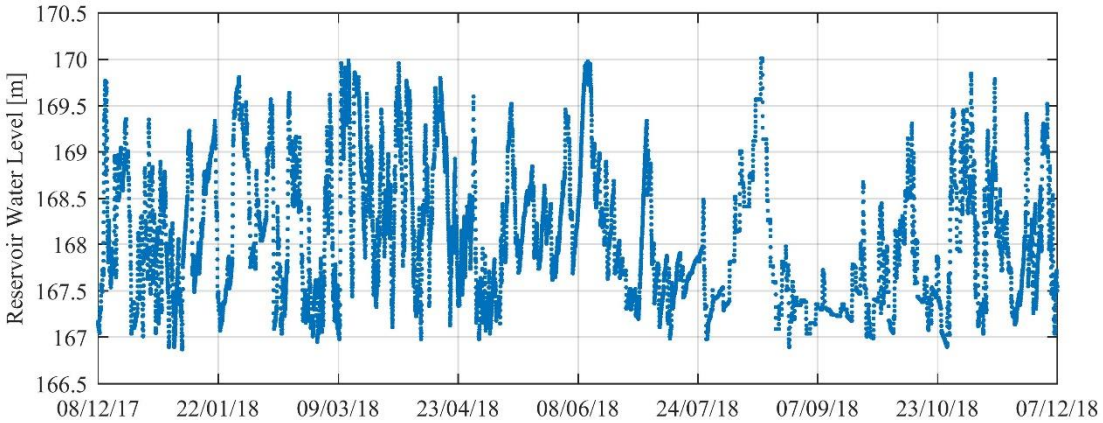

Figure 7.10 – Time evolution of reservoir water level (from 08/12/2017 to 07/12/2018).

A zoom in the evolution of the natural frequencies of the first two vibration modes is presented in Figure 7.11. The general variations presented by the frequencies of these two modes seems to be in accordance with the variation patterns that follow the evolution of water level, but higher natural frequency values are found during the summer, when compared to those verified during winter months, while water level keeps varying between 167 and 170m during the entire year. More specifically, the average value of the first mode natural frequency between December 2017 and January 2018 is around 3.0 Hz, while the average between August and September 2018 is about 3.15 Hz, indicating the existence of a second major source of data variability affecting the structure, which is probably related with temperature.

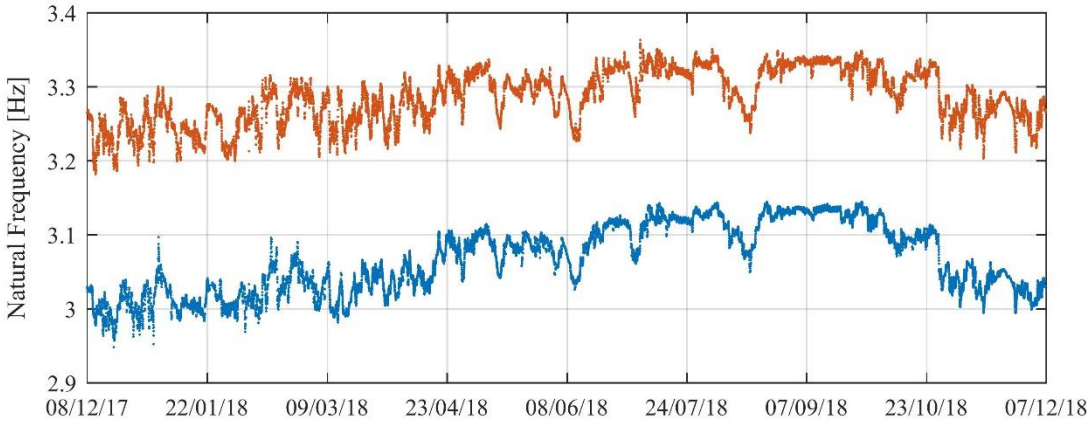

Figure 7.11 – Time evolution of 12-hour moving average of natural frequencies: zooming the first two modes.

Damping ratios were tracked as well, and the evolution of each modes damping ratios during the same period of analysis is presented independently for each mode in Figure 7.12, using 3-hour averages for clearer visualization. All the modes present a cloud of points that mostly lays between 1 and 2 %. While the evolution of the second and third modes damping ratios seem to be the most stable, in the case of the fifth mode wider variations are verified, in accordance with the fact that this mode natural frequencies are heavily affected by water level as well.

Nevertheless, in the cases of the first and fourth modes damping ratios, it is clear that generally higher values were identified during the winter months and lower values during the summer, indicating a strong influence of temperature in the evolution of these two modes damping ratios, even more important than the influence of reservoir water level. It is worth mention that both the first and fourth modes present modal configurations with antisymmetric shapes.

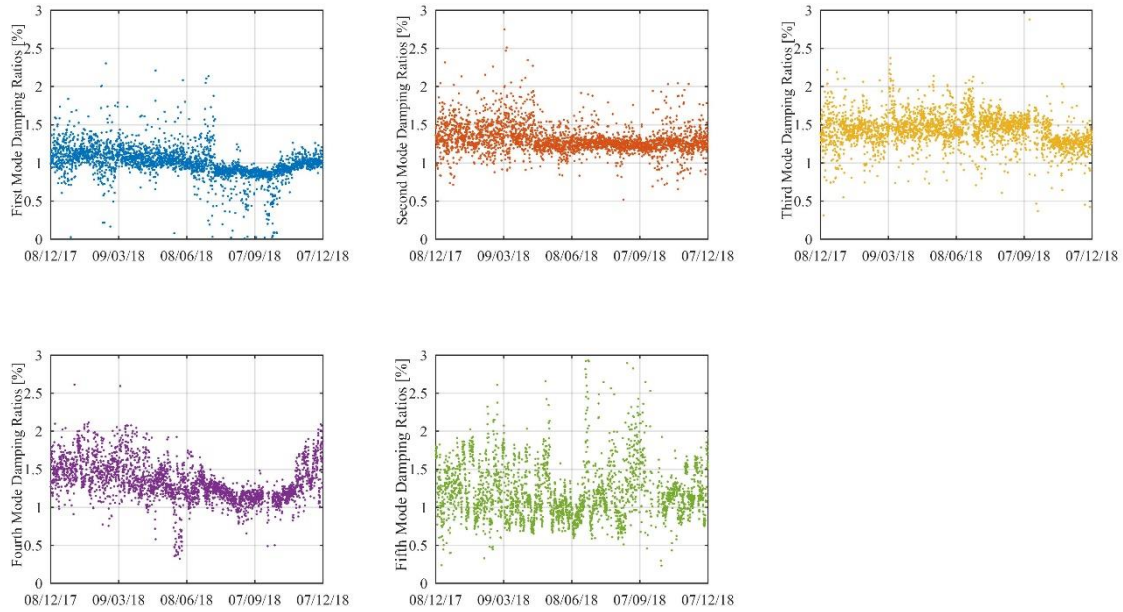

Figure 7.12 – Time evolution of damping ratios between 07/12/2017 and 08/12/2018.

Finally, a summary of the dam's modal properties is presented in Table 7.2, including the mean and standard deviation frequencies and damping ratios during the first year of monitoring, and minimum and maximum natural frequency values as well. Minimum and maximum damping ratios were not presented since, contrary to what happens during the tracking of natural frequencies, no limits are used in the tracking of damping ratios, besides the fact that all values must be positive, thus a few outliers with no significance are present in the identified data, which would misrepresent the true maximum and minimums.

It is worth mention that the fifth mode natural frequency varies between 5.5 and 7.0 Hz, even if the reservoir water level only varied about 3 m during the studied period. This very peculiar behaviour is going to be further studied.

Table 7.2 – Modal parameters averages for Foz Tua dam first five modes during the first year of continuous monitoring

Mode	$f_{[\text{Min}\,;\,\text{Max}]}$ [Hz]	f_{mean} [Hz]	f_{std} [Hz]	ξ_{mean} [%]	ξ_{std} [%]
1	[2.84 ; 3.24]	3.07	0.048	1.00	0.358
2	[3.09 ; 3.47]	3.29	0.040	1.30	0.336
3	[3.95 ; 4.72]	4.31	0.113	1.43	0.307
4	[5.22 ; 6.16]	5.73	0.166	1.33	0.316
5	[5.53 ; 7.00]	6.55	0.290	1.19	0.462

7.4. FINAL CONSIDERATIONS

This chapter started with the description of Foz Tua arch dam and the continuous dynamic monitoring system that was installed in the dam in December 2017 and has been working since then. The disposition of the accelerometers in the dam is constrained by the position of the main spillway gates, thus the bulk of the sensors (eight) are installed in the second visit gallery, while the other four accelerometers are disposed in the upper visit gallery, two on each side of the spillway.

The monitoring system worked properly during the first year of monitoring, being able to characterize both very low vibrations levels (in the order of micro g) and medium to high vibration levels provoked by the operation of the power production plant, small earthquakes and water discharges. The reduced number of lost setups during the first year of monitoring demonstrates the robustness and reliability of the monitoring system.

Using the time series of accelerations recorded by the monitoring system during its first day of monitoring and the SSI-Cov method, the dams modal properties were identified, namely the natural frequencies, damping ratios and mode shapes of the first six vibrations modes. The natural frequencies of the six modes can be found between 2 Hz and 8 Hz, and their damping ratios present values between 1 % and 2 %. The tools implemented for automatic operational modal analysis, which had been described in chapter 5, were then used to continuously identify the structures modal properties from the data collected by the monitoring system.

The dam's first five vibration modes, have been successfully tracked during this first year of monitoring with identification rates between 80 % and 95 %. The turbines rotation frequency (3.09 Hz) and its harmonics pollute the measured data whenever the power plant is operating, but no major influence in the number of misidentifications was detected due to this factor. The values of natural frequencies presented high variability during the monitoring period, thus moving references based on water level had to be used within the tracking algorithm for it to be able to track the dam's fifth mode, while the first four vibration modes were successfully tracked using fixed references. Due to the high variability presented by the sixth mode natural frequency, it was not possible to track this mode with successful identification rates. Therefore, improvements should be introduced in the tracking algorithms to correct its inability to properly track the dam's sixth vibration mode.

The study of the evolution of the structures modal properties unveiled a straight inverse relation between natural frequencies and the level of water in the reservoir. This effect overlaps the increase in stiffness due to the dam's contraction joints closing when the weight of the water grows, which

should lead to a increase in natural frequency values. The effect of seasonal temperature variations on natural frequencies, though not directly studied, was identified as well, through the fact that natural frequencies present higher average values during the summer, and lower average values during the winter, while the water level remains stable inside a 3 m variation range. The effects of water level and temperature on damping ratios were also characterized.

Concluding, the dynamic monitoring system installed at Foz Tua arch dam has been providing important data about the dynamic behaviour of this concrete arch dam that can be used to accurately calibrate numerical models, but also to closely monitor the instrumented structure. Since one year of monitoring has now been completed, the major operational and environmental factors affecting the structure's dynamic behaviour should be well characterized, thus it will be possible to create a damage detection procedure such as the one implemented in Baixo Sabor arch dam, preventing the proliferation of small damages through the detection of abnormal structural behaviour and guaranteeing timely maintenance procedures that should lead to the prolonging of the structure life span with high safety standards.

Finally, it is worth noting the relevance of this application, since the large frequency variations verified due to such small water level fluctuations represent a unique result and a remarkable challenge to the automatic modal tracking tools.

8. CONCLUSIONS AND FUTURE RESEARCH

8.1. CONCLUSIONS

This work mainly consisted in exploring the potential of operational modal analysis in the testing and monitoring of concrete dams. In this context, several processing tools were developed, implemented and applied in many field tests and two main case studies, allowing and efficient processing, and concluding in accurate results that were corroborated by previous tests or numerical models whenever available. The time-series recorded during both the ambient vibration tests and the continuous monitoring were transformed into features that can be correlated with other data from the structure and the environment, providing the owners with useful information, which can be delivered continuously and automatically.

The thesis started with an overview on dams and the particularities of the dam-foundation-reservoir system, and the solutions to numerically model it. Then, the work focused on operational modal analysis and four state-of-art identification techniques were described: Peak-Picking (PP); Enhanced Frequency Domain Decomposition (EFDD), Covariance driven Stochastic Subspace Identification (SSI-Cov) and poly-Least Squares Complex Frequency Domain (p-LSCF). The PP and SSI-Cov methods were then intensively used with the time-series collected at Alto Lindoso, Bouçã, Castelo do Bode, Caldeirão, Santa Luzia and Aguieira dams during the ambient vibration tests performed in these dams. The PP, because of its versatility and readiness, and the SSI-Cov, since it produced accurate estimates of modal properties and allowed to characterize the uncertainties associated with these estimates.

On the use of operational modal analysis in the context of continuous dynamic monitoring, an overview of the tools available to mitigate the effects of operational and environmental factors on natural frequencies, with the aim of obtaining features suited for damage detection, was followed by the presentation of the vibration-based monitoring campaigns of two recently built concrete arch dams: Baixo Sabor and Foz Tua dams.

The research developed in the scope of this thesis resulted in a set of main conclusions that synthesise the partial conclusions that were previously presented at the end of each chapter:

- There are many different types of dams and the choice of which typology to use in each development is mainly dependent on the characteristics of the site where it will be inserted and on the purposes it will be built for. However, independently from their typologies, most dams will likely be subjected to major external actions, such as seismic activity, and to slow, time-driven deterioration. Therefore, continuous inspections and monitoring are necessary to guarantee high-standard operation;

- Modal analysis provides important information about structures from a global perspective that can be very useful in the monitoring of the structure health condition, complementing the information that can be gathered from other destructive and non-destructive types of testing and inspection. Nevertheless, the identification of modal properties may also play an important role in the validation of structural design assumptions, in the calibration or updating of numerical models and in the implementation of continuous monitoring systems. The low levels of vibration expected when performing ambient vibration tests in dams require the consideration of high-quality equipment, and on the other hand it should be taken into account that, in the case of a power plant operating nearby the dam, the data collected may be polluted with harmonics from the turbines rotation, whenever the power plant is operating.

- The modal parameters of a structure estimated from ambient vibration measurements are always subject to bias and variance errors. Therefore, tests and data processing must be conducted with extreme care, in order to reduce the number of error sources and to mitigate the effects of those that cannot be completely supressed. To mitigate bias errors, stabilization diagrams are of good use, through the elimination of spurious modes due to physical and mathematical sources, and helping in the detection of a possible under-estimation of the system order. However, unlike bias errors, which can be mitigated,

variance errors can only be estimated, they cannot be removed, thus it is important to be able to quantify the uncertainty related with these errors. In this context, a version of the SSI-Cov method that allows the quantification of the uncertainty associated with modal properties estimates was implemented;

- Ambient vibration tests have been successfully performed in six concrete dams with distinct characteristics and typologies, including four arch dams with very different heights (Alto Lindoso dam, Santa Luzia dam, Bouçã dam and Caldeirão dam), an arch-gravity dam (Castelo do Bode dam) and a multiple arch dam (Aguieira dam), thus showing the suitability of operational modal analysis to concrete dams. Two distinct acquisition systems were available to perform the tests and each of them was used depending on the characteristics and geometry of the structure: a central acquisition system connected to accelerometers through electrical cables and portable autonomous recorders with an internal tri-axial force balance accelerometer. Good results were achieved using data collected from both the acquisition systems. Generally, the recorded vibration levels go from a few micro g in quiet conditions to many tens of micro g when traffic crosses the dam or human activities with machinery occur nearby. In the case of the power plant fully operating, vibration levels are constantly closer to milli g. It was verified that in general, MEMs accelerometers are not yet suited for the dynamic testing of dams based on ambient vibrations, while piezoelectric accelerometers may be used for this purpose, though not providing results so good as the ones provided by force-balance sensors.

- The procedure proposed for the tracking of natural frequencies in structures whose modal properties are largely affected by operational and environmental conditions proved to be efficient. Using moving references with values based on the evolution of the reservoir water level reduced the number of misidentifications verified in the tracking of Baixo Sabor dam natural frequencies and allowed to track the fifth mode of Foz Tua dam, which was not possible to track using fixed references. It is worth mention, nonetheless, that considerably large intervals should be used around the moving references so that data variability is preserved and the number of identifications does not decrease.

- The quantification of the uncertainties associated with the estimates of modal properties is extremely useful. On the one hand, it is profitable during the modal identification process itself, helping to distinguish spurious modes or machinery induced frequencies from physical modes. On the other hand, it provides information about the true values of modal

properties, allowing to build confidence intervals that help the analyst to decide if a specific estimate should or not be trusted, for instance when using modal properties for model updating. Additionally, the tool for uncertainty quantification was used in the automatic operational modal analysis of Baixo Sabor dam. More specifically, the estimates of uncertainties were included in the algorithm for modal tracking, helping to reduce the number of misidentifications and eliminating poles with high uncertainties, thus producing estimates of modal properties with higher quality that characterize better the evolution of the dam dynamic behaviour.

- The study of the evolution of Baixo Sabor dam modal properties, which were automatically identified for more than three years, allowed to test the ability of alternative static multiple linear regression models to minimize the effects of operational and environmental conditions on natural frequencies. After testing the possibility of using the uncertainties of natural frequencies as weights, a set of different, but similar, weighted and unweighted models were used to reproduce the evolution of each vibration mode natural frequencies with high coefficients of determination, using reservoir water level, ambient and concrete temperatures and concrete hardening as predictors. However, since a new profile of concrete temperatures occurred after the period used to build the models and the time gap between concrete temperature measurements led to (temporally confined) misrepresentations of the real data by the data produced by the regressions models, it was impossible to use the residuals resulting from the application of these models as inputs for damage detection.

  Nevertheless, the direct application of principal components analysis to natural frequencies proved to be an efficient procedure in the removing of data variability due to operational and environmental factors, thus producing features that resulted in stable control charts.

- The simulations performed using the numerical model of Baixo Sabor dam developed by the Concrete Dams Department of LNEC, allowed to ascertain the intensity of the frequency shifts that would be verified in the dam if such damages occurred. For a broad analysis, different damage intensities and different water levels were tested. Afterwards, data from the continuous monitoring was polluted with these frequency shifts and the control charts previously built, and tested to guarantee no false identifications of damage would occur, were used to try to detect such damages. In the end, it was demonstrated that the adopted processing strategy, from the application of automatic operational modal

analysis to the mitigation of variability due to external factors through the application of the principal components analysis, allows the detection of realistic damages only a few days after their occurrence.

- The good results obtained during the first year of operation of the monitoring system installed in Foz Tua arch dam, both through the characterization of vibration levels and in terms of tracking of modal properties, show the success achieved with the application in Baixo Sabor dam is neither casual nor isolated, and that the equipment and methodologies used are suited for the continuous vibration-based monitoring of concrete arch dams. It is worth mention the strong relation found between reservoir water level and modal properties (even stronger than in the case of Baixo Sabor), and that after an entire year of monitoring the dynamic behaviour of the structure should now be fully characterized and damage detection tools tested.

8.2. FUTURE RESEARCH

The work presented in this thesis contains useful contributions for the development of ambient vibration tests and continuous dynamic monitoring of dams, some of which are extensible to the vibration-based testing and monitoring of other civil engineering structures. Nevertheless, additional research would be important to consolidate the knowledge acquired and to reach other capabilities, making the technology and procedures used in this work even more advantageous and common, both in the scientific community and in the industry. In this sense, a few research topics related with the developed work are presented in the following paragraphs:

- Relations between the uncertainties associated with modal properties and operational and environmental factors should be studied, in order to assess the necessity to use slightly different identification processing procedures to obtain better results, depending for instance on vibration levels;

- The effectiveness of using tools for the removing of harmonics from time-series of accelerations should be compared to the results obtained with the approach used in the continuous monitoring of Baixo Sabor dam, which consists in eliminating estimates that are likely to correspond to the rotation of turbines in the power plant, or its harmonics, during modal tracking, after the modal identification is performed;

- Since continuous monitoring data about concrete temperatures in Baixo Sabor dam is not available, other methods to mitigate the effects of operational and environmental conditions on natural frequencies that do not depend on predictors, such as Local PCA, Second Order Blind Identification (SOBI), Co-integration or algorithms based in Neural Networks should be implemented and tested, and the results obtained should be compared with the ones provided by the models developed in the context of this thesis using MLR and PCA;

- Static data from the continuous monitoring of Baixo Sabor dam could be used to test the ability of the tools implemented for damage detection, comparing the results obtained with static and dynamic data and studying the possibility of improving the damage detection procedure combining the two types of data;

- The possibility of reaching a higher level in Rytter's scale for the assessment of damage, namely the second level of the scale (localization of damage), should be tested, for instance considering the uncertainties associated with ordinate estimates from mode shapes, since it

has been verified in an example with a real damaged structure, that ordinate estimates closer to the part of the structure where the damage was located where associated with much higher uncertainties;

- The analysis of the data collected with the dynamic monitoring system installed in Foz Tua arch dam is still in an early stage. Parallel to the work developed with Baixo Sabor dam, the observed variations of natural frequencies are going to be correlated with operational and environmental data and models to reduce the effect of these factors on natural frequencies will be developed, which will allow to test the ability of the monitoring system for damage detection.

9. REFERENCES

Abdel-Ghaffar, A. M., & Scott, R. F. (1981). VIBRATION TESTS OF FULL-SCALE EARTH DAM. *Journal of the Geotechnical Engineering Division, 107*(3), 241-269.

Abdulamit, A., Demetriu, S., Aldea, A., Neagu, C., & Gaftoi, D. (2017). Ambient Vibration Tests at Some Buttress Dams in Romania. *Procedia Engineering, 199*, 2196-2201. doi:https://doi.org/10.1016/j.proeng.2017.09.183

Akkose, M., Bayraktar, A., & Dumanoglu, A. A. (2008). Reservoir water level effects on nonlinear dynamic response of arch dams. *Journal of Fluids and Structures, 24*(3), 418-435. doi:10.1016/j.jfluidstructs.2007.08.007

Alembagheri, M., & Ghaemian, M. (2013). Damage assessment of a concrete arch dam through nonlinear incremental dynamic analysis. *Soil Dynamics and Earthquake Engineering, 44*, 127-137. doi:10.1016/j.soildyn.2012.09.010

Allemang, R. J., & Brown, D. L. (1982). *A Correlation Coefficient for Modal Vector Analysis.* Paper presented at the International Modal Analysis Conference, Orlando, Florida, USA.

Altunişik, A., Kalkan, E., & Başağa, H. (2018). *Structural behavior of arch dams considering experimentally validated prototype model using similitude and scaling laws* (Vol. 22).

Altunisik, A. C., Gunaydin, M., Sevim, B., & Adanur, S. (2017). System identification of arch dam model strengthened with CFRP composite materials. *Steel and Composite Structures, 25*(2), 231-244. doi:10.12989/scs.2017.25.2.231

Altunişik, A. C., Günaydin, M., Sevim, B., Bayraktar, A., & Adanur, S. (2016). Retrofitting Effect on the Dynamic Properties of Model-Arch Dam with and without Reservoir Water Using Ambient-Vibration Test Methods. *Journal of Structural Engineering (United States), 142*(10). doi:10.1061/(ASCE)ST.1943-541X.0001520

Alves, S. W., & Hall, J. F. (2006). System identification of a concrete arch dam and calibration of its finite element model. *Earthquake Engineering and Structural Dynamics, 35*(11), 1321-1337. doi:10.1002/eqe.575

Amberg, F. (2015). *Stability of concrete dams - Some basic requirements.* Paper presented at the 13th ICOLD Benchmark Workshop on the Numerical Analysis of Dams, Lausanne - Switzerland.

Amezquita-Sanchez, J. P., & Adeli, H. (2016). Signal Processing Techniques for Vibration-Based Health Monitoring of Smart Structures. *Archives of Computational Methods in Engineering, 23*(1), 1-15. doi:10.1007/s11831-014-9135-7

APREN. (2019). *Yearbook - Portugal needs our energy*. Retrieved from https://www.apren.pt/contents/documents/anuario-2019-aprenebook-v2-5562.pdf

Azevedo, N. M., & Lemos, J. V. (2006). Hybrid discrete element/finite element method for fracture analysis. *Computer Methods in Applied Mechanics and Engineering, 195*(33-36), 4579-4593. doi:10.1016/j.cma.2005.10.005

Batista, A. L. (1998). *Análise do Comportamento ao Longo do Tempo de Barragens Abóbada.* (PhD), Universidade Técnica de Lisboa, Lisboa.

Batista, A. L., & Matos, D. S. (2016). *Aspetos Relevantes do Apoio do LNEC à EDP na Instrumentação das Barragens de Betão Construídas entre 2011 e 2016* Paper presented at the 2º Encontro Nacional Sobre Qualidade e Inovação na Construção, Lisbon.

Bayraktar, A., Sevim, B., & Can Altunişik, A. (2011). Finite element model updating effects on nonlinear seismic response of arch damreservoirfoundation systems. *Finite Elements in Analysis and Design, 47*(2), 85-97. doi:10.1016/j.finel.2010.09.005

BBC, N. (2019). Brumadinho dam collapse: Hope fades for hundreds missing in Brazil. Retrieved from https://www.bbc.com/news/world-latin-america-47017551

Bellino, A., Fasana, A., Garibaldi, L., & Marchesiello, S. (2010). PCA-based detection of damage in time-varying systems. *Mechanical Systems and Signal Processing, 24*(7), 2250-2260. doi:10.1016/j.ymssp.2010.04.009

Belouchrani, A., Abed-Meraim, K., Cardoso, J. F., & Moulines, E. (1997). A blind source separation technique using second-order statistics. *IEEE Transactions on Signal Processing, 45*(2), 434-444. doi:10.1109/78.554307

Bendat, J. S., & Piersol, A. G. (1980). *Engineering Applications of Correlation and Spectral Analysis.* New York, USA: John Wiley & Sons.

Bérubé, M.-A., Duchesne, J., Dorion, J. F., & Rivest, M. (2002). Laboratory assessment of alkali contribution by aggregates to concrete and application to concrete structures affected by alkali–silica reactivity. *Cement and Concrete Research, 32*(8), 1215-1227. doi:http://doi.org/10.1016/S0008-8846(02)00766-4

Betâmio de Almeida, A., Matias Ramos, C., Santos, M. A., & Viseu, T. (2003). *Dam Break Flood Risk Management in Portugal*. Lisbon, Portugal: Laboratório Nacional de Engenharia Civil.

Bićanić, N. (2004). Discrete Element Methods *Encyclopedia of Computational Mechanics*: John Wiley & Sons, Ltd.

Bobet, A., Fakhimi, A., Johnson, S., Morris, J., Tonon, F., & Yeung, M. R. (2009). Numerical models in discontinuous media: review of advances for rock mechanics applications. *Journal of Geotechnical and Geoenvironmental Engineering, 135*(11), 1547-1561.

Branco, J. A. (2004). *Uma Introdução à Análise de Clusters*. Paper presented at the XII Congresso Anual da Sociedade Portuguesa de Estatística.

Bretas, E. M., Lemos, J. V., & Lourenço, P. B. (2014). A DEM based tool for the safety analysis of masonry gravity dams. *Engineering Structures, 59*, 248-260. doi:http://doi.org/10.1016/j.engstruct.2013.10.044

Brincker, R., Ventura, C., & Andersen, P. (2001). *Damping Estmation by Frequency Domain Decomposition.* Paper presented at the IMAC 19, International Modal Analysis Conference, Kissimmee, Florida, USA.

Brincker, R., Zhang, L., & Andersen, P. (2000). *Modal Identification from Ambient Responses using Frequency Domain Decomposition.* Paper presented at the IMAC 18, International Modal Analysis Conference, San Antonio, USA.

Brownjohn, J. M. W. (2007). Structural health monitoring of civil infrastructure. *Philosophical Transactions of the Royal Society A: Mathematical, Physical and Engineering Sciences, 365*(1851), 589-622. doi:10.1098/rsta.2006.1925

Brownjohn, J. M. W., Magalhaes, F., Caetano, E., & Cunha, A. (2010). Ambient vibration re-testing and operational modal analysis of the Humber Bridge. *Engineering Structures, 32*(8), 2003-2018. doi:10.1016/j.engstruct.2010.02.034

Bukenya, P., Moyo, P., Beushausen, H., & Oosthuizen, C. (2014). Health monitoring of concrete dams: A literature review. *Journal of Civil Structural Health Monitoring, 4*(4), 235-244. doi:10.1007/s13349-014-0079-2

Calcina, S. V., Eltrudis, L., Piroddi, L., & Ranieri, G. (2014). Ambient vibration tests of an arch dam with different reservoir water levels: Experimental results and comparison with finite element modelling. *Scientific World Journal, 2014*. doi:10.1155/2014/692709

Câmara, R., Oliveira, S., & Portugal, A. (1993). *Estudo do comportamento dinâmico da barragem do Alto Lindoso*. Retrieved from

Campos, A., López, C. M., & Aguado, A. (2016). Diffusion–reaction model for the internal sulfate attack in concrete. *Construction and Building Materials, 102, Part 1*, 531-540. doi:http://doi.org/10.1016/j.conbuildmat.2015.10.177

Cantieni, R. (2005). *Experimental methods used in system identification of civil engineering structures.* Paper presented at the Proceedings of the 1st International Operational Modal Analysis Conference, IOMAC 2005.

Carden, E. P., & Brownjohn, J. M. W. (2008). Fuzzy clustering of stability diagrams for vibration-based structural health monitoring. *Computer-Aided Civil and Infrastructure Engineering, 23*(5), 360-372. doi:10.1111/j.1467-8667.2008.00543.x

Cauberghe, B. (2004). *Applied Frequency-Domain System Identificatioin in the Field of Experimental and Operational Modal Analysis.* (PhD Thesis), Vrije Universiteit Brussel, Belgium.

Chen, S.-H. (2015). Gravity Dams *Hydraulic Structures* (pp. 283-395). Berlin, Heidelberg: Springer Berlin Heidelberg.

Chopra, A. K., & Wang, J. (2012). *Comparison of recorded and computed earthquake response of arch dams.* Paper presented at the Proc. of the 15th World Conference on Earthquake Engineering.

Clough, R. W., Ghannat, Y., & Qui, X. F. (1987). *Dynamic reservoir interaction with Monticello Dam*. Retrieved from

Clough, R. W., & Penzien, J. (1995). *Dynamics of Structures* (I. McGraw-Hill Ed. Second ed.). Berkeley, USA.

Clough, R. W., & Wilson, E. L. (1999). *Early finite element research at Berkeley.* Paper presented at the Fifth US National Conference on Computational Mechanics.

CNPGB, C. N. P. d. G. B. Retrieved from http://cnpgb.apambiente.pt/gr_barragens/gbportugal/Lista.htm

Comanducci, G., Magalhães, F., Ubertini, F., & Cunha, Á. (2016). On vibration-based damage detection by multivariate statistical techniques: Application to a long-span arch bridge. *Structural Health Monitoring, 15*(5), 505-524. doi:10.1177/1475921716650630

Cruz, P., Materón, B., & Freitas, M. (2009). *Concrete Face Rockill Dams*. São Paulo: CRC Press.

Cundall, P. A. (1971). *A computer model for simulatin progressive large scale movements in blocky rock systems*. Nancy: Rock fracture (ISRM).

Cundall, P. A. (1989). Numerical experiments on localization in frictional materials. *Ingenieur-Archiv, 59*(2), 148-159. doi:10.1007/BF00538368

Cunha, A. (1990). *Dinâmica estrutural estocástica: aplicações à engenharia sísmica.* (PhD), FEUP, Porto.

Cunha, A., & Caetano, E. (2006). Experimental modal analysis of civil engineering structures. *Sound and Vibration, 40*(6), 12-20.

Cunha, A., Caetano, E., & Delgado, R. (2001). Dynamic tests on large cable-stayed bridge. *Journal of Bridge Engineering, 6*(1), 54-62. doi:10.1061/(ASCE)1084-0702(2001)6:1(54)

DAM_AGE. (2016-2018). Advanced Online Dynamic Structural Health Monitoring of Concrete Dams *PTDC/ECM-EST/0805/2014.*

Dams, P. N. C. o. L. (1992). *Large Dams in Portugal*.

Darbre, G. R., De Smet, C. A. M., & Kraemer, C. (2000). Natural frequencies measured from ambient vibration response of the arch dam of Mauvoisin. *Earthquake Engineering and*

Structural Dynamics, 29(5), 577-586. doi:10.1002/(SICI)1096-9845(200005)29:5<577::AID-EQE924>3.0.CO;2-P

Darbre, G. R., & Proulx, J. (2002). Continuos ambient-vibration monitoring of the arch dam of Mauvoisin. *Earthquake Engineering and Structural Dynamics, 31*(2), 475-480. doi:10.1002/eqe.118

De Troyer, T., Guillaume, P., Pintelon, R., & Vanlanduit, S. (2009). Fast calculation of confidence intervals on parameter estimates of least-squares frequency-domain estimators. *Mechanical Systems and Signal Processing, 23*(2), 261-273. doi:http://dx.doi.org/10.1016/j.ymssp.2008.04.009

Deinum, P. J., Dungar, R., Ellis, B. R., Jeary, A. P., Reed, G. A. L., & Severn, R. T. (1982). Vibration tests on emosson arch dam, Switzerland. *Earthquake engineering & structural dynamics, 10*(3), 447-470. doi:10.1002/eqe.4290100308

Delgado, R. (1984). *O Método dos Elementos Finitos na Análise Dinâmica de Barragens Incluindo a Interação Sólido-Líquido.* (PhD thesis), Faculdade de Engenharia da Universidade do Porto.

Deraemaeker, A., Reynders, E., De Roeck, G., & Kullaa, J. (2008). Vibration-based structural health monitoring using output-only measurements under changing environment. *Mechanical Systems and Signal Processing, 22*(1), 34-56. doi:10.1016/j.ymssp.2007.07.004

Diord, S., Magalhães, F., Cunha, Á., & Caetano, E. (2017). High spatial resolution modal identification of a stadium suspension roof: Assessment of the estimates uncertainty and of modal contributions. *Engineering Structures, 135*, 117-135. doi:http://dx.doi.org/10.1016/j.engstruct.2016.12.060

Döhler, M., Lam, X.-B., & Mevel, L. (2013). Uncertainty quantification for modal parameters from stochastic subspace identification on multi-setup measurements. *Mechanical Systems and Signal Processing, 36*(2), 562-581. doi:http://dx.doi.org/10.1016/j.ymssp.2012.11.011

Döhler, M., & Mevel, L. (2013). Efficient multi-order uncertainty computation for stochastic subspace identification. *Mechanical Systems and Signal Processing, 38*(2), 346-366. doi:10.1016/j.ymssp.2013.01.012

Duffaut, P. (2013). The traps behind the failure of Malpasset arch dam, France, in 1959. *Journal of Rock Mechanics and Geotechnical Engineering, 5*(5), 335-341. doi:https://doi.org/10.1016/j.jrmge.2013.07.004

EDP, E. d. P. Retrieved from http://www.a-nossa-energia.edp.pt/centros_produtores/

El-kafafy, M., Accardo, G., Peeters, B., Janssens, K., De Troyer, T., & Guillaume, P. (2015). *A fast maximum likelihood-based estimation of a modal model.* Paper presented at the Conference Proceedings of the Society for Experimental Mechanics Series.

Ellis, B. R., & Jeary, A. P. (1984). On the forced vibration testing of dams. *Proceedings of the 8th World Conference on Earthquake Engineering (WCEE), San Francisco, Calif., 21-28 July 1984, 5*, 119-126.

Escuder-Bueno, I., Galán, D., & Serrano, A. (2013). *Need for transient thermal models, with daily inputs, to explain the displacements of arch gravity dams.* Paper presented at the ICOLD - 12th International Benchmark Workshop on Numerical Analysis of Dams, Graz - Austria.

Evans, J. R., Allen, R. M., Chung, A. I., Cochran, E. S., Guy, R., Hellweg, M., & Lawrence, J. F. (2014). Performance of Several Low-Cost Accelerometers. *Seismological Research Letters, 85*(1), 147-158. doi:10.1785/0220130091

Ewins, D. J. (2000). *Modal Testing: Theory, Practice and Application*. Baldock, England: Research Studies Press Ltd.

Fan, W., & Qiao, P. (2011). Vibration-based damage identification methods: A review and comparative study. *Structural Health Monitoring, 10*(1), 83-111. doi:10.1177/1475921710365419

Faria, R. (1994). *Avaliação do Comportamento Sísmico de Barragens de Betão Através de um Modelo de Dano Contínuo.* (PhD), Faculdade de Engenharia da Universidade do Porto.

Farrar, C. R., Doebling, S. W., & Nix, D. A. (2001). Vibration-based structural damage identification. *Philosophical Transactions of the Royal Society A: Mathematical, Physical and Engineering Sciences, 359*(1778), 131-149. doi:10.1098/rsta.2000.0717

Felber, A. J. (1993). *Development of a Hybrid Bridge Evaluation System.* (PhD Thesis), The University of British Columbia.

Filkins, D. (2017). A Bigger Problem Than Isis? *The New Yorker*.

Frangopol, D. M. (2011). Life-Cycle performance, management, and optimisation of structural systems under uncertainty: Accomplishments and challenges. *Structure and Infrastructure Engineering, 7*(6), 389-413. doi:10.1080/15732471003594427

Frangopol, D. M., & Soliman, M. (2016). Life-cycle of structural systems: recent achievements and future directions. *Structure and Infrastructure Engineering, 12*(1), 1-20. doi:10.1080/15732479.2014.999794

Frigerio, A., & Mazza, G. (2013). *The rehabilition of Beauregard Dam: the contribution of the numerical modeling.* Paper presented at the ICOLD - 12th International Benchmark Workshop on Numerical Analysis of Dams, Graz - Austria.

García-Palacios, J. H., Soria, J. M., Díaz, I. M., & Tirado-Andrés, F. (2016). Ambient modal testing of a double-arch dam: The experimental campaign and model updating. *Journal of Physics: Conference Series, 744*(1). doi:10.1088/1742-6596/744/1/012037

García, F., Aznárez, J. J., Cifuentes, H., Medina, F., & Maeso, O. (2014). Influence of reservoir geometry and conditions on the seismic response of arch dams. *Soil Dynamics and Earthquake Engineering, 67*, 264-272. doi:10.1016/j.soildyn.2014.10.008

Gauron, O., Boivin, Y., Ambroise, S., Saidou Sanda, A., Bernier, C., Paultre, P., . . . Roth, S.-N. (2018). Forced-Vibration Tests and Numerical Modeling of the Daniel-Johnson Multiple-Arch Dam. *Journal of Performance of Constructed Facilities, 32*(2), 04017137. doi:10.1061/(ASCE)CF.1943-5509.0001137

Gentile, C., Ubertini, F., Cavalagli, N., Guidobaldi, M., Materazzi, A. L., & Saisi, A. (2014). *Dynamic investigation of the "san Pietro" bell-tower in Perugia.* Paper presented at the Proceedings of the International Conference on Structural Dynamic , EURODYN.

Goethals, I., Vanluyten, B., & De Moor, B. (2004). *Reliable spurious mode rejection using self learning algorithms.* Paper presented at the Proceedings of the 2004 International Conference on Noise and Vibration Engineering, ISMA.

Goldgruber, M. (2014). *Proceedings of the ICOLD - 12th International Benchmark Workshop on Numerical Analysis of Dams*.

Gomes, J., & Carvalho, E. (2014). *Ensaios de Vibração Forçada para a Caracterização do Comportamento Dinâmico de Barragens de Betão. Aplicação à Barragem de Cahora Bassa*. Paper presented at the 5ª Jornadas Portuguesas de Engenharia de Estruturas, Lisbon.

Gomes, J., & Lemos, J. V. (2016a). *Characterization of the dynamic behavior of an arch dam by means of forced vibration tests*. Paper presented at the 1st Meeting of EWG Dams and Earthquakes, Saint Malo, France.

Gomes, J., & Lemos, J. V. (2016b). *Ensaios de Vibração Forçada para a Caracterização do Comportamento Dinâmico de Barragens de Betão*. Paper presented at the 10º Congresso Nacional de Mecânica Experimental, Lisbon.

Gomes, J., Pereira, S., Magalhães, F., Lemos, J. V., & Cunha, Á. (2018). *Input-output vs output-only modal identification of Baixo Sabor concrete arch dam*. Paper presented at the 9th European Workshop on Structural Health Monitoring (EWSHM 2019), Manchester, UK.

Gomes, J. P., & Lemos, J. V. d. (2016). *Caracterização do Comportamento Dinâmico de Barragens de Betão Utilizando Ensaios de Vibração Forçada*. Paper presented at the 10º Congresso Nacional de Sismologia e Engenharia Sísmica, Ponta Delgada, Açores, Portugal.

Gomes, J. P., & Magalhães, F. (2015). *Barragem de montante do aproveitamento hidroelétrico do Baixo Sabor. Caracterização do comportamento dinâmico da barragem através de monitorização em contínuo. Relatório de instalação.* Retrieved from

Google. Google Maps. Retrieved from https://www.google.pt/maps/

Gordon, A. (1999). *Classification* (C. Hall Ed. 2nd edition ed.): Chapman & Hall.

Goursat, M., Döhler, M., Mevel, L., & Andersen, P. (2011). Crystal Clear SSI for Operational Modal Analysis of Aerospace Vehicles. In T. Proulx (Ed.), *Structural Dynamics, Volume 3: Proceedings of the 28th IMAC, A Conference on Structural Dynamics, 2010* (pp. 1421-1430). New York, NY: Springer New York.

Guillaume, P., Verboven, P., Vanlanduit, S., Van der Auweraer, H., & Peeters, B. (2003). *A Poly-Reference Implementation of the Least-Squares Complex Frequency-Domain Estimator*. Paper presented at the IMAC 21, International Modal Analysis Conference, Kissimmee, Florida, USA.

Gunn, R. M., & Tzenkov, A. D. (2015). Theme A - Seismic Safety Evaluations of a Concrete Dam Based on Guidelines *Proceedings of the ICOLD - 13th International Benchmark Workshop on Numerical Analysis of Dams*. Lausanne - Switzerland.

Hall, J. F. (1988). The dynamic and earthquake behaviour of concrete dams: review of experimental behaviour and observational evidence. *Soil Dynamics and Earthquake Engineering, 7*(2), 58-121. doi:10.1016/S0267-7261(88)80001-0

Hamidian, D., Seyedpoor, S. M., & Salajegheh, J. (2013). An investigation of dam-water-foundation rock interaction effects on linear and nonlinear earthquake response of concrete arch dams. *Asian Journal of Civil Engineering, 14*(1), 111-122.

Hay, W. W. (2016). HOH—The Keystone of Earth's Climate *Experimenting on a Small Planet: A History of Scientific Discoveries, a Future of Climate Change and Global Warming* (pp. 390-420). Cham: Springer International Publishing.

Henkel, M. (2015). *21st Century Homestead: Sustainable Agriculture II: Farming and Natural Resourses*: Lulu. com.

Hermans, L., & Van Der Auweraer, H. (1999). MODAL TESTING AND ANALYSIS OF STRUCTURES UNDER OPERATIONAL CONDITIONS: INDUSTRIAL APPLICATIONS. *Mechanical Systems and Signal Processing, 13*(2), 193-216. doi:http://dx.doi.org/10.1006/mssp.1998.1211

Heylen, W., Lammens, S., & Sas, P. (2007). *Modal Analysis Theory and Testing*. Katholieke Universiteit Leuven, Belgium.

Hu, J., & Wu, S. (2019). Statistical modeling for deformation analysis of concrete arch dams with influential horizontal cracks. *Structural Health Monitoring, 18*(2), 546-562. doi:10.1177/1475921718760309

ICOLD, C.-. Commission Internationale des Grands Barrages - International Comission on Large Dams. Retrieved from http://www.icold-cigb.net/

Instituto da Água, I. A. (2001). *Curso de Exploração e Segurança de Barragens*. Lisboa.

Itasca, D. (2017). Three-dimensional Distinct Element Code. Version 5.2. Minneapolies, USA: Itasca Consulting Group.

Jansen, R. B. (1980). *Dam and Public Safety. A Water Resources Technical Publication.* Denver, USA: U. S. Department of the Interior - Bureau of Reclamation.

Johnson, R. A., & Wichern, D. W. (2007). *Applied Multivariate Statistical Analysis* (6th ed.).

Juang, J. N. (1994). *Applied System Identification*. New Jersey, USA: Prentice Hall Englewood Cliffs.

Kambhatla, N., & Leen, T. K. (1997). Dimension Reduction by Local Principal Component Analysis. *Neural Computation, 9*(7), 1493-1516. doi:10.1162/neco.1997.9.7.1493

Kullaa, J. (2004). *Structural health monitoring of a crane in variable configurations.* Paper presented at the Proceedings of the 2004 International Conference on Noise and Vibration Engineering, ISMA.

Lau, D. T., Noruziaan, B., & Razaqpur, A. G. (1998). Modelling of contraction joint and shear sliding effects on earthquake response of arch dams. *Earthquake Engineering and Structural Dynamics, 27*(10), 1013-1029. doi:10.1002/(SICI)1096-9845(199810)27:10<1013::AID-EQE765>3.0.CO;2-0

Lemos, J., & Antunes, N. (2011). Modelling of arch dam foundation failure scenarios—case studies of Baixo Sabor and Alto Ceira dams. *Dam Engineering, 21*(4), 299.

Lemos, J. V. (1987). *A Distinct Element Method for Dynamic Analysis of Jointed Rock with Application to Dam Foundations and Fault Motion.* (PhD), University of Minnesota.

Lemos, J. V., Gomes, J., & Pereira, S. (2019). *Modelling Dam-Water Dynamic Interaction. Numerical Options and Experimental Validation*. Paper presented at the 7th ECCOMAS Thematic Conference on Computational Methods in Structural Dynamics and Earthquake Engineering (COMPDYN 2019), Crete, Greece.

Lemos, J. V., Oliveira, S., & Mendes, P. (2008). *Analysis of the dynamic behaviour of cabril dam considering the influence of contraction joints.* Paper presented at the 7th European Conference on Structural Dynamics, EURODYN 2008.

Li, H. N., Ren, L., Jia, Z. G., Yi, T. H., & Li, D. S. (2016). State-of-the-art in structural health monitoring of large and complex civil infrastructures. *Journal of Civil Structural Health Monitoring, 6*(1), 3-16. doi:10.1007/s13349-015-0108-9

LNEC, FEUP, & Ambisig. (2015). Barragem de montante do aproveitamento hidroelétrico do Baixo Sabor. Caracterização do comportamento dinâmico da barragem através de monitorização em contínuo. Relatório de instalação.

Loh, C.-H., Chen, C.-H., & Hsu, T.-Y. (2011). Application of advanced statistical methods for extracting long-term trends in static monitoring data from an arch dam. *Structural Health Monitoring, 10*(6), 587-601. doi:10.1177/1475921710395807

Londe, P. (1987). The Malpasset Dam failure. *Engineering Geology, 24*(1-4), 295-329. doi:10.1016/0013-7952(87)90069-X

Magalhães, F. (2010). *Operational Modal Analysis for Testing and Monitoring of Bridges and Special Structures.* (PhD), Faculdade de Engenharia da Universidade do Porto.

Magalhães, F., Caetano, E., & Cunha, Á. (2008). Operational modal analysis and finite element model correlation of the Braga Stadium suspended roof. *Engineering Structures, 30*(6), 1688-1698. doi:10.1016/j.engstruct.2007.11.010

Magalhães, F., Caetano, E., Cunha, Á., Flamand, O., & Grillaud, G. (2012). Ambient and free vibration tests of the Millau Viaduct: Evaluation of alternative processing strategies. *Engineering Structures, 45*, 372-384. doi:10.1016/j.engstruct.2012.06.038

Magalhães, F., & Cunha, A. (2011). Explaining operational modal analysis with data from an arch bridge. *Mechanical Systems and Signal Processing, 25*(5), 1431-1450. doi:10.1016/j.ymssp.2010.08.001

Magalhães, F., Cunha, A., & Caetano, E. (2009). Online automatic identification of the modal parameters of a long span arch bridge. *Mechanical Systems and Signal Processing, 23*(2), 316-329. doi:10.1016/j.ymssp.2008.05.003

Magalhães, F., Cunha, A., & Caetano, E. (2012). Vibration based structural health monitoring of an arch bridge: From automated OMA to damage detection. *Mechanical Systems and Signal Processing, 28*, 212-228. doi:10.1016/j.ymssp.2011.06.011

Magalhães, F., Cunha, Á., & Caetano, E. (2008). Dynamic monitoring of a long span arch bridge. *Engineering Structures, 30*(11), 3034-3044. doi:10.1016/j.engstruct.2008.04.020

Maia, N., & Silva, J. (1997). *Theoretical and Experimental Modal Analysis*: Research Studies Press Ltd.

Makha, R., & Moyo, P. (2012). *Observations from the calibration of an arch dam model using ambient modal properties.* Paper presented at the Concrete Repair, Rehabilitation and Retrofitting III - Proceedings of the 3rd International Conference on Concrete Repair, Rehabilitation and Retrofitting, ICCRRR 2012.

Martins, N., Caetano, E., Diord, S., Magalhães, F., & Cunha, T. (2014). Dynamic monitoring of a stadium suspension roof: Wind and temperature influence on modal parameters and structural response. *Engineering Structures, 59*, 80-94. doi:10.1016/j.engstruct.2013.10.021

Mata, J. (2011). Interpretation of concrete dam behaviour with artificial neural network and multiple linear regression models. *Engineering Structures, 33*(3), 903-910. doi:10.1016/j.engstruct.2010.12.011

Mathworks. (2016). Matlab. R2016a.

Mendes, P. (2010). *Observação e Análise do Comportamento Dinâmico de Barragens de Betão.* (PhD), Faculdade de Engenharia da Universidade do Porto.

Mendes, P., Oliveira Costa, C., Almeida Garrett, J., & Oliveira, S. (2007). Development of a monitoring system to Cabril dam with operational modal analysis. *The Proceedings of the 2nd Experimental Vibration Analysis for Civil Engineering Structures (EVACES), Porto*.

Mendes, P., & Oliveira, S. (2007). *Study of dam-reservoir dynamic interaction using vibration tests on a physical model.* Paper presented at the Proceedings of the 2nd International Operational Modal Analysis Conference, IOMAC 2007.

Mendes, P., & Oliveira, S. (2009). *Influence of the Intake Tower Dynamic Behaviour on Modal Identification of Cabril Dam.* Paper presented at the IOMAC-3rd International Operational Modal Analysis Conference.

Montgomery, D. C. (2009). *Statistical quality control: a modern introduction*. New York: John Wiley & Sons.

Munjiza, A. A. (2004). *The combined finite-discrete element method*: John Wiley & Sons.

Ni, Y. Q., Zhou, H. F., & Ko, J. M. (2009). Generalization capability of neural network models for temperature- frequency correlation using monitoring data. *Journal of Structural Engineering, 135*(10), 1290-1300. doi:10.1061/(ASCE)ST.1943-541X.0000050

Nour, A., Cherfaoui, A., Gocevski, V., & Léger, P. (2016). Probabilistic seismic safety assessment of a CANDU 6 nuclear power plant including ambient vibration tests: Case study. *Nuclear Engineering and Design, 304*, 125-138. doi:10.1016/j.nucengdes.2016.05.004

Novak, P., Moffat, A. I. B., & Nalluri, C. (2007). *Hydraulics in Civil and Enrironmental Engineering* (T. Francis Ed. Fourth ed.). London and New York.

Okuma, N., Etou, Y., Kanazawa, K., & Hirata, K. (2008). *Dynamic properties of a large arch dam after forty-four years of completion* Paper presented at the The 14th World Conference on Earthquake Engineering, Beijing, China.

Oliveira, G. (2016). *Vibration-Based Structural Helath Monitoring of Wind Turbines.* (PhD), Faculty of Engineering of the University of Porto.

Oliveira, G., Magalhães, F., Cunha, Á., & Caetano, E. (2016). Development and implementation of a continuous dynamic monitoring system in a wind turbine. *Journal of Civil Structural Health Monitoring, 6*(3), 343-353. doi:10.1007/s13349-016-0182-7

Oliveira, G., Magalhães, F., Cunha, Á., & Caetano, E. (2018). Continuous dynamic monitoring of an onshore wind turbine. *Engineering Structures, 164*, 22-39. doi:10.1016/j.engstruct.2018.02.030

Oliveira, S. (2000). *Modelos para Análise do Comportamento de Barragens de Betão Considerando a Fissuração e os Efeitos do Tempo. Formulações de Dano.* (PhD), Faculdade de Engenharia da Universidade do Porto.

Oliveira, S., & Faria, R. (2006). Numerical simulation of collapse scenarios in reduced scale tests of arch dams. *Engineering Structures, 28*(10), 1430-1439. doi:10.1016/j.engstruct.2006.01.012

Oñate, E. (2009). *Strutural Analysis with the FInite Element Method. Linear Statics. Volume 1. Basics and Solids.* (First Edition ed.). Barcelona, Spain: Springer.

Overschee, P. V., & Moor, B. D. (1996). *Subspace Identification for Linear Systems - Theory, Implementation, Applications*: Kluwer Academic Publishers.

Pacheco, J., Oliveira, G., Magalhães, F., Moutinho, C., & Cunha, Á. (2018). Evaluation of low cost vibration based damage detection systems. *Journal of Physics: Conference Series, 1037*(5), 052005.

Pande, G., Beer, G., & Williams, J. (1990). Numerical methods in rock mechanics.

Pappa, R. S., James Iii, G. H., & Zimmerman, D. C. (1998). Autonomous modal identification of the Space Shuttle tail rudder. *Journal of Spacecraft and Rockets, 35*(2), 163-169. doi:10.2514/2.3324

Paultre, P., Proulx, J., & Carbonneau, C. (2002). An experimental evaluation of ice cover effects on the dynamic behaviour of a concrete gravity dam. *Earthquake Engineering and Structural Dynamics, 31*(12), 2067-2082. doi:10.1002/eqe.205

Pedro, J. O. (1977). *Dimensionamento das barragens abóbada pelo método dos elementos finitos.* (Thesis to become LNEC specialist (Memory nº 479)), Lisbon, Portugal.

Peeters, B. (2000). *System Identification and Damage Detection in Civil Engineering.* (PhD thesis), Katholieke Universiteit Leuven.

Peeters, B., Cornelis, B., Janssens, K., & Van der Auweraer, H. (2007). *Removing disturbing harmonics in operational modal analysis.* Paper presented at the Proceedings of International Operational Modal Analysis Conference, Copenhagen, Denmark.

Peeters, B., & Van der Auweraer, H. (2005). *PolyMax: a Revolution in Operational Modal Analysis*. Paper presented at the IOMAC, International Operational Modal Analysis Conference, Copenhagen, Denmark.

Penman, A. D. M. (1989). 18 - Dams A2 - Blake, LS *Civil Engineer's Reference Book (Fourth Edition)* (pp. 18/11-18/37): Butterworth-Heinemann.

Pereira Gomes, J., Magalhães, F., Monteiro, G., Palma, J., Pereira, S., & Silva Matos, D. (2018). *Seismic Monitoring System of Baixo Sabor Scheme for Structural Dynamic Behaviour Monitoring and Risk Management.* Paper presented at the ICOLD 2018, Vienna, Austria.

Pereira, S., Magalhães, F., Gomes, J. P., Cunha, Á., & Lemos, J. V. (2018). Dynamic monitoring of a concrete arch dam during the first filling of the reservoir. *Engineering Structures, 174*, 548-560. doi:10.1016/j.engstruct.2018.07.076

Pietrangeli, S. (2015). Design of the Highest RCC dam. Retrieved from http://www.pietrangeli.com/project/pubblications.htm

Pina, C., & Gomes, J. (1996). *Barragem do Cabril. Ensaio de vibração forçada.* Retrieved from Lisboa, Portugal:

Pintelon, R., Guillaume, P., & Schoukens, J. (2007). Uncertainty calculation in (operational) modal analysis. *Mechanical Systems and Signal Processing, 21*(6), 2359-2373. doi:http://dx.doi.org/10.1016/j.ymssp.2006.11.007

Portugal, A. (1990). *Caracterização do comportamento dinâmico de barragens de betão através de ensaios "in situ".* (Master thesis), Instituto Superior Técnico.

Portugal, A. C., & Caetano, E. (1992). *Experimental Evaluation of the Dynamic Characteristics of Portuguese Dams*. Paper presented at the Proceedings of the Tenth World Conference on Eartquake Engineering, Vols 1-10.

Priscu, R., Popovici, A., Stematiu, D., & Stere, C. (1985). *Earthquake engineering for large dams*. New York.

Proulx, J., Paultre, P., Rheault, J., & Robert, Y. (2001). An experimental investigation of water level effects on the dynamic behaviour of a large arch dam. *Earthquake Engineering and Structural Dynamics, 30*(8), 1147-1166. doi:10.1002/eqe.55

Rainieri, C., & Fabbrocino, G. (2014). Operational modal analysis of civil engineering structures. *Springer, New York, 142*, 143.

Rainieri, C., Magalhaes, F., Gargaro, D., Fabbrocino, G., & Cunha, A. (2019). Predicting the variability of natural frequencies and its causes by Second-Order Blind Identification. *Structural Health Monitoring, 18*(2), 486-507. doi:10.1177/1475921718758629

Reynders, E. (2009). *System Identification and Modal Analysis in Structural Mechanics.* (PhD Thesis), Katholieke Universiteit Leuven, Belgium.

Reynders, E., Houbrechts, J., & De Roeck, G. (2012). Fully automated (operational) modal analysis. *Mechanical Systems and Signal Processing, 29*, 228-250. doi:10.1016/j.ymssp.2012.01.007

Reynders, E., Maes, K., Jansen, M., Lombaert, G., & De Roeck, G. (2014). *Identification and uncertainty quantification of the dynamic properties of a mid-rise building under ambient wind excitation.* Paper presented at the Proceedings of the International Conference on Structural Dynamic , EURODYN.

Reynders, E., Pintelon, R., & De Roeck, G. (2008). Uncertainty bounds on modal parameters obtained from stochastic subspace identification. *Mechanical Systems and Signal Processing, 22*(4), 948-969. doi:10.1016/j.ymssp.2007.10.009

Rodrigues, J. (2004). *Identificação Modal Estocástica.* (PhD), Faculdade de Engenharia da Universidade do Porto.

RSB. (2018). Regulamento de Segurança de Barragens. Portugal: Diário da República.

Rytter, A. (1993). *Vibrational Based Inspection of Civil Engineering Structures.* (PhD thesis), Aalbord University.

Salawu, O. S., & Williams, C. (1995). Bridge assessment using forced-vibration testing. *Journal of Structural Engineering (United States), 121*(2), 161-173. doi:10.1061/(ASCE)0733-9445(1995)121:2(161)

Santasusana, M. I. (2012). *Continuum modelling using the Discrete Element Method. Theory and implementation in an object-oriented software platform.* Spain.

Santos, J. P. (2014). *Smart Structural Health Monitoring Techniques for Novelty Identification in Civil Engineering Structures.* (PhD thesis), IST - University of Lisbon.

Santos, J. P., Crémona, C., Orcesi, A. D., & Silveira, P. (2013). Multivariate statistical analysis for early damage detection. *Engineering Structures, 56*, 273-285. doi:10.1016/j.engstruct.2013.05.022

Santos, N., Colaço, A., Costa, P. A., & Calçada, R. (2016). Experimental analysis of track-ground vibrations on a stretch of the Portuguese railway network. *Soil Dynamics and Earthquake Engineering, 90*, 358-380. doi:10.1016/j.soildyn.2016.09.003

Savage, B. M., & Johnson, M. C. (2001). Flow over ogee spillway: Physical and numerical model case study. *Journal of Hydraulic Engineering, 127*(8), 640-648. doi:10.1061/(ASCE)0733-9429(2001)127:8(640)

Scionti, M., Lanslots, J., Goethals, I., Vecchio, A., Van der Auweraer, H., Peeters, B., & De Moor, B. (2003). *Tools to improve detection of structural changes from inflight flutter data.* Paper presented at the 8th Internation Conference on Recent Advances in Structural Dynamics, Southampton, UK.

Scionti, M., & Lanslots, J. P. (2005). Stabilisation diagrams: Pole identification using fuzzy clustering techniques. *Advances in Engineering Software, 36*(11-12), 768-779. doi:10.1016/j.advengsoft.2005.03.029

Serafim, J. (1987). A Note on the Earthquake Performance of Arch Dams. *Proceedings of Joint China-U.S. Workshop on Earthquake Behavior of Arch Dams*.

Sevim, B., Altunisik, A. C., & Bayraktar, A. (2013). Structural identification of concrete arch dams by ambient vibration tests. [Structural identification of concrete arch dams by ambient vibration tests]. *1*. doi:10.12989/ACC2013.1.3.227

Sevim, B., Altunişik, A. C., & Bayraktar, A. (2012a). Earthquake behavior of berke arch dam using ambient vibration test results. *Journal of Performance of Constructed Facilities, 26*(6), 780-792. doi:10.1061/(ASCE)CF.1943-5509.0000264

Sevim, B., Altunişik, A. C., & Bayraktar, A. (2012b). Experimental evaluation of crack effects on the dynamic characteristics of a prototype arch dam using ambient vibration tests. *Computers and Concrete, 10*(3), 277-294.

Shi, W., Shan, J., & Lu, X. (2012). Modal identification of Shanghai World Financial Center both from free and ambient vibration response. *Engineering Structures, 36*, 14-26.

Soal, K., Govers, Y., Bienert, J., & Bekker, A. (2018). *Automatic modal parameter selection using a statistical model and a Kalman filter*.

Song, Z., Liu, Y., & Yang, Q. (2016). Experimental and numerical investigation on the stability of a high arch dam with typical problems of nonsymmetry: Baihetan Dam, China. *Bulletin of Engineering Geology and the Environment, 75*(4), 1555-1570. doi:10.1007/s10064-015-0819-5

Soo Lon Wah, W., Owen, J. S., Chen, Y. T., Elamin, A., & Roberts, G. W. (2019). Removal of masking effect for damage detection of structures. *Engineering Structures, 183*, 646-661. doi:10.1016/j.engstruct.2019.01.005

Structurae, M. Retrieved from https://structurae.net/en/structures/dams/multiple-arch-and-buttress-dams

Suzuki, A., Hoshiai, T., Nakata, H., Otomaru, T., Oki, M., Taniguchi, H., . . . Kuroda, S. (2019). *Modal analysis of two different types of fixed implant-supported prostheses embedded in edentulous maxillae* (Vol. 536).

Tan, H., & Chopra, A. K. (1996). Dam-foundation rock interaction effects in earthquake response of arch dams. *Journal of Structural Engineering, 122*(5), 528-538.

Times, N. (2018). The 3$ Billion Plan to Turn Hoover Dam Into a Giant Battery. *The New York Times*.

Tua, A. d. D. R. d. V. d. (2016). Aproveitamento Hidroelétrico de Foz Tua. Retrieved from http://www.valetua.pt/

Ubertini, F., Comanducci, G., & Cavalagli, N. (2016). Vibration-based structural health monitoring of a historic bell-tower using output-only measurements and multivariate statistical analysis. *Structural Health Monitoring, 15*(4), 438-457. doi:10.1177/1475921716643948

UN, U. N.-. (2015). World Population 2015. Retrieved from https://esa.un.org/unpd/wpp/Publications/Files/World_Population_2015_Wallchart.pdf

Verboven, P., Guillaume, P., Cauberghe, B., Parloo, E., & Vanlanduit, S. (2003). *Stabilization Charts and Uncertainty Bounds for Frequency Domain Linear Least Squares Estimators*.

Verboven, P., Parloo, E., Guillaume, P., & Van Overmeire, M. (2002). Autonomous structural health monitoring - Part I: Modal parameter estimation and tracking. *Mechanical Systems and Signal Processing, 16*(4), 637-657. doi:10.1006/mssp.2002.1492

Wang, B. S., & He, Z. C. (2007). Crack detection of arch dam using statistical neural network based on the reductions of natural frequencies. *Journal of Sound and Vibration, 302*(4–5), 1037-1047. doi:https://doi.org/10.1016/j.jsv.2007.01.008

Wang, H., & Li, D. (2006). Experimental study of seismic overloading of large arch dam. *Earthquake Engineering and Structural Dynamics, 35*(2), 199-216. doi:10.1002/eqe.517

Wang, H., & Li, D. (2007). Experimental study of dynamic damage of an arch dam. *Earthquake Engineering and Structural Dynamics, 36*(3), 347-366. doi:10.1002/eqe.637

WECouncil, W. E. C.-. (2016). *World Energy Resources 2016*. Retrieved from London: www.worldenergy.org

Wei-Hua, H. (2012). *Operational modal analysis and continuous dynamic monitoring of footbridges.* (PhD), Faculty of Engineering of University of Porto.

Westergaard, H. M. (1933). Water pressures on dams during earthquakes. *Trans. ASCE, 98*(1835), 418-433.

Williams, J. R., & Pentland, A. P. (1992). Superquadrics and modal dynamics for discrete elements in interactive design. *Engineering Computations, 9*(2), 115-127.

Worden, K., & Dulieu-Barton, J. M. (2004). An Overview of Intelligent Fault Detection in Systems and Structures. *Structural Health Monitoring, 3*(1), 85-98.

Worden, K., Sohn, H., & Farrar, C. R. (2002). Novelty detection in a changing environment: Regression and inter polation approaches. *Journal of Sound and Vibration, 258*(4), 741-761. doi:10.1006/jsvi.2002.5148

Yan, A. M., Kerschen, G., De Boe, P., & Golinval, J. C. (2005a). Structural damage diagnosis under varying environmental conditions - Part I: A linear analysis. *Mechanical Systems and Signal Processing, 19*(4), 847-864. doi:10.1016/j.ymssp.2004.12.002

Yan, A. M., Kerschen, G., De Boe, P., & Golinval, J. C. (2005b). Structural damage diagnosis under varying environmental conditions - Part II: Local PCA for non-linear cases. *Mechanical Systems and Signal Processing, 19*(4), 865-880. doi:10.1016/j.ymssp.2004.12.003

Yang, J., Jin, F., Wang, J. T., & Kou, L. H. (2017). System identification and modal analysis of an arch dam based on earthquake response records. *Soil Dynamics and Earthquake Engineering, 92*, 109-121. doi:10.1016/j.soildyn.2016.09.039

Zelin, D., Qianqian, W., & Jing, W. (2016). Analysis on stability of an Arch Dam with interlayer shear zones. *KSCE Journal of Civil Engineering, 20*(6), 2262-2269. doi:10.1007/s12205-015-0017-9

Zhang, C., Jin, F., Pan, J., & Long, Y. (2013). Chapter 4 - Seismic Safety Evaluation of High Concrete Dams1: Part 2: Earthquake Behavior of Arch Dams – Case Study *Seismic Safety Evaluation of Concrete Dams* (pp. 79-99): Butterworth-Heinemann.

Zhang, L. M., Xu, Y., & Jia, J. S. (2009). Analysis of earth dam failures: A database approach. *Georisk, 3*(3), 184-189. doi:10.1080/17499510902831759

Zienkiewicz, O. C., Taylor, R. L., & Fox, D. (2014). The Finite Element Method for Solid and Structural Mechanics *The Finite Element Method for Solid and Structural Mechanics (Seventh Edition)* (pp. i). Oxford: Butterworth-Heinemann.